



Doctoral Thesis

Internally consistent thermodynamic database for fluid-rock interaction Tools, methods and optimization

Author(s):

Miron, George D.

Publication Date:

2016

Permanent Link:

<https://doi.org/10.3929/ethz-a-010655112> →

Rights / License:

[In Copyright - Non-Commercial Use Permitted](#) →

This page was generated automatically upon download from the [ETH Zurich Research Collection](#). For more information please consult the [Terms of use](#).

Internally consistent thermodynamic database for fluid-rock interaction: tools, methods and optimization

A thesis submitted to attain the degree of
DOCTOR OF SCIENCES of ETH ZURICH
(Dr. sc. ETH Zurich)

presented by
GEORGE DAN MIRON
MSc. in Earth Sciences ETH Zürich

born on 19.07.1985

citizen of Romania

accepted on the recommendation of
Prof. Dr. Christoph A. Heinrich, examiner
Prof. Dr. Thomas Wagner, co-examiner
Prof. Dr. Lukas Baumgartner, co-examiner
Dr. Dmitrii A. Kulik, co-examiner

Contents

ABSTRACT	VII
Zusammenfassung	IX
Acknowledgments	XIII
1. Introduction	1
1.1. Why thermodynamic modeling?	2
1.2. From data to models	3
1.3. Type of experimental data	4
1.3.1. Thermophysical and thermochemical measurements.....	4
1.3.2. Phase equilibrium experiments	6
1.3.3. Solubility experiments.....	6
1.4. Equation of state and activity models	7
1.5. Uncertainties	10
1.6. Thermodynamic compilations and databases	16
1.7. Internal consistency	18
1.8. Tools and methods	20
References	21
2. GEMSFITS: Code package for optimization of geochemical model parameters and inverse modeling	25
Abstract	26
2.1. Introduction	27
2.2. Review of software for optimization of thermodynamic model parameters	29
2.3. Key features of GEMSFITS	30
2.4. Methods and data	31
2.4.1. Architecture of GEMSFITS	32
2.4.2. Experimental and task database management	33
2.4.3. Parameter optimization code	36
2.4.4. GEMS3K chemical solver and its input data	39
2.4.5. GUI and help functionality	40
2.4.6. The gemsfit2 task specification	42
2.4.7. Optimization library	43
2.4.8. Weighting and outliers	44
2.4.9. Statistics.....	44

2.4.10.	Confidence intervals for parameters by Monte Carlo simulation	44
2.4.11.	Fit-independent statistics.....	45
2.5.	Application examples	46
2.5.1.	Boehmite solubility and Al speciation	47
2.5.2.	Ti in quartz: Solid-solution geothermometry	52
2.6.	Discussion	56
2.7.	Outlook	59
	Acknowledgments.....	59
	References.....	59
2A.	Application of GEMSFITS for multi-parameter optimization in the C-S-H-N-K aqueous solid solution systems	63
2A.1.	Introduction	64
2A.2.	The CASHNK multi-site solid solution model	64
2A.2.	Parameterization of multi-site solid-solution models of C-S-H with alkali and aluminium contents	68
2A.3.	Conclusions	77
	References.....	78
3.	Internally consistent thermodynamic data for aqueous species in the system Na-K-Al-Si-O-H-Cl	81
	Abstract	82
3.1.	Introduction	83
3.2.	Thermodynamic framework.....	85
3.3.	Ion association properties of major electrolytes	88
3.3.1.	NaCl ⁰ association constant.....	90
3.3.2.	KCl ⁰ association constant.....	91
3.3.3.	NaOH ⁰ association constant.....	91
3.3.4.	KOH ⁰ association constant.....	91
3.3.5.	HCl ⁰ association constant.....	92
3.4.	Selection of experimental solubility data.....	92
3.4.1.	Quartz solubility.....	94
3.4.2.	Corundum solubility.....	96
3.4.3.	Gibbsite, boehmite and diasporite solubility	97
3.4.3.1.	Gibbsite solubility.....	98
3.4.3.2.	Boehmite solubility.....	99

3.4.3.3.	Diaspore solubility	100
3.4.4.	Solubility of feldspars, aluminosilicates, and silicate assemblages	100
3.4.4.1.	Feldspar solubility	101
3.4.4.2.	Aluminosilicate solubility	101
3.4.4.3.	Solubility of silicate mineral assemblages	101
3.5.	Parameter optimization methods	103
3.6.	Results	111
3.6.1.	System Si-O-H-Cl	112
3.6.2.	System Al-O-H-Cl.....	112
3.6.3.	System Al-Si-O-H-Cl	116
3.6.4.	System K-Na-Al-Si-O-H-Cl.....	116
3.7.	Discussion	126
3.7.1.	System Si-O-H-Cl	128
3.7.2.	System Al-O-H-Cl.....	128
3.7.3.	System Al-Si-O-H-Cl	130
3.7.4.	System K-Na-Al-Si-O-H-Cl.....	130
3.7.5.	Thermodynamics of the aqueous K ⁺ and Na ⁺ ions.....	131
3.7.6.	Thermodynamics of Na- and K-bearing minerals	132
3.7.7.	Internally consistent thermodynamic database.....	134
3.7.8.	Agreement with CODATA for Na ⁺ and K ⁺ ions.....	135
3.8.	Conclusions and outlook	136
	Acknowledgements	137
	Supplementary tables	137
	References.....	143
4.	Extension of internally consistent thermodynamic dataset for aqueous species to the system Ca-Mg-Na-K-Al-Si-O-H-C-Cl.....	155
	Abstract.....	156
4.1.	Introduction.....	156
4.2.	Thermodynamic framework.....	158
4.3.	Carbon dioxide solubility in water	159
4.4.	Carbon species	162
4.4.1.	Carbonate and bicarbonate	162
4.4.2.	Metal-bicarbonate and -carbonate complexes	164
4.4.2.1.	Ca complexes	164

4.4.2.2.	Mg complexes	165
4.4.2.3.	Na complexes	166
4.4.2.4.	K complexes	167
4.5.	Ion association properties of Ca and Mg with hydroxide and chlorine	167
4.5.1.	Hydroxide species	168
4.5.1.1.	CaOH ⁺ association constant.....	168
4.5.1.2.	MgOH ⁺ association constant.....	169
4.5.2.	Ca and Mg chloride species	170
4.5.2.1.	CaCl ⁺ and CaCl ₂ ⁰ association constants	170
4.5.2.2.	MgCl ⁺ and MgCl ₂ ⁰ association constants	173
4.6.	Ca and Mg silicate species	174
4.7.	Selection of experimental solubility data.....	175
4.7.1.	System Ca-Mg-Al-Si-O-H	175
4.7.2.	System Ca-Mg-Al-Si-Cl-O-H	176
4.7.3.	System Ca-Mg-Cl-O-H-C	178
4.8.	Parameter optimization methods.....	179
4.9.	Results.....	180
4.9.1.	System Ca-Mg-Al-Si-O-H	186
4.9.2.	System Ca-Mg-Al-Si-Cl-O-H	188
4.9.3.	System Ca-Mg-Cl-O-H-C	191
4.10.	Discussion	194
4.10.1.	System Ca-Mg-Al-Si-O-H	194
4.10.2.	System Ca-Mg-Al-Si-Cl-O-H	196
4.10.3.	System Ca-Mg-Cl-O-H-C	198
4.10.4.	Standard state properties of Ca and Mg ions	199
4.11.	Conclusions and outlook	201
	Acknowledgements	202
	References.....	202
5.	Outlook.....	211
	References.....	218
	Curriculum Vitae - George Dan Miron	221

ABSTRACT

Aqueous fluids are of great importance in a variety of chemical and geochemical processes. From the Earth's crust to the mantle, fluids and fluid-rock interaction play a key role in element distribution and mobility. As geochemists we are largely interested in the elemental mobility and interactions throughout the Earth's geological, hydrological, and biological systems. What are the factors that govern the mobility of different elements? How do some elements get concentrated to form an economic ore deposit? How do some trace elements such as radioactive elements get leached and transported from disposed radioactive waste? What would be the impact of surface fluids on different industrial materials such as concrete? Such question can be answered by field investigations, experimental studies and numerical simulations. With the increase in computational power large advances were made in the development of numerical models for geochemical processes close in complexity to real natural systems. The geochemical simulations are powerful methods that help us understand the processes governing the natural fluid-rock systems helping us answer questions as the ones above. An important advantage of computer simulations is that it allows us to systematically explore and understand the governing processes at conditions and over time scales not accessible to direct observation or laboratory experiments.

The results of the geochemical computations models rely critically on the robustness of the geochemical models and, hence, on the availability, accuracy, precision and consistency of thermodynamic (and kinetic) parameters.

The main objective of this thesis was to develop an internally consistent thermodynamic dataset for fluid-rock equilibria in the core system Na-K-Al-Si-O-H-Cl with the extension to Ca-Mg-C. Part of this work was to investigate and develop methods and tools for optimizing the thermodynamic properties of aqueous species in a consistent way.

The first part of the thesis deals with the parameter optimization tool, GEMSFITS, developed for fitting internally consistent input parameters of chemical thermodynamic models against experimental data. GEMSFITS codes can import, manage and query extensive sets of the experimental data accumulated in database files which does not need a priori knowledge of the data structure. Many types of experimental data can be inserted. The tool can simultaneously refine many parameters of several types, independent or constrained, against selected different type of experimental data, using a suite of local and global, gradient or non-gradient based parameter optimization algorithms (NLOpt library ab-initio.mit.edu/nlopt). The optimized parameters are reported with confidence intervals generated using Monte Carlo simulations. Statistical evaluation of fitting results such as sensitivities of measured data and parameters, distributions, correlation coefficients are also available. GEMSFITS is part of the GEM Software package for geochemical modeling (<http://gems.web.psi.ch/>).

The second part of the thesis deals with generating an internally consistent thermodynamic dataset for fluid-rock equilibria in the core system Na-K-Al-Si-O-H-Cl. A large collection of experiments on mineral solubility covering a wide range of temperature pressure and composition

conditions was critically evaluated. Data on association equilibria of major electrolytes (NaCl, KCl, HCl, NaOH, KOH) was evaluated and used to separately refine the standard state properties and equation of state parameters of neutral ion pairs. The selected experimental data was used to simultaneously optimize the standard state Gibbs energies of aqueous ions and complexes but maintaining the agreement with the association equilibria for ion pairs and complexes that were independently derived from conductance and potentiometric data. The work on this system served as a proof of concept for the optimization strategy.

In the third part of the thesis the core dataset was extended with the addition of Ca, Mg, and C to the core system. The experimental data on solubility the solubility of Ca-Mg silicates, hydroxides, and carbonate minerals was critically evaluated. The association equilibria of important complexes (calcium and magnesium hydroxide and chloride species, aqueous carbon dioxide, carbonate and bicarbonate with and without alkali and alkali-metal complexes) was revised. Their standard state properties and equation of state parameters were separately optimized based on experimentally derived association constant data from conductance, potentiometric and exceptionally from solubility measurements. The standard state Gibbs energies of aqueous ions and complexes in the system Ca-Mg-Na-K-Al-Si-O-H-C-Cl were simultaneously optimized against the full selection of experimental data form the core system and the extension.

The new dataset is consistent with the Holland and Powell (1998) mineral dataset (Thermocalc dataset ds55) and with all experimental mineral phase equilibria used to derive these data, as well as with experimental constraints on aqueous speciation equilibria. The main assumption was that the mineral database (ds55) is “fully consistent” and no adjustment of the thermodynamic properties of minerals was done. The dataset reproduces all available fluid-mineral phase equilibria and mineral solubility data with good accuracy over a wide range in temperature, pressure and composition (25 to 800°C; 1 bar to 5 kbar; salt concentrations up to 5 molal).

The method used in this study provides a clear guide to future experimentation, by highlighting the most sensitive gaps in fluid-mineral phase equilibria experiments. More experimental data is needed to solve existing discrepancies and provide missing data on the stability of calcium and magnesium hydroxide and chloride complexes, different carbonate and bicarbonate complexes, and also silica-potassium, calcium-silica, magnesium-silica complexes.

The method developed in this study together with the GEMSFITS optimization tool allows repeating the optimization procedure whenever new and improved experimental constraints become available, better thermodynamic models are developed, when different speciation model is used, and more chemical elements are added. For the future it is desirable that the standard-state properties of minerals, aqueous species and complexes will be simultaneously optimized to create a next-generation internally consistent dataset for fluid-mineral equilibria. The goal is always to have better thermodynamic models as well as accurate and consistent thermodynamic data for these models.

Zusammenfassung

Wässrige Lösungen (Fluide) sind von grosser Bedeutung für eine Vielzahl chemischer und geochemischer Prozesse. Fluide und Interaktionen zwischen Fluiden und Gesteinen spielen eine zentrale Rolle in Bezug auf Verteilung sowie Beweglichkeit chemischer Elemente in der Erdkruste als auch im Erdmantel. Als Geochemiker interessieren wir uns v.a. für die Beweglichkeit und die Interaktionen chemischer Elemente in sämtlichen geologischen, hydrologischen und biologischen Systemen. Welches sind die Faktoren, welche die Beweglichkeit verschiedener Elemente bestimmen? Wie werden gewisse Elemente genügend konzentriert, um wirtschaftlich bedeutsame Erzlagerstätten zu bilden? Wie werden gewisse Spurenelemente sowie radioaktive Elemente aus radioaktiven Endlagern ausgelaugt und wegtransportiert? Was wäre der Einfluss oberflächennaher Fluide auf industrielle Materialien wie beispielsweise Beton? Mithilfe von Felduntersuchungen, Experimenten und numerischen Simulationen können solche Fragen beantwortet werden. Mit zunehmender Rechnerleistung wurden grosse Fortschritte der numerischen Modellierung geochemischer Prozesse erzielt, welche sich in ihrer Komplexität natürlichen Systemen annähern. Diese geochemischen Simulationen sind wirkungsvolle Methoden, welche uns helfen die Prozesse zu verstehen, die natürliche Fluid-Gesteins Systeme bestimmen und sie helfen uns ebenfalls die oben gestellten Fragen zu beantworten. Computersimulationen haben den grossen Vorteil, dass sie uns erlauben die massgeblichen Prozesse für Umgebungsbedingungen und Zeiträume systematisch zu untersuchen, welche über diejenigen hinausgehen, welche mithilfe direkter Beobachtung oder durch Experimente studiert werden können.

Die Ergebnisse solcher geochemischer Berechnungen sind dabei stark von der Robustheit der verwendeten geochemischen Modelle abhängig und somit ebenfalls von der Verfügbarkeit sowie der Richtigkeit, der Präzision und der Konsistenz der verwendeten thermodynamischen (und kinetischen) Parameter abhängig.

Das Hauptziel der vorliegenden Arbeit war die Entwicklung einer innerlich konsistenten thermodynamischen Datenbank der Fluid-Gesteins-Interaktionen des Kernsystems Na-K-Al-Si-O-H-Cl inklusive einer Erweiterung für Ca-Mg-C. Teil der Arbeit war die Entwicklung und die Untersuchung von Methoden zur Optimierung thermodynamischer Eigenschaften aquatisierter Spezies auf eine konsistente Art und Weise.

Der erste Teil der Arbeit befasst sich mit dem GEMSFITS Parameter Optimierungswerkzeug, welches entwickelt wurde, um innerlich konsistente Eingabeparameter thermodynamischer chemischer Modelle mit experimentellen Daten in Übereinstimmung zu bringen. GEMSFITS Codes können umfangreiche experimentelle Datenmengen importieren und bearbeiten, welche in Datenbank Dokumenten gespeichert sind, und welche keine a priori Kenntnis der zugrundeliegenden Datenstruktur voraussetzen. Viele unterschiedliche Arten experimenteller Daten können somit eingefügt werden. GEMSFITS kann gleichzeitig Parameter verschiedenster Art (unabhängig oder eingeschränkt) gegenüber ausgewählter verschiedener experimenteller

Daten verbessern. Dies geschieht unter Verwendung lokaler und globaler, gradient- oder nicht gradientbasierter Parameter Verbesserungs Algorithmen (NLOpt Bibliothek ab-initio.mit.edu/nlopt). Die optimierten Parameter werden mit Konfidenzintervallen angegeben, welche mithilfe von Monte-Carlo Simulationen bestimmt werden. Ebenfalls verfügbar sind statistische Auswertungen, Sensitivitäten der gemessenen Daten und Parameter, Verteilungen sowie Korrelationskoeffizienten. GEMSFITS ist ein Teil des GEM Softwarepakets für geochemische Modellierungen (<http://gems.web.psi.ch>).

Der zweite Teil der Arbeit beschäftigt sich mit dem Aufbau eines intern konsistenten thermodynamischen Datensatzes für Fluid-Gesteins Gleichgewichte im Kernsystem Na-K-Al-Si-O-H-Cl. Zu diesem Zweck wurde eine grosse Sammlung von Minerallöslichkeitsexperimenten über einen weiten Bereich von Temperatur, Druck und Zusammensetzung kritisch evaluiert. Die Daten über Assoziationsgleichgewichte der wichtigen Elektrolyte (NaCl, KCl, HCl, NaOH, KOH) wurden evaluiert und dazu verwendet die Standardzustandseigenschaften und Zustandsgleichungen für neutrale Ionenpaare gesondert weiterzuentwickeln. Die ausgewählten experimentellen Daten wurden verwendet um die Gibbs Energien unter Standardbedingungen von wässrigen Ionen und Komplexen simultan zu optimieren. Dabei wurde die Übereinstimmung mit den Assoziationsgleichgewichten für Ionenpaare und Komplexe, die unabhängig über die Leitfähigkeit und potentiometrische Daten hergeleitet wurden, beibehalten. Dieses System diente als Nachweis für die Gültigkeit des Konzeptes für die Optimierungsstrategie.

Im dritten Teil der Arbeit wurde der Kerndatensatz um die Elemente Ca, Mg und C erweitert. Experimentelle Daten über die Löslichkeit von Ca-Mg Silikaten, Hydroxiden und Karbonatmineralen wurde kritisch evaluiert und die Assoziationsgleichgewichte von wichtigen Komplexen (Calcium- und Magnesiumhydroxiden, Chlorid Verbindungen, wässrigen Kohlendioxiden, Karbonaten und Bikarbonaten mit und ohne Alkalimetallkomplexen) wurden überarbeitet. Basierend auf experimentellen Assoziationskonstanten aus Leitfähigkeits-, potentiometrischen- und gelegentlich Löslichkeitsmessungen wurden die Standardzustandseigenschaften und Zustandsgleichungen gesondert optimiert. Die Gibbs Energien unter Standardbedingungen von wässrigen Ionen und Komplexen im System Ca-Mg-Na-K-Al-Si-O-H-C-Cl wurden mithilfe der vollständigen Auswahl von experimentellen Daten des Kernsystems und der Erweiterung simultan optimiert.

Der neue Datensatz stimmt sowohl mit dem Mineraldatensatz (Thermocalc dataset ds55) von Holland und Powell (1998) und mit allen experimentellen Mineralphasengleichgewichten, die diesen Daten zugrunde liegen, als auch mit experimentellen Bedingungen von wässrigen Bildungsgleichgewichten überein. Die Prämisse bestand hauptsächlich daraus, dass der Mineralien-Datensatz (ds55) "vollständig konsistent" ist und keinerlei Anpassungen an den thermodynamischen Eigenschaften der Mineralien vorgenommen wurde. Der Datensatz reproduziert die verfügbaren Fluid-Mineral Phasengleichgewichte und Minerallöslichkeitsdaten über einen weiten Bereich von Temperatur, Druck und Zusammensetzung (25 bis 800°C; 1 bar bis 5 kbar; Salzkonzentrationen bis zu 5 molal) mit guter Genauigkeit.

Die Methode, die in dieser Arbeit verwendet wurde, stellt einen guten Leitfaden für zukünftige Experimente dar, indem sie die empfindlichsten Lücken in Fluid-Mineral Phasengleichgewichtsexperimenten beleuchtet. Mehr experimentelle Daten werden benötigt um die existierenden Widersprüche zu lösen und fehlende Daten zur Stabilität von Calcium- und Magnesiumhydroxiden, Chloridkomplexen, verschiedenen Karbonat- und Bikarbonatkomplexen, Silicium-Kalium-, Calcium-Silicium-, und Magnesium-Silicium-Komplexen zu ergänzen.

Die Methode, die in dieser Arbeit entwickelt wurde, und das GEMSFITS Optimierungswerkzeug ermöglichen es das Optimierungsverfahren zu wiederholen sobald neue und verbesserte experimentelle Bedingungen zur Verfügung stehen, bessere thermodynamische Modelle entwickelt werden, unterschiedliche Speziationsmodelle verwendet werden oder mehr chemische Elemente hinzugefügt werden. In Zukunft wäre es wünschenswert, dass die Standardzustandseigenschaften von Mineralen, wässrigen Lösungen und komplexen simultan optimiert werden, um eine neue Generation intern konsistenter Datensätze für Fluid-Mineral Gleichgewichte zu schaffen. Das Ziel sind sowohl ständig verbesserte thermodynamische Modelle, als auch richtige und konsistente thermodynamische Daten für diese Modelle.

Acknowledgments

I want to thank Christoph Heinrich (Stöff) for believing in me throughout my master and PhD time spent at ETH. He inspired me to come to ETH Zürich in the first place, to do my Master studies. I will always appreciate the process-oriented thinking that Stöeff teaches to his students, and of course the famous “back of the envelope calculation”. Because in most cases the simplest explanation is also the correct one.

Special thanks goes to Thomas Wagner who had the idea for the project and considered me capable of doing the job. He had to put a lot of trust in me to work on such a project, with him supervising from Helsinki. Although he is more of an emotional person, I have always appreciated that he is doing his best to be an objective researcher and teacher. I have learned many things from him, starting from thermodynamics and modeling and ending with writing a scientific manuscript, especially improving the layout and the figures.

A big thanks goes to Dmitrii Kulik (Dima) with whom I spent a great time improving my programming and geochemical modeling knowledge. During my PhD he was one of my biggest source of feedback and I am grateful that throughout our collaboration we managed to produce a very useful tool for other scientists. Dima is a good role-model of how to combine theory and practice, geology, chemistry, and computer science and always be up to date with many of the advances in science and technology.

Special thanks goes to Britt Meyer who was very helpful with all the administrative problems and was always very responsive in all kind of paper-work situations.

I am very grateful to have been a part of the Fluids and Mineral Deposits group. I want to thank my colleagues who were besides me during the good and the bad times of the PhD. A big thank you to my office colleagues: Achille, Katerina, Maike, Szandra, but also to: Albrecht, Daniela, Denis, Dominik, Ingrid (Ying-Jui, pronounced Ying-Ray ☺), James, Julian, Markus, Pilar, Sam, Simon, Thomas (ThoDri), Yannick, and previous members of the group: Gillian, Jung-Hun, Klara, Matt, Phillip, Tobias, Ingo, Ferdinand. I am also thankful to all the colleagues from the department of Earth Sciences, with whom I had interesting discussions but also a lot of fun during my time at ETH.

I want also to thank Selim for all the “mensa time”, but not only.

I was inspired by my secondary school teacher of chemistry, Mihaela Hadarean, biology, Aurelia Farcas, high-school teacher of geography, Iosof Gabriela, and of Romanian language, Doina Tonca. Special thank you for my university teachers: Sorin Filipescu, my first contact with geology, Marcel Benea, to whom I am grateful for being my diploma supervisor, and Nicolae Har, a great teacher that inspires many students through his enthusiasm and didactic skills.

Special thanks go to Pawel for all the fruitful discussions about parameter fitting but also for being beside me all this time.

I would also like to thank my family: sister, Ilinca, mother, Daniela, father, Gheorghe, grandmother, Maria, who supported me during all my studies, especially during the time when I was far from home.

1. Introduction

1.1. Why thermodynamic modeling?

Fluid-rock interaction processes are of central importance for a wide range of geological systems such as hydrothermal ore deposits, hydrothermal systems at mid-ocean ridges, fluid flow in subduction zones and geothermal reservoirs. Information about these processes can be retrieved from field studies, experimental studies or predictive methods such as geochemical modeling. In field studies samples are often affected by many processes which happened over large periods of geological time. The results are therefore often ambiguous and difficult to interpret. Experiments on simple systems are rather straightforward to perform, but experimental studies of more complex fluid-mineral equilibria face a number of considerable methodological and technical challenges. The use of computer simulations such as reactive transport (coupled fluid flow and geochemical reactions between fluids and minerals) can give valuable insights into the key physical and chemical processes in many geological systems. Advances in computational methods and technology have facilitated the development of efficient and comprehensive (geo)chemical thermodynamic and physical-chemical models for simulation of the behavior of natural systems. Geochemical modeling has the advantage that it can simulate multicomponent-multiphase systems at different pressure-temperature conditions and over timescales that are not accessible to direct observation and laboratory experiments. These simulations are useful for solving environmental problems (e.g. long-term prediction of radioactive waste disposal or contamination of groundwater), designing and improving industrial processes (e.g. formation and stability of different materials), and understanding the evolution of geochemical systems from the surface to the deep Earth. In particular, geochemical reactive-transport simulations that couple thermodynamic fluid-mineral equilibria, kinetics of mineral dissolution and precipitation, and fluid flow in the subsurface have become essential for understanding and predicting the processes in geosystems relevant for carbon dioxide sequestration, exploitation of geothermal energy, and formation of mineral resources (e.g. Reed, 1982; Steefel and Maher, 2009; Xu et al., 2001).

Thermodynamic modeling can be divided into two essential parts: models and parameter datasets. Thermodynamic models are mathematical relations between different physical properties of the system. In the ideal case, the thermodynamic models are developed obeying basic thermodynamic principles and are based on solid theoretical foundations. Some models, however, are just empirical representation of observed data. They are called empirical models. Models which have a sound theoretical background usually have high predictive capabilities, while empirical models mostly fail to predict properties outside their calibration conditions. In many cases it can be extremely difficult to develop a theoretical model and thus an empirical model can be more suited for a certain problem. Often models are constructed by combining theoretical and empirical parts.

Thermodynamic datasets are collections of values for the fundamental thermodynamic properties of substances and other model parameters like empirical parameters, parameters of solution mixing, surface and kinetics model parameters, etc. They are often compiled from direct measurements of the thermodynamic properties or indirectly derived from other experimental data. Different thermodynamic datasets have parameters with different levels of accuracy and internal

consistency. Therefore “*even if the thermodynamic model is rigorous, a blind faith in the database attached to a computer program can be a recipe for disaster*” - Anderson (2005). None of the existing thermodynamic datasets contain values for all possible substances, and often the reported parameters were not derived in an internally consistent way. For example, we can independently obtain the best values of the $\Delta_f G_{298,1}^0$ of pyrophyllite, H₂O, kaolinite, and SiO₂⁰, from different sources of experimental data. However, these values can be in disagreement (would be inconsistent) with the experimental data of the reaction: pyrophyllite + H₂O = kaolinite + SiO₂⁰. Often one thermodynamic dataset is consistent just with certain thermodynamic models, and, therefore, values of parameters taken from different datasets can be inconsistent with each other. It is important to note that “internally consistent” does not necessarily mean “more accurate”. But an internally consistent set of parameters will accurately reproduce the experimental data used to derive it, and can be extremely efficient in reproducing complex multi-component.

1.2. From data to models

Experimental data on simple and well controlled systems can give us insights into more complex systems. These measurements contain information on the fundamental thermodynamic properties that describe the system. Some types of experiments are especially useful for extracting values of the reference properties and model parameters, which can be then used to model more complex systems. To extract useful numbers from experimental data, first, we need quantitative models that relate the experimental observations (measured properties) to the thermodynamic parameters. Secondly, we need an algorithm that can find the combination of parameters which best describes the input experimental data, within the measurement errors. When calculating or optimizing fundamental properties, it is important to do it in such a way, that they are mutually consistent. To produce a reliable estimate of the thermodynamic properties of the chemical system components, it is necessary to use a large number of independent constraints which have to be considered simultaneously (Engi, 1992). A combination of constraints from measurements of fundamental properties, reaction data, phase-equilibria, and solubility allows refinement of the thermodynamic properties of individual components (species) (Engi, 1992). To derive an internally consistent thermodynamic database, a large number of experiments of different type of data covering a wide range of temperature, pressure, composition conditions have to be processed simultaneously to minimize the difference between the calculated and measured experimental values and avoid systematic errors. It is important to consider that when working on a method of data analysis and processing, for deriving an internally consistent database “*we make a clear distinction between our ideal goal and the practical results we can achieve*” - Engi (1992). Often there is not enough experimental data to cover all the temperature-pressure-composition space that we want to model in our calculations, or there are not enough constraints on the mineral fluid-speciation equilibria, to make a refinement of all parameters possible at the same time. In such cases, assumptions have to be made in a form of constraints or rough approximations of parameters for which there is no experimental data. After refining the system parameters, it is crucial that the

geochemical calculations are done in the same thermodynamic framework (i.e. using the same equation of state, models) as was used in the parameters refinement process (Engi, 1992).

A frequently applied method in parameter optimization is the least squares (non-linear) regression. Special algorithms were developed to find the best parameter combination for which the sum of squared residuals (differences between measured and calculated values) has the minimum possible value. The least-squares regression method was employed by Powell and Holland (1985), Holland and Powell (1998) and Holland and Powell (2011), for generating an internally consistent thermodynamic database for minerals. The experimental data they used were mineral phase equilibria. During optimization they assumed a normally distributed Gaussian probability between the half phase equilibria brackets. This was criticized by researchers employing linear mathematical algorithms for their optimization (e.g. Berman et al., 1986). Kolassa (1991) analyzed this method and came to the conclusion that the distribution is far from normal and that the assumption that equilibrium is found in the middle of the brackets would result in parameters which are inconsistent with some equilibrium constraints (Engi, 1992). Holland and Powell (1990) responded to the criticism of Berman et al. (1986), Berman (1988) and introduced weighting related to the bracket width to reduce this effect in their fit. While there are some debates on which data optimization method should be used for treating equilibrium brackets experiments (Berman et al., 1986; Engi, 1992; Holland and Powell, 1990), in the case of solubility experiments, the measured properties represent equality constraints. This means that the least-squares optimization method chosen in the current study is appropriate.

1.3. Types of experimental data

Different type of experiments can be related to thermodynamic properties. These can be direct measurements such as calorimetry, or so called indirect experiments such as reaction equilibria between different minerals or between minerals and a fluid phase (solubility experiments). It follows from the thermodynamic principles that one can use thermodynamic properties derived from simple experimental settings to model more complex systems. Complex experiments trying to duplicate natural conditions as close as possible are often difficult to interpret and thus can be of limited usefulness for extracting fundamental properties (Anderson, 2005). It is desired to have many simple experiments covering a wide range of conditions. In some cases, the experiments need not be too simple, so that the component we want to study is correctly represented by the experiment.

1.3.1. Thermophysical and thermochemical measurements

Electrochemical cells can be used to accurately extract the Gibbs energy of reactions and dissolved substances. A potentiometric cell, where a reversible electrochemical reaction takes place, is used to measure the electrode potential (also known as electromotive force) which is then related to the standard Gibbs energy of the chemical reaction (Lvov and Palmer, 2004). Standard electrode potentials for many reactions have been measured at ambient conditions but there is

limited data available at elevated temperatures and pressures (Lvov and Palmer, 2004). Standard state free energies of formation for ions such as K^+ and Na^+ were determined from electrode potential measurements between amalgams and aqueous and non-aqueous solutions (Cerquetti et al., 1968; Dill et al., 1968; Smith and Taylor, 1940).

Another source for the Gibbs energy, enthalpy, entropy and heat capacity are calorimetric measurements. Solution calorimetry is often used to determine the enthalpy of formation of minerals and aqueous species. This method is based on several calorimetric cycles / reactions which, combined in a series of algebraic calculations, lead to the desired heat of formation. Usually, to get the heat of formation of one component one needs the heats of more than two other reactions. The large number of reactions that have to be considered often leads to a large accumulated error in the final value for the desired enthalpy of formation of the component. The large accumulated errors into this property is also one of the arguments used by Powell and Holland (1985) for choosing to optimize just the enthalpy of formation of minerals in their database. Cryogenic calorimetry is often used for determining the heat capacity at very low temperatures. Integrating these values from temperatures very close to absolute 0 up to 298.15 K lets us get the standard state entropy at 298.15 K (Robie, 1987). Differential scanning calorimetry is the experimental technique used to determine the heat capacity as a function of temperature. The investigated sample and a reference material are slowly heated. The temperatures of the sample and reference materials are always kept equal. Heat capacity of the sample can be inferred based on the difference of heats supplied to the sample and the reference material.

Molar volumes of minerals can be determined using X-Ray diffraction. The change in the molar volume of minerals with temperature and pressure is rather low and it is approximated by using a constant molar volume or accounting for the small changes using simple models. In the case of aqueous components, the molar volume is far from constant and largely changes with temperature, pressure and composition. Two frequent methods for studying the molar volumes in aqueous solutions are density measurements, which measure the densities of a solution at different conditions, and dilatometer measurements, which directly measure the change in solution volume. These measurements are then related through activity models to the infinite dilution standard state volume. They are also used for extracting the activity model parameters from the variation of the molar volume with composition.

Electrolyte solutions are much better conductors than pure water solvent. Their conductance is dependent on the degree of association. For example, if some of the Na^+ and Cl^- ions associate to form the $NaCl^0$ neutral ion pair, the conductance of the solution decreases. Conductance measurements are thus important for determining the degree of association of solutes and the stability constants of associated species. The derived values of the ion pairs equilibrium constants are often dependent on the models used to relate them to the measured electrical conductance, and on the activity models used to extrapolate them to infinite dilution. At low concentrations (< 0.01 mol/kg water), the existing conductance equations and activity models can be used to accurately determine the limiting conductance and ion association constants (Corti, 2008; Sharygin et al., 2002).

The isopiestic (constant pressure) method is used to derive the activity of a component in a multicomponent system using the measured activity coefficient of a standard for different concentrations of a solute. This relationship comes from the Gibbs-Duhem equation, which states that the solution components are not always independent of one another (Anderson, 2005). This method is useful for extracting activity model parameters but also standard state properties.

1.3.2. Phase equilibrium experiments

Phase equilibrium experiments are done to study the reaction between different phases. A detailed chemical characterization of the experimental results allows the calculation of fundamental thermodynamic parameters of the phases involved in the reaction. Reversal phase-equilibrium experiments are used for constraining mineral stabilities. The relative stabilities of reactant and product minerals are studied over a wide range of pressures and temperatures. These experiments are then used to approximate the equilibrium which is bounded by the experimental P-T half brackets. This is done by fitting the parameters of univariant equilibrium to pass it between all the experimental half-brackets. In this process the standard state properties of the product and reactant mineral phases are optimized (Berman et al., 1986; Powell and Holland, 1985).

1.3.3. Solubility experiments

Solubility experiments are a subgroup of the phase equilibrium experiments. They involve the equilibrium between one or more solid phase (and/or gas) and an aqueous solution. For this kind of experiments, it is important to demonstrate the attainment of equilibrium. This is done by doing the experiments from both undersaturated and supersaturated conditions. In some cases, proximity to equilibrium is approximated by a “sufficiently long” time of the experiment or by the constant concentration value measured in a time series experiment. The most accurate results from solubility measurements are obtained by sampling the aqueous solution at equilibrium conditions. Often these experiments are done at elevated temperatures and pressures, where the experimental technique does not allow sampling of the solution at equilibrium conditions. In these cases, the experimental capsule is quenched to room conditions, and then the solution is analyzed. This method is plagued by possible backward reactions and changes in the sample composition. The pH of the aqueous solution is an essential property in solubility experiments and gives important information about the stability and speciation of aqueous components. Determining the pH of the solution at the experimental conditions is a difficult task. In many experiments the pH at the equilibrium conditions is estimated from the measured pH of the quenched solution. This can be largely affected by the change in speciation and other quench related reactions. The hydrogen-electrode concentration cell (HECC) method is useful to monitor the H^+ ions concentration at the conditions of the experiments (Bénézech et al., 2001; Palmer et al., 2001). This method is used only up to 300 °C at SWVP (saturated water vapor pressure) due to difficulties in accounting for non-idealities (activity coefficients) of the standard solution used in the experiments at supercritical conditions (Lvov and Palmer, 2004). Improved in situ spectroscopic methods (i.e. Raman spectrometry) are now used to study the solubility of various minerals in diamond anvil

cells at extreme conditions (Facq et al., 2014). Synthetic fluid inclusion method is used for sampling the aqueous phase at the experimental conditions (Schmidt et al., 1998). An important factor when retrieving thermodynamic properties from solubility experiments is the accurate knowledge of the speciation in the aqueous phase and the properties of the components. Missing species or inaccurate properties of components can lead to accumulated errors in the optimized property of other components. Because the solubility and phase equilibrium experiments involve reactions, the thermodynamic parameters optimized from such experiments are not independent, but are determined by all the properties of reactants and products involved in the reaction. To minimize the error between different components and ensure internal consistency, it is thus important to simultaneously evaluate multiple experimental systems (multiple reactions) covering a wide range of temperature-pressure-composition conditions.

1.4. Equation of state and activity models

For calculating the standard state Gibbs energy at the temperature T and pressure P of interest of all the components in a chemical system we would need to know the $\Delta_f G_{298,1}^0$ and $S_{298,1}^0$ at the reference temperature $T_r = 298.15\text{K}$ and reference pressure $P_r = 10^5\text{Pa}$ (1bar) and the change in molar volume and heat capacity with pressure and temperature. For minerals the changes in volume can be approximated to be close to zero, while the changes in heat capacity with temperature are taken from calorimetric experiments fitted to a heat capacity function (e.g Maier-Kelley function). In the case of aqueous phase components, things become more complicated because the standard partial molar volumes of the aqueous ions and species vary with temperature and pressure. One of the most widely used model for calculating the standard state partial molal Gibbs energy of aqueous components at the temperature and pressure of interest is the HKF (Helgeson-Kirkham-Flowers) equation of state (Helgeson et al., 1981). It is a semi empirical model that can evaluate the change in the standard state partial molal volume and heat capacity with pressure and temperature using several constant parameters. To calculate the standard state Gibbs energy at the temperature and pressure of interest for an aqueous species in the framework of HKF, the values for the standard partial molal Gibbs energy, standard partial molal entropy, and the HKF parameters at reference conditions are needed. For most ions and some aqueous species, the HKF parameters were obtained by Tanger and Helgeson (1988). The authors used experimental standard partial molal volumes, isothermal compressibilities, and isobaric heat capacities of several aqueous electrolytes (e.g., HCl, NaCl, KCl, NaOH, KOH; Tanger and Helgeson, 1988) over a range of temperatures. They regressed this experimental data to obtain the HKF equation of state parameters for the respective electrolytes. From the resulting values, they calculated the HKF parameters for the ions using the constraint that a given parameter of the electrolyte is equal to the sum of the respective parameters of its constituent ions. Although some of the standard state properties and HKF parameters of aqueous species have been derived from different experiments (e.g. solubility, association reaction data), there are numerous aqueous species which have scarce or no data. Shock and Helgeson (1988) and later studies by Shock and Helgeson (1990), Sassani and Shock (1992),

Shock et al. (1997), Sverjensky et al. (1997), and Plyasunov and Shock (2001) proposed several empirical correlations between the standard state properties and HKF parameters, so it is possible to estimate missing properties for many aqueous species, for which there is no experimental data. The experiments on the partial molal heat capacity and volume available at the time of the earlier studies were restricted to low temperatures - below 100 °C, and mostly below 50 °C, making some extrapolations not always in agreement with more recent experiments (Plyasunov and Shock, 2001; Tremaine et al., 2004). While there is experimental data at ambient conditions, a lot of experimental data related to the aqueous phase is missing at elevated pressure and temperature conditions. The fact that these correlations make it possible to predict properties for aqueous components with no or scarce experimental data made the HKF model widely used in high temperature and pressure geochemical applications. Other models used to describe the properties of solutions at elevated conditions are the so called “density models”. In contrast to the HKF model, which is based on the static permittivity (dielectric constant) of the solvent, the density models are based on the volumetric properties (Anderson et al., 1991; Dolejš and Manning, 2010; Holland and Powell, 1998).

The HKF model calculates the thermodynamic properties in their standard state (i.e. at infinite dilution). To calculate chemical equilibrium of a real system, the activity coefficients (γ) have to be calculated using an activity model. Models based on the Debye-Hückel theory (Debye and Hückel, 1923) with different extensions are frequently used in low electrolyte concentrations. One such extension is the D-H-Helgeson (Helgeson et al., 1981) which is used in connection with the HKF equation of state for the standard state properties. Another way to calculate activity coefficients is using the Pitzer formulations (Pitzer, 1973). While the HKF model refers to the properties in the standard state and needs a separate activity model, the Pitzer equations lead to excess properties, calculating the real system properties. The HKF parameters can be fitted to experimental data only after extrapolating to infinite dilution, while the Pitzer parameters are fitted to the actual experimental data at various concentrations (Anderson, 2005). The Pitzer model describes very well systems at conditions close to the Earth’s surface and for concentrated solutions. There are little or no parameters known for high pressure and temperature conditions and the model does not explicitly consider the formation associated species and ion pairs. The HKF model complemented by the D-H-Helgeson activity model is more suitable for low concentrated solutions and aqueous solutions related to metamorphic and hydrothermal fluids at conditions where speciation and ion pairing become important. In this study an extended Debye-Hückel equation (Helgeson et al., 1981) was used to calculate the activity coefficients for charged species (see Chapter 3, Eqs. 3.2-3.4).

Since the parameters of this activity model were not optimized and taken as such from different sources, a test was done to evaluate the impact of different parameters on the calculated solubility values. The solubility of corundum was modeled at 600 °C and 2000 bar from 0.5 to 5 mNaOH concentration. A comparison was made between the results using the extended term activity model parameter for NaOH reported by Pokrovskii and Helgeson (1995), as 0.098 (pressure and

temperature dependent) and the value of 0.03 (pressure and temperature independent) suggested by Dolejš and Wagner (2008).

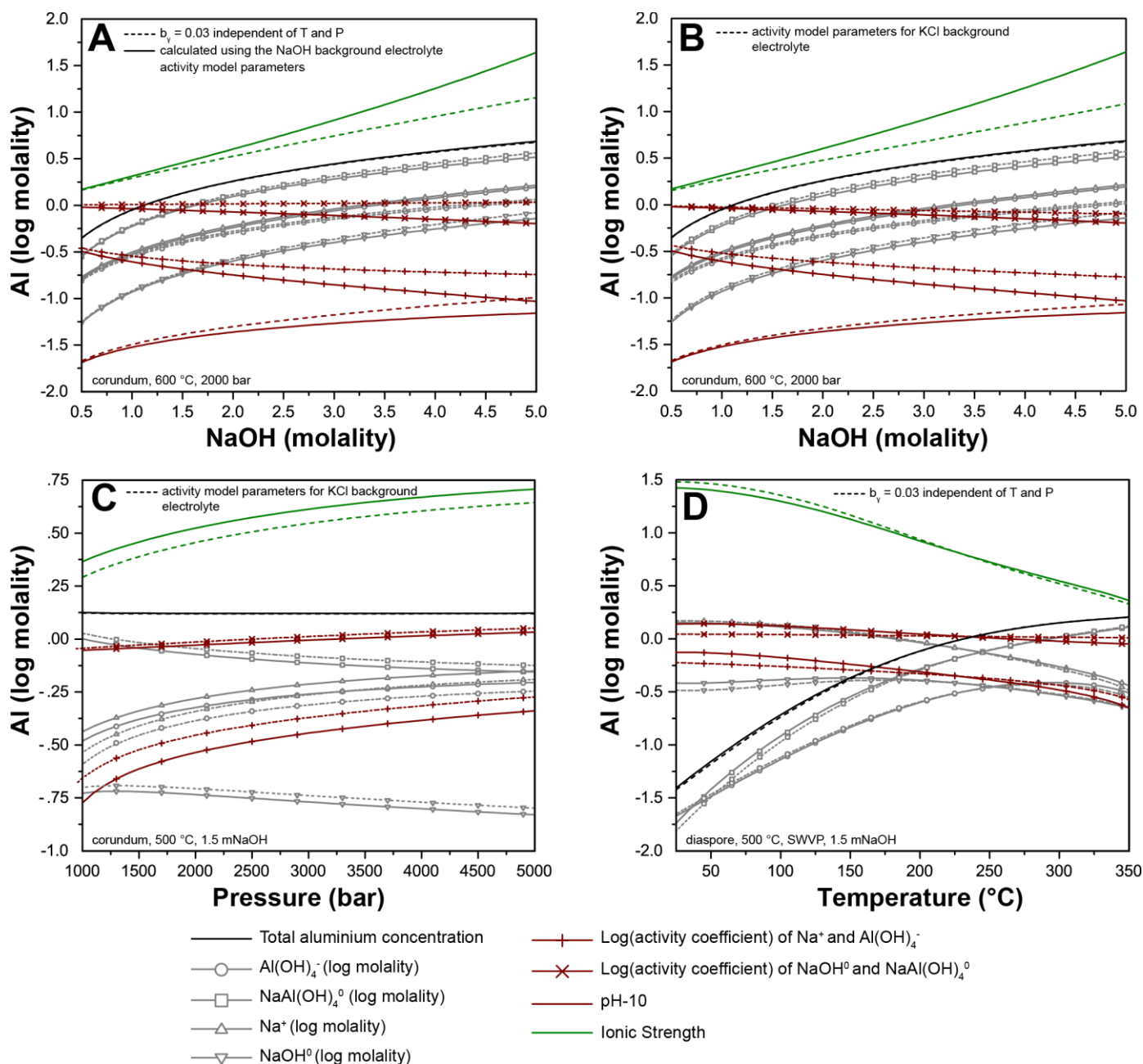


Figure 1.1 Test for the effect of different activity model parameters for calculating the total aluminium concentration in NaOH solutions in equilibrium with corundum and diaspora at different conditions. Continuous lines are calculated using the activity model parameters as reported by Pokrovskii and Helgeson (1995) for NaOH background electrolyte. Dashed lines represent values calculated using different values for the activity model parameters (see figure legend). (A), (B) and (C) corundum solubility, (D) diaspora solubility.

In Fig. 1.1 one can see that up to 5 molal NaOH concentration the difference in the calculated aluminium solubility is almost identical for the two cases. Although there are large differences in the calculated activity coefficients and concentrations of the charged and neutral species due to the mass balance and the interdependence between the components coming out of the Gibbs-Duhem relation, these differences cancel out in the total concentration of aluminium. The same system

was modeled using the \hat{a} and b_γ parameters for a KCl background electrolyte solution (Pokrovskii and Helgeson, 1997a; Fig. 1.1B). The solubility of corundum was calculated at constant temperature and 1.5 mNaOH concentration with changing pressure (Fig. 1.1C) and the solubility of diaspore was calculated at the same NaOH concentration with changing temperature at SWVP (Fig. 1.1D). The comparisons were done between using the parameters for NaOH background electrolyte and using the parameters for KCl background electrolyte, or using a b_γ of 0.03 independent of temperature and pressure. In all cases of using different activity model parameters, the difference between the calculated total dissolved aluminum is very small. The only noticeable differences are between the amount of different species and their activities, which increase with concentration. At very low concentrations, the differences between the activities of the species should be minimal since the extended term contribution is decreasing with concentration. This test demonstrates that the activity model chosen for this study has a minimum impact on the calculations of the total elemental concentrations used for comparison with their experimental measured counterparts and representing the main contribution in the parameter optimization.

1.5. Uncertainties

Uncertainties in geochemical modeling are difficult to fully quantify. This is due to the complex mathematical structure of the thermodynamic models. The total uncertainty is related to the uncertainties in the thermodynamic data and the uncertainties in the calculation procedure (Anderson, 1977). Usually the thermodynamic parameters are also correlated and just a simple error propagation will overestimate the uncertainty (Holland and Powell, 1985; Wolery et al., 2007), and thus the actual error on the resulted thermodynamic value is difficult to quantify. This is why a common practice when building a thermodynamic database is to give higher priority to internal consistency than accuracy. This means that the parameters from this database will accurately reproduce the constraining experimental measurements, inside the thermodynamic framework used to extract them even if they are not the most accurate (Wolery et al., 2007).

Large part of the uncertainties in the thermodynamic data and geochemical calculations come from the way the original data is processed. The thermodynamic properties which are not directly measured contain uncertainties both from original data measurements and from the models which relate the original data with the derived parameters. These models can have their own parameters which have associated uncertainties. The calorimetric measurements on minerals have an average uncertainty around 4-6 kJ/mol. Solubility measurements have in the good cases errors around 1% for the soluble salts and around about 10 % for elements which are less soluble but still much above the limit of detection (Wolery et al., 2007). As the concentration of an element gets close to the limit of detection the uncertainty also increases.

To test the sensitivity of the calculated aqueous phase composition to changes in the $\Delta_f G_{298,1}^0$ of aqueous species, we simulated the solubility of microcline-muscovite-quartz mineral assemblage in pure water from 200 °C to 550 C°, at 1000 bars (1 mol of each mineral reacting with 10 g of water). The major Al species at the condition of the simulation is $\text{Al}(\text{OH})_4^-$, which is over

2.5 orders of magnitude more abundant than $\text{Al}(\text{OH})_3^0$. The $\Delta_f G_{298,1}^0$ of $\text{Al}(\text{OH})_4^-$ aqueous species was incremented in steps until a value +7000 J/mol from the original value (Table 1.1). Any change in the $\Delta_f G_{298,1}^0$ of the aqueous species involved in the solubility linearly affects the Gibbs energy of the reaction. The final value of +7000 J/mol corresponds to a difference of 0.64 log units at 200 °C and to 0.44 log units at 550 C° in the logK of the solubility reaction. In Table 1.1 the deviations in percentages are shown as a function of temperature and of the change in the $\Delta_f G_{298,1}^0$ of $\text{Al}(\text{OH})_4^-$. In general, the differences for aluminium decrease with temperatures while in the case of potassium the differences increase. This is due to the formation of more microcline, which contains more potassium and less aluminium than muscovite. In this way we have less potassium in the fluid but more aluminium with the stepwise increase in the $\Delta_f G_{298,1}^0$ of $\text{Al}(\text{OH})_4^-$. As a result, with increasing temperature, the error in the calculated potassium increases, while the error in calculated aluminium decreases. The error in calculated potassium reaches a maximum around 500 °C from where it slightly decreases. This is because the KAlO_2^0 species becomes more abundant with temperature, and start to have a meaningful concentration from this temperature. This effect counter balances the difference in aluminium concentration but also in potassium concentration.

In Fig.1.2 the computed aqueous composition is shown using the initial value $\Delta_f G_{298,1}^0$ of $\text{Al}(\text{OH})_4^-$ and using a value 7000 J/mol more positive. One can see that the difference of the total calculated concentration of aluminium in solution, between these two cases at the same temperature, decreases from more than 1 log unit, at lower temperatures, to less than 0.5 log units, at higher temperatures. This is due to different combined effects. One is the effect of increasing pH, for the +7000 J/mol case. This means that the activity of OH^- in solution is also increased. This leads to more $\text{Al}(\text{OH})_4^-$ forming and thus an increase in total aluminium which acts to cancel the lower stability of the species (+7000 J/mol effect). Another reason for this decrease in the difference with increasing temperature is the change in the activity / activity coefficient of $\text{Al}(\text{OH})_4^-$. Its value decreases more with temperature for the case when $\Delta_f G_{298,1}^0$ of $\text{Al}(\text{OH})_4^-$ is made 7000 J/mol more positive. The lower activity coefficient has the effect that more $\text{Al}(\text{OH})_4^-$ forms in the solution, thus reducing the difference in the total dissolved aluminium between the two cases. In this multi element system one can notice that a change in the properties of the aluminium species is correlated with changes in other elements as well. The difference between the calculated amount of dissolved potassium increases between the two cases with increasing temperature. This is due to the formation of more microcline in the +7000 J/mol case, which contains more potassium and less aluminium than muscovite. The formation of microcline as opposed to muscovite is also a cause of the increase in the pH of the aqueous phase in the +7000 J/mol case compared to the initial value case.

In many geological fluid systems, chlorine is an important component (see: Fyfe et al., 1978). With increasing temperature in the chlorine bearing systems, the associated species between chlorine and the alkaline, alkaline-earth elements start to form. The standard state properties of these species are important in determining the composition of the aqueous phase. One of the

essential species common to all chlorine systems is the neutral HCl^0 ion pair. This species influences the pH, but also has a role in the availability of chlorine for other chlorine species to form.

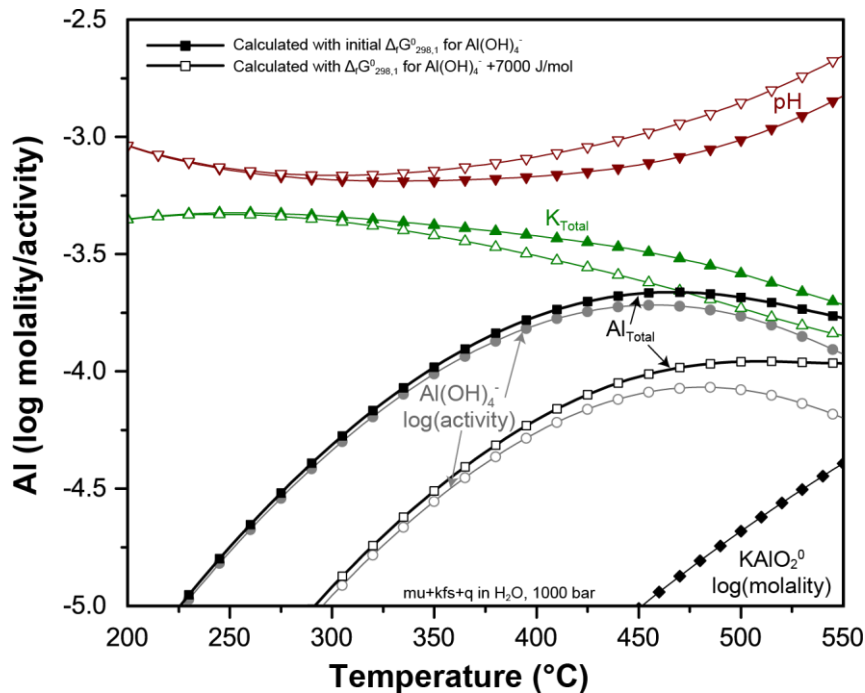


Figure 1.2 Simulated solubility of mineral assemblage muscovite+microcline+quartz in water at 1000 bar with changing temperature. Lines with full symbols represent the calculated aqueous composition using the initial value of the $\Delta_f G_{298,1}^0$ of $\text{Al}(\text{OH})_4^-$. Lines with empty symbols represent the calculated aqueous composition with the $\Delta_f G_{298,1}^0$ of $\text{Al}(\text{OH})_4^-$ 7000 J/mol more positive.

To test the effect of changed standard state properties of HCl^0 ion pair, the solubility of diopside-talc-quartz was calculated at 600 °C and 2000 bars in a solution of 1m CaCl_2 . At these conditions, CaCl_2^0 , MgCl_2^0 , Cl^- and HCl^0 are the main chlorine species. If we consider that the $\Delta_f G_{298,1}^0$ of HCl^0 would be off by 3000 J/mol (~ 0.18 log units), the necessary correction to the $\Delta_f G_{298,1}^0$ of CaCl_2^0 , MgCl_2^0 would be around 6800 J/mol (~ 0.41 log units) to get the same aqueous composition. This shows that the impact of the standard state properties is not uniform and that at high temperatures the properties of HCl^0 are essential. In many studies, the properties of HCl^0 were taken from different sources and used in the process of obtaining the association properties of other chlorine species. Even a small change in the HCl^0 properties leads to large differences between the resulting properties of the other chlorine species. This can be one of the reasons for the discrepancies of the determined association constant values between different studies. Saccoccia and Seyfried (1990) calculated the dissociation constant for MgCl^+ from talc-quartz solubility experiments and found that their value at 400 °C and 500 bar is 0.68 log units more positive than the one reported in the study of Frantz and Marshall (1982). They also noted that just an adjustment of -0.2 log units to the dissociation constant of HCl^0 could account for the discrepancy.

Table 1.1 Calculated relative differences (in percentage) for the total dissolved molality of Al (aluminium) and K (potassium) in equilibrium with muscovite+microcline+quartz using the value for $\Delta_f G_{298,1}^0$ of $\text{Al}(\text{OH})_4^-$ (Initial) and a stepwise increase of the $\Delta_f G_{298,1}^0$ (New): (Initial – New)/Initial*100

ΔG	T (°C)	200	225	250	275	300	325	350	375	400	425	450	475	500	525	550
+50	Al	1.22	1.16	1.09	1.03	0.96	0.89	0.82	0.74	0.67	0.60	0.53	0.48	0.43	0.38	0.32
	K	0.00	0.01	0.02	0.03	0.06	0.08	0.12	0.16	0.20	0.23	0.26	0.28	0.28	0.27	0.25
+100	Al	2.46	2.33	2.20	2.07	1.93	1.79	1.64	1.49	1.34	1.20	1.07	0.96	0.86	0.76	0.65
	K	0.01	0.03	0.04	0.07	0.11	0.17	0.24	0.32	0.40	0.47	0.53	0.56	0.57	0.55	0.50
+200	Al	4.89	4.62	4.37	4.11	3.85	3.57	3.28	2.98	2.68	2.40	2.15	1.93	1.72	1.52	1.29
	K	0.03	0.05	0.09	0.14	0.22	0.33	0.47	0.64	0.80	0.94	1.06	1.12	1.13	1.09	1.00
+400	Al	9.56	9.05	8.57	8.08	7.58	7.04	6.48	5.90	5.31	4.77	4.27	3.83	3.43	3.02	2.57
	K	0.05	0.10	0.17	0.27	0.43	0.65	0.93	1.25	1.58	1.87	2.09	2.22	2.25	2.17	1.98
+600	Al	14.00	13.28	12.58	11.88	11.16	10.40	9.58	8.74	7.89	7.09	6.36	5.71	5.11	4.50	3.84
	K	0.08	0.14	0.24	0.40	0.64	0.96	1.38	1.85	2.34	2.77	3.10	3.30	3.35	3.23	2.95
+1000	Al	22.24	21.15	20.10	19.04	17.94	16.77	15.51	14.19	12.86	11.59	10.42	9.37	8.39	7.40	6.31
	K	0.13	0.23	0.39	0.64	1.02	1.55	2.22	3.00	3.79	4.51	5.06	5.39	5.48	5.30	4.84
+2000	Al	39.54	37.85	36.19	34.51	32.75	30.86	28.80	26.59	24.31	22.06	19.95	18.00	16.16	14.27	12.18
	K	0.23	0.41	0.70	1.17	1.86	2.83	4.09	5.56	7.08	8.47	9.56	10.23	10.43	10.12	9.27
+3000	Al	52.98	51.01	49.05	47.05	44.94	42.65	40.12	37.36	34.43	31.48	28.63	25.94	23.34	20.64	17.65
	K	0.30	0.55	0.95	1.59	2.54	3.90	5.66	7.74	9.92	11.94	13.54	14.56	14.91	14.51	13.32
+5000	Al	71.53	69.52	67.49	65.38	63.13	60.64	57.82	54.65	51.14	47.41	43.62	39.85	36.07	32.03	27.45
	K	0.41	0.75	1.31	2.20	3.56	5.50	8.07	11.15	14.45	17.59	20.16	21.87	22.56	22.10	20.38
+7000	Al	82.70	80.98	79.20	77.32	75.28	72.99	70.36	67.31	63.81	59.92	55.76	51.41	46.83	41.77	35.92
	K	0.48	0.87	1.53	2.59	4.23	6.58	9.74	13.57	17.76	21.82	25.25	27.63	28.71	28.29	26.22

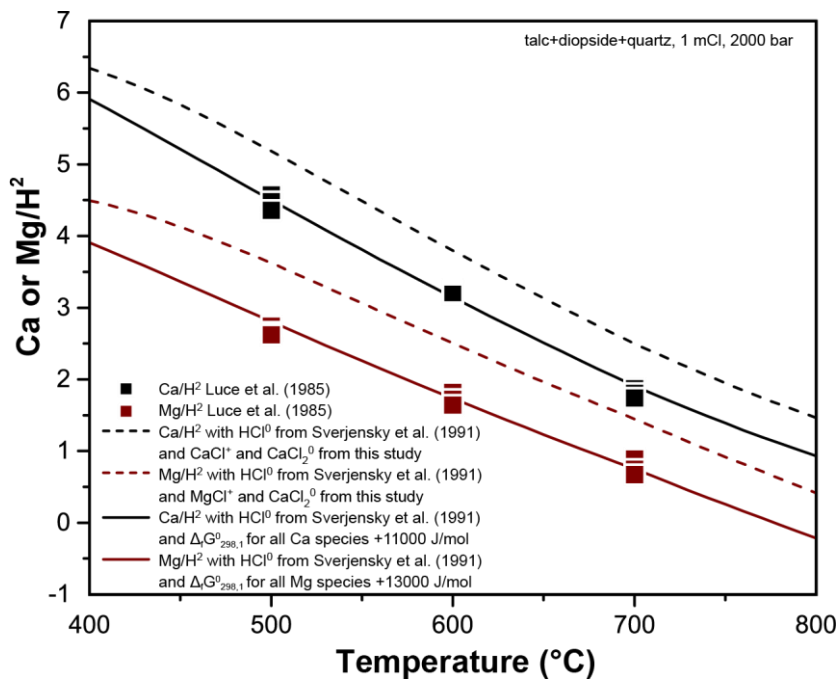


Figure 1.3 Comparison between the measured (Luce et al., 1985) and calculated Ca or Mg/H² (total) molality ratios from an aqueous solution with 1 molal Cl concentration, at 1000 bars, with increasing temperature, and in equilibrium with talc+diopside+quartz. The standard state properties and HKF parameters for HCl⁰ were taken from Sverjensky et al. (1991); the properties of Ca⁺², Mg⁺², MgOH⁺ and CaOH⁺ were taken from SUPCRT92 (Johnson et al., 1992; Shock et al., 1997). The dotted line was calculated using the standard state properties and HKF of CaCl⁺, CaCl₂⁰, MgCl⁺, and MgCl₂⁰ derived in this study. The continuous line was calculated using the HKF parameters of the calcium and magnesium chloride species derived in this study but with the $\Delta_f G_{298,1}^0$ of calcium and magnesium ions and complexes increased by 11000 and 13000 J/mol, respectively.

Another example is modeling the dissolved $\text{Ca}_{\text{tot}}/\text{H}^2_{\text{tot}}$ ratio in equilibrium with diopside-talc-quartz mineral assemblage and using the standard state properties and HKF parameters reported by Sverjensky et al. (1991) as opposed to the ones reported by Tagirov et al. (1997), which are also used in this study (Fig. 1.3). One can see in Fig. 1.3 that there is a large disagreement between the measured (Luce et al., 1985) and calculated values (dashed lines). The temperature trend seems to agree though. To achieve an agreement between the calculated (full lines) and measured values, the $\Delta_f G_{298,1}^0$ of Ca⁺², CaOH⁺, CaCl⁺, CaCl₂⁰ had to be increased by 11000 J, while the $\Delta_f G_{298,1}^0$ of Mg⁺², MgOH⁺, MgCl⁺, MgCl₂⁰ had to be increased by 13000 J. In Fig. 1.4 the $\Delta_f G_{298,1}^0/1000$ for HCl⁰ is plotted at different temperatures and pressures for the two different sources. This is an example of an inconsistency between two sets of standard state properties and HKF parameters for HCl⁰ and the large impact it has on the modeled aqueous solution. It also shows that, if the temperature and pressure trends of the properties of the aqueous species are appropriate, the remaining discrepancies can be corrected just by adjusting the $\Delta_f G_{298,1}^0$ of the ions

while maintaining the agreement with the ion association equilibria using reaction constraints. The same principle is applied in this study.

These examples show that the uncertainty in the Gibbs energy of aqueous species can have a tremendous impact on the modeling of mineral solubility. The effect can be temperature-, pressure- and composition-dependent. The relationships are not simple and changes in the properties of aqueous species are correlated. Therefore, a simple error propagation in this kind of geochemical calculations can lead to unreasonable uncertainties.

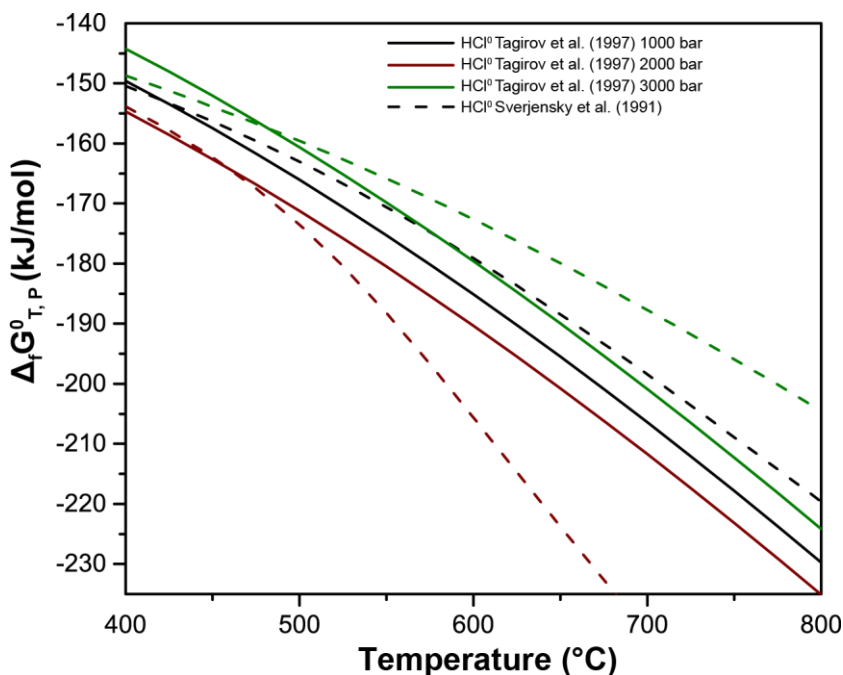


Figure 1.4 Comparison between the calculate Gibbs free energies of HCl^0 using the standard state properties and HKF parameters from Tagirov et al. (1997) and Sverjensky et al. (1991).

Some of the uncertainties in the calculated equilibrium composition come from the approximate character of the thermodynamic models used to calculate the thermodynamic properties of the system's components. In case of the HKF model the uncertainties in the estimated parameters are propagated to the uncertainties of the calculated partial molal properties. If all errors of the HKF parameters would be added up (all have the same sign), this would result in a maximum additional error of the $\Delta G_{T,P}^0$ between 2.4 kJ/mol at 500 °C and 2 kbar and 6.0 kJ/mol at 1000 °C and 5 kbar (Shock and Helgeson, 1988). More likely, these additional uncertainties should be below 2 kJ/mol (around 0.1 units in logK).

A good way of determining the uncertainties in correlated parameters is using the Monte Carlo method (Miron et al., 2015; Motulsky and Christopoulos, 2003). This method was investigated in applications for calculating errors related to geochemical calculation as early as 1976 by G. M. Anderson (Anderson, 1976). In this method the input experimental data is randomly varied according to their residuals' distribution and new sets of parameters are optimized in each case. After a large number of calculations, the resulting parameters will describe the distribution of all possible parameters from the variation of the experimental data. The measure of the dispersion of

this distribution represents the uncertainty in the parameters (Anderson, 1976). The Monte Carlo method is also employed for uncertainty calculations in this study.

1.6. Thermodynamic compilations and databases

There are different types of databases for thermodynamic properties that have been developed over the years. Two important categories are: (1) compilations of thermodynamic properties from different sources and (2) databases that were generated by refining the parameters against different types of experimental data (separate for different components or simultaneously). Several compilations containing the thermodynamic properties for key aqueous species exist. A comprehensive review was made by Wolery et al. (2007). These compilations contain standard state properties for pure substances such as gaseous species and stoichiometric compounds, but usually not for complex aqueous species. Two of these compilations, which are most used in geochemical applications are: **NIST89**, and **CODATA89**.

NIST89 is a product of the National Institute of Standards and Technology (NIST). The set of thermodynamic values was published in several reports such as Wagman et al. (1982) The dataset contains the recommended standard thermodynamic properties ($\Delta_f G_{298,1}^0$, $\Delta_f H_{298,1}^0$, $S_{298,1}^0$, and $Cp_{298,1}^0$) for a large number of elements and gas, aqueous and solid components. While it is generally considered as a reliable source, it has been criticized for the lack of details on how the data was extracted or why some of the values were selected instead of other possible alternatives (Wolery et al., 2007).

CODATA89 (Committee on Data for Science and Technology) is a result of the work of several CODATA task groups over the 1970s and 1980s, on updating and improving the recommendations for key thermodynamic data. The latest published work was CODATA Key Values for Thermodynamics by Cox et al. (1989). The thermodynamic properties given are the reference standard state enthalpies of formation and standard state entropies. CODATA also suffers from similar drawbacks as NIST89. It is difficult to trace back the way the data was selected or derived. Compared to NIST89, CODATA89 gives uncertainties in the reported data which represent “worst case” results (Wolery et al., 2007).

Wolery et al. (2007) made a comparison between these two datasets and found that most of the disagreements are on the order of tens of Joules, mostly less than 500 J. However, they also found disagreements going above 500 J and even up to 7 kJ for a few components, such as discrepancies for Al^{3+} (6.5 kJ/mol), HPO_4^{2-} (6.8 kJ/mol), $H_2PO_4^-$ (6.9 kJ/mol), and F^- (2.7 kJ/mol). Although Wagman was an author in both CODATA89 (second author to Cox) and NIST89 (first author), the discrepancies between the two datasets were not addressed by the authors (Wolery et al., 2007).

Gibbs free energies and enthalpies cannot be measured absolutely and by convention they are related to the formation from chemical elements in their standard state forms (Wolery et al., 2007). This means that the reference standard state data found in thermodynamic compilations are in fact related to other data such as the entropy of elements in their standard states. For example, the

values given in Cox et al. (1989) are not Gibbs energies of formation but standard enthalpies of formation. One can calculate the reference standard state Gibbs energy of formation using the reported standard state entropies (not entropies of formation) and the entropy of elements in their standard states. Wolery et al. (2007) made a review of different sources for the entropies of the chemical elements in their standard states. They concluded that there are discrepancies, but they are relatively small in most cases. For example, the elemental entropy of Ca in the reference form (zero oxidation state) reported in CODATA89 is 41.59 J/molK, while the one reported by Robie and Hemingway (1995) is 42.90 J/molK. This would amount to a difference of 390 J/mol in the calculated standard state Gibbs free energy at 298.15 K and 1 bar for a Ca containing component. An issue mentioned by Wolery et al. (2007) could also be that the reference of the elemental entropy is zero oxidation state while the oxidation state in the components of interest may be different.

Some thermodynamic databases contain more complex components like associated species for aqueous phase, gas, and mineral components.

SUPCRT92 is the name of the computer program developed by Johnson et al. (1992) for calculating the standard state properties of aqueous, gases, and solid components from their reference conditions to elevated temperatures and pressures conditions (using the HKF equation of state for aqueous species). The thermodynamic database associated with SUPCRT92 is a result of numerous studies originating from the work of Harold C. Helgeson (Helgeson et al. 1978) and continued in numerous studies mainly done by Helgeson and his students (Oelkers and Helgeson, 1988; Pokrovskii and Helgeson, 1995; Shock and Helgeson, 1988; Sverjensky et al., 1997). It contains the standard state properties and HKF parameters for many aqueous inorganic and organic species, but also standard state properties of gas components and pure mineral endmembers. Although the dataset was established in 1992 (Johnson et al., 1992), some components were subsequently updated with improved reference standard state thermodynamic properties and HKF parameters for several chemical subsystems. For example, the properties of aluminium species were later refined by Pokrovskii and Helgeson (1995) and Pokrovskii and Helgeson (1997b), or the later developed correlations and refined standard state properties from Sverjensky et al. (1997) and Shock et al. (1997). The thermodynamic properties of minerals present in this database are based on the review of Helgeson et al. (1978). Many of these values were, however, updated and superseded by more recent compilations and internally consistent datasets such as from Berman (1988), Robie and Hemingway (1995), and Holland and Powell (1990).

Another thermodynamic database which contains minerals, aqueous and gas species is the **LLNL** database. This database is used in the **EQ3/6** (Wolery, 1992) and **PHREEQC** (Parkhurst and Appelo, 2013) computer programs. The LLNL contains the reaction constants (logK) values for many reactions containing aqueous species, minerals and gases. These logK values were mainly derived from SUPCRT92 properties. The database uses the B-dot Debye-Hückel activity model and it is applicable up to 300 °C on the SWVP curve. The thermodynamic data from EQ3/6 and PHREEQC databases contain also Pitzer activity model parameters. These are useful when modeling concentrated solutions, but the calculations are limited to low temperatures (mostly

below 100 °C) and pressures (SWVP). Recently Appelo (2015) extended the applicability of the Pitzer database for selected elements and components up to 200 °C and 1000 bars. The mineral properties from these databases are mainly taken from Helgeson et al. (1978), Robie and Hemingway (1995), and other sources. These databases were not derived in an internally consistent way but represent just critically assessed compilations.

Some of the existing databases, with applications in petrology, consider only the properties of mineral endmembers with addition of the thermodynamic properties for pure H₂O or H₂O-CO₂-CH₄ mixtures, and possibly melt components. Three most important mineral databases which were derived in an internally consistent way are summarized below. While there are differences between these datasets, due to the fact that most of the experimental data used by the authors overlap there is in fact a relative agreement between them.

The **BERMAN** internally consistent mineral database (Berman, 1988) was obtained using linear mathematical programming. The standard state thermodynamic parameters of each mineral were refined using the calorimetric and phase-equilibria data available at that time. A few non ideal solid-solution models were also incorporated.

Gottschalk (1997) produced an internally consistent thermodynamic database for minerals using a limited number of calorimetric measurements and phase equilibria. The standard molar enthalpies of formation and standard molar entropies were refined using an iterative regression. In this method, all the experimental data is considered in the beginning (irrespective if it is conflicting or not) but during the iterative process, the conflicting data is systematically eliminated.

The **Holland and Powell** database (Holland and Powell, 1985; Holland and Powell, 1990, 1998; Holland and Powell, 2011; Powell and Holland, 1985) is one of the most extensive and most used database for minerals in petrologic studies. The enthalpies of formation of pure solid mineral components were refined using least-squares regression. Uncertainties and correlations are reported for all parameters. Other thermochemical data such as the heat capacity and entropy were treated separately. The mineral properties in this database were refined using the most recent (at that time) calorimetric and phase-equilibrium data. Many more non-ideal solid-solution models are consistent with the “Thermocalc” dataset ds55 (referred to as HP02) (Holland and Powell, 1998) as compared to the more recent version of the database (Holland and Powell, 2011).

1.7. Internal consistency

Engi (1992) has formulated four conditions for internal consistency in a thermodynamic database:

1. The thermodynamic framework used to derive the parameters from experimental data has to be compatible with the basic thermodynamic principles.
2. When extracting the parameters from the experimental data, a uniform set of reference standard state conditions and physical constants should be used (e.g. reference temperature and pressure, gas constant, atomic weights).

3. The refinement of the parameters should be done by simultaneously processing all of the experimental data to obtain a “best compromise”. A parameter set that best reproduces the data.
4. The optimized parameters should be compatible with all relevant experimental and field data (within the uncertainties), except the rejected data based on critical evaluation of the employed methods.

Furthermore, he classifies the datasets in three quality groups:

1. *“formally consistent, if only the first two points are satisfied”*
2. *“partially consistent, if the third point is also guaranteed”*
3. *“fully consistent, if points 1, 2, 3 and 4 are ensured”*

In this study, the derived thermodynamic database fulfils all four points of consistency being a fully internally consistent database.

As noted before, it is important to understand that the level of consistency does not necessarily correlate positively with the accuracy of the parameters. When building an internally consistent database, it is important to use all types of the available experimental data covering a large pressure, temperature and composition interval.

Often, when deriving a thermodynamic database, anchor components (substances) are used. Their thermodynamic properties are independently constrained from calorimetry or other types of experiments (e.g. conductance data). An error in one anchor component is then propagated to all the other dependent components. For example, in the case of the mineral database from SUBCRT92, the reference standard state properties of aluminosilicates were derived using the standard state properties of kaolinite as anchor for the Al_2O_3 component in the other aluminium bearing minerals. This was done in a complex chain of reactions holding the results from previous steps constant, thus accumulating errors. The reference standard state Gibbs energy of formation of kaolinite was not retrieved from calorimetry, but from solubility data of a natural groundwater assumed to be in equilibrium with kaolinite and gibbsite. The resulting standard state Gibbs energy of kaolinite does not only depend on the assumption of equilibrium in the system but also on the set of thermodynamic properties used for gibbsite. This could be one of the reasons for the conflict in data for aluminosilicates between Helgeson 1978, Robie and Hemingway, 1995, and also the newest databases for minerals (Holland and Powell, 1998).

It is often the case, that most of the error on the standard state properties of different components is accumulated in the enthalpy or Gibbs energy of formation. A simultaneous refinement of the Gibbs energy of formation of components against experimental data can result in an internally consistent database. But, while the Gibbs energy of formation may contain the largest uncertainty of all the thermodynamic parameters, the restriction of optimizing only this parameter can be a source of systematic errors. It can be so because other thermodynamic data can be a large source of error (Engi, 1992). It is thus important that the other thermodynamic properties are also evaluated and that they are consistent as well. These are usually extracted from different reliable independent sources.

In the best case scenario all thermodynamic parameters for both minerals and aqueous components (even gas components) should be optimized simultaneously against different types of experimental data; from thermochemical and thermophysical measurements to different phase equilibrium experiments covering a wide temperature, pressure and composition space. In many cases mineral phase-equilibria and solubility experiments used simultaneously can largely improve the consistency of thermodynamic data for rock-fluid equilibria. Usually, it is best if some thermodynamic data such as association data from conductance measurements of aqueous species or heat capacity measurements of minerals can be treated independently before it is used to refine thermodynamic parameters.

1.8. Tools and methods

To proceed in investigating different methods and principles for deriving an internally consistent thermodynamic database the following points have to be considered:

1. Access to a large collection of experimental data.
2. An efficient numerical method to perform thermodynamic computations for all experimental chemical systems.
3. Use of different system properties to simultaneously refine the parameters.
4. A complex algorithm that can find the optimum combination of parameters for which the sum of differences between the calculated and the measured experimental data is at a minimum.
5. A way to propagate and determine the uncertainty of the optimized parameters.

To test and define the strategies for deriving an internally consistent dataset for aqueous species, the following tasks were performed in this study:

1. A large number of mineral solubility experiments were collected and critically evaluated (quartz, corundum, gibbsite, aluminosilicates, feldspars, micas). Experimental datasets were assessed for the quality of data (attainment of equilibrium, no impurities, no re-precipitation during the experiment). The agreement between different experimental datasets was checked.

2. Results from new high-precision conductance experiments on electrolyte association were used to derive more reliable and accurate equilibrium constants.

3. The conductance and potentiometric data on the association constants of several complexes were collected to constrain the properties of such complexes for those cases where they are insensitive to the solubility data.

4. A computational method was developed that allows to freely optimize the properties of some aqueous species while constraining others through reactions using the data from speciation equilibria.

5. The GEMSIFTS fitting tool was developed for regressing consistent thermodynamic parameters against various types of experimental data. GEMSIFTS optimization tool has the following characteristics:

- a. Simultaneously refines many parameters of several types, independent or constrained.

b. Manages a large experimental database which does not need a priori knowledge of the data structure; many types of experimental data can be inserted.

c. Uses a suite of local and global, gradient or non-gradient based parameter optimization algorithms (NLOpt library ab-initio.mit.edu/nlopt).

d. Performs a statistical evaluation of fitting results: sensitivities of measured data and parameters, distributions, correlation coefficients, and parameter confidence intervals from Monte Carlo simulations.

e. GEMSFITS uses GEMS3K chemical solver (Kulik et al., 2013) includes the TSolMod library (Wagner et al., 2012) of equations of state and activity models of solution phases (part of GEM-Selektor).

f. Is equipped with a graphical user interface (GUI) and is parallelized.

During the global optimization process, the Gibbs free energy (or enthalpy) of formation of several ions and aqueous species is adjusted while entropy, heat capacity, molar volume, thermal expansion, compressibility and related HKF parameters are accepted without further modification. The standard state properties of the rock-forming minerals are accepted as is from the internally consistent dataset of Holland and Powell (HP02) (Holland and Powell, 1998). The mineral database is assumed to be “fully consistent” and their properties are not changed during the optimization. Thermodynamic equilibrium was calculated with the GEM-Selektor v.3 code (Kulik et al., 2013) using the revised Helgeson-Kirkham-Flowers (HKF) model (Tanger and Helgeson, 1988). The extended Debye-Hückel aqueous electrolyte model (Helgeson et al., 1981) was used for calculating the activity coefficients of individual species. The confidence intervals of the parameters are estimated from the scatter of the experimental data points using a Monte Carlo method (Miron et al., 2015).

References

- Anderson, G.M. (1976) Error propagation by the Monte Carlo method in geochemical calculations. *Geochim Cosmochim Acta* 40, 1533-1538.
- Anderson, G.M. (1977) The Accuracy and Precision of Calculated Mineral Dehydration Equilibria, in: Fraser, D. (Ed.), *Thermodynamics in Geology*. Springer Netherlands, 115-136.
- Anderson, G.M. (2005) *Thermodynamics of Natural Systems*. Cambridge University Press, Cambridge, 648p.
- Anderson, G.M., Castet, S., Schott, J. and Mesmer, R.E. (1991) The density model for estimation of thermodynamic parameters of reactions at high temperatures and pressures. *Geochim Cosmochim Acta* 55, 1769-1779.
- Appelo, C.A.J. (2015) Principles, caveats and improvements in databases for calculating hydrogeochemical reactions in saline waters from 0 to 200 °C and 1 to 1000 atm. *Appl Geochem* 55, 62-71.
- Bénézech, P., Palmer, D.A. and Wesolowski, D.J. (2001) Aqueous high-temperature solubility studies. II. The solubility of boehmite at 0.03 m ionic strength as a function of temperature and pH as determined by in situ measurements. *Geochim Cosmochim Acta* 65, 2097-2111.
- Berman, R.G. (1988) Internally-Consistent Thermodynamic Data for Minerals in the System Na₂O-K₂O-CaO-MgO-FeO-Fe₂O₃-Al₂O₃-SiO₂-TiO₂-H₂O-CO₂. *Journal of Petrology* 29, 445-522.
- Berman, R.G., Engi, M., Greenwood, H.J. and Brown, T.H. (1986) Derivation of Internally-Consistent Thermodynamic Data by the Technique of Mathematical Programming: a Review with Application the System MgO-SiO₂-H₂O. *Journal of Petrology* 27, 1331-1364.

- Cerquetti, A., Longhi, P. and Mussini, T. (1968) Thermodynamics of aqueous hydrochloric acid from the emf. of hydrogen-chlorine cells. *Journal of Chemical & Engineering Data* 13, 458-461.
- Corti, H.R. (2008) *Electrical Conductivity in Hydrothermal Binary and Ternary Systems, Hydrothermal Experimental Data*. John Wiley & Sons, Ltd, 207-226.
- Cox, J.D., Wagman, D.D. and Medvedev, V.A. (1989) *CODATA Key Values for Thermodynamics*. Hemisphere Publishing Company, New York.
- Debye, P. and Hückel, E. (1923) The theory of electrolytes. I. Lowering of freezing point and related phenomena. *Physikalische Zeitschrift* 24, 22.
- Dill, A.J., Itzkowitz, L.M. and Popovych, O. (1968) Standard potentials of potassium electrodes and activity coefficients and medium effects of potassium chloride in ethanol-water solvents. *The Journal of Physical Chemistry* 72, 4580-4586.
- Dolejš, D. and Manning, C.E. (2010) Thermodynamic model for mineral solubility in aqueous fluids: theory, calibration and application to model fluid-flow systems. *Geofluids* 10, 20-40.
- Dolejš, D. and Wagner, T. (2008) Thermodynamic modeling of non-ideal mineral–fluid equilibria in the system Si–Al–Fe–Mg–Ca–Na–K–H–O–Cl at elevated temperatures and pressures: Implications for hydrothermal mass transfer in granitic rocks. *Geochim Cosmochim Acta* 72, 526-553.
- Engi, M. (1992) Thermodynamic data for minerals: a critical assessment, in: Price, G., Ross, N. (Eds.), *The Stability of Minerals*. Springer Netherlands, 267-328.
- Facq, S., Daniel, I., Montagnac, G., Cardon, H. and Sverjensky, D.A. (2014) In situ Raman study and thermodynamic model of aqueous carbonate speciation in equilibrium with aragonite under subduction zone conditions. *Geochim Cosmochim Acta* 132, 375-390.
- Frantz, J.D. and Marshall, W.L. (1982) Electrical conductances and ionization constants of calcium chloride and magnesium chloride in aqueous solutions at temperatures to 600°C and pressures to 4000 bars. *Am J Sci* 282, 1666-1693.
- Fyfe, W.S., Price, N.J. and Thompson, A.B. (1978) *Fluids in the earth's crust: their significance in metamorphic, tectonic, and chemical transport processes*. Elsevier Scientific Pub. Co.
- Gottschalk, M. (1997) Internally consistent thermodynamic data for rock-forming minerals in the system SiO₂–TiO₂–Al₂O₃–CaO–MgO–FeO–K₂O–Na₂O–H₂O–CO₂. *European Journal of Mineralogy* 9, 175-223.
- Helgeson, H.C., Delaney, J.M., Nesbitt, H.W. and Bird, D.K. (1978) Summary and critique of the thermodynamic properties of rock-forming minerals. *Amer. J. Sci.* 278A, 230.
- Helgeson, H.C., Kirkham, D.H. and Flowers, G.C. (1981) Theoretical prediction of the thermodynamic behavior of aqueous electrolytes by high pressures and temperatures; IV, Calculation of activity coefficients, osmotic coefficients, and apparent molal and standard and relative partial molal properties to 600 degrees C and 5kb. *Am J Sci* 281, 1249-1516.
- Holland, T.J.B. and Powell, R. (1985) An internally consistent thermodynamic dataset with uncertainties and correlations: 2. Data and results. *Journal of Metamorphic Geology* 3, 343-370.
- Holland, T.J.B. and Powell, R. (1990) An enlarged and updated internally consistent thermodynamic dataset with uncertainties and correlations: the system K₂O–Na₂O–CaO–MgO–MnO–FeO–Fe₂O₃–Al₂O₃–TiO₂–SiO₂–C–H₂–O₂. *Journal of Metamorphic Geology* 8, 89-124.
- Holland, T.J.B. and Powell, R. (1998) An internally consistent thermodynamic data set for phases of petrological interest. *Journal of Metamorphic Geology* 16, 309-343.
- Holland, T.J.B. and Powell, R. (2011) An improved and extended internally consistent thermodynamic dataset for phases of petrological interest, involving a new equation of state for solids. *Journal of Metamorphic Geology* 29, 333-383.
- Johnson, J.W., Oelkers, E.H. and Helgeson, H.C. (1992) SUPCRT92: A software package for calculating the standard molal thermodynamic properties of minerals, gases, aqueous species, and reactions from 1 to 5000 bar and 0 to 1000°C. *Computers & Geosciences* 18, 899-947.
- Kolassa, J.E. (1991) Confidence intervals for thermodynamic constants. *Geochim Cosmochim Acta* 55, 3543-3552.

- Kulik, D.A., Wagner, T., Dmytrieva, S.V., Kosakowski, G., Hingerl, F., Chudnenko, K.V. and Berner, U. (2013) GEM-Selektor geochemical modeling package: revised algorithm and GEMS3K numerical kernel for coupled simulation codes. *Comput Geosci* 17, 1-24.
- Luce, R.W., Cygan, G.L., Hemley, J.J. and D'Angelo, W.M. (1985) Some mineral stability relations in the system CaO-MgO-SiO₂-H₂O-HCl. *Geochim Cosmochim Acta* 49, 525-538.
- Lvov, S.N. and Palmer, D.A. (2004) Chapter 11 - Electrochemical processes in high-temperature aqueous solutions, in: Palmer, D.A., Fernández, D.P., Harvey, A.H. (Eds.), *Aqueous Systems at Elevated Temperatures and Pressures*. Academic Press, London, pp. 377-408.
- Miron, G.D., Kulik, D.A., Dmytrieva, S.V. and Wagner, T. (2015) GEMSFITS: Code package for optimization of geochemical model parameters and inverse modeling. *Appl Geochem* 55, 28-45.
- Motulsky, H. and Christopoulos, A. (2003) *Fitting models to biological data using linear and non-linear regression: a practical guide to curve fitting*. Oxford University Press, Oxford.
- Oelkers, E.H. and Helgeson, H.C. (1988) Calculation of the thermodynamic and transport properties of aqueous species at high pressures and temperatures: Aqueous tracer diffusion coefficients of ions to 1000°C and 5 kb. *Geochim Cosmochim Acta* 52, 63-85.
- Palmer, D.A., Bénézech, P. and Wesolowski, D.J. (2001) Aqueous high-temperature solubility studies. I. The solubility of boehmite as functions of ionic strength (to 5 molal, NaCl), temperature (100–290°C), and pH as determined by in situ measurements. *Geochim Cosmochim Acta* 65, 2081-2095.
- Parkhurst, D.L. and Appelo, C.A.J. (2013) Description of input and examples for PHREEQC version 3—A computer program for speciation, batch-reaction, one-dimensional transport, and inverse geochemical calculations U.S. Geological Survey Techniques and Methods 6, 497p.
- Pitzer, K.S. (1973) Thermodynamics of electrolytes. I. Theoretical basis and general equations. *The Journal of Physical Chemistry* 77, 268-277.
- Plyasunov, A.V. and Shock, E.L. (2001) Correlation strategy for determining the parameters of the revised Helgeson-Kirkham-Flowers model for aqueous nonelectrolytes. *Geochim Cosmochim Acta* 65, 3879-3900.
- Pokrovskii, V.A. and Helgeson, H.C. (1995) Thermodynamic properties of aqueous species and the solubilities of minerals at high pressures and temperatures; the system Al₂O₃-H₂O-NaCl. *Am J Sci* 295, 1255-1342.
- Pokrovskii, V.A. and Helgeson, H.C. (1997a) Calculation of the standard partial molal thermodynamic properties of KCl⁰ and activity coefficients of aqueous KCl at temperatures and pressures to 1000°C and 5 kbar. *Geochim Cosmochim Acta* 61, 2175-2183.
- Pokrovskii, V.A. and Helgeson, H.C. (1997b) Thermodynamic properties of aqueous species and the solubilities of minerals at high pressures and temperatures: the system Al₂O₃-H₂O-KOH. *Chemical Geology* 137, 221-242.
- Powell, R. and Holland, T.J.B. (1985) An internally consistent thermodynamic dataset with uncertainties and correlations: 1. Methods and a worked example. *Journal of Metamorphic Geology* 3, 327-342.
- Reed, M.H. (1982) Calculation of multicomponent chemical equilibria and reaction processes in systems involving minerals, gases and an aqueous phase. *Geochim Cosmochim Acta* 46, 513-528.
- Robie, R.A. (1987) Calorimetry, in: Ulmer, G.C., Barnes, H.L. (Eds.), *Hydrothermal experimental techniques*. Wiley, New York, pp. 389-422.
- Robie, R.A. and Hemingway, B.S. (1995) *Thermodynamic Properties of Minerals and Related Substances at 298.15 K and 1 Bar (105 Pascals) Pressure and at Higher Temperatures*. U.S. Government Printing Office.
- Saccoccia, P.J. and Seyfried Jr, W.E. (1990) Talc-quartz equilibria and the stability of magnesium chloride complexes in NaCl-MgCl₂ solutions at 300, 350, and 400°C, 500 bars. *Geochim Cosmochim Acta* 54, 3283-3294.
- Sassani, D.C. and Shock, E.L. (1992) Estimation of standard partial molal entropies of aqueous ions at 25°C and 1 bar. *Geochim Cosmochim Acta* 56, 3895-3908.
- Schmidt, C., Chou, I.M., Bodnar, R.J. and Bassett, W.A. (1998) Microthermometric analysis of synthetic fluid inclusions in the hydrothermal diamond-anvil cell. *American Mineralogist* 83, 13.

- Sharygin, A.V., Wood, R.H., Zimmerman, G.H. and Balashov, V.N. (2002) Multiple Ion Association versus Redissociation in Aqueous NaCl and KCl at High Temperatures. *The Journal of Physical Chemistry B* 106, 7121-7134.
- Shock, E.L. and Helgeson, H.C. (1988) Calculation of the thermodynamic and transport properties of aqueous species at high pressures and temperatures: Correlation algorithms for ionic species and equation of state predictions to 5 kb and 1000°C. *Geochim Cosmochim Acta* 52, 2009-2036.
- Shock, E.L. and Helgeson, H.C. (1990) Calculation of the thermodynamic and transport properties of aqueous species at high pressures and temperatures: Standard partial molal properties of organic species. *Geochim Cosmochim Acta* 54, 915-945.
- Shock, E.L., Sassani, D.C., Willis, M. and Sverjensky, D.A. (1997) Inorganic species in geologic fluids: Correlations among standard molal thermodynamic properties of aqueous ions and hydroxide complexes. *Geochim Cosmochim Acta* 61, 907-950.
- Smith, E.R. and Taylor, J.K. (1940) Standard electrode potential of sodium. *Journal of Research of the National Bureau of Standards* 25, 16.
- Steeffel, C.I. and Maher, K. (2009) Fluid-Rock Interaction: A Reactive Transport Approach. *Reviews in Mineralogy and Geochemistry* 70, 485-532.
- Sverjensky, D., Shock, E. and Helgeson, H. (1997) Prediction of the thermodynamic properties of aqueous metal complexes to 1000 C and 5 kb. *Geochim Cosmochim Acta* 61, 1359-1412.
- Sverjensky, D.A., Hemley, J.J. and D'Angelo, W.M. (1991) Thermodynamic assessment of hydrothermal alkali feldspar-mica-aluminosilicate equilibria. *Geochim Cosmochim Acta* 55, 989-1004.
- Tagirov, B.R., Zotov, A.V. and Akinfiyev, N.N. (1997) Experimental study of dissociation of HCl from 350 to 500°C and from 500 to 2500 bars: Thermodynamic properties of HCl°(aq). *Geochim Cosmochim Acta* 61, 4267-4280.
- Tanger, J.C. and Helgeson, H.C. (1988) Calculation of the thermodynamic and transport properties of aqueous species at high pressures and temperatures; revised equations of state for the standard partial molal properties of ions and electrolytes. *Am J Sci* 288, 19-98.
- Tremaine, P., Zhang, K., Bénézeth, P. and Xiao, C. (2004) Chapter 13 - Ionization equilibria of acids and bases under hydrothermal conditions, in: Palmer, D.A., Fernández, D.P., Harvey, A.H. (Eds.), *Aqueous Systems at Elevated Temperatures and Pressures*. Academic Press, London, 441-492.
- Wagman D.D., Evans W.H., Parker V.B., et al. (1982). The NBS tables of chemical thermodynamic properties. Selected values for inorganic and C1 and C2 organic substances in SI units. *J. Phys. Chem. Ref. Data* 11, Suppl. 2.
- Wagner, T., Kulik, D.A., Hingerl, F.F. and Dmytrieva, S.V. (2012) GEM-Selektor geochemical modeling package: TSolMod library and data interface for multicomponent phase models. *The Canadian Mineralogist* 50, 1173-1195.
- Wolery, T.J. (1992) EQ3/6, a software package for geochemical modeling of aqueous systems: Package overview and installation guide (Version 70), United States, 70p.
- Wolery, T.J., Jove-Colon, C., Rard, J., Sutton, M., Helean, K., Finch, B. and Nowak, J. (2007) Qualification of Thermodynamic Data for Geochemical Modeling of Mineral-Water Interactions in Dilute Systems. In *Energy*. Edited by: US Department of Energy. Bechtel SAIC Company, Las Vegas, Nevada, USA.
- Xu, T., Sonnenthal, E., Spycher, N., Pruess, K., Brimhall, G. and Apps, J. (2001) Modeling Multiphase Non-Isothermal Fluid Flow and Reactive Geochemical Transport in Variably Saturated Fractured Rocks: 2. Applications to Supergene Copper Enrichment and Hydrothermal Flows. *Am J Sci* 301, 34-59.

2. GEMSIFTS: Code package for optimization of geochemical model parameters and inverse modeling

George D. Miron^a, Dmitrii A. Kulik^b, Svitlana V. Dmytrieva^c, Thomas Wagner^d

^aInstitute of Geochemistry and Petrology, ETH Zurich, Switzerland, dan.miron@erdw.ethz.ch

^bLaboratory for Waste Management, Paul Scherrer Institut, 5232 Villigen PSI, Switzerland

^cInstitute of Environmental Geochemistry, Kyiv, Ukraine

^dDepartment of Geosciences and Geography, University of Helsinki, Finland

Published in: **Applied Geochemistry 55 (2015): 28-45.**

<http://dx.doi.org/10.1016/j.apgeochem.2014.10.013>

Abstract

GEMSFITS is a new code package for fitting internally consistent input parameters of GEM (Gibbs energy minimization) geochemical-thermodynamic models against various types of experimental or geochemical data, and for performing inverse modeling tasks. It consists of the `gemsfit2` (parameter optimizer) and `gfshell2` (graphical user interface) programs both accessing a NoSQL database, all developed with flexibility, generality, efficiency, and user friendliness in mind. The parameter optimizer `gemsfit2` includes the GEMS3K chemical speciation solver (<http://gems.web.psi.ch/GEMS3K>), which features a comprehensive suite of non-ideal activity- and equation-of-state models of solution phases (aqueous electrolyte, gas and fluid mixtures, solid-solutions, (ad)sorption). The `gemsfit2` code uses the robust open-source NLOpt library for parameter fitting, which provides a selection between several nonlinear optimization algorithms (global, local, gradient-based), and supports a large-scale parallelization. The `gemsfit2` code can also perform comprehensive statistical analysis of the fitted parameters (basic statistics, sensitivity, Monte Carlo confidence intervals), thus supporting the user with powerful tools for evaluating the quality of the fits and the physical significance of the model parameters. The `gfshell2` code provides menu-driven setup of optimization options (data selection, properties to fit and their constraints, measured properties to compare with computed counterparts, and statistics). The practical utility, efficiency, and geochemical relevance of GEMSFITS is demonstrated by examples of typical classes of problems that include fitting of parameters of thermodynamic mixing models, optimization of standard state Gibbs energies of aqueous species and solid-solution end-members, thermobarometry, inverse titrations, and optimization problems that combine several parameter- and property types.

Keywords: parameter optimization, regression tool, thermodynamic modeling, Gibbs energy minimization, experimental database

2.1. Introduction

Advances in computational methods and technology have facilitated the development of efficient and comprehensive (geo)chemical thermodynamic and physical-chemical models for simulation of the behavior and complex feedbacks of natural systems. Computational thermodynamics has many applications in geochemistry, petrology, chemical engineering, chemistry, and materials research, because multicomponent-multiphase systems can be simulated at pressure-temperature conditions and over timescales that are not accessible to direct observation and laboratory experiments. These simulations are useful for solving environmental problems (e.g. long-term prediction of radioactive waste disposal or contamination of groundwater), designing and improving industrial processes (e.g. formation and stability of different materials), and understanding the evolution of geochemical systems from the surface to the deep Earth. In particular, geochemical reactive-transport simulations that couple thermodynamic fluid-mineral equilibria, kinetics of mineral dissolution and precipitation, and fluid flow in the subsurface have become essential for understanding and predicting the processes in geosystems relevant for carbon dioxide sequestration, exploitation of geothermal energy, and formation of mineral resources (Steeffel and Lasaga, 1994; Steeffel et al., 2005; Xu et al., 2011; Zhang and Parker, 2012; Hoffmann et al., 2012).

One of the main steps in thermodynamic equilibrium modeling is to calculate the molar Gibbs free energy of all components of all phases as a function of temperature, pressure, and composition. The equilibrium state (at fixed composition, temperature and pressure) is then determined by the global minimum of the total Gibbs energy of the system. The Gibbs Energy Minimization (GEM) algorithm (Karpov et al., 1997; Kulik et al., 2013) finds the unknown phase assemblage and speciation of all phases by minimizing the total Gibbs energy of the system while maintaining the mass balance. Conversely, the Law of Mass Action (LMA) algorithm (Reed, 1982) finds the equilibrium speciation by solving a system of nonlinear equations that combine mass balance and mass action expressions. The method directly minimizes the mass balance residuals and performs additional loops if the stable phase assemblage is not known in advance. Although LMA algorithms can perform faster in simple chemical systems, the GEM method is better suited for solving for the equilibrium in complex heterogeneous chemical systems with many non-ideal multicomponent solution phases (Kulik et al., 2013; Leal et al., 2014). The main input and output parameters and properties used in the GEM approach are listed in Table 2.1.

As any numerical model, a chemical-thermodynamic model is a mathematical formulation that describes the relevant features of a natural system or its parts. Key components of thermodynamic models are the control (input) parameters, which may be empirical (e.g. compositions of fluids and rocks, fluid/rock ratios) or may represent some physical-chemical properties of the system (thermodynamic properties, temperature, pressure). For example, the Helgeson-Kirkham-Flowers equation of state (HKF EoS) (Helgeson et al., 1981; Shock and Helgeson; Tanger and Helgeson, 1988; Shock et al., 1992), which describes the temperature and pressure dependence of the standard-state thermodynamic properties of aqueous species, uses 7 semi-empirical parameters.

These parameters are not accessible to direct observation or measurement, but need to be derived by regressing experimental data for measurable quantities (mineral solubility, heat capacity and volume of aqueous solutions).

Table 2.1 GEM method input and output parameters/properties.

GEM input	GEM output
<ul style="list-style-type: none"> • List of independent components (elements) • List of phases • List of species (dependent components) in all phases • Standard state Gibbs free energy (G°) for each species at T, P of interest • Bulk (elemental) chemical composition • Temperature T and pressure P of interest • Parameters of activity models for components of solution phases 	<ul style="list-style-type: none"> • Chemical system speciation (mole amounts of dependent components in all phases) • Total volume and Gibbs energy of the system • Activity coefficients of dependent components in their respective phases • Amount, volume, mass, and bulk elemental composition of the multicomponent phases • Effective aqueous ionic strength (IS), pH, pe, Eh (in aqueous systems).
Optional:	
<ul style="list-style-type: none"> • Specific surface areas of phases • Kinetic rate parameters for phases • Additional metastability restrictions for some phase components 	

Regression of model parameters involves adjusting them by iterative numerical methods in such a way that the differences between model-calculated properties and their experimentally determined counterparts become minimal. Input parameters derived using different models and separate sets of the experimental data may not be mutually consistent and will lead to unrealistic model predictions. Simultaneous processing of large sets of experimental data and regressing them with the same thermodynamic model ensures that the derived thermodynamic properties are internally consistent and accurately reproduce the experimental data (Anderson and Crerar, 1993). To make this possible, a single code framework must integrate a comprehensive collection of appropriate thermodynamic models, an efficient numerical method to perform the thermodynamic computations, a numerically stable and efficient optimization algorithm to adjust the parameter values, and an extensible, flexible collection of the experimental data and parameter optimization tasks.

GEMSFITS is a code package that can adjust any input parameters or properties (see Table 2.1) for GEM-based modeling of (geo)chemical equilibria, provided that experimental datasets are available and that the input parameters are sensitive to them. This is a much more extended scope than that of the previous prototype GEMSFIT (Hingerl et al., 2014), which was aimed only at fitting interaction parameters of thermodynamic activity models. The GEMSFITS codes are fully

compatible with the GEM-Selektor software package (<http://gems.web.psi.ch/GEMS3>) and the GEMS3K numerical kernel (Kulik et al., 2013). The GEMSFITS package consists of `gemsfit2` (parameter optimizer) and `gfshell2` graphical user interface (GUI) codes, which both access the same NoSQL database files. The package offers a general and flexible way for handling the experimental database, setting up parameter optimization or inverse modeling tasks, and visualizing and analyzing the results of the fitting. The `gemsfit2` code can efficiently run complex multi-dimensional parameter optimization problems and can be parallelized. In this paper, we describe the main features and computational methods of the GEMSFITS package and demonstrate the efficiency of its application to chemical-thermodynamic problems of aqueous geochemistry and petrology.

2.2. Review of software for optimization of thermodynamic model parameters

Generic fitting code packages like MATLAB (MathWorks, 2012), HOPSPACK (Plantenga, 2009), UCODE (Poeter and Hill, 1998), DAKOTA (Eldred et al., 2007), or PEST (Doherty and Hunt, 2010) perform nonlinear parameter estimation using data exchange via input and output files; the user has to manually implement all thermodynamic models involved in the parameter fitting. In many cases, complex scripts are needed to call the objective function subroutine that compares the model output properties with their empirical (experimental) counterparts. One of the benefits of these methods is that they are independent of the modeling software package.

Another approach is to couple the optimization routine to a chemical solver. The FITEQL code (Herbelin, 1999) uses nonlinear least-square optimization for determining chemical equilibrium constants from experimental solubility and titration data. Due to limitations of the implemented algorithms, the program has convergence issues in more complex fitting problems. Furthermore, because of a lack of normalization options, the fitting results are more sensitive to the data points with high absolute values (Karamalidis and Dzombak, 2010). The program comes together with the MINEQL LMA chemical solver that can be used to perform calculations only in aquatic systems with pure solids, simple ideal solid-solutions, and/or adsorption at low temperature (0-50 °C) and low to moderate ionic strength (<0.5 M) (Westall et al., 1976). This substantially limits the range of possible applications.

The PhreePlot package (Kinniburgh and Cooper, 2011) includes the embedded PHREEQC LMA chemical solver (Parkhurst and Appelo, 2013) and thus has a direct access to all chemical speciation models available in PHREEQC. However, preparing a more complex fitting task in PhreePlot (e.g., when experiments with more than one dependent value are regressed and/or when parameters belong to separate models) is regarded as quite an advanced task (Kinniburgh and Cooper, 2011). The program involves only local non-gradient based (derivative-free) optimization algorithms, and the output summary statistics is minimal (calculation of confidence intervals and sensitivity and parameter correlation analysis are not performed). The possibilities for optimization of several model parameters against large experimental datasets are limited because the code is not

parallelized. The LMA algorithm used in PHREEQC also makes the parameter regression for complex non-ideal solution models or non-ideal fluid mixtures not possible.

2.3. Key features of GEMSFITS

In comparison with the software packages reviewed above, GEMSFITS offers a robust collection of non-linear (global, local, gradient based, and non-gradient based) optimization algorithms, coupled with the efficient GEMS3K chemical solver (Kulik et al., 2013) that includes a broad range of mixing models for solution phases collected in the `TSOLMod` library (Wagner et al., 2012). Another relevant feature of GEMSFITS is that it can store, retrieve, and manage in a flexible and efficient way large amounts of structured experimental data in a NoSQL database. This feature also allows the user to produce and store different optimization tasks using various selections of data sets and experimental samples. In contrast, other available codes (see Section 2) do not provide the convenient tools for managing the experimental data and optimization tasks, which makes it very difficult to develop and maintain comprehensive datasets with experimental data for large chemical systems.

Unlike the earlier prototype GEMSFIT (Hingerl et al., 2014) that used an structured query language (SQL) database server, the GEMSFITS codes can manage and access the experimental data collected in databases in the industry-winning NoSQL BSON format (Binary JSON JavaScript Object Notation; <http://www.mongodb.com/nosql-explained>; <http://bsonspec.org/>). This difference is important, because in SQL databases, the individual records (e.g., for experiments or samples) are stored similar to rows in tables, whose columns contain properties (e.g., chemical element amount, temperature, pressure) that all must be initially specified. Different data types are stored in separate tables that are connected with the join tables needed to execute complex selection queries (e.g., selecting experiments with a certain phase). The SQL relational database implementation becomes extremely complex when describing hierarchical chemical systems with all properties, phases and components, because it has to rely on dozens of data and join tables.

Conversely, a NoSQL database (as used in GEMSFITS) stores the data as documents, each defined as a JSON object. The simplest object is a { *<key>* : *<value>* } pair, for instance { "temperature" : 298.15 }. The *<value>* can be either a constant (string, number, binary data block), an ordered array of values [*<value1>*, *<value2>*, ...], or a nested key-value pair. This allows describing complex hierarchical data structures in a natural, straightforward and human-readable way, similar to structured types in object-oriented programming languages. Each JSON document can contain any number of nested key-value pairs. Compared to the structure of SQL databases, which require a defined schema before adding the data (i.e., SQL databases need to know all column headers in all tables in advance), the NoSQL databases allow inserting data without a predefined schema because every JSON document (database record) may, in principle, have a different data structure. This approach is much better suited for storing large volumes of weakly structured data without making any changes to the already stored documents, and implementing

future extensions of the database. Thus, the NoSQL database can store definitions of complex chemical systems or experimental data, which are flexible and easy to process in codes based on object oriented programming.

Based on our experience with the earlier prototype GEMSFIT (Hingerl et al., 2014), the GEMSFITS package has been completely redesigned to efficiently solve the following classes of parameter optimization problems (combinations are possible as well):

- 1) Fitting of interaction parameters of mixing models including aqueous activity models;
- 2) Optimization of thermodynamic properties such as standard state Gibbs free energy $\Delta_f G_{298}^0$ of compounds, or equilibrium constants of chemical reactions;
- 3) Thermobarometry (finding temperature and pressure of formation for the known phase speciation);
- 4) Inverse titrations (e.g. finding the bulk composition that results in prescribed pH);
- 5) Combined (nested) titration-solubility, titration-adsorption and similar fitting problems.

Thus, the GEMSFITS package has the capability to optimize any GEMS3K input properties or parameters (see Table 2.1). Several parameters from different groups can be fitted simultaneously, either as unconstrained parameters, or some of them can be bounded, reaction-constrained or linearly-constrained. GEMSFITS can perform extensive statistical evaluation of the fitted parameter values, thus helping the user to evaluate the quality and physical significance of the regression results. The program can also be executed on parallel computer architectures, reducing the amount of computing time, and making it possible to run very large optimization problems with the Monte Carlo generated statistics. The GEMSFITS package is available for free download from <http://gems.web.psi.ch/GEMSFITS>, eventually open-source.

2.4. Methods and data

The GEMSFITS package is composed of the `gemsfit2` parameter optimizer and the `gfshell2` graphical user interface (GUI), both accessing the same NoSQL database in JSON/BSON (EJDB, <http://ejdb.org>) format where the experimental data, the fitting task definitions, and the task calculation results are stored. This functionality enables the user to access and manage the database, to specify the fitting tasks by editing their definitions, to run the parameter optimization (optionally generating statistics of the fitted model parameters), to view, and to plot and print fitting results and statistics. In this way, an efficient and flexible workflow of GEM input parameter optimization is made possible.

The setup of the fitting task (to be performed by the `gemsfit2` code) is provided in the task input specification file that can be exported from the `gfshell2` or prepared using any external text editor. The task setup controls the selection of experimental data from the database, defines what model output values are retrieved, and how they will be compared within the global and/or nested objective function. Furthermore, it selects the model input parameters that should be fitted (and provides initial values, optionally lower and upper bounds), and defines the choice of

the optimization method, the sample weighting rules, and the options for statistics. Upon execution, the `gemsfit2` code reads the task specification input file, the GEMS3K chemical system definition files, and the NoSQL database with experimental data, performs the requested calculations (writes the steps into a log file), and finally writes the results into output files in comma-separated values (csv) format (results can be imported into NoSQL database in connection with the fitting task that generated them).

2.4.1. Architecture of GEMSFITS

The GEMSFITS software package consists of four main components:

- 1) The `NoSQL` database (collection of documents describing experimental samples, fitting task definitions, and fitting task results) in BSON/JSON format, with tools for the database management;
- 2) The `gemsfit2` parameter optimization code that reads the experimental data from the database, executes a “fitting task” as described in the task specification file (exported from the task definition database record, or edited separately), and writes results into a set of csv format output files;
- 3) The GEMS3K chemical solver (including the `TSolMod` library of mixing models) (Wagner et al., 2012; Kulik et al., 2013) embedded into the `gemsfit2` code, which reads the chemical system definition from the set of GEMS3K input files provided, and calculates chemical equilibria and/or phase activity models whenever called by the parameter optimizer;
- 4) The `gfshell2` GUI with graphics widget and help viewer that assist the user in accessing the database, preparing the input files, running the fitting tasks, and exploring the results. It keeps track of the task definition (which generates the task specification file) and task results records in the database, and provides text editors and graphics for input and result data.

The GEMSFITS GUI-based workflow is organized in projects consisting of one or more fitting tasks, as illustrated in Fig. 2.1. A project defines one general parameter optimization application. Each project refers to an experimental database file and a set of GEMS3K chemical system definition files. A fitting task is defined by a task specification record containing all the settings for the optimization process. The user can configure alternative task definitions with different optimization options, save task definitions to the database, run these different optimization tasks, and view and save their results.

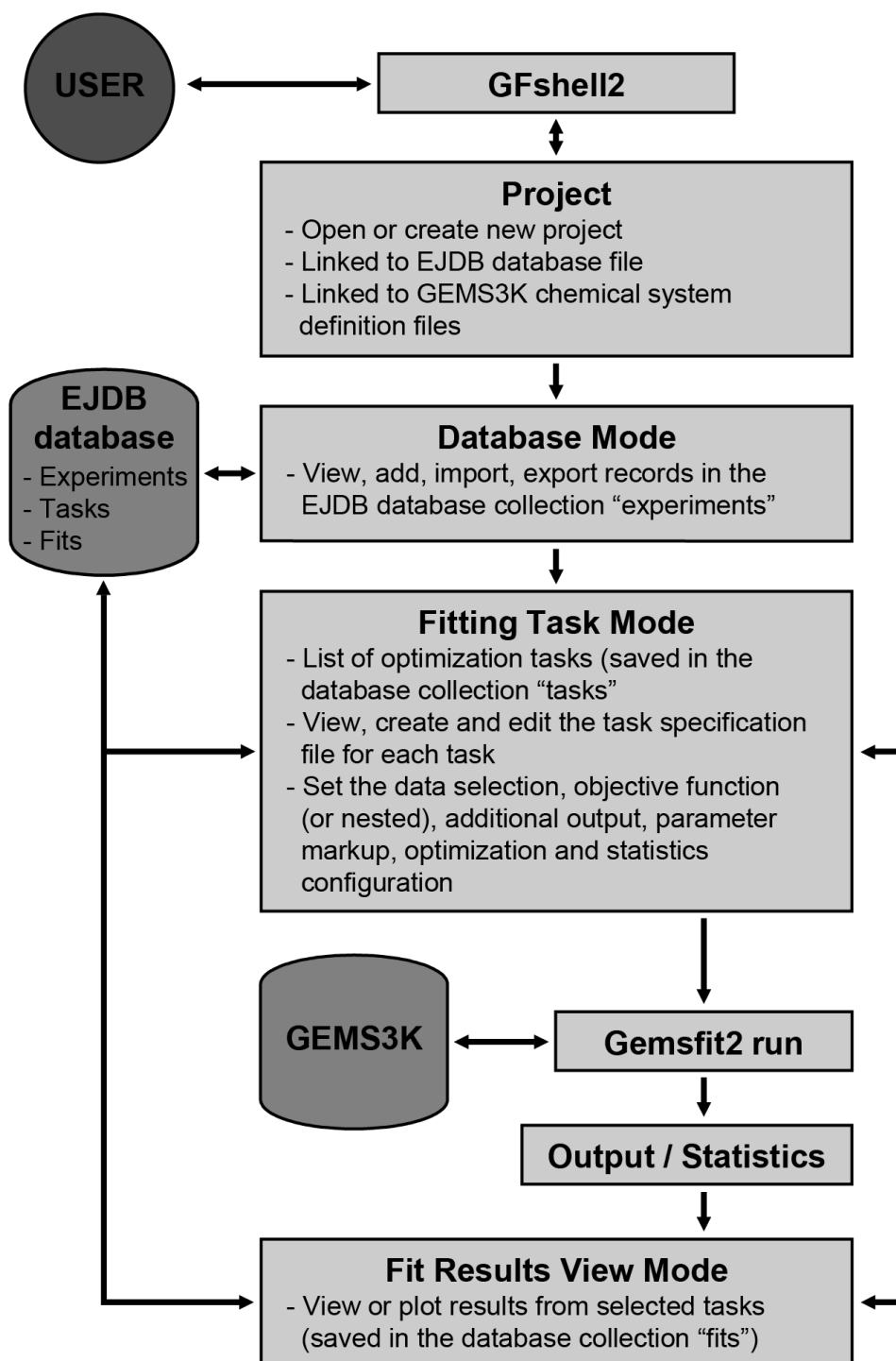


Figure 2.1 Flow chart of the `gfshell2` code illustrating the four main modes of code operation (Project Mode, Database Mode, Fitting Task Mode and Fit Results View Mode) and the links to the EJDB database.

2.4.2. Experimental and task database management

Currently, the NoSQL database is implemented as files within the local computer application using the EJDB library (Embedded JSON Data Base engine, <http://ejdb.org>), which is a lightweight variant of the MongoDB database (<http://mongodb.org>). GEMSFITS databases can be transferred to a MongoDB server in the future, if required for distributed database development projects. The

database is initially created, extended, or updated by importing the experimental data in csv format, using the `gfshell2` menus. The csv files can be exported from pre-formatted spreadsheets.

The database operations can be performed directly in the database using the `EJDB console` (<http://ejdb.org>) or via the `gfshell2` GUI. The latter allows also for exporting the data into JSON format files. The database stores the data in a BSON (Binary JSON) format (<http://bsonspec.org/>).

An advantage of the JSON format is that the data is represented through a hierarchical structure as { <key>: <value> } pairs, such as { "phase": "aq_gen" }. In place of <value>, an array of ordered values [<value1>, <value2>, ...] can be used, e.g. { "phase": ["aqueous", "gaseous", "calcite"] }, or a subordinated { <key>: <value> } pair, for instance { "phase": { "aggrstate": "electrolyte", "name": "aqueous" } }. This recursive notation can represent any hierarchical, structured, and ordered data objects such as those used in advanced object-oriented programming languages. This format makes it easy to handle data that describe various experimental settings and chemical systems, allowing for streamlined expansion of new database documents (records) without modifying the already existing data records or the entire database architecture.

Table 2.2 Main types of experimental data that can be added to the database and used in calculation of the objective function for the sum of residuals (Measured results).

Experiments description	System composition	Measured results
<ul style="list-style-type: none"> • Experimental dataset (expdataset) • Sample name (sample) • Comment • Temperature (sT) • Pressure (sP) • Volume (sV) of the system 	<ul style="list-style-type: none"> • Chemical composition of the system in formula units (<i>comp</i>) • Upper and lower additional metastability constraints for phases or species (<i>UMC</i>, <i>LMC</i>) • Unit of measurement and estimated error for all entries 	<ul style="list-style-type: none"> • Concentration of elements (independent components <i>IC</i>) in aqueous phase • Mole amount of independent components (<i>IC</i>) in phases-solutions • Mole ratios (<i>MR</i>) of elements in gaseous, solid, melt, and aqueous phases • Phase properties: mass (<i>Q</i>), volume (<i>pV</i>), excess Gibbs energy of mixing (<i>Gex</i>), density (<i>RHO</i>), <i>pH</i>, <i>pe</i>, <i>eH</i>, ionic strength (<i>IS</i>), alkalinity (<i>alk</i>), surface area (<i>sArea</i>), osmotic coefficient of water (<i>oscw</i>) • Amounts or concentrations of dependent components (<i>DC</i>) in non-aqueous phases • Units of measurement and estimated experimental errors for all entries

The `EJDB` stores all data records ('documents') in 'collections'. A collection is a group of documents having similar (but not necessarily the same) structure. In a `GEMSFITS` project database, the experimental data is stored in the collection "experiments". The optimization task specification is saved in the "tasks" collection; after each successful optimization run, the results can be saved in the "fits" collection of the project database file. In this way, the data records can be viewed, edited and used at any later time. Experimental data records are identified by two keywords "expdataset" and "sample", a combination of which should be unique in the entire database collection, and forms a 'data record key'. The "expdataset" value (string) typically refers

to a paper or a report, or part of it describing a substantially different setup of the experiments. The “sample” value (string) refers to a single sample or a measurement point with defined temperature, pressure, and composition. The experimental data consists usually of three subsets or sections, which are ‘Experiment description’, ‘System composition’, and ‘Measured results’ (Table 2.2).

The major advantage of using the EJDB with standalone files is that these files are part of the GEMSFITS application and can be easily packaged together with the rest of the fitting project, without requiring access to a database server. Because EJDB uses the same BSON C Application Programming Interface (API) as the MongoDB, the data can be backed-up to JSON format files (<http://www.json.org/>) and restored from them into a MongoDB server (Plugge et al., 2010), if necessary.

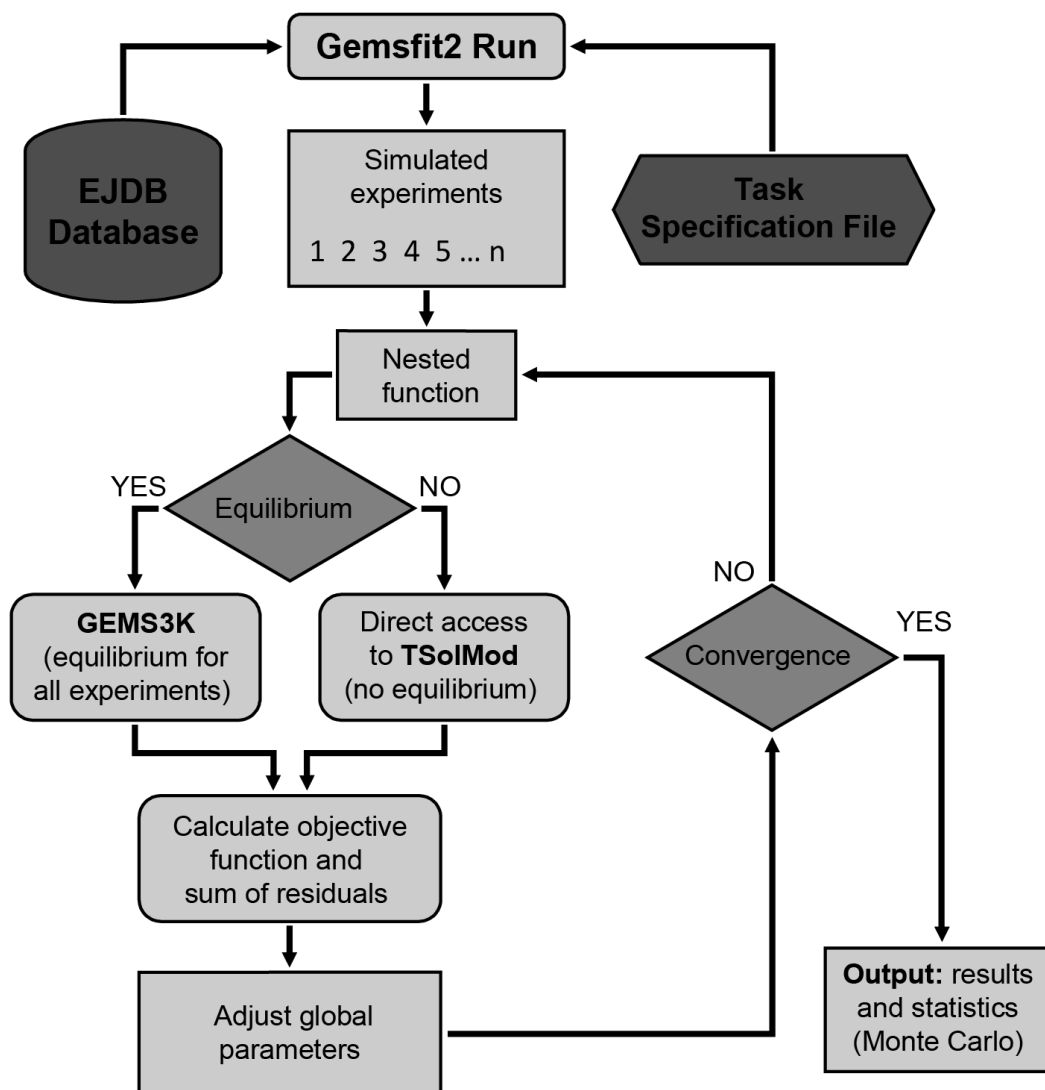


Figure 2.2 Flow chart of the `gemsfit2` global optimization loop illustrating the connections to GEMS3K and TsoIMod code libraries.

2.4.3. Parameter optimization code

The `gemsfit2` code performs the actual parameter optimization as described in the task specification file, according to the flow chart shown in Fig. 2.2. The program reads in the experimental data from the database according to the "DataSelect" query. Using the GEMS3K input chemical system definition files, `gemsfit2` creates an array of chemical system definitions in the computer memory, one per 'experimental sample'. At the next step, the program checks if there is any nested objective function defined in the "DataTarget" section of the task specification file. If no nested function is defined, the program proceeds with computing the equilibrium state for each given sample by calling the embedded GEMS3K chemical speciation solver. For certain objective functions, an alternative to computing the equilibrium is to use direct access to the `TSolMod` code library (Wagner et al., 2012) of geochemical-thermodynamic mixing models. This significantly reduces computational time in cases when the equilibrium phase composition is known and the calculation of phase equilibrium is not necessary (e.g., optimizing activity model parameters against data such as osmotic coefficients of aqueous solutions or excess Gibbs energies of a solid-solution).

Table 2.3 Functions for calculating the residuals and weights in `gemsfit2`.

Residual functions and weights
$F = \sum_{i=1}^n w_i (f_i - y_i)^2 w_o w_e w_{Tu}$
$F = \sum_{i=1}^n w_i \left(\frac{f_i}{\bar{y}} - \frac{y_i}{\bar{y}} \right)^2 w_o w_e w_{Tu}$
$w_i = \frac{1}{\sigma_i}$
$w_i = \frac{1}{\sigma_i^2}$
$w_i = \frac{1}{y_i^2}$
$w_i = \frac{\bar{y}}{\sigma_i^2}$
$w_i, w_o, w_e, w_{Tu} = 1 \text{ (default)}$

Properties: f : computed property; y : measured property; \bar{y} : measured property average; σ : error; n : number of experiments; F : sum of residuals; w_i : weight related to error or measured property value; w_o : weight related to an objective function term (e.g. measurements of Si concentration can have a different weight than the ones of Ca concentration); w_e : individual experiment weight.

The sum of residuals is computed using the objective function terms that are defined in the "DataTarget" section. Each term describes what measured data should be compared with the computed counterpart (e.g., measured concentrations of dissolved elements like Al and Si in solubility experiments). The sum of residuals can be computed as a classical "sum of squares" or other implemented variants, and several alternative weighting methods can be applied (Table 2.3). The sum of residuals (the "target") is then transferred to the chosen optimization algorithm, which will generate new input parameter values, trying to minimize the sum of residuals. This loop consists of computing the equilibria (or phase property) for all samples, calculating the sum of residuals, and refining the fitting parameters. It is repeated until the defined threshold for convergence is reached. At the end of the optimization process, the output (results and statistics) is written into csv formatted text output files.

The nested objective function, for the first time implemented in `gemsfit2`, allows the possibility to set up a fitting task in which the GEM input properties for each experiment (such as temperature, pressure and bulk elemental composition) must always be adjusted against measured data such as pH, alkalinity, or fugacities of gases (Fig. 2.3). Typical examples of such experimental data include pH-dependent solubility data for minerals, or pH edges for ion adsorption, where pH is measured, but not explicitly defined in the experimental sample compositions. Most GEM algorithms do not allow to set pH, alkalinity or fO_2 as a direct input. For a given system definition, these activity-based measurable output properties can only be adjusted to desired (measured) values by changing the bulk composition (e.g., titration with acid or base), temperature or pressure.

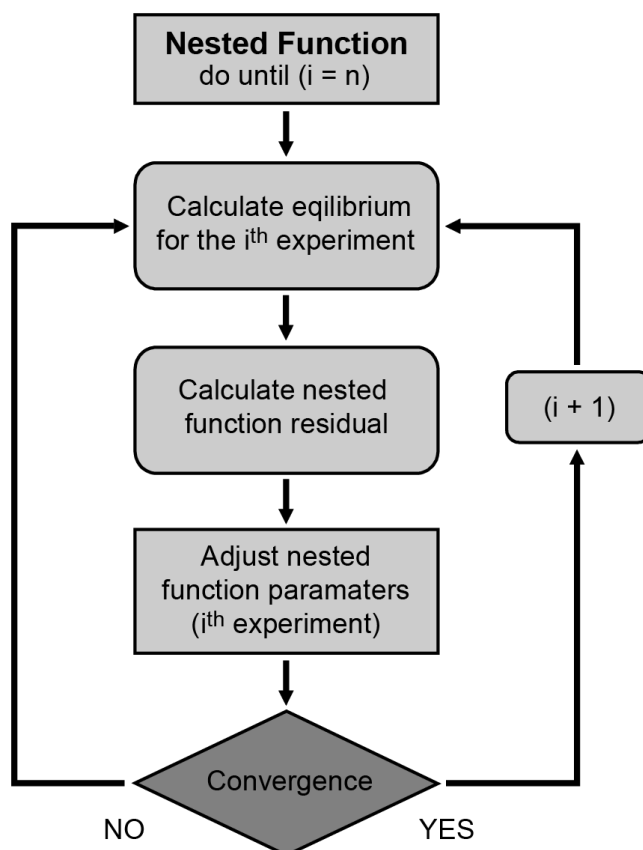


Figure 2.3 Flow chart of the `gemsfit2` nested objective function loop (inverse modeling).

If a nested objective function is defined in the "DataTarget" section of the task specification file, the program first loops through all simulated experiments (samples). For each experiment, the program calculates the absolute difference between the measured and the computed property specified in the nested function (any GEM output with experimental counterpart, e.g., pH). The optimization algorithm then adjusts the parameters involved in the nested function until the computed properties achieve the best agreement with the measured ones. When the optimization algorithm converges, the same procedure is done for the next simulated experiment, until the end of the list of experiments. After executing the nested function optimization for all simulated experimental samples, the program proceeds with the main loop for optimizing the global fitting parameters using the top-level objective function (Fig. 2.2). If no top-level objective function is defined, the program writes the results of the nested function optimization into a csv file as the inverse modeling result.

Parameters that can be optimized by the `gemsfit2` code are summarized in Table 2.4. Parameters that influence the computed properties in many experiments are optimized using the global objective function (with one or more terms) by minimizing the total sum of residuals

$$\min (total S_{res}) = \sum_0^M F_0 \quad (2.1)$$

where F_0 is the sum of residuals calculated as described in Table 2.3, and M is the number of terms in the global objective function.

Parameters specific to an individual experiment only (inverse modeling) are optimized using the nested objective function, by minimizing the absolute residual values of the difference between the computed property f and the measured property y

$$\min (res_i) = \min |f_i - y_i| \quad (2.2)$$

Table 2.4 Main classes of adjustable parameters for fitting tasks and parameter fitting modes.

Parameter	Fitting mode	Objective function
• Standard state Gibbs free energy (25 °C and 1 bar) of phase components "G0"	• Free (F) • Reaction constrained (R) • Set (S)	Global
• Mixing models interaction parameter coefficients "PMc", "DMc" • DQF parameters of end members pure gas fugacities "fDQF"	• Free (F) • Set (S)	Global
• Temperature and pressure "TK", "P"	• Free (F) • Set (S)	Nested
• Element bulk composition "bIC"	• Independent (F) • Linearly constrained (L) • Set (S)	Nested

Three different parameter-fitting modes can be used, which are free (independent) (F), reaction constrained (R), and linearly constrained (L) fitting. Parameters marked as free 'F' are optimized independently of each other. Some standard-state molar Gibbs energies of components (25 °C and

1 bar), marked as ‘R’, can be optimized using an additional reaction constraint. This means that at each optimization step, the new value is re-calculated using a (user-provided) reaction equilibrium constant K and the independently optimized values of molar Gibbs energies of any other species that take part in the reaction:

$$R_p = -RT \ln K + \sum_{j=1}^{N_r} P_j c_j \quad (2.3)$$

Here, R_p is the value of the reaction-constrained parameter, R is the gas constant, T is the temperature in Kelvin, K is the equilibrium constant, N_r is the number of parameters involved in the reaction other than the constrained one, P_j is the value of the parameter involved in the reaction (can be reaction constrained, freely fitted, or fixed), and c_j is the reaction stoichiometry coefficient. The reaction always involves one species constrained by the equilibrium constant, and several others that are independently fitted or have been fixed. To give an example, the solubility data for halite (NaCl) could be fitted by regressing the properties of aqueous Na^+ and Cl^- species, but adjusting the properties of the aqueous species NaCl^0 through equilibrium constants obtained for the ion association reaction ($\text{Na}^+ + \text{Cl}^- = \text{NaCl}^0$) from independent sets of experiments (e.g., conductance data). Note that temperature and pressure cannot be adjusted simultaneously with implicitly T and P dependent parameters such as "G0" or "PMc". Bulk composition parameters, if marked with ‘L’, can be linearly constrained to independently fitted composition variables, in order to reproduce the stoichiometry of compounds such as titrants.

An additional “Set” mode (S) is available, to set the input parameter to a new value (different from that initially given in GEMS3K input files, perhaps already fitted in a previous step) to be kept constant during the optimization procedure. This limits the applicability of that new parameter value to a given task while not affecting other tasks.

2.4.4. GEMS3K chemical solver and its input data

GEMS3K (Kulik et al., 2013) is a chemical equilibrium speciation solver that performs modeling of multiphase-multicomponent geochemical equilibria using a GEM algorithm. GEMS3K provides a built-in selection of equation-of-state and activity models for multicomponent phases available in the `TSolMod` class library (Wagner et al., 2012). The chemical system definition (CSD) and the thermodynamic data arrays are usually set up and exported to GEMS3K input files using the GEM-Selektor v.3 (GEMS3) code package. When setting up the chemical modeling project in GEM-Selektor GUI, the user is guided through a stepwise wizard where the elements comprising the system compositions, the thermodynamic database, and the thermodynamic models of mixing in aqueous and gaseous phases are selected. When defining the chemical system (including components, species and phases), the user can select for each phase one of several non-ideal mixing and activity models or equations of state, depending on the thermodynamic framework of the model. The `TSolMod` class library contains most of the commonly used mixing models for aqueous solutions, gas mixtures, fluid mixtures and solid-solutions (Wagner et al., 2012).

Internally, the `gemsfit2` code calls GEMS3K in the ‘-init’ mode to read GEMS3K CSD input files for creating an array of nodes for chemical systems representing the selected experimental samples, to further simulate these experiments. During the parameter optimization, the chemical equilibrium state and speciation are calculated for each sample using the GEMS3K solver, or the solution models are directly accessed and the phase properties calculated without computing the complete equilibrium. This is all done based on the chemical system definition specified in the GEMS3K input files.

The screenshot shows the GEMSfits GUI in Database Mode. The main window is titled "GEMSfits: Optimization of GEM Input Parameters". The menu bar includes "Project", "Record", "Database", "Calculate", and "Help". The toolbar contains icons for navigation and editing. The "Data or Task Editor" panel displays a table with the following data:

sample	expdataset
1 C_01	CH04
2 C_02	CH04
3 C_03	CH04
4 Cw_01	CH04D
5 Cw_03	CH04D
6 Cw_04	CH04D
7 T0.05	GC65
8 T0.07	GC65

The "Search Query Editor" panel shows a JSON query:

```
{
  "expdataset": {"$in": ["CH04", "CH04D", "GC65"]},
  "sample": {"$in": ["C_01", "Cw_01", "T0.05",
    "C_02", "Cw_03", "T0.07",
    "C_03", "Cw_04"]},
  "sT": {"$bt": [1, 30]},
  "sP": {"$bt": [1, 500]}
}
```

The "Data or Task Editor" panel shows a JSON entry for sample "Cw_01":

```
{
  "sample": "Cw_01",
  "expdataset": "CH04D",
  "sT": 22,
  "sP": 1,
  "sbcomp": [
    {
      "comp": "SiO2@",
      "Q": 10,
      "unit": "g"
    },
    {
      "comp": "H2O@",
      "Q": 1000,
      "unit": "g"
    },
    {
      "comp": "Ca(OH)2",
      "Q": 18.25,
      "unit": "g"
    }
  ],
  "expphases": [
    {
      "phase": "aq_gen",
      "phprop": [
        {
          "prop": "pH",
          "Q": 12.37,
          "error": 0.03,
          "unit": "-loga"
        }
      ],
      "phIC": [
        {
          "IC": "Si",
          "Q": 2e-05,
          "error": 1e-05,
        }
      ]
    }
  ]
}
```

The "IComp (Elements)" panel shows a periodic table with elements Ca, H, Nit, O, Si, and Zz. The "Phases/Components" panel lists various chemical species:

- aq_gen: Ca+2, CaOH+, Ca(HSiO3)+, CaSiO3@, HSiO3-, SiO2@, SiO3-2, H2@, N2@, O2@, OH-, H+, H2O@
- gas_gen: H2, N2, O2
- C-S-H-Q: CSH-JenD, CSH-JenH, CSH-TobD, CSH-TobH
- Portlandite: Portlandite
- Silica-amorph: Silica-amorph, Amor-Sl

The "Run Status" panel shows "Record filtered".

Figure 2.4 Screen image of the `gfshell2` graphical user interface illustrating the appearance of the Database Mode. The view shows the query result that was retrieved from the experimental database and one sample entry in JSON format. The column on the right-hand side shows the chemical system definition (lists of components, phases and species) that is read from the GEMS3K files.

2.4.5. GUI and help functionality

The graphical user interface `gfshell2` is designed to assist the user throughout the complete workflow of parameter optimization, including editing of the database, setup of the fitting task, running the regression procedure, and analyzing the results. The `gfshell2` operates in ‘Database Mode’, ‘Fitting Task Mode’, and ‘Fit Results View Mode’ (Fig. 2.1). Any fitting project created

in `gfshell12` GUI refers to an experimental database file and to a set of GEMS3K chemical system definition files.

In *Database Mode*, the experimental records from the project database can be viewed in a list and edited in JSON format (Fig. 2.4). Bulk data can be backed up and restored from JSON format files or imported and exported from preformatted spreadsheet files previously saved in csv format. Database selection queries can be added and edited in the “Search Query Editor”. The record (sample) list retrieved from the database by a search query can be then exported into the task specification file with the help of a menu command.

In *Fitting Task Mode*, the task specification file is viewed and edited (Fig. 2.5). The specification file contains all the options related to one fitting run. The task specification is viewed in JSON format, where each key has a value and the options. For instance, the pair `"DataSelect": "search_query"` has the value represented by the database search query, or the key-value pair `"OptAlgo": "GN_ISRES"` defines the type of optimization algorithm to be used. Fitting task specifications can be edited, saved to database, or new tasks created from them, and they can all be exported to task input files and executed in the `gemsfits2` code.

The screenshot displays the GEMSFITS GUI with the following components:

- Task List Table:**

taskid	projectid
1 idmix3em	csqhsol
2 idmix4em	csqhsol
3 mix4em_logm_ip2_b2	csqhsol
4 mix4em_logm_ipfi_b1	csqhsol
5 mix4em_logm_rw_a3	csqhsol
6 mix4em_logm_rwf_b0	csqhsol
7 mix4em_logm_rwip2_b3	csqhsol
8 mix4em_logm_w_a1	csqhsol
9 mix4em_logm_w_a2	csqhsol
10 template	csqhsol
- JSON Specification (Task 5):**

```
{
  "taskid": "mix4em_logm_rw_a3",
  "projectid": "csqhsol",
  "MPI": 4,
  "DataSource": 0,
  "DataDB": "../EJDB/csqhsoldata",
  "DataCollection": "experiments",
  "SystemFiles": "../GEMS/CSHQsol-dat.lst",
  "DataSelect": {
    "usedatasets": [
      "GC65"
    ]
  },
  "DataTarget": {
    "Target": "name",
    "TT": "lsq",
    "WT": "inverr3",
    "OFUN": [
      {
        "EPH": "aq_gen",
        "CT": "IC",
        "CN": "Ca",
        "unit": "log_molal",
        "WT": 3
      },
      {
        "EPH": "aq_gen",
        "CT": "IC",
        "CN": "Si",
        "unit": "log_molal",
        "WT": 5
      },
      {
        "EPH": "C-S-H-Q",
        "CT": "MR",
        "CN": "Ca/Si",
        "unit": "molratio",
        "WT": 3
      }
    ]
  }
}
```
- Chemical System Definition:**
 - IComp (Elements): Ca, H, Nit, O, Si
 - Phases/Components:
 - aq_gen: Ca+2, CaOH+, Ca(HSiO3)+, CaSiO3@, HSiO3-, SiO2@, SiO3-2, H2@, N2@, O2@, OH-, H+, H2O@
 - gas_gen: H2, N2, O2
 - C-S-H-Q: CSH-JenD, CSH-JenH, CSH-TobD, CSH-TobH
 - Portlandite: Portlandite
 - Silica-amorph: Amor-Sl
- Search Query Editor:** (Empty)
- Run Status:** Text in the editor is in valid JSON format

Figure 2.5 Screen image of the `gfshell12` graphical user interface illustrating the appearance of the Fitting Task Mode. The view shows the list of fitting tasks, the specification file for one task in JSON format and the chemical system definition.

sample	expdataset	sT	sP	aq_gen.Ca.meas(y)	aq_gen.Ca.calc(y)	residual	aq_gen.Si.meas(y)	aq
0	T0.05	GC65	25	1	-3.1307683	-3.0186821	-0.11208613	-2.636388
1	T0.07	GC65	25	1	-3.0315171	-3.018685	-0.012832013	-2.5850267
2	T0.14	GC65	25	1	-2.8326827	-3.0186799	0.18599728	-2.4685211
3	T0.23	GC65	25	1	-2.7746907	-3.0186781	0.24398738	-2.3635121
4	T0.32	GC65	25	1	-2.7212464	-3.0186777	0.2974313	-2.3904056
5	T0.41	GC65	25	1	-2.7099654	-3.0186786	0.30871317	-2.4089354
6	T0.43	GC65	25	1	-2.7055338	-3.0186784	0.31314459	-2.412289
7	T0.68	GC65	25	1	-2.69897	-3.050869	0.35189903	-2.4236586
8	T0.76	GC65	25	1	-2.756962	-3.1141873	0.35722531	-2.8326827
9	T0.93	GC65	25	1	-2.6716204	-2.8781244	0.20650399	-3.60206

Figure 2.6 Screen image of the `gfshell12` illustrating the appearance of the Fit Result Viewing mode with different spreadsheet tabs (Fitted Parameters, Fit for Samples, Summary Statistics, Sensitivity Data, Quantile Residuals, Monte Carlo Residuals, Inverse Modeling Results, `gemsfit2 log`).

In the *Fit Results View Mode*, the results can be imported from `gemsfit2` output csv files, viewed, and plotted. This functionality is useful for rapid evaluation of the quality of the fitting results. In this mode, the `gemsfit2` output can be displayed in several tabs in a spreadsheet format (Fig. 2.6). The output contains:

- 1) *Fitted Parameters* with the initial and fitted values of the parameters and the associated parameter statistics;
- 2) *Fit for Samples* containing the dependent/calculated and measured properties, residuals, as well as the weights and other user pre-defined output (Fig. 2.6);
- 3) *Sum Statistics* with the summary statistics describing the quality of the fit;
- 4) *Sensitivity Data* containing the calculated sensitivities for each measured value to each regressed parameter;
- 5) *Quantile Residuals* with the ordered residuals and their respective quantiles (points taken at regular intervals form the cumulative distribution function of the residuals);
- 6) *MC results* containing the resulting parameter values for each Monte Carlo generated optimization run;
- 7) *Inverse Modeling Results*;
- 8) *gemsfit2 log* containing some diagnostic information related to the fitting run.

2.4.6. The `gemsfit2` task specification

The fitting task specification contains all the options and information that are required by `gemsfit2` for performing the computations. It exists as a property-value JSON format editable in `gfshell12`. It has four main sections, which are ‘Data Selection’ (starts with keyword "DataSelect"), ‘Data Target’ (with "DataTarget"), ‘Parameter Markup’ (with different parameter lists/arrays e.g. "G0" for Gibbs free energy parameters; "bIC" for elemental bulk

composition), and ‘Optimization and Statistics’ (with different options such as "OptAlgo" for defining the algorithm; "StatMCruns" for defining the number of Monte Carlo runs). Before running the task, each section must be defined and edited by the user. The query for selecting the experimental data, the definition of the objective function, and the markup of the parameters to be adjusted are all defined as JSON objects. Using the `gfshell2` program, any task input file can be imported and edited in JSON format, and then saved in the “tasks” collection of the project database. The task specification is automatically exported into the `gemsfit2` input file when the task calculation is started from `gfshell2`.

Table 2.5 Optimization algorithms in `gemsfit2`.

Optimization algorithms (NLOpt library)
<p>Global (only bound-constrained problems):</p> <ul style="list-style-type: none"> • GN_ISRES: Improved Stochastic Ranking Evolution Strategy (Runarsson and Xin, 2005) • GN_CRS: Controlled Random Search with local mutation (Kaelo and Ali, 2006) • GN_ESCH: Evolutionary algorithm (da Silva Santos et al., 2010) • GN_ORIG_DIRECT: Dividing Rectangles algorithm (Jones et al., 1993) • GN_ORIG_DIRECT_L: A locally-biased form of the DIRECT algorithm (Gablonsky and Kelley, 2001) • GD_MLSL: Multi-Level Single-Linkage (Rinnooy Kan and Timmer, 1987)
<p>Local:</p> <ul style="list-style-type: none"> • LN_BOBYQA: Bound Optimization By Quadratic Approximation (Powell, 2009) • LN_SBPLX: modified Subplex (Rowan, 1990) algorithm • LN_NEWUOA: using quadratic approximation (Powell, 2004), superseded by BOBYQA (above) • LN_PRAXIS: PRincipal AXIS method (Brent, 1972) • LD_MMA: Method of Moving Asymptotes (Svanberg, 2002) • LD_SLSQP: Sequential Least-Squares Quadratic Programing (Kraft, 1994) • LD_VAR1: shifted limited-memory variable-metric algorithm (Vlcek and Luksan, 2006)

In the definition of optimization algorithms, G stands for Global, L for Local, N for non-derivative, and D for derivative (gradient-based).

2.4.7. Optimization library

Handling complex parameter optimization tasks with numerous parameters and a complex objective function requires a versatile selection of efficient and numerically robust optimization algorithms. Multi-dimensional fitting exercises almost invariably result in convergence difficulties, because of possible local minima and/or highly correlated fitting parameters. For this reason, `gemsfit2` uses the NLOpt nonlinear optimization library (<http://initio.mit.edu/nlopt>) that was also employed in the earlier prototype (Hingerl et al., 2014). This library provides several global and local minimization algorithms, which can be gradient or non-gradient based (derivative-free). The algorithms implemented in NLOpt and thus available in `gemsfit2` are listed in Table 2.5. In the ‘Optimization’ section of the task specification, several options can be used to control the use of NLOpt, e.g., the type of algorithm, a global upper and lower bound percentage for all

parameters, the relative and absolute tolerance for the convergence criterion, the initial step of the parameters, and the maximum number of iterations.

2.4.8. Weighting and outliers

In many datasets, outlying samples may result in significantly degrading the quality of the fitting and may also cause convergence problems for the fitting algorithms. The simplest way of dealing with extreme outliers is to exclude them from the selection of experiments from the database.

Another option available in `gemsfit2` for moderately outlying samples is to assign the outliers a lower weight. This can be done systematically using a Tuckey's Biweight function that reduces the influence of outliers (Motulsky and Christopoulos, 2004). The function uses a cutoff value C calculated as the median of all absolute values of residuals multiplied with an arbitrary scaling factor (6 by default) set in the task specification file. Each sample whose absolute value of the residual exceeds C is assigned a weight of 0 (i.e., it will be ignored during the fitting). Other samples are given weights determined by the following equation (where R_i is the absolute value of residual, i is the sample index, and C is the cutoff value as defined before):

$$w_{Tui} = \left(1 - \left(\frac{R_i}{C} \right)^2 \right)^2 \quad (4)$$

Sample weights are recomputed at each iteration of the optimization algorithm. These weights are computed for each different data type that is included in the objective function term (e.g., different medians for dissolved aqueous Al and Si concentrations). Weights can be set for each individual experimental sample, but also for each term of the objective function, as user defined values. More than one weighting option can be selected for one fitting task; Table 2.3 gives an overview of all possible weighting options.

2.4.9. Statistics

The majority of the statistics options implemented in `gemsfit2` remain the same (with minor corrections) as in the early prototype GEMSFIT; a detailed summary of them can be found in Hingerl et al. (2014). The main statistics features that can be analyzed are goodness of fit, sensitivity analysis, correlation of parameters (Hill and Tiedeman, 2007), and confidence intervals from Monte Carlo simulations (Motulsky and Christopoulos, 2004). All the statistics options can be set in the 'Statistics' section of the task specification.

2.4.10. Confidence intervals for parameters by Monte Carlo simulation

The philosophy of this method is to generate many datasets (experimental pseudo-data), and perform the optimization of fitting parameters for each generated dataset (Motulsky and Christopoulos, 2004). The resulting distributions of adjusted (fitted) parameters are then used to calculate their standard deviations and confidence intervals. The random scatter is generated as an array of values randomly extracted from a synthetic set of normally distributed data, which have the mean value and the standard deviation equal to that of the residuals resulting from the nonlinear

regression. Another option is using a “bootstrap sampling” (DiCiccio and Efron, 1996) of the residuals (useful when the residuals are not normally distributed). This is done by randomly sampling the residuals with the possibility of sampling one residual more than once. The random scatter is then added either to the computed property values or to the respective experimental values, as in eq. (2.5) or (2.6) (option set in the Statistics section of the task specification):

$$y_{i,new} = y_{i,old} + s_i \quad (2.5)$$

$$y_{i,new} = f_{i,old} + s_i \quad (2.6)$$

Here, y_i represents the measured value, f_i is the computed value, s_i represents the random scatter value, and subscripts *new* and *old* refer to the new ‘synthetic’ measured value and the one used in the actual fitting before the Monte Carlo iterations.

The resulting randomly modified values are then used as new “measured values” for the optimization procedure. The random scatter is computed for each objective function term (different types of data that are included into the objective function) on a normalized scale. For example, one scatter array is computed for all aluminum solubility measurements, and a separate one is computed for the silicon solubility measurements. In the case of bootstrap sampling, the random scatter is computed for each type of the data and the experimental dataset (i.e. one literature reference or set of experiments).

The MC procedure is repeated many times (>100), to make it possible to evaluate the standard deviation of fitted parameter values, which represents the error of the parameters for the given scatter of the experimental data. Symmetric confidence intervals are estimated from standard deviations of parameters by multiplying them with a suitable quantile of Student’s t-distribution (Hill and Tiedeman, 2007).

Due to the large amount of computing required for the Monte-Carlo simulations or, in some cases, for the nested functions and global algorithms, these options may be very time consuming. For this reason, the `gemsfit2` code is parallelized, and it can manage many processing tasks using the OpenMP (Open Multi-Processing) shared-memory multiprocessing library (<http://openmp.org/>). The master process is split into parallel tasks (depending on the type of configuration) that are simultaneously executed, thus dramatically reducing the required computation time.

2.4.11. Fit-independent statistics

The fit-independent statistics are calculated without invoking the optimized parameter values, using only sensitivities and weights (Hill and Tiedeman, 2007). Sensitivities represent the change in the computed value (y_i) divided by the change in the respective parameter value (b_j). They are calculated using central differences, in which the parameters are both increased and decreased. Mathematically speaking, sensitivity is a partial derivative of a computed value (y_i) with respect to the parameter (b_j). It is approximated from the finite difference:

$$\left(\frac{\partial y_i}{\partial b_j}\right)_b \approx \left(\frac{y_i(b_j + \Delta b_j) - y_i(b_j - \Delta b_j)}{2\Delta b_j}\right) \quad (2.7)$$

The change in the parameter value is calculated using a perturbator value (Δ), which can be set in the `gemsfit2` task specification file. In most cases, when using a small perturbator value, the calculated sensitivities approach the real sensitivities (Poeter and Hill, 1998), although a too small value could result in insignificant changes in the computed values. It is recommended to investigate the effect of different perturbation values until an optimal one is found. The sensitivities indicate the importance of the observations for determining the estimated parameter.

To better reflect the importance of observations in the parameter optimization, sensitivities have to be scaled. This is because their units are calculated as the measured value divided by the parameter, both of which can have very different units. For this purpose, sensitivities of each observation and parameter are multiplied by the value of the parameter (b_j) and by the weight assigned to the observation (w_i), resulting in the dimensionless-scaled sensitivities (*DSS*):

$$DSS_{ij} = \left(\frac{\partial y_i}{\partial b_j}\right)_b |b_j| w_i^{0.5} \quad (2.8)$$

Information about the sensitivity of one parameter to the observations is provided by the composite scaled sensitivities (*CSS*) (Hill and Tiedeman, 2007). They are calculated for each parameter using the dimensionless-scaled sensitivities, as follows (n is the number of observations):

$$CSS_j = \sum_{i=1}^n \left[\frac{(DSS_{ij})^2}{n} \right]^{1/2} \quad (2.9)$$

The variance-covariance matrix is then calculated as:

$$VarCov(b) = s^2 (X^T w X)^{-1} \quad (2.10)$$

$$X = \left(\frac{\partial y_i}{\partial b_j}\right)_b \quad (2.11)$$

where $VarCov(b)$ is a square matrix (the size of which is the number of parameters); s^2 is the error variance, i.e., the weighted squared sum of squared residuals divided by the degrees of freedom (number of observations minus the number of parameters); X is the matrix of sensitivities; and w is the weight matrix. The correlation coefficient between the j^{th} and the k^{th} parameter is then calculated as follows:

$$PCC(j, k) = \frac{VarCov(j, k)}{VarCov(j, j)^{1/2} VarCov(k, k)^{1/2}} \quad (2.12)$$

2.5. Application examples

The practical utility and efficiency of the GEMSFITS code package is demonstrated with examples that represent typical classes of optimization problems in geochemical-thermodynamic modeling. These include (1) fitting of interaction parameters of mixing models, (2) optimization

of thermodynamic properties such as the standard molal Gibbs energies of aqueous species or the equilibrium constants of formation reactions, (3) thermobarometry, (4) inverse titrations, and (5) combined nested problems.

2.5.1. Boehmite solubility and Al speciation

Aluminum is an important element in many rock-forming minerals. Because of its low solubility, Al determines fluid-mineral equilibria and the reaction progress during fluid-rock interaction (Pokrovski, 1998; Bénézech et al., 2001; Tagirov and Schott, 2001; Manning, 2006; Mookherjee et al., 2014). Modeling aluminum solubility in geologic fluids has always been problematic and controversial due to the inconsistency of thermodynamic data that involve Al, contradictions between different experimental studies of the pH-dependent solubility of Al minerals, discrepant thermodynamic properties of aluminum-bearing minerals that were used for extracting properties of aqueous Al species from solubility experiments, and because different activity models were used in deriving thermodynamic properties of aluminum aqueous species (Tagirov and Schott, 2001).

In this example, the standard molal Gibbs energies ($\Delta_f G_{298}^0$) of aqueous aluminum species at 25°C and 1 bar were fitted using in situ boehmite solubility experiments performed by Bénézech et al. (2001). The $\Delta_f G_{298}^0$ of Al^{3+} , AlOH^{2+} , $\text{Al}(\text{OH})_2^+$, $\text{Al}(\text{OH})_3^0$ and $\text{Al}(\text{OH})_4^-$, were simultaneously fitted. The thermodynamic properties of boehmite $\text{AlOOH}_{(\text{cr})}$ were accepted from Verdes et al. (1992) and Hemingway et al. (1991), and these have also been used by Bénézech et al. (2001) for interpreting their experimental results. Thermodynamic properties of aqueous species at the experimental conditions were calculated in the GEM-Selektor v.3 code using the revised Helgeson-Kirkham-Flowers (HKF) model (Helgeson et al., 1981); water properties were calculated from the Haar-Gallagher-Kell (HGK) model (Kestin et al., 1984). The extended Debye-Hückel aqueous electrolyte model (Helgeson et al., 1981; Oelkers and Helgeson, 1990) was used for calculating the activity coefficients of individual species. The standard state thermodynamic properties and HKF parameters of other species present in the system were taken from Shock and Helgeson (1988) for OH^- , Cl^- , Na^+ , from Tagirov et al. (1997) for HCl^0 , from Sverjensky et al. (1997) for NaCl^0 and from Shock et al. (1997) for NaOH^0 .

The boehmite solubility experiments were performed over a wide range of pH (from 2 to 10) at a salt concentration of 0.03 mol/kg (NaCl), at temperatures between 100 and 290°C, and at saturated water vapor pressures. The experimental method, described in Palmer et al. (2001), has been demonstrated to produce consistent results for numerous samples. The pH of the system was measured in situ using a hydrogen-electrode concentration cell (Bénézech et al., 2001).

To be able to simulate the exact experimental conditions in the GEM-Selektor v.3 code, the complete chemical composition for each system (experimental sample) must be known. Because concentrations of HCl and NaOH (that were used to adjust the pH in the experiments) were not reported by Bénézech et al. (2001), we had to apply the inverse titration approach in GEM-Selektor for adjusting the pH in each experiment (sample) to the experimentally measured value, using the

nested objective function as implemented in the `gemsfit2` code. The bulk composition of each simulated experimental sample was first adjusted by adding HCl and NaOH titrants by the free fitting of Na and Cl amounts ('F' type) with linearly constrained O and H amounts ('L' type) to reproduce the titrant stoichiometries.

Table 2.6 Initial and regressed (final) values of $\Delta_f G_{298}^0$ (kJ mol⁻¹) for selected aluminum species. The uncertainty (2σ) represents 2 times the standard deviation estimated from 1000 Monte Carlo runs.

Species	(¹)Initial $\Delta_f G_{298}^0$	(²)Final $\Delta_f G_{298}^0$	(²)Error (2σ)	(³)Final $\Delta_f G_{298}^0$	(³)Error (2σ)	(⁴)Final $\Delta_f G_{298}^0$	(⁵)Final $\Delta_f G_{298}^0$
AlOOH(cr)	-917.82	-917.82	1.9	-917.82	1.9	-917.82	-917.82
Al ³⁺	-487.5	-486.8	1.4	-486.3	0.5	-486.4	-486.4
AlOH ²⁺	-696.3	-695.8	10.0	-695.1	0.7	-695.2	-695.3
Al(OH) ₂ ⁺	-899.5	-897.9	1.2	-898.6	1.0	-897.1	-898.0
Al(OH) ₃ ⁰	-1101.7	-1105.0	1.0	-1104.6	0.9	-1106.2	-1104.9
Al(OH) ₄ ⁻	-1305.8	-1307.2	0.4	-1307.2	0.4	-1303.9	-1307.2
NaAl(OH) ₄ ⁰	-1567.4	-1567.4		-1567.4		-1567.4	-1567.4
Sum of squares	23.03	13.99		13.97		27.12	13.96

(¹)The initial $\Delta_f G_{298}^0$ value for AlOOH(cr) was adopted from Verdes et al. (1992) initial values for all aqueous Al species were taken from Tagirov and Schott (2001). The $\Delta_f G_{298}^0$ values for AlOOH(cr) and NaAl(OH)₄⁰ were fixed in the regression.

(²)Case A, the $\Delta_f G_{298}^0$ of all species was fitted independently.

(³)Case B1, the $\Delta_f G_{298}^0$ of Al³⁺ was fitted directly, while the $\Delta_f G_{298}^0$ of the AlOH²⁺ species was constrained by applying the equilibrium constant for the species-forming hydrolysis reaction (Al³⁺ + H₂O = AlOH²⁺ + H⁺). For this species, the 2σ error was calculated from the error of the $\Delta_f G_{298}^0$ for Al³⁺ and the error of the equilibrium constant for the species-forming reaction.

(⁴)Case B2, fitted by setting all initial values of $\Delta_f G_{298}^0$ smaller with 10.0 kJ/mol. The $\Delta_f G_{298}^0$ of Al³⁺ was fitted directly, while the $\Delta_f G_{298}^0$ of the AlOH²⁺ species was constrained by applying the equilibrium constant for the species-forming reaction.

(⁵)Case B2, same as (⁴) and using as starting values the final values of (⁴).

Using `gemsfit2`, the $\Delta_f G_{298}^0$ values of the aqueous Al species were adjusted and three different fitting cases were considered. In the first case (A), the regression yielded $\Delta_f G_{298}^0$ values for Al³⁺, AlOH²⁺, Al(OH)₂⁺, Al(OH)₃⁰ and Al(OH)₄⁻ fitted independently. In the second case (B1), the $\Delta_f G_{298}^0$ of AlOH²⁺ was constrained through the equilibrium constant for the species-forming reaction (Al³⁺ + H₂O = AlOH²⁺ + H⁺). In an additional third case (B2), the initial values for all standard state Gibbs energies were set to 10 kJ/mol more negative, while keeping the same reaction constraint as in the second task (B1). Although the species NaAl(OH)₄⁰ is included in the chemical

system, it is not controlling solubility at low Na concentrations and the $\Delta_f G_{298}^0$ was therefore fixed at the value from Tagirov and Schott (2001). Initial values of the $\Delta_f G_{298}^0$ and other standard molal thermodynamic properties for the aqueous aluminum species were adopted from Tagirov and Schott (2001). Only the $\Delta_f G_{298}^0$ values were adjusted during regression, while other standard molal properties of aqueous species were kept unchanged.

In all three fitting tasks, the local BOBYQA (Powell, 1994) optimization algorithm was used, and the search bounds for parameters were set to $\pm 5\%$ of the initial value. Initial values, final values, and the associated uncertainties for all fitting runs are given in Table 2.6. The standard sum of squares function was used with equal weights of 1.0 for all experimental data points:

$$F = \sum_{i=1}^n w_i (f_i - y_i)^2 \quad (2.13)$$

The solubility data were treated as \log_{10} of the molality. In all runs, the resulting final $\Delta_f G_{298}^0$ values of each species were similar, within their uncertainties (set to two times the standard deviation as estimated using the Monte Carlo method by simulating 1000 random sets of experiments).

Table 2.7 Parameter correlation matrix for the final regressed $\Delta_f G_{298}^0$ values of Al species.

	Al ³⁺	AlOH ²⁺	Al(OH) ₂ ⁺	Al(OH) ₃ ⁰	Al(OH) ₄ ⁻
Al ³⁺	1.0	-0.71	0.30	-0.11	-0.02
AlOH ²⁺		1.0	-0.56	0.25	0.04
Al(OH) ₂ ⁺			1.0	-0.65	0.16
Al(OH) ₃ ⁰				1.0	-0.29
Al(OH) ₄ ⁻					1.0

The correlation matrix was calculated for the case where $\Delta_f G_{298}^0$ values of all species were fitted independently.

In the first task (A), all $\Delta_f G_{298}^0$ values were independently fitted ('F' type). In systems with several independently fitted parameters, where the target function is not highly sensitive to each parameter, typically some fitted parameters are highly correlated, which makes it difficult to obtain physically meaningful values and to find the optimum solution. In the chemical system investigated, the total solubility is not very sensitive to the independent contributions of Al³⁺, AlOH²⁺ and Al(OH)₂⁺ at pH values below 5, where their predominance fields overlap (Fig. 2.7). The situation is different at neutral to alkaline pH, where Al(OH)₃⁰ and Al(OH)₄⁻ dominate the speciation. Uncertainties resulting from the independent fitting show that the $\Delta_f G_{298}^0$ values of all species except AlOH²⁺ could be constrained within reasonable bounds, and that the high

uncertainty associated with the $\Delta_f G_{298}^0$ of this species is clearly due to correlations. The resulting correlation coefficients of the independently fitted parameters can be found in Table 2.7; they show that the correlation coefficient between AlOH^{2+} with Al^{3+} is statistically significant ($r = -0.71$).

Therefore, for the second case (B1), the $\Delta_f G_{298}^0$ value of AlOH^{2+} was reaction-constrained ('R' type) using the equilibrium constants associated with the hydrolysis reaction:



$$\Delta_r G^0 = -RT \ln K \quad (2.15)$$

Values of equilibrium constants ($\log_{10}K$) for the above reaction for each experimental temperature were taken from Palmer and Wesolowski (1993), who determined them by a potentiometric method. After each optimization iteration, the new value for $\Delta_f G_{298}^0$ of AlOH^{2+} was recalculated using the $\log_{10}K$ of the above reaction and a new independently adjusted $\Delta_f G_{298}^0$ of Al^{3+} . The final results (Table 2.6) of the two fitting approaches show that the $\Delta_f G_{298}^0$ value of Al^{3+} is quite well constrained.

In the third task (B3), the initial values of $\Delta_f G_{298}^0$ of all Al species were set to 10 kJ/mol more negative than in two previous tasks, in order to investigate the significance of initial guesses for the final regressed parameters; all other settings were kept the same. In the first run, the BOBYQA algorithm converged to a local minimum (Table 2.6), clearly identified by the sum of squares being two times larger than in the two other tasks. A second run was performed using the final values from the first run as initial values. This time, the algorithm converged to a similar minimum as for the preceding cases, and the final values were almost identical.

The main improvement compared to other datasets for aqueous Al speciation is that the final optimized $\Delta_f G_{298}^0$ values were derived fully consistent with the selected aqueous electrolyte model (extended Debye-Hückel equation), the HKF EoS, the selected thermodynamic properties of boehmite, and all the selected experimental data. This opens up the possibility to derive alternative geochemical-thermodynamic datasets using different standard state data for the solubility-controlling mineral phases, different sets of aqueous species, different activity coefficient models (e.g., derive standard state properties based on a Pitzer model), or different experimental datasets. Furthermore, if new high-quality experimental data would become available in the future, thermodynamic properties of the aqueous Al species could be re-derived using the same approach. The key message here is that GEMSFITS optimized values will always be consistent with the selected models and input data, best reproducing the experimental data. Figure 7 shows \log_{10} activity values of aluminum species and total aluminum concentration as function of increasing pH, comparing directly the values calculated with the initial thermodynamic data and with the final adjusted ones. Experimental data points are plotted for comparison, and final regressed $\Delta_f G_{298}^0$ values obviously show a much better agreement with the experimental Al solubility data.

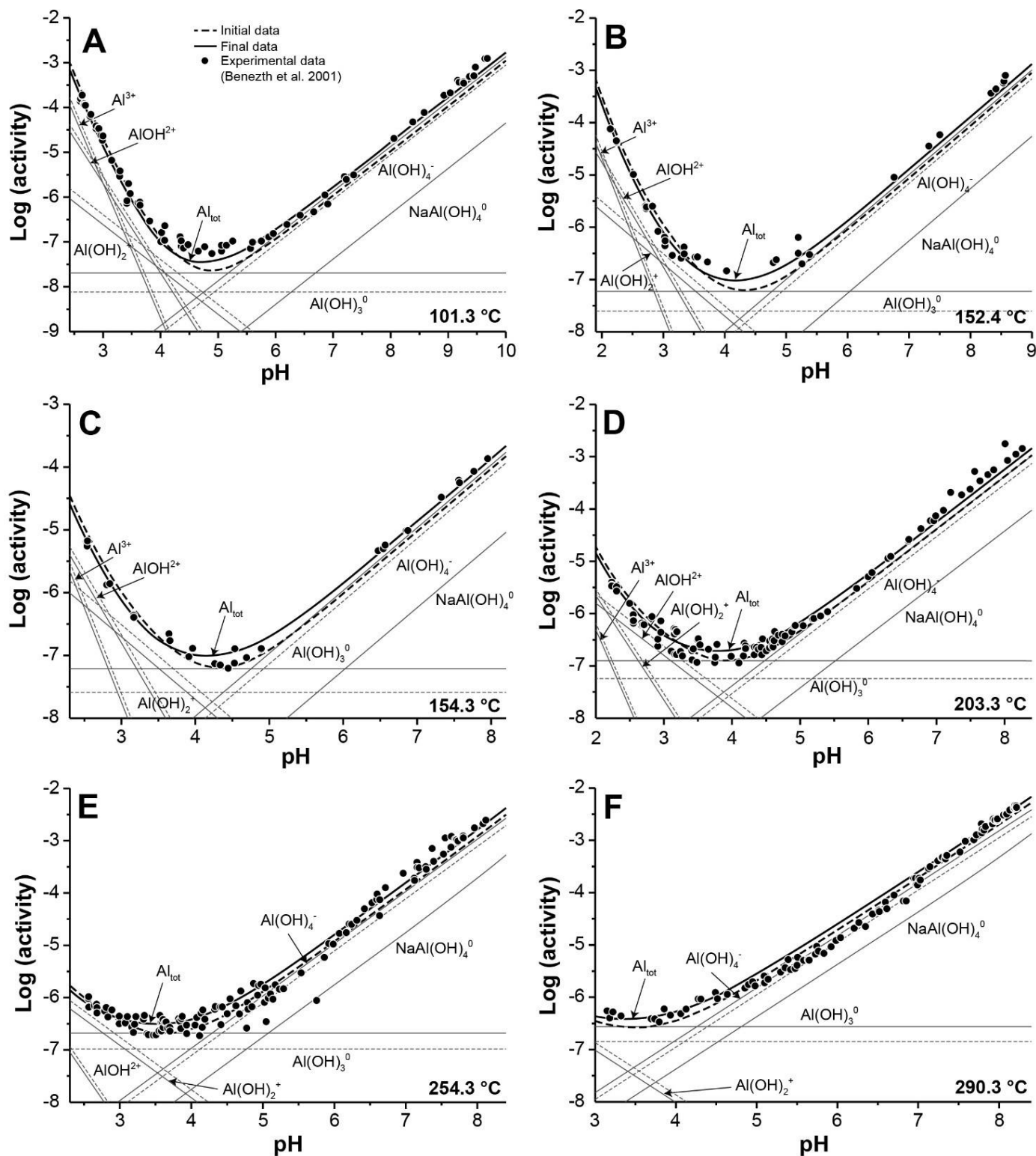


Figure 2.7 Plots showing the aluminum solubility and speciation as function of increasing pH and the total aluminum concentration, calculated with GEM-Selektor before (dashed lines) and after the optimization (solid lines) of the standard state properties of the aqueous Al species Al^{3+} , AlOH^{2+} , Al(OH)_2^+ , Al(OH)_3^0 and Al(OH)_4^- . Filled circles represent the experimental data points. Plots are shown for temperatures of (A) 101.3 °C, (B) 152.4 °C, (C) 154.3 °C, (D) 203.3 °C, (E) 254.3 °C and (F) 290.3 °C.

2.5.2. Ti in quartz: Solid-solution geothermometry

Several authors studied the temperature and pressure dependence of the substitution of Ti for Si in quartz (Ostapenko et al. 1987; Wark and Watson, 2008; Thomas et al., 2010; Huang and Audétat, 2012). This solid-solution is commonly applied as a thermobarometer (Rusk et al., 2008; Smith et al., 2010; Wilson et al., 2012; Kidder et al., 2013).

The objective of this example was to test the optimization of mixing model parameters for solid-solutions using GEMSFITS. Therefore, a regular SiO₂-TiO₂ (quartz-rutile) solid-solution model was constructed in the GEM-Selektor database. Then three coefficients (constant term and linear terms for temperature and pressure dependence) of the regular interaction parameter were fitted against the experimental data (Wark and Watson, 2008; Thomas et al., 2010). The optimized solid-solution model was then used in a GEMSFITS inverse modeling task aimed at determining the temperature of quartz crystallization using measured Ti concentration data in natural quartz samples from Kidder et al. (2013) along with those from low-grade metamorphic quartz veins in accretionary-wedge sediments of the Swiss Alps (Miron et al., 2013).

The solubility of Ti in quartz in the presence of pure rutile was experimentally measured between 600 and 1000 °C and between 5 and 20 kbar using a piston-cylinder apparatus (Wark and Watson, 2008; Thomas et al., 2010). A total number 31 data from these experimental studies were added to the GEMSFITS TiQ database. The chemical system was set up using GEM-Selektor and exported to a set of GEMS3K input files. The Peng-Robinson multicomponent fluid model (Anderson and Crerar, 1993) was used to describe the fluid phase (with fluid species H₂O, H₂ and O₂). The solid phases in the system were pure rutile and a quartz-rutile solid-solution phase. Thermodynamic properties of solid-solution end-members were taken from the Holland and Powell (1998) database (as revised in Thermocalc datafile ds55). The regular binary mixing model (Anderson and Crerar, 1993) was used, where the end-member activity coefficient is calculated from a single interaction parameter:

$$RT \ln \gamma_{\text{SiO}_2} = X_{\text{TiO}_2} (1 - X_{\text{SiO}_2}) W_{\text{SiO}_2\text{-TiO}_2} \quad (2.16)$$

$$RT \ln \gamma_{\text{TiO}_2} = X_{\text{SiO}_2} (1 - X_{\text{TiO}_2}) W_{\text{SiO}_2\text{-TiO}_2} \quad (2.17)$$

Here, γ_{SiO_2} and γ_{TiO_2} represent the activity coefficients, and X_{SiO_2} and X_{TiO_2} the mole fractions of SiO₂ and TiO₂ in quartz. $W_{\text{SiO}_2\text{-TiO}_2}$ is the regular interaction parameter, which is a simple function of temperature and pressure:

$$W_{\text{SiO}_2\text{-TiO}_2} = a + bT + cP \quad (2.18)$$

Here, T is the temperature in Kelvin and P is the pressure in bar. The coefficients a , b and c are adjustable parameters in the regression of experimental data (measured Ti concentrations in quartz at given temperature and pressure).

Table 2.8 Results of optimization runs for the Ti-in-quartz solid solution model.

Coefficient	⁽¹⁾ Initial	⁽¹⁾ Final (global)	⁽²⁾ Final (local)	⁽²⁾ Error (2 σ)	⁽²⁾ CSS	⁽³⁾ Final (local)	⁽³⁾ Error (2 σ)
<i>a</i>	10000 (1000 – 100000)	60300	60316	2300	35.4	60717	1100
<i>b</i>	-1 (-100 – 100)	-1.168	-1.159	0.568	1.32	-1.577	0.42
<i>c</i>	1 (-100 – 100)	1.791	1.780	0.180	13.5	1.762	0.1

Coefficients *a*, *b* and *c* of the interaction parameter $W = a + bT + cP$. The uncertainty (2σ) represents the 2 times standard deviation of the parameters from 1000 Monte Carlo runs. Numbers in parentheses represent the parameter bounds during optimization. CSS: composite scaled sensitivities.

⁽¹⁾Case A1, initial and final values as well as errors for the runs where the global optimization algorithm was applied.

⁽²⁾Case A2, final values and errors obtained from the optimization runs using the local optimization algorithm. The final values of the runs with the global optimization algorithm were used as initial guesses for the subsequent runs with the local optimization algorithm.

⁽³⁾Case A3, final values and errors obtained from the optimization runs where the measured Ti concentration in quartz was used as $\ln(X_{TiO_2}^{Quartz})$

For the first fitting task (A1), a global optimization setup was prepared (Table 2.8). The chosen global fitting algorithm was *GN_ISRES* (Runarsson and Xin, 2005), and the weighting used was the inverse square of the measured value. Results of fitting tasks are listed in Table 2.8, and calculations from the model are compared to experimental data in Fig. 2.8. Optimized values of the *a*, *b* and *c* coefficients obtained from the global optimization run were then used as initial values for the second task (A2) using the BOBYQA (Powell, 1994) local optimization algorithm. Parameter correlation coefficients using the local algorithm are given in Table 2.9, showing that coefficients *a* and *c* are highly correlated (-0.91). Parameter composite scaled sensitivities from the statistical analysis show that the second coefficient (*b*), which describes the temperature dependence of the interaction parameter, is the least sensitive to the experimental data.

Table 2.9 Correlation matrix for the final regressed values of the interaction parameter coefficients ($W = a + bT + cP$) of the Ti in quartz solid solution model.

	<i>a</i>	<i>b</i>	<i>c</i>
<i>a</i>	1.0	0.32	-0.91
<i>b</i>		1.0	-0.02
<i>c</i>			1.0

A third fitting task (A3) was produced using the initial values of parameters obtained from the first task (A1), but setting the calculated and measured concentrations of Ti in quartz in the natural logarithm scale. The resulting parameter values are almost identical to the ones obtained from the second fitting task, but their computed errors (2 times the standard deviation of the parameters resulting from 1000 Monte Carlo runs) are half as large as the errors from the second fitting task (Table 2.8). The change in error values is a consequence of the change in the shape of the minimized function surface due the conversion to logarithmic scale.

Thomas et al. (2010) used the following equation to describe their data:

$$RT \ln X_{\text{TiO}_2}^{\text{quartz}} = -a + bT(K) - cP(\text{kbar}) + RT \ln a_{\text{TiO}_2} \quad (2.19)$$

where R is the universal gas constant, T is temperature in Kelvin, P is pressure in kbar, $\ln X_{\text{TiO}_2}^{\text{quartz}}$ is the mole fraction of TiO_2 in quartz, and a_{TiO_2} is the activity of TiO_2 in the system. Their fitted values for the coefficients (a : -60952 ± 3177 ; b : 1.52 ± 0.39 ; c : 1741 ± 63) agree within uncertainty with those obtained from our regression. This is because eq. (2.19) can be converted into a form that is equivalent to the regular mixing model (eqs. 2.16, 2.17 and 2.18) using the definition of the activity of end-members:

$$\ln X_{\text{TiO}_2}^{\text{Quartz}} = \ln a_{\text{TiO}_2} - \ln \gamma_{\text{TiO}_2}^{\text{Quartz}} \quad (2.20)$$

For the binary regular model:

$$RT \ln \gamma_{\text{TiO}_2}^{\text{Quartz}} = (X_{\text{SiO}_2}^{\text{Quartz}})^2 W_{\text{SiO}_2-\text{TiO}_2} \quad (2.21)$$

When Ti is present at trace element concentrations in quartz, the mole fraction of the SiO_2 end-member can be closely approximated with unity, leading to the simplified expression:

$$\ln \gamma_{\text{TiO}_2}^{\text{Quartz}} = \frac{W_{\text{SiO}_2-\text{TiO}_2}}{RT} \quad (2.22)$$

This can be substituted into eq. (2.20) to arrive at a form that is identical to eq. (2.19).

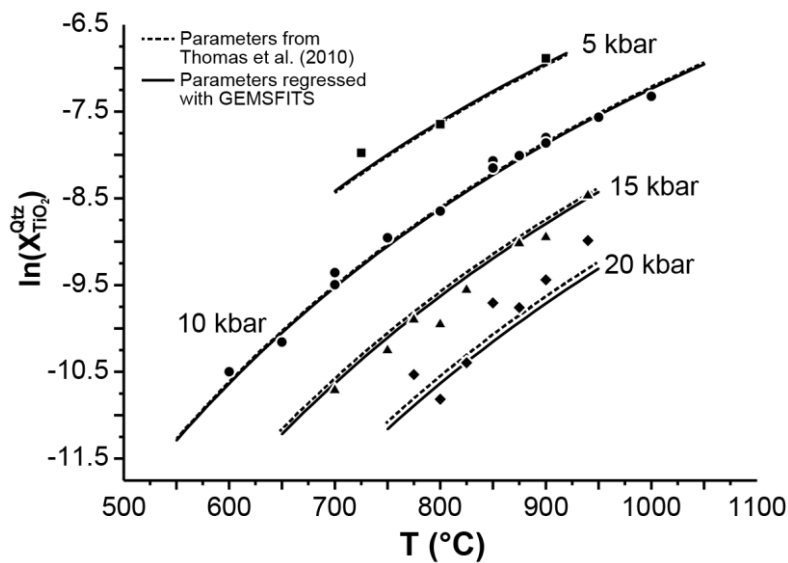


Figure 2.8 Plot illustrating the temperature dependence of Ti concentrations in quartz. Filled circles are experimental data points (Wark and Watson, 2008; Thomas et al., 2010) and curves are calculated from thermodynamic solid-solution models.

In an application to field-based geochemical data, the optimized coefficients obtained from the second fitting task (Table 2.8) were used to determine the temperature of crystallization of quartz (Table 2.10) in the presence of rutile from 6 natural samples reported by Kidder et al. (2013). For this inverse modeling problem, the Ti concentration data from Kidder et al. (2013) and our own data from quartz veins in low-grade metamorphic rocks from the Central Swiss Alps (Miron et al., 2013) were added to the TiQ database file. All samples had 300 °C as starting value for the temperature. The parameter marked for fitting in the GEMSFITS task input file was temperature "TK" and in the "DataTarget" section, a nested function was used to compare the measured concentrations of Ti in quartz with the calculated ones. The `gemsfit2` code adjusted the temperatures for each sample independently, until the calculated amount of Ti in solid-solution with quartz was close to the analyzed concentrations. The resulting equilibrium temperatures are in good agreement with the temperatures estimated from other independent geothermometers for the same samples. Other applications similar to the one above could be developed for modeling of trace element partitioning. One can easily use GEMSFITS for adjusting the mixing model parameters for different solid-solutions between major and trace elements in minerals (e.g. Zr in rutile, Zr in titanite, etc.).

Table 2.10 Application of Ti in quartz geothermometry to two field examples.

Sample	Ti in quartz (ppm)	⁽¹⁾ P (bar)	⁽¹⁾ T (°C)	⁽¹⁾ Error (2σ)	⁽²⁾ T (°C)	⁽²⁾ Error (2σ)	Reference
ms-004	0.19	2600	237	26	234	24	K
ms-34	0.48	3100	276	28	273	22	K
ms-342	0.52	3000	279	28	277	22	K
q-005	0.54	2800	282	28	274	22	K
q-123b	0.30	3100	256	27	257	21	K
q-148j	0.72	3200	295	29	292	23	K
Thuisis	1.00	3000*	320*	20*	302	23	M

Temperatures were calculated using analyzed Ti concentrations in quartz, applying the solution model calibration from (Thomas et al., 2010) and this study.

⁽¹⁾Sample median temperatures reported by Kidder et al. (2013) (ref. 'K') and calculated by using TitaniQ thermometer (Thomas et al., 2010) and (*) estimated using mineral geothermometry (Miron et al., 2013). Pressures calculated using a geothermal gradient of 25°Km⁻¹ and the mean temperature values reported by Kidder et al. (2013). Ref. 'M': G.D.Miron, unpublished data.

⁽²⁾Temperatures calculated using inverse modeling with the solution model calibration obtained in this study. The analytical 2σ error has been propagated from the error on the regressed interaction parameters.

2.6. Discussion

The GEMSFITS code package can adjust separately or simultaneously any GEM input property parameters (standard state Gibbs energies of formation, interaction parameters of thermodynamic mixing models or equations of state, pressure, temperature, input bulk composition), provided that sufficient experimental data are available that can be compared to their computed counterparts. This is a substantial extension compared to the previous prototype (Hingerl et al., 2014), which had only capabilities for fitting the interaction parameters of aqueous activity models.

The user-defined objective function with one or multiple terms (one term for each type of property) makes it possible to calculate the sum of residuals for any measurable property from experiments performed in different, but related systems. GEMSFITS can therefore fit parameters simultaneously for several chemical systems and many individual experimental data points. The quality of fit can be improved by assigning conditional weights to experimental data points using a range of methods (Table 2.3). Weights can also be placed on each term of the objective function, thereby giving more weight to selected types of measured data (e.g., placing more weight on solubility data than on volumetric or calorimetric data of aqueous electrolytes). Weighting can also be used to normalize the observed and computed data, because even for a linear regression model it is recommended that all data sets are expressed in the same scale (Motulsky and Christopoulos, 2004). For datasets that cover a large range in parameter space (e.g., experimental solubility data that span several orders of magnitude in concentration), the data should be brought to the same units or at least to similar magnitudes, in order to avoid that the high-magnitude properties would strongly bias the fitting results.

In the `gemsfit2` code, one way of bringing the experimental data to the same magnitude is by using the squared inverse measured value as a weight multiplier. For certain types of data such as dissolved aqueous concentrations, the logarithmic scale is clearly preferable. A potential problem when using the logarithmic scale is that the residuals are asymmetric, i.e., that the absolute value of the positive residual is numerically larger than that of the negative residual (even if the residuals in the non-logarithmic scale are absolutely equal). It is often difficult to decide which experimental points should be treated as outliers. Samples identified as outliers can be skipped from the fitting task, or assigned a low weight (close to zero). A general way of treating outliers is using the GEMSFITS implementation of the Tuckey's Biweight method (Motulsky and Christopoulos, 2004), which gives increasingly less weight to the points further away from the ideal value.

Well constrained parameters for mixing models in non-ideal solution phases are important for accurately calculating activities of solutes or end-members, which is essential for realistic modeling of (geo)chemical systems. These models can have a large number of parameters (e.g., the Pitzer model; Pitzer and Kim, 1974), which imposes high demands on the fitting method. Therefore, it is important to utilize numerically robust and stable optimization algorithms and to perform thorough statistical analysis of the fitting results. The `gemsfit2` code therefore provides

a selection of different global and local, gradient based or gradient-free, algorithms that can solve multidimensional non-linear optimization problems. Local optimization algorithms may experience problems when the surface of the function to be minimized is complex and has local minima. In this case, the parameter optimization may converge to incorrect values that represent a local rather than the global minimum. Global algorithms are much slower, but can search for the true global minimum. However, global algorithms are less precise close to the minimum compared to the local algorithms. Thus, a ‘smart’ procedure combines a global optimization run and then uses the resulting parameters as initial guesses with rather close upper and lower bounds in a subsequent local refinement step. Compared to a global algorithm, the parameter search space of a local algorithm is smaller, and this increases the calculation time required to find the optimal solution of the fitting problem.

The standard state molar (molal) Gibbs energy values $\Delta_f G_{298}^0$ of dependent components (e.g., aqueous species, solid-solution end-members, pure condensed substances, gaseous and fluid species) can be adjusted as free (‘F’) parameters, or by application of reaction-type (‘R’) constraints. Complex chemical systems contain many dependent components, which considerably increases the dimensionality of the fitting problem and makes it more difficult for the optimization algorithms to converge. Furthermore, some of the regressed $\Delta_f G_{298}^0$ values may be highly correlated and may not be physically meaningful. For complex systems, the reaction-type constraints can greatly speed up the fitting process for poorly constrained or highly correlated $\Delta_f G_{298}^0$ values, especially if only low-quality or insufficient experimental data are available (see the example on fitting the $\Delta_f G_{298}^0$ values of aqueous aluminum species).

Inverse GEM modeling tasks include thermobarometry calculations and inverse titrations. Thermobarometry finds the temperature and/or pressure based on analyzed compositions of solution phases (e.g., Mg-Fe exchange equilibria between garnet and biotite, Ti concentration in quartz etc.). Mineral solid-solutions record the P - T history of the rocks by continuous adjustment of the element partitioning between coexisting mineral phases, driven by changes in P - T conditions (Spear, 1993; Powell and Holland, 2008). The response and sensitivity of element exchange reactions to changes in temperature and pressure is determined from well-defined laboratory experiments or analytical data for rock samples where independent information on P - T conditions is available (Zhou et al., 1994; Dale et al., 2000; Worley and Powell, 2000). These data are used to calibrate thermodynamic models that describe the mixing properties of the mineral solid-solution phases involved in the element partition reactions. Thermodynamic models can then be used to estimate the P - T conditions that natural rock samples have experienced.

Inverse titrations involve the iterative adjustment of the bulk composition of the chemical system to match the calculated output properties with their given (experimental) counterparts (e.g., pH, pe, activities/fugacities of species in gas/fluid phases or in aqueous solution). Commonly, the exact amounts of titrants employed in the experiments to adjust some parameters such as pH are not reported in the publications, but only the measured output parameters (e.g. pH) are provided.

For such cases, “nested” objective functions can be defined in GEMSFITS, and parameter optimization can be performed using experimental data such as measured mineral solubility as function of pH (as in the boehmite solubility example), or pH edges for adsorption of aqueous ions on solid surfaces. The `gemsfit2` code then adjusts the amount of titrant through the nested inverse titration functions, until the computed equilibrium pH is in agreement with the measured pH at a prescribed precision. This option has to be treated carefully, because it could result in undesired changes in the ionic strength of aqueous solutions.

In GEMSFITS, the experimental data are currently kept in a NoSQL database as local files within the project folder. The database contents can be exported to JSON text files for backup or further to be uploaded to a MongoDB server, if necessary. Maintenance of the database and editing data records can be straightforwardly performed through the `gfshell2` graphical user interface. Compared to the SQL database that was used in the early prototype (Hingerl et al., 2014), the NoSQL database is much better suited for storing weakly structured data that describe samples with variable experimental conditions. In the NoSQL database, there is no need to know the data structure in advance before creating the database or even inserting new records (documents) into an existing database. The way in which the experiments are stored, handled and selected in GEMSFITS permits to test the fitting of many data combinations from different experimental settings, as well as to remove experimental data sets or single outliers without the need to prepare different experimental data input files for each fitting task. The latter is often required by other fitting tools (Herbelin, 1999; Karamalidis and Dzombak, 2010; Kinniburgh and Cooper, 2011).

A major advantage of GEMSFITS is that both standard statistical and Monte Carlo based methods are available for analysis of the regression results. Monte Carlo methods are essential if the documentation of the analytical errors of the experimental data in the original publications is unavailable, incomplete, or lacking appropriate consideration of all sources of uncertainty. When using the Monte Carlo method, performing global optimization of large systems, or optimizing a large number of fitting parameters, the `gemsfit2` code can take advantage of the parallelization, which substantially decreases the computing time required to complete a fitting task.

For example, fitting the Ti-in-quartz solid-solution model required to optimize 3 parameters using the global algorithm (ISRES) with 20000 iterations. To complete this task, the program executed 3.2 times faster when parallelized on 4 processor threads compared to one thread (32 compared to 101 seconds). When fitting standard state properties of aqueous Al species (using 4 free parameters and one parameter constrained by the species-forming reaction) with a local algorithm (BOBYQA), the program needed 54 iterations to converge and executed 3.4 times faster when parallelized on 4 processor threads compared to one thread (644 compared to 2220 seconds). The speedup gained from parallelization will become more important in large chemical systems, where the number of fitting parameters and number of experiments will dramatically increase. Producing internally consistent thermodynamic datasets for large chemical systems will involve simultaneous regression of many standard state Gibbs energies of species using thousands of experimental data points. This work will only be feasible when taking advantage of the code parallelization that GEMSFITS offers.

The GEMSFITS codes will be made freely distributable and open-source, as part of the GEM Software collection (<http://gems.web.psi.ch>). This will give other scientists the opportunity to use the codes and the possibility to improve them further. Free (as ‘freedom’) software is of great importance in modern research communities where scientists share their knowledge in a way that others can build upon and use it freely in their research.

2.7. Outlook

All the new features described above make the GEMSFITS code package a general, flexible, efficient, and user-friendly practical tool for fitting any input parameters of geochemical-thermodynamic models. Future implementations will include extensions to fit the parameters of electrostatic sorption models and mineral dissolution/precipitation kinetic models that are part of the current development version of the GEMS3K codes. When completed, these models will be included into the release version of GEMS and made available to the scientific community. This will increase the range of applications of GEMSFITS to surface adsorption studies and mineral-aqueous reaction kinetics. Furthermore, GEMSFITS will be extended to be capable of fitting parameters of all equation-of-state models that are implemented into the GEM-Selektor v.3 code. Another long-term goal is to create an experimental database server accessible online via web applications that would be updated and improved using the scientific expertise and resources of different participants. This data can then be easily selected and used with GEMSFITS for optimizing various models for a large number of applications in geochemistry, petrology, chemical engineering, and materials science.

Acknowledgments

This project was supported by ETHIRA grant ETH-19-11-2 from ETH Zürich. Additional funding to DK was provided by Nagra, Wettingen. We thank Pawel Kuczera for helpful discussions concerning parameter fitting approaches and related statistical data analysis.

References

- Anderson, G.M., Crerar, D.A., 1993. *Thermodynamics in Geochemistry: The equilibrium model*. Oxford University Press, 588 p.
- Bénézech, P., Palmer, D.A., Wesolowski, D.J., 2001. Aqueous high-temperature solubility studies. II. The solubility of boehmite at 0.03 m ionic strength as a function of temperature and pH as determined by in situ measurements. *Geochim. Cosmochim. Acta* 65, 2097-2111.
- Brent, R., 1972. *Algorithms for Minimization without Derivatives* Prentice-Hall, Englewood Cliffs, New Jersey, 195p.
- Dale, J., Holland, T., and Powell, R., 2000. Hornblende-garnet-plagioclase thermobarometry; a natural assemblage calibration of the thermodynamics of hornblende. *Contrib. Mineral. Petrol.* 140, 353-362.
- DiCiccio, T.J., Efron, B., 1996. Bootstrap confidence intervals (with Discussion). *Stat. Sci.* 11, 189-228.
- Doherty, J. E., Hunt, R.J., 2010. *Approaches to Highly Parameterized Inversion: A Guide to Using PEST for Groundwater-Model Calibration*: US Geological Survey.

- Eldred, M.S., Giunta, A.A., van Bloemen Waanders, B.G., Wojtkiewicz, S.F., Hart, W.E., Alleva, M.P., 2007. DAKOTA, a multilevel parallel object-oriented framework for design optimization, parameter estimation, uncertainty quantification, and sensitivity analysis: Version 4.1. Sandia National Laboratories Albuquerque.
- Gablonsky, J.M., Kelley, C.T., 2001. A locally-biased form of the DIRECT algorithm. *J. Global Optimization* 21, 27-37.
- Helgeson, H.C., Kirkham, D.H., Flowers, G.C., 1981. Theoretical prediction of the thermodynamic behavior of aqueous electrolytes by high pressures and temperatures. IV. Calculation of activity coefficients, osmotic coefficients, and apparent molal and standard and relative partial molal properties to 600 °C and 5kb. *Amer. J. Sci.* 281, 1249-1516.
- Hemingway, B.S., Robie, R.A., Apps, J.A., 1991. Revised values for the thermodynamic properties of boehmite, AlO(OH), and related species and phases in the system Al-H-O. *Amer. Mineral.* 76, 445-457.
- Herbelin, A.L., 1999. FITEQL a computer program for determination of chemical equilibrium constants from experimental data. Oregon State University, Corvallis.
- Hill, M.C., Tiedeman, C.R., 2007. Effective groundwater model calibration: With analysis of data, sensitivities, predictions, and uncertainty.
- Hingerl, F., Kosakowski, G., Wagner, T., Kulik, D., Driesner, T., 2014. GEMSFIT: a generic fitting tool for geochemical activity models: *Computat. Geosci.* 18, 227-242.
- Hoffmann, J., Kräutle, S., Knabner, P., 2012. A general reduction scheme for reactive transport in porous media. *Computat. Geosci.* 16, 1081-1099.
- Holland, T.J.B., Powell, R., 1998. An internally consistent thermodynamic data set for phases of petrological interest. *J. Metam. Geol.* 16, 309-343.
- Huang, R., Audétat, A., 2012. The titanium-in-quartz (TitaniQ) thermobarometer: A critical examination and recalibration. *Geochim. Cosmochim. Acta* 84, 75-89.
- Johnson, J.W., Oelkers, E.H., Helgeson, H.C., 1992. SUPCRT92: A software package for calculating the standard molal thermodynamic properties of minerals, gases, aqueous species, and reactions from 1 to 5000 bars and 0°C to 1000°C. *Comput. Geosci.* 18, 890-947.
- Jones, D.R., Perttunen, C.D., Stuckmann, B.E., 1993. Lipschitzian optimization without the lipschitz constant. *J. Optim. Theory Appl.* 79, 157.
- Kaelo, P., Ali, M.M., 2006. Some variants of the controlled random search algorithm for global optimization. *J. Optim. Theory Appl.* 130, 253-264.
- Karamalidis, A.K., Dzombak, D.A., 2010. Data compilation and treatment methods. *Surface Complexation Modeling*, John Wiley & Sons, 45-57.
- Karpov, I.K., Chudnenko, K.V., Kulik, D.A., 1997. Modeling chemical mass transfer in geochemical processes; thermodynamic relations, conditions of equilibria and numerical algorithms. *Amer. J. Sci.* 297, 767-806.
- Kestin, J., Sengers, J.V., Kamgar-Parsi, B., Levelt-Sengers, J.M., 1984. Thermophysical properties of fluid H₂O. *J. Phys. Chem. Ref. Data* 13, 175-183.
- Kidder, S., Avouac, J.P., Chan, Y.C., 2013. Application of titanium-in-quartz thermobarometry to greenschist facies veins and recrystallized quartzites in the Hsüehshan range, Taiwan. *Solid Earth* 4, 1-21.
- Kinniburgh, D., Cooper, D., 2011. PhreePlot: Creating graphical output with PHREEQC.
- Kraft, D., 1994. Algorithm 733: TOMP-Fortran modules for optimal control calculations. *ACM Transact. Mathem. Software* 20, 262-281.
- Kulik, D.A., Wagner, T., Dmytrieva, S.V., Kosakowski, G., Hingerl, F., Chudnenko, K.V., Berner, U., 2013. GEM-Selektor geochemical modeling package: revised algorithm and GEMS3K numerical kernel for coupled simulation codes. *Computat. Geosci.* 17, 1-24.
- Leal A.M.M., Blunt M, LaForce T., 2014. Efficient chemical equilibrium calculations for geochemical speciation and reactive transport modelling, *Geochim. Cosmochim. Acta* 131, 301-322.
- Manning, C.E., 2006. Mobilizing aluminum in crustal and mantle fluids. *J. Geochem. Explor.* 89, 251-253.
- MathWorks, 2012. MATLAB and Statistics Toolbox Release 2012b, The MathWorks Inc., Natick, Massachusetts, United States.

- Miron, G., Wagner, T., Wälle, M., Heinrich, C.A., 2013. Major and trace-element composition and pressure–temperature evolution of rock-buffered fluids in low-grade accretionary-wedge metasediments, Central Alps. *Contrib. Mineral. Petrol.* 165, 981-1008.
- Mookherjee, M., Keppler, H., Manning, C.E., 2014. Aluminum speciation in aqueous fluids at deep crustal pressure and temperature. *Geochim. Cosmochim. Acta* 133, 128-141.
- Motulsky, H., Christopoulos, A., 2004. Fitting models to biological data using linear and non-linear regression: a practical guide to curve fitting. Oxford University Press, Oxford, 352 p.
- Oelkers, E.H., Helgeson, H.C., 1990. Triple-ion anions and polynuclear complexing in supercritical electrolyte solutions. *Geochim. Cosmochim. Acta* 54, 727-738.
- Ostapenko, G.T., Gamarnik, M.Y., Gorogotskaya, L.I., Kuznetsov, G.V., Tarashchan, A.N., Timoshkova, L.P., 1987. Isomorphism of titanium substitution for silicon in quartz: experimental data. *Mineral Zh.* 9, 30-40.
- Palmer, D.A., Benezeth, P., Wesolowski, D.J., 2001. Aqueous high-temperature solubility studies. I. The solubility of boehmite as functions of ionic strength (to 5 molal, NaCl), temperature (100-290°C), and pH as determined by in situ measurements. *Geochim. Cosmochim. Acta*, 65, 2081-2095.
- Palmer, D.A., Wesolowski, D.J., 1993. Aluminum speciation and equilibria in aqueous solution: III. Potentiometric determination of the first hydrolysis constant of aluminum(III) in sodium chloride solutions to 125°C. *Geochim. Cosmochim. Acta* 57, 2929-2938.
- Parkhurst, D.L., Appelo, C.A.J., 2013. Description of input and examples for PHREEQC version 3: a computer program for speciation, batch-reaction, one-dimensional transport, and inverse geochemical calculations. *U.S. Geological Survey Techniques and Methods* 6, 497.
- Pitzer, K.S., Kim, J.J., 1974. Thermodynamics of electrolytes. IV. Activity and osmotic coefficients for mixed electrolytes. *J. Amer. Chem. Soc.* 96, 5701-5707.
- Plantenga, T.D., 2009. HOPSPACK2.0 user manual: Version 2.0.2. Sandia Technical Report 2009-6265.
- Plugge, E., Hawkins, T., Membrey, P., 2010. The definitive guide to MongoDB: The NoSQL database for cloud and desktop computing, APress, 328 p.
- Poeter, E.P., Hill, M.C., 1998. Documentation 722 of UCODE: A computer code for universal inverse modeling. U.S. Geological Survey, Denver.
- Pokrovski, G.S., Schott, J., Salvi, S., Gout, R., Kubicki, J.D., 1998. Structure and stability of aluminum-silica complexes in neutral to basic solutions. Experimental study and molecular orbital calculations. *Min. Mag.*, 62A, 1194-1195.
- Powell, M.J.D., 1994. A direct search optimization method that models the objective and constraint functions by linear interpolation. *Proceedings of the Sixth Workshop on Optimization and Numerical Analysis, Oaxaca, Mexico*, 51.
- Powell, M.J.D., 2004. The NEWUOA software for unconstrained optimization without derivatives. *Proceedings of the 40th Workshop on Large Scale Nonlinear Optimization (Erice, Italy, 2004)*.
- Powell, R., Holland, T.J.B., 2008. On thermobarometry. *J. Metam. Geol.* 26, 155-179.
- Reed, M.H., 1982. Calculation of multicomponent chemical equilibria and reaction processes in systems involving minerals, gases and an aqueous phase. *Geochim. Cosmochim. Acta* 46, 513-528.
- Rinnooy, A.H.G.K., Timmer, G.T., 1987. Stochastic global optimization methods. *Mathem. Progr.* 39, 27-78.
- Rowan, T., 1990. Functional Stability Analysis of Numerical Algorithms. Ph.D. thesis, Department of Computer Sciences, University of Texas at Austin.
- Runarsson, T.P., Xin, Y., 2005. Search biases in constrained evolutionary optimization. *IEEE Transact.* 35, 233-243.
- Rusk, B.G., Lowers, H.A., Reed, M.H., 2008. Trace elements in hydrothermal quartz: relationships to cathodoluminescence textures and insights into vein formation. *Geology* 36, 547–550.
- Silva Santos, C.H., Goncalves, M.S., Hernandez-Figueroa, H.E., 2010. Designing novel photonic devices by bio-inspired computing. *IEEE Photonics Tech. Lett.* 22, 1177-1179.
- Smith, V.C., Shane, P., Nairn, I., 2010. Insights into silicic melt generation using plagioclase, quartz and melt inclusions from the caldera-forming Rotoiti eruption, Taupo volcanic zone, New Zealand. *Contrib. Mineral. Petrol.* 160, 951-971.

- Spear, F.S., 1993. *Metamorphic phase equilibria and Pressure-Temperature-Time paths*. Mineralogical Society of America, 799 pp.
- Steeffel, C.I., Lasaga, A.C., 1994. A coupled model for transport of multiple chemical species and kinetic precipitation/dissolution reactions with application to reactive flow in single phase hydrothermal systems. *Amer. J. Sci.* 294, 529-592.
- Steeffel, C.I., DePaolo, D.J., Lichtner, P.C., 2005. Reactive transport modeling: An essential tool and a new research approach for the Earth sciences. *Earth Planet. Sci. Lett.* 240, 539-558.
- Shock, E.L., Helgeson, H.C., 1988. Calculation of the thermodynamic and transport properties of aqueous species at high pressures and temperatures: Correlation algorithms for ionic species and equation of state predictions to 5 kb and 1000°C. *Geochim. Cosmochim. Acta* 52, 2009-2036.
- Shock, E.L., Oelkers, E.H., Johnson, J.W., Sverjensky, D.A., Helgeson, H.C., 1992. Calculation of the thermodynamic properties of aqueous species at high pressures and temperatures. Effective electrostatic radii, dissociation constants and standard partial molal properties to 1000 °C and 5 kbar. *J. Chem. Soc. Farad. Trans.* 88, 803-826.
- Shock, E. L., Sassani, D. C., Willis, M., and Sverjensky, D. A., 1997. Inorganic species in geologic fluids: Correlations among standard molal thermodynamic properties of aqueous ions and hydroxide complexes. *Geochim. Cosmochim. Acta* 61, 907-950.
- Svanberg, K., 2002. A class of globally convergent optimization methods based on conservative convex separable approximations. *SIAM J. Optim.* 12, 555-573.
- Sverjensky, D., Shock, E., Helgeson, H., 1997. Prediction of the thermodynamic properties of aqueous metal complexes to 1000 C and 5 kb. *Geochim. Cosmochim. Acta* 61, 1359-1412.
- Tagirov, B.R., Zotov, A.V., Akinfiev, N.N., 1997. Experimental study of dissociation of HCl from 350 to 500°C and from 500 to 2500 bars: Thermodynamic properties of HCl⁰(aq). *Geochim. Cosmochim. Acta* 61, 4267-4280.
- Tagirov, B., Schott, J., 2001. Aluminum speciation in crustal fluids revisited. *Geochim. Cosmochim. Acta* 65, 3965-3992.
- Tanger, J.C., Helgeson, H.C., 1988. Calculation of the thermodynamic and transport properties of aqueous species at high pressures and temperatures: Revised equations of state for the standard partial molal properties of ions and electrolytes. *Amer. J. Sci.* 288, 19-98.
- Thomas, J.B., Watson, E.B., Spear, F.S., Shemella, P.T., Nayak, S.K., Lanzirrotti, A., 2010. TitaniQ under pressure: the effect of pressure and temperature on the solubility of Ti in quartz. *Contrib. Mineral. Petrol.* 160, 743-759.
- Verdes, G., Gout, R., Castet, S., 1992. Thermodynamic properties of the aluminate ion and of bayerite, boehmite, diaspore and gibbsite. *Eur. J. Mineral.* 4, 767-792.
- Vlcek, J., Luksan, L., 2006. Shifted limited-memory variable metric methods for large-scale unconstrained minimization. *J. Computat. Appl. Math.* 186, 365-390.
- Wagner, T., Kulik, D.A., Hingerl, F.F., Dmytrieva, S.V., 2012. GEM-Selektor geochemical modeling package: TSolMod library and data interface for multicomponent phase models. *Can. Mineral.* 50, 1173-1195.
- Westall, J.C., Zachary, J.L., Morel, F.M.M., 1976. MINEQL: A computer program for the calculation of chemical equilibrium composition of aqueous systems. *Inst. of Technol., Cambridge*.
- Wilson, C., Seward, T., Allan, A., Charlier, B., Bello, L., 2012. A comment on: 'TitaniQ under pressure: the effect of pressure and temperature on the solubility of Ti in quartz', by Jay B. Thomas, E. Bruce Watson, Frank S. Spear, Philip T. Shemella, Saroj K. Nayak and Antonio Lanzirrotti. *Contrib. Mineral. Petrol.* 164, 359.
- Worley, B., Powell, R., 2000. High-precision relative thermobarometry; theory and a worked example. *J. Metam. Geol.* 18, 91-101.
- Xu, T., Spycher, N., Sonnenthal, E., Zhang, G., Zheng, L., Pruess, K., 2011. TOUGHREACT Version 2.0: A simulator for subsurface reactive transport under non-isothermal multiphase flow conditions. *Comp. Geosci.* 37, 763-774.
- Zhang, F., Yeh, G.T., Parker, J.C. (Eds.), 2012. *Groundwater Reactive Transport Models*. Behtham Publishers, 254 p.
- Zhou, T., Dong, G., Phillips, G. N., 1994. Chemographic analysis of assemblages involving pyrophyllite, chloritoid, chlorite, kaolinite, kyanite, quartz; application to metapelites in the Witwatersrand goldfields, South Africa. *J. Metam. Geol.* 12, 655-666.

2A. Application of GEMSFITS for multi-parameter optimization in the C-S-H-N-K aqueous solid solution systems

Dmitrii A. Kulik^a, **George D. Miron**^b, Barbara Lothenbach^c

^aLaboratory for Waste Management, Paul Scherrer Institut, 5232 Villigen PSI, Switzerland

^bInstitute of Geochemistry and Petrology, ETH Zurich, Switzerland

^cLaboratory for Concrete and Construction Chemistry, Empa, Switzerland

2A.1. Introduction

C-S-H (calcium silicate hydrate) is the main phase of hydrated Portland cement, blended or alkali activated cements systems. C-S-H is “glue” in mortar and concrete, and it is also a major buffer against degradation of cements where it can sorb significant amount of alkalis and can take up other elements such as aluminium. C-S-H is a gel-like phase of variable composition and typically shows incongruent solubility upon carbonation or decalcification. Concentrations of dissolved Si and Ca vary strongly with the calcium to silicon (Ca/Si) ratio of the solid, as shown in many experimental investigations of the solubility of synthetic C-S-H (cf. Walker et al., 2015; Lothenbach and Nonat, 2015).

Several thermodynamic models describing the C-S-H solubility trends have been developed, starting from simple empirical fits up to structurally consistent solid solution models (Kulik, 2011). Understanding of the incorporation of aluminium and alkali in C-S-H is important for improving the solid solution models for thermodynamic predictions of composition and alteration of hydrated cements. However, the experimental data on solubility and sorption in C-S-H systems containing K, Na and Al have long been incomplete and partly controversial.

Recent systematic experimental studies on the uptake of aluminium, alkali and anions on the C-S-H composition and water uptake have been carried out in various laboratories (L’Hopital, 2014; Lothenbach and Nonat, 2015). The obtained datasets need to be converted into a consistent thermodynamic framework. Therefore, we aimed at developing a structurally consistent multi-site solid solution model for C-S-H that would integrate not only alkali- and aluminium uptake, but also its effects on volume and density under moderate temperature changes (7 to 80 °C). Due to complexity of the multi-site solid solution models having 10 or more parameters to be adjusted at the same time, this is hardly possible without application of dedicated methods and software for calculation of equilibria in complex aqueous-solid solution systems (GEM-Selektor and GEMS3K codes (Kulik et al., 2013) with TSolMod library of solution models (Wagner et al., 2012)) and for multiple parameter optimization (the GEMSFITS code (Miron et al., 2015)).

2A.2. The CASHNK multi-site solid solution model

Our new multi-site solid solution model, CASHNK, takes advantage of the presently available understanding of C-S-H tobermorite-like structure, extending and refining earlier solid solution models (Kulik and Kersten, 2001; Lothenbach and Winnefeld, 2006; Kulik 2011; Myers et al., 2014). The spectroscopic data (L’Hopital, 2014; Renaudin et al., 2009) and molecular dynamic simulations (Pegado et al., 2014) suggest that in C-S-H structure (Fig. A2.1, Table A2.1) substitutions may simultaneously occur within three different sublattice sites.

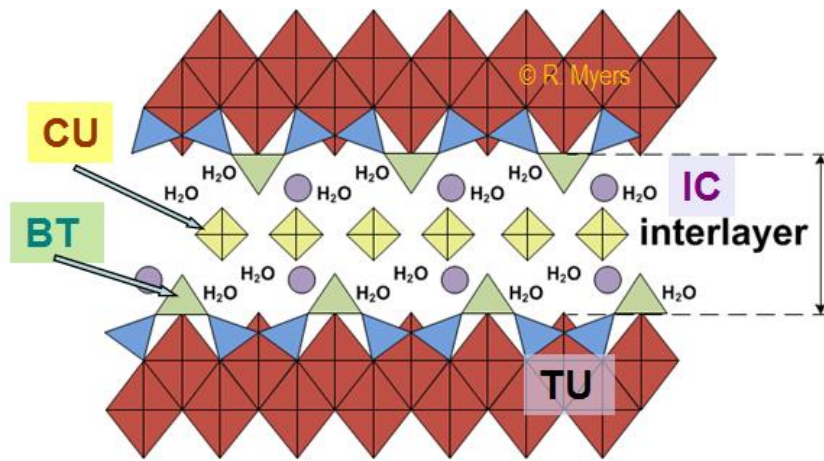


Figure A2.1. Structural sites (sublattices) C-S-H tobermorite-like structure (after Myers et al., 2014).

Table A2.1. Sites and substituting moieties defining the CASHNK solid solution model.

Sublattices (sites):	TU (tobermorite dimeric unit)	IC (interlayer cation exchange)	BT (bridging tetrahedral unit)	CU (additional Ca unit)
Moieties (species); their one-letter codes	$\text{Ca}_2\text{Si}_2\text{O}_5(\text{OH})_4$	T (H_3O) ₂ CaH_2O $\text{AlOH}(\text{H}_2\text{O})_2$ (NaH_2O) ₂ (KH_2O) ₂	H C A N K SiO_2 Va AlOOH	S v A Va $\text{Ca}(\text{OH})_2$ AlOOH v

Va (v) denotes vacancies (different moieties on different sublattices). Charges on IC moieties (+2) and on TU unit (-2) are not shown because they cancel out in any CASHNK compound. The number of H_2O molecules in IC moieties is chosen in accord with the data on density and water content in C-S-H at 25 % relative humidity (Muller et al., 2013).

As seen in Table A2.1, the SiO_2 moiety can only be substituted in BT sites, whereas Ca can be substituted in IC and CU sites, and Al – in BT, IC and CU sites. Vacancies in the BT sublattice define the defect-tobermorite structure. All possible end members can be generated by combining one moiety for each sublattice (45 end members in total, including 8 for C-S-H without Al, Na and K; 27 for C-A-S-H). For easier identification, each moiety is coded with one letter (Table A2.1). For instance, the least-calcium-rich end member with $\text{Ca}/\text{Si} = 0.67$ is THSv , $\{(\text{H}_3\text{O})_2\}$: $\{\text{SiO}_2\}$: $\{\text{Va}\}$: $[\text{Ca}_2\text{Si}_2\text{O}_5(\text{OH})_4]$. In this formula, colons separate sublattices with substitutions, and moieties are taken in braces. The ‘T’ moiety is the same for all end members and, for this reason, it is kept at the end of the end-member compound formula. The THSv compound formally has the infinite silicate “dreierketten” chain length CL (as any other tobermorite-like compound with ‘S’ or ‘A’ moiety in the BT sublattice). Any compound with a vacancy ‘v’ in the BT sublattice has $CL = 2$. The mean chain length MCL can be estimated by summation of all dimeric end member mole fractions x_{j2} (Kulik, 2011):

$$MCL = 3 / \sum_{j_2} x_{j_2} - 1 \quad (\text{A2.1})$$

which allows CASHNK solid solution models to describe both stability/solubility and structural changes in C-S-H phases.

A multi-site solid solution with two or more sublattices and two or more moieties substituted on each sublattice is called *reciprocal*. This term can be understood using the simplest two-site solid solution phase {A,B}{X,Y} (e.g. Wood and Nicholls, 1978; Hillert, 1998). All possible compositions can be represented on a ‘composition square’ made of end members AX, BX, AY, BY. However, only three of them are needed to describe any bulk composition of this phase. For instance, the center of the square can be obtained by mixing equal amounts of either AX and BY or AY and BX, hence the name ‘reciprocal’. Any three of four end members can be declared as ‘independent’, while the remaining one will be ‘dependent’ because all its properties can be obtained from those of ‘independent’ end members and that of a reciprocal reaction (rr)



with a standard molar Gibbs energy effect

$$\Delta_{rr}G^{\circ} = G^{\circ}_{AX} + G^{\circ}_{BY} - G^{\circ}_{AY} - G^{\circ}_{BX} \quad (\text{A2.3})$$

The chemical potential of the j-th end-member is represented as:

$$\mu_j = G^{\circ}_j + RT \ln x_j + RT \ln \lambda_j + RT \ln f_j + RT \ln \gamma_j \quad (\text{A2.4})$$

where $\ln x_j$ is the mole fraction; f_j is the activity coefficient due to excess Gibbs energy; $\ln \lambda_j = \ln a_j^{(con)} - \ln x_j$; $a_j^{(con)}$ is the ideal part of activity related to the configurational entropy (Price, 1985); and γ_j is the reciprocal activity coefficient, which is unity (ideal behaviour) for all end members if and only if $\Delta_{rr}G^{\circ} = 0$ for all possible reciprocal reactions. For the above example of {A,B}{X,Y} solid solution, one can derive (Wood and Nicholls, 1978)

$$RT \ln \gamma_{AX} = -y_B y_Y \Delta_{rr}G^{\circ} \quad RT \ln \gamma_{BY} = -y_A y_X \Delta_{rr}G^{\circ} \quad (\text{A2.5})$$

$$RT \ln \gamma_{AY} = +y_B y_X \Delta_{rr}G^{\circ} \quad RT \ln \gamma_{BX} = +y_A y_Y \Delta_{rr}G^{\circ} \quad (\text{A2.6})$$

where y_A, y_B are the site fractions of A or B on the first sublattice, and y_X, y_Y – that of X or Y on the second sublattice (they can be easily computed from end-member mole fractions). From the above equations, reciprocal non-ideality terms appear to reflect the energies of interaction upon simultaneous substitutions in two sublattices. This formalism of reciprocal reactions can be extended for the case when more than two moieties substitute on each of two sublattices; the number of end members and especially reciprocal reactions dramatically increases in such cases.

It is difficult to apply reciprocal reactions to solid solutions with simultaneous substitutions in three or more sublattices. Fortunately, Sundman and Ågren (1981) suggested a method for computing reciprocal activity coefficient terms in this general case. We have implemented this method in TSolMod library in addition to calculation of configurational terms and substitution interaction terms implemented earlier (Wagner et al., 2012). Now, the GEMS3K code can compute all terms in chemical potentials of end members, and, thus, rigorously model complex mixing in solid solutions like the CASHNK. Accordingly, all input parameters (G° same notation as $\Delta_f G_{298,1}^{\circ}$ values of end members, interaction parameters) can be optimized using the GEMSFITS code in their multiplicity.

To represent intra-site non-ideal interactions for substitutions of moieties (indexed with m) on sublattices (indexed with s), the approach of Berman and Brown (1984), Berman (1990) is applied because of its relative simplicity and compatibility with the ‘petrologic’ style of defining end members with more than one moiety on a sublattice site.

Ideal contribution to the end member (indexed with j) activity used in a sublattice model of k -th phase:

$$a_j^{(con)} = \prod_s \prod_m \left(y_{s,m} \frac{\eta_s}{\eta_{j,s,m}} \right)^{\eta_{j,s,m}}, \quad m \in M_k \quad s \in \Xi_k \quad j \in L_k \quad (\text{A2.7})$$

is common to Berman’s and CEF (Compound Energy Formalism) approach, with a CEF (Hillert, 2001) limitation that $\eta_{j,s,m} = \eta_s$ for any end member, as in the present CASHNK model. Here, η_s is the *site multiplicity*, and $\eta_{j,s,m}$ is a ‘moiety-site multiplicity’, i.e. the number of moles of m -th moiety on s -th site in one mole of j -th end member.

The non-ideal interaction contribution of moieties on sublattice sites to j -th end-member activity is defined as the sum of respective sublattice contributions:

$$RT \ln f_j = \sum_s f_{j,s}, \quad s \in \Xi_k \quad (\text{A2.8})$$

$$f_{j,s} \equiv RT \sum_m \ln \gamma_{j,s,m} \quad (\text{A2.9})$$

$$RT \ln \gamma_{j,s,m} = y_{j,s,m}^o \sum_t y_d y_e y_f W_{def,s} \left(Q_{s,m} \frac{y_{j,s,m}^o}{y_{s,m}} - \Theta \right), \quad t \in W_s \quad (\text{A2.10})$$

where the index m refers only to moieties that are present on s -th site in j -th end member; $Q_{s,m}$ is the number of d, e, f subscripts equal to m (0, 1 or 2); Θ is the order of interaction (symmetric: 1; asymmetric: 2); and W_s is the subset of indexes p of entries in the list of interaction parameters that refer to s -th sublattice. The $d, e,$ or f subscript can be an index m of any moiety that exists on the s -th site. Hence, $W_{def,s}$ is the interaction parameter for a particular combination of moieties substituting each other on the s -th site. The T, P dependence of the interaction parameter is represented by three coefficients $a, b,$ and c (J,K,bar):

$$W = a - b \cdot T + c \cdot P \quad (\text{A2.11})$$

In the case of symmetric interaction, the f subscript does not exist, and above equations take the form:

$$RT \ln \gamma_{j,s,m} = y_{j,s,m}^o \sum_t y_d y_e W_{de,s} \left(Q_{s,m} \frac{y_{j,s,m}^o}{y_{s,m}} - 1 \right), \quad t \in W_s \quad (\text{A2.12})$$

For the asymmetric interactions,

$$RT \ln \gamma_{j,s,m} = y_{j,s,m}^o \sum_t y_d y_e y_f W_{def,s} \left(Q_{s,m} \frac{y_{j,s,m}^o}{y_{s,m}} - 2 \right), \quad t \in W_s \quad (\text{A2.13})$$

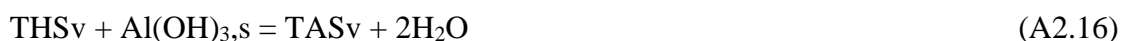
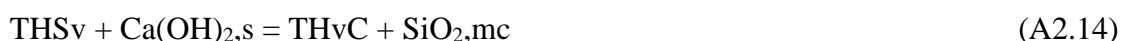
where either d and e or e and f indexes refer to the same moiety on s -th site in the case of a pseudo-binary interaction, and all three indexes are different in a ternary interaction.

So far, this approach ignores cross-site interactions (which at least partially can be accounted for by using the reciprocal terms), to some extent considered in the excess energy terms in CEF (Compound energy formalism) approach (Sundman and Agren, 1981; Hillert, 1988, 2001).

The resulting CASHNK multi-site solid solution model is flexible, structurally plausible, and can be rigorously described using the Compound Energy Formalism (Hillert 2001) with the thermodynamic properties computed using the GEM Software. The difficulty is that such a multi-

site model requires many end members, most of which do not exist in pure state, and probably many site interaction parameters. This necessitates (i) the systematic prediction of initial thermodynamic properties of end members from their composition, and (ii) the usage of an advanced GEM input parameter optimization tool such as the GEMSFITS code (Miron et al., 2015).

The initial thermodynamic dataset for 45 end members of the CASHNK model, consistent with the PSI-Nagra 12/07 and Cemdata'14 TDBs, was generated as follows. Two end members – THSv and TCvv – were selected as reference compounds, with standard thermodynamic properties at 1 bar, 25 °C obtained, respectively, by upscaling those of TobH and T2C end-members of the CSH3T solid solution model (Kulik, 2011) without the gel-water content. Standard properties of other end member compounds were derived from exchange reactions like



and so on, assuming zero effects of reaction ($\Delta_r G^\circ=0$, $\Delta_r S^\circ=0$, $\Delta_r Cp^\circ=0$, $\Delta_r V^\circ=0$), and all zero standard properties of vacancy Va. Properties of the following compounds were used: from Cemdata and PSI-Nagra databases - $\text{Ca(OH)}_{2,s}$ – portlandite (CH); $\text{Al(OH)}_{3,s}$ – gibbsite; H_2O – water; from (Wagman et al., 1982): solid $\text{KOH}_{,s}$ and $\text{NaOH}_{,s}$; by simultaneous adjustment to typical low-Ca C-S-H solubility data $[\text{Ca}]=1.6\text{e-}3$ M and $[\text{Si}]=3.8\text{e-}3$ M: THSv and $\text{SiO}_{2,mc}$ – microcrystalline silica. Calculations were performed using the ReacDC module of GEM-Selektor v.3.2. We assumed the uncertainty of such initial estimates of standard Gibbs energy per mole G° of end members in about 50 kJ/mol, except 10 kJ/mol for THSv and TCvv end members.

2A.2. Parameterization of multi-site solid-solution models of C-S-H with alkali and aluminium contents

Our CASHNK multi-site (sublattice) solid solution model aims to describe the effect of aluminium and alkali sorption on C-S-H solubility and structure. It is based on a defect-tobermorite structure, in which three sites (interlayer IC, bridging tetrahedra BT, and additional calcium unit CU) with substitutions of Ca, K, Na, Si, Al moieties or vacancies can be identified (Lothenbach and Nonat, 2015). All end members were generated by permutation of moieties on their respective structural sites. Such apparently complex solid solution models with many end-members and many site interaction parameters, easily computed with the GEM software, can reproduce stability and water content of C-S-H, as well as its structural properties such as MCL (mean chain length). The objective was to obtain a consistent thermodynamic data set for the CASHNK model by stepwise multi-parameter optimization for sub-models against selected C-S-H solubility datasets and known trends in MCL or in Al distribution between structural sites as functions of Ca/Si ratio in C-S-H. Such a demanding parameterization effort would not be possible without a dedicated software tool GEMSFITS (Miron et al. 2015), developed as part of in-house GEM software

(<http://gems.web.psi.ch>). The following strategy was used in fitting the solid solution model against the available data.

- (1) Start with the C-S-H sub-system (initial G° of 8 end members) with zero interaction parameters; proceed with fitting G° values of end members against the C-S-H solubility and MCL data, then fine-tune the model by optimizing the on-site interaction parameters. Keep all parameters fitted at this step fixed in subsequent parameterization stages.
- (2) Extend the C-S-H sub-system to C-S-H-K by adding 4 potassium-containing end members; fit G° values of these end members to available solubility data, then fine-tune interaction parameters, if necessary.
- (3) Apply the same procedure as at Stage 2 to derive the C-S-H-N sub-system with added 4 sodium-containing end members. Keep all parameters optimized at steps 1 to 3 fixed in subsequent parameterization stages.
- (4) Step back to the C-S-H sub-system and extend it to C-A-S-H system by adding 19 Al-containing end members; adjust G° values of 19 end members to solubility data, then fine-tune the interaction parameters; check against the available MCL data, solubility and aluminium speciation data in GEM-Selektor trial calculations.
- (5) Merge C-S-H-K and C-A-S-H sub-systems and extend it to C-A-S-H-K sub-system by adding 5 end members that simultaneously contain Al and K; adjust G° values of these end members and newly-added interaction parameters to the available solubility data.
- (6) Merge C-S-H-N and C-A-S-H sub-systems and extend it to the C-A-S-H-N sub-system by adding 5 end members that simultaneously contain Al and Na; adjust G° values of these newly-added end members and newly-added interaction parameters to the available solubility data.
- (7) Verify the parameterized CASHNK solid solution model by forward modelling of C-A-S-H-N-K solubility in various sub-systems; if needed, adjust the interaction parameters between K and Na moieties.

In the following, we illustrate this strategy by stage (1), which involves optimization of 11 parameters to obtain an internally consistent thermodynamic dataset for the CSH sub-model of the CASHNK solid solution model.

At this step of GEMSFITS parameterization, we used the following experimental C-S-H solubility datasets:

CH04D: “Curve C^w” or double decomposition data (Chen et al., 2004);

ELH: C-S-H co-precipitation data (L’Hopital et al., 2014);

Haas: Data from (Haas and Nonat, 2015; Haas, 2012).

The trends in all three datasets are very similar, common to C-S-H obtained by co-precipitation synthesis methods. The least-square objective function included M parts as follows (cf. Miron et al., 2015):

$$\min(\text{total } \Sigma_{res}) = \sum_{q=1}^M w_q F_q \quad (\text{A2.18})$$

where F_q is the q -th sum of residuals, w_q is the weight coefficient related to q -th part of the objective function, and

$$F_q = \sum_{i=1}^N w_{q,i} w_i w_{Tu,i} (y_{q,i} - f_{q,i})^2 \quad (\text{A2.19})$$

where N is the number of experimental samples; $f_{q,i}$ is the q -th property computed for i -th experimental sample; $y_{q,i}$ is the q -th property measured in i -th experimental sample; $w_{q,i}$ is the weight coefficient related to (input) error of measured q -th property value in i -th sample; w_i is the individual (input) weight coefficient for i -th sample; and $w_{Tu,i}$ is the Tuckey biweight coefficient to suppress the outliers (see Miron et al., 2015, eq. 4). By default, all weight multipliers equal to 1. In this work, the samples weights $w_i = 1$ were used if not stated otherwise, and $w_{q,i}$ weights were calculated (the *inverr3* option) as

$$w_{q,i} = 1/y_{q,i}^2 \quad (\text{A2.20})$$

The objective function was constructed from $M = 4$ parts (Table A2.2).

Table A2.2: Setup of objective function for C-S-H fitting steps using the global or local optimization.

q	$y_{q,i}$ (measured)	$f_{q,i}$ (computed)	w_q (step 1)	w_q (step 2)	w_q (step 3)	w_q (step 4)
1	$\log_{10}m(\text{Ca}_{\text{AQ}})$	$\log_{10}m(\text{Ca}_{\text{AQ}})$	1	1	1	1
2	$\log_{10}m(\text{Si}_{\text{AQ}})$	$\log_{10}m(\text{Si}_{\text{AQ}})$	1	1	1	0.3
3	$n(\text{Ca})/n(\text{Si})$ in C-S-H	$n(\text{Ca})/n(\text{Si})$ in CSH	1	1	0.1	0.1
4	MCL (restored NMR)	MCL from eq (1)	0.001	1	0.1	0.3

The overall quality of the fit for each individual experimental dataset is defined by the normalized root mean square error (NRMSE):

$$\text{NRMSE} = \sqrt{\frac{\sum_i^N [y(i) - f(i)]^2}{\sum_i^N y(i)^2}} \quad (\text{A2.21})$$

where y_i represent the measured (experimental) value, f_i is the calculated value, and N is the number of experiments. The mean chain length was calculated from the mole fractions of dimeric end members using eq (1). In the GEMSFITS task definition, MCL is calculated from GEM output as:

$$\text{"expr": "3/sum(\{TCvC\}, \{TCvv\}, \{THvC\}, \{THvv\}) - 1"} \quad (\text{A2.22})$$

where braces denote mole fractions of the respective end members.

Based on a striking similarity of C-S-H solubility data for samples obtained by co-precipitation or double-decomposition methods, the CH04D, ELH and Haas datasets were taken together. Of 62 samples in total, 2 were excluded as outliers ("4k", "4j" from the CH04D dataset).

At the first round of fitting, we used the global fitting method GN_ESCH (genetic evolutionary algorithm) with relative and absolute tolerances of 0.01 and maximum 2000 loops.

At *step 1*, the only 8 freely adjustable parameters were the G_{298}^0 values of all 8 end members of the CSH phase (all interaction parameters W in the Berman model were zeroed off). The lower

bounds (LB) for G°_{298} values of all end members except THSv were set 50 kJ/mol more negative than initial values (IV) taken from Table A2.5; the upper bounds (UB) for G°_{298} values of all end members except THSv were set 50 kJ/mol more positive than initial values (IV). For the THSv end member, UB was set 10 kJ/mol more positive and LB – 10 kJ/mol more negative than the initial value. The MCL part ($q=4$) of the objective function was suppressed by setting its weight to $w_4 = 0.001$.

From the fitting results (not shown), it was evident that the fit for Ca_{AQ} is good, for Si_{AQ} is reasonable (too high at target $\text{C/S} > 0.9$); and the fit for MCL was bad at $0.75 < \text{C/S} < 1.3$.

Conversely, to improve the MCL fit, i.e. the structural consistency of the sublattice solid solution model of CSH, the objective function must include the MCL data with the high weight $w_4 \geq 0.1$, comparable to that for the solubility data. However, the ^{29}Si MAS NMR data from which the MCL data was derived are scarce and not available for all samples in all datasets. Fortunately, the available MCL data plot very well into the same trend as function of Ca/Si ratio in C-S-H for all three co-precipitation datasets (Fig. A2.2).

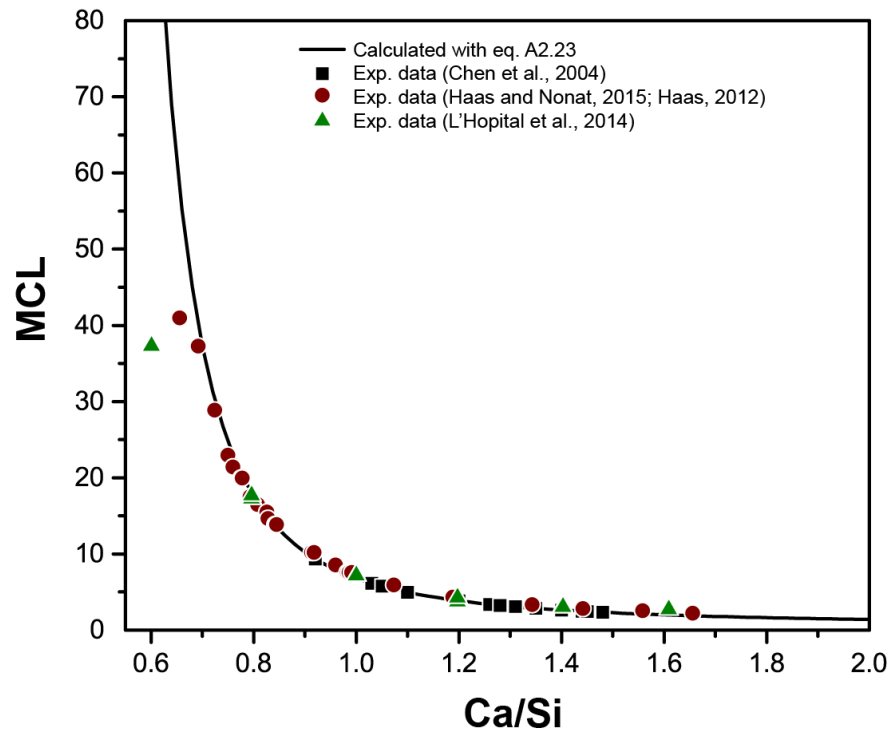


Figure A2.2. MCL data plotted against Ca/Si ratio in C-S-H. MCL-fit is the curve of eq. (A2.23). Scattered symbols denote the experimental data sets.

Keeping in mind that the MCL data result from deconvolution of NMR peaks and, thus, are not very precise, we have regressed the data from Chen et al. 2004 and L'Hopital, 2014 (using the SigmaPlot software) with an exponential decay function

$$MCL = (0.391 \pm 0.083) \exp \frac{(2.302 \pm 0.267)}{c/s - (0.195 \pm 0.035)} \quad (\text{A2.23})$$

where C/S stands for the Ca/Si ratio in C-S-H. With this function, which fits the measured MCL data well, the MCL values were restored for all data points in all three experimental datasets, and then used in the fourth part of the objective function (Table A2.2) as the “regressed” MCL data.

At **step 2**, to improve the fit for MCL, the previous GEMSFITS task was cloned into another task where the default weight $w_4 = 1$ was restored, and run with the same global algorithm and settings as in step 1. The results of this exercise showed a perfect fit for the MCL data, but bad fit for both Ca and Si solubility data. Clearly, the solid solution model without the excess Gibbs energy terms cannot fit well the solubility and the MCL trend at the same time. To prepare an initial dataset for local fitting runs and for introducing the G_{ex} interaction parameters, the fitted G° values were compared, and their averages were taken as initial values, with the bounds UB (upper bound) and LB (lower bound) taken slightly greater as half-differences.

At **step 3**, the GEMSFITS task was cloned into a new task, and the initial values for G°_{298} of end members were taken from fitted values from step 2, with LB values set as (IV – 10 kJ/mol), and UB values as (IV + 10 kJ/mol). $G^\circ_{298} = -851.0$ kJ/mol was set for SiO_2, am phase to improve the convergence of the optimization. The weight for the MCL part was set to intermediate value $w_4 = 0.1$.

The model was fitted at this stage with the local LN_BOBYQA optimization algorithm (with initial parameter values obtained from global fitting steps and parameter brackets of 10 kJ/mol), using the asymmetric or the symmetric Berman model for excess Gibbs energy of mixing (in GEM-Selektor v.3.2 implementation) on top of the sublattice model with reciprocal terms. As there are two substituting moieties per structural site in the CSH model, and cross-site interaction parameters are not permitted, this leads to six interaction parameters of the asymmetric model (Table A2.3) or three interaction parameters of the symmetric model (Table A2.4).

Table A2.3. Site interaction parameters (Berman) for the CSH asymmetric model of mixing.

Sublattice	Site index s	Interaction parameter	Name in GEMSFITS	Interacting moieties		
IC	0	$W_{\text{HHC},0}$	CSH[0 0]	H_2OH^+	H_2OH^+	
		$W_{\text{HCC},0}$	CSH[1 0]	H_2OH^+	$\text{H}_2\text{OCa}^{2+}$	$\text{H}_2\text{OCa}^{2+}$
BT	1	$W_{\text{SSv},1}$	CSH[2 0]	SiO_2	SiO_2	Va
		$W_{\text{Svv},1}$	CSH[3 0]	SiO_2	Va	Va
CU	2	$W_{\text{CCv},2}$	CSH[4 0]	$\text{Ca}(\text{OH})_2$	$\text{Ca}(\text{OH})_2$	Va
		$W_{\text{Cvv},2}$	CSH[5 0]	$\text{Ca}(\text{OH})_2$	Va	Va

Table A2.4. Site interaction parameters (Berman) for the CSH symmetric model of mixing.

Sublattice	Site index s	Interaction parameter	Name in GEMSFITS	Interacting moieties
IC	0	$W_{\text{HC},0}$	CSH[0 0]	H_2OH^+ $\text{H}_2\text{OCa}^{2+}$
BT	1	$W_{\text{Sv},1}$	CSH[1 0]	SiO_2 Va
CU	2	$W_{\text{Cv},2}$	CSH[2 0]	$\text{Ca}(\text{OH})_2$ Va

Comparison of fits with symmetric and asymmetric Berman model shows that they are of the same (good) overall quality, although the symmetric model yields slightly worse fit of MCL data but better fit for dissolved Ca_{AQ} concentrations. This fact allows considering the symmetric non-ideality (with binary parameters) as the basis for further extension of the CSH model because of less number of fitting parameters.

Parameters fitted for symmetric case (Table A2.5) were entered into GEM-Selektor project CASHNK, and forward Process calculations were performed to test the quality and performance of the parameterized CSH model. It was found that a strong smoothing parameter (s.p. 0.001 or less) is required in GEM calculations to obtain smooth curves of end-member properties (the bulk properties of the whole phase and solubility curves were smooth even at much larger smoothing parameter of 0.01; no convergence at s.p. ≥ 0.1). The results are shown in Fig. A2.3.

Table 2A.5. Initial and fitted parameters of the CSH multi-site solid solution sub-model.

Parameter, end member	Initial estimate (kJ/mol)	Fitted value (kJ/mol)	Confidence interval 95% (MC)	Sensitivity	Fitted – Initial (kJ/mol)
G_{298}° TCSC	-6205.14	-6225.45	4.45	55.5	-20.31
G_{298}° TCSv	-5308.13	-5328.42	2.54	83.5	-20.29
G_{298}° TCvC	-5354.53	-5336.29	7.51	59.1	18.24
G_{298}° TCvv	-4457.51	-4456.72	0.50	148.0	0.79
G_{298}° THSC	-6014.85	-6042.95	0.66	352.1	-28.1
G_{298}° THSv	-5117.84	-5124.53	0.25	316.3	-6.69
G_{298}° THvC	-5164.24	-5155.60	1.34	109.2	8.64
G_{298}° THvv	-4267.22	-4264.86	0.41	318.1	2.36
$W_{\text{HC},0}$	0	-2.29	0.95	0.66	-2.29
$W_{\text{Sv},1}$	0	-10.77	0.75	1.11	-10.77
$W_{\text{Cv},2}$	0	-19.28	1.32	0.95	-19.28

Monte Carlo (MC) sampling was performed in 300 trials (see details in Miron et al., 2015).

Evidently, the optimization of 11 parameters has led to good fits to both solubility and MCL data (with reasonable estimates of density and non-gel water content of C-S-H – not shown). From

Table A2.5, it can be seen that the initial estimates of thermodynamic properties of end-members (and initial zero interaction parameters), in fact, have much smaller uncertainty (20 - 30 kJ/mol or less) than initially assumed uncertainty 50 kJ/mol used in global fitting steps. In Fig. A2.3C one can see peaks at mole fractions of THSC and THvv endmembers around Ca/Si = 0.96 of about equal height. Because THSC corresponds to chain length of infinity and THvv to chain length of 2, the MCL is close to 5 in accord with the assumed ordering in C-S-H corresponding to the T5C endmember of the earlier CSH3T model of C-S-H solid-solution (Kulik, 2011, Table A2.3).

Table A2.6. Aqueous speciation at bulk Ca/Si = 1.6.

Species	Log ₁₀ (molal)	%Ca, aq	%Si, aq
Ca ⁺²	-1.7916	79.0900	
CaOH ⁺	-2.3718	20.7919	
CaHSiO ₃ ⁺	-7.0757	0.0004	0.3349
CaSiO ₃ , aq	-4.6191	0.1177	95.8475
HSiO ₃ ⁻	-6.1209		3.0183
SiO ₂ , aq	-8.8741		0.0053
SiO ₃ ⁻²	-6.7009		0.7939
N ₂ , aq	-3.1879		
O ₂ , aq	-5.8819		
OH ⁻	-1.4369		
H ⁺	-12.3867		

pH = 12.48, Ca_{aq, total} = 20.43 mm, Si_{aq, total} = 0.0251 mm. Note that in the GEMS database, CaSiO₂(OH)₂(aq) is represented as CaSiO₃, aq under assumption that $K = 1$ of the reaction $\text{CaSiO}_2(\text{OH})_2(\text{aq}) = \text{CaSiO}_3, \text{aq} + \text{H}_2\text{O}$.

Our structurally consistent model somewhat over-predicts the experimental data for dissolved Si at Ca/Si ratios above 1, as nearly all earlier C-S-H solubility models (Kulik, 2011; Lothenbach and Winnefeld, 2006). Inspection of aqueous speciation of silicon at bulk Ca/Si ratio about 1.6 (calculated with GEM-Selektor), Table A2.6, reveals that the predominant species at these conditions is CaSiO₃, aq complex.

Selection of data for this complex in PSI-Nagra database 12/07 (Hummel, 2014; Thoenen et al. 2014) is based on a single set of results of potentiometric titrations of Si(OH)₄(aq) in the presence of Ca²⁺ and Mg²⁺ in 1 M NaClO₄ up to pH 9 reported by (Santschi and Schindler, 1974). In this work, in order to avoid the formation of polymeric silicate species as well as the precipitation of amorphous silica, the total ligand concentration did not exceed $2.3 \cdot 10^{-3}$ M. In preliminary experiments it was found that the complexes formed are rather weak. Comparatively high concentrations of both the reacting metal ions and the inert salt were therefore required. The results of this experimental study are not unambiguous in terms of the speciation model. Based on chemical arguments, interpretation of the experimental data could be done in terms of two equilibria.



Leading to the values $\log_{10}K^0(\text{eq. A2.24}) = (1.2 \pm 0.1)$ and $\log_{10}K^0(\text{eq. A2.25}) = (4.6 \pm 0.2)$. Note that the underlying experimental data were obtained at $\text{pH} < 9$, although in pH region between 11.5 and 12.5 relevant for solubility of Ca-rich C-S-H, the $\text{CaSiO}_3, \text{aq}$ ($\text{CaSiO}_2(\text{OH})_2(\text{aq}) = \text{CaSiO}_3, \text{aq} + \text{H}_2\text{O}$) complex becomes really predominant. Therefore, the uncertainty of $\log_{10}K^0(\text{eq. A2.25})$ must be much greater than ± 0.2 and can only be reduced when new experimental data for Ca-Si complexation at pH between 9 and 13 become available.

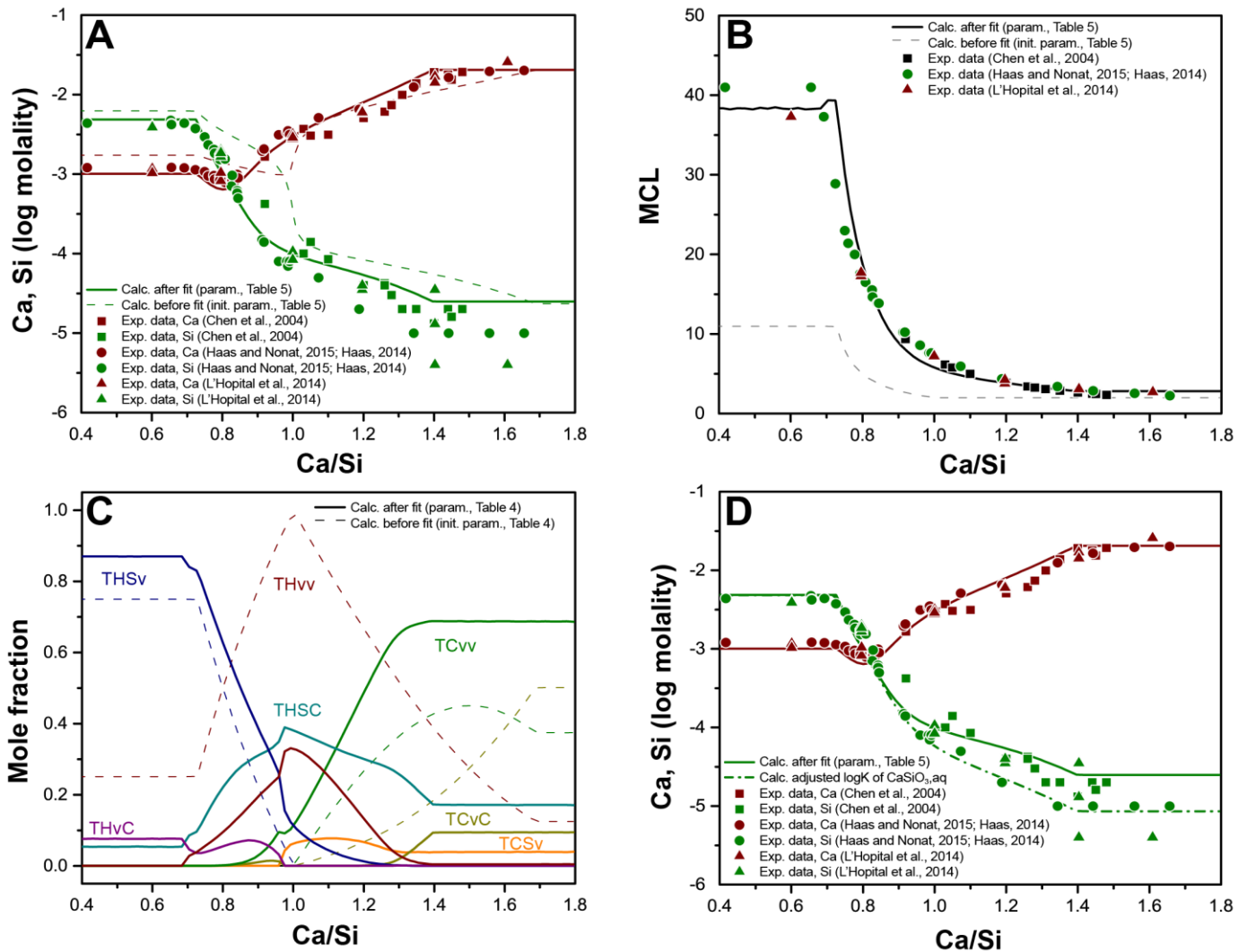


Figure A2.3. GEM-Selektor v.3 diagrams for the parameterized C-S-H model: A: solubility, B: MCL data, C: end-member mole fractions. Dotted curves correspond to the initial parameter values from Table A2.5; solid curves result from using the fitted parameter values. Panel D compares the same calculation with fitted parameters as in (A) (solid curves) and that with G°_{298} of the $\text{CaSiO}_3, \text{aq}$ aqueous complex corrected by +2.854 kJ/mol or -0.5 logK units less stable (dotted curves). Scattered symbols correspond to the same composite dataset of 60 co-precipitation samples that has been used in fitting exercises (data EL14, Chen04 and Haas14), including the regressed MCL data.

Indirect testing of a hypothesis that $\log_{10}K^{\circ}(\text{eq. A2.25}) = 4.6$ is too strong can be performed on our C-S-H aqueous – solid solution model against the available C-S-H solubility data.

A GEM speciation calculation at bulk Ca/Si = 1.6 (0.16 mol CH, 0.1 mol SiO₂, 1 kg H₂O, 1 mol N₂) at 1 bar, 25 C reveals (Table A2.6) that CaSiO_{3,aq} complex contains 96% of total dissolved Si, but only 0.12% of total dissolved Ca.

It is seen also that in this system (with stable CSH and portlandite), the total dissolved Si is about 2.5 times higher than typical experimental values about 0.01 mm. To fix this by adjusting the stability of CaSiO_{3,aq} complex, its initial $G^{\circ}_{298} = -1517.557$ kJ/mol was changed to $G^{\circ}_{298} = -1514.703$ kJ/mol by adding 2.854 kJ/mol or $-0.5 \log_{10}K$ units, and the speciation calculation was repeated (Table A2.7). Now the total dissolved Si is less than $1 \cdot 10^{-5}$ m, although the CaSiO_{3,aq} complex is still predominant with 88%. The impact of such correction on the C-S-H solubility diagram is seen on Fig. A2.3D. We also tried the adjustment of G°_{298} of CaHSiO₃⁺ by 0.5 $\log_{10}K$ units, but this had no visible effect on the solubility diagram of C-S-H (Fig. A2.3A) because at pH above 9.7 this complex remains insignificant.

At **step 4**, we undertook one more fitting exercise with GEMSFITS to see how the adjustment of stability of the CaSiO_{3,aq} complex can improve the overall fit of the CSH solid solution model against the solubility data. The fitting task was cloned from that used at step 3, and the initial $G^{\circ}_{298} = -1517.557$ kJ/mol of CaSiO_{3,aq} was adjusted (by 1.5 to 3.0 kJ/mol). In a series of calculations, we found that the optimal fit can be achieved at $G^{\circ}_{298} = -1515.845$ kJ/mol (1.713 kJ/mol more positive, or 0.3 pK units). The results are given in Fig. A2.4 and Table A2.8.

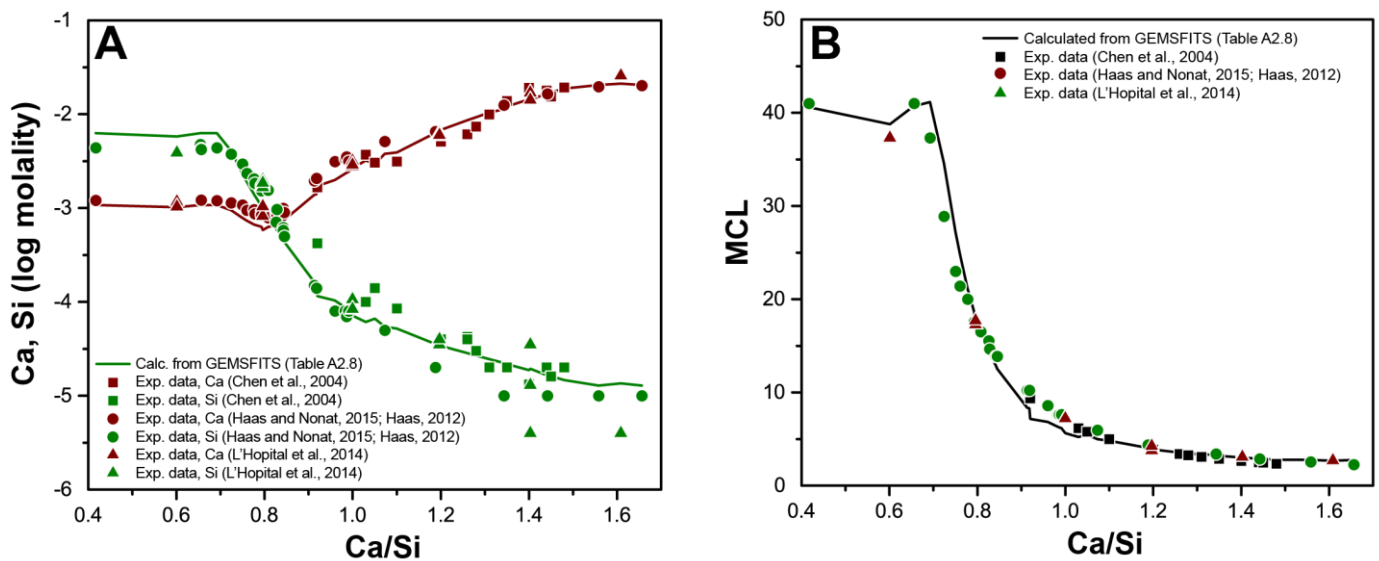
Table A2.7. Speciation at bulk Ca/Si = 1.6 with G°_{298} of CaSiO_{3,aq} corrected by +2.854 kJ/mol (0.5 pK).

Species	lg(molal)	%Ca, aq	%Si, aq
Ca ⁺²	-1.7917	79.1563	
CaOH ⁺	-2.3720	20.8061	
CaHSiO ₃ ⁺	-7.0756	0.0004	0.9719
CaSiO _{3, aq}	-5.1190	0.0373	87.9479
HSiO ₃ ⁻	-6.1207		8.7609
SiO _{2, aq}	-8.8737		0.0155
SiO ₃ ⁻²	-6.7008		2.3038
N _{2, aq}	-3.1879		
O _{2, aq}	-5.8819		
OH ⁻	-1.4370		
H ⁺	-12.3866		

pH = 12.48, Ca_{aq, total} = 20.41 mm, Si_{aq, total} = 0.00865 mm

Table A2.8. Initial (from Table A2.5) and re-adjusted parameters of the CSH sub-model.

Parameter, end member	Initial estimate (kJ/mol)	Fitted value (kJ/mol)	Confidence interval 95% (MC)	Sensitivity	Fitted – Initial (kJ/mol)
G°_{298} TCSC	-6225.45	-6225.68	1.807	111.9	-0.23
G°_{298} TCSv	-5328.42	-5327.71	1.207	142.5	0.71
G°_{298} TCvC	-5336.29	-5335.98	7.234	72.3	0.31
G°_{298} TCvv	-4456.72	-4456.67	0.598	202.5	0.05
G°_{298} THSC	-6042.95	-6042.74	0.314	794.8	0.21
G°_{298} THSv	-5124.53	-5124.59	0.273	421.5	-0.06
G°_{298} THvC	-5155.60	-5155.01	1.021	185.9	0.59
G°_{298} THvv	-4264.86	-4265.12	0.237	819.9	-0.26
$W_{HC,0}$	-2.29	-3.27	0.888	1.99	-0.98
$W_{SV,1}$	-10.77	-10.78	0.328	1.74	-0.01
$W_{CV,2}$	-19.28	-19.56	0.633	2.10	-0.28

**Figure A2.4.** GEMSFITS plots for the re-parameterized C-S-H model (Table 8): A: solubility (in log molal units), B: MCL data.

2A.3. Conclusions

This worked example of simultaneous fitting of 11 parameters of the CSH sub-model of the sublattice CASHNK model shows the efficiency of GEMSFITS code in obtaining internally consistent thermodynamic datasets by using various kinds of experimental and spectroscopic data. The description in this chapter covers only the first stage of the multi-stage fitting process, described in full in other manuscripts (Kulik, Miron, Lothenbach, 2016, in preparation).

In parallel, the fitting results show that the stability constant of the CaSiO_3,aq ($\text{CaSiO}_2(\text{OH})_2,\text{aq}$) aqueous complex as given in the PSI-Nagra 12/07 database is about 0.3 to 0.5 pK units too high. Reconsideration of experimental data (Santschi and Schindler, 1974) shows that at $\text{pH} < 9$ the neutral species, CaSiO_3,aq , is minor and its stability as determined in eq. A2.25 is quite uncertain. It turns out that the C-S-H solubility data at $\text{Ca/Si} > 1$ can be the only source to constrain the stability of this species (to make it 0.3 – 0.4 pK units less stable, to $\log_{10}K^0 = 4.3 \pm 0.4$ in eq. A2.25) in fitting the aqueous solid-solution models of C-S-H.

References

- Berman RG (1990). Mixing properties of Ca-Mg-Fe-Mn garnets. *Am. Mineral.* 75, 328–344.
- Berman RG, Brown TH (1984). A thermodynamic model for multi-component melts, with application to the system $\text{CaO-Al}_2\text{O}_3\text{-SiO}_2$. *Geochim. Cosmochim. Acta* 45 661–67.
- Chen J.J., Thomas J.J., Taylor H.F.W., Jennings H.M. (2004). Solubility and structure of calcium silicate hydrate. *Cement and Concrete Research* 34, 1499-1519.
- Haas, J., 2012. Etude expérimentale et modélisation thermodynamique du système $\text{CaO-SiO}_2\text{-(Al}_2\text{O}_3\text{)-H}_2\text{O}$. Université de Bourgogne, Dijon, France, pp. 183.
- Haas, J., Nonat, A., (2015). From C–S–H to C–A–S–H: Experimental study and thermodynamic modeling, *Cement and Concrete Research* 68, 124-138.
- Hillert, M. (1998). Phase equilibria, phase diagrams and phase transformations: Their thermodynamic basis. Cambridge Univ. Press, Cambridge.
- Hillert M. (2001). The compound energy formalism. *J. Alloys and Compounds* 320, 161–176.
- Hummel, W., Berner, U., Curti, E., Pearson, F.J., Thoenen, T. (2002). Nagra/PSI Chemical Thermodynamic Data Base 01/01. Nagra Technical Report NTB 02-16, Nagra, Wetingen, Switzerland, and Universal Publishers, Parkland, Florida, 565 pp.
- Hummel, W. (2014). The PSI/Nagra Chemical Thermodynamic Database 12/07 (Update of the Nagra/PSI TDB 01/01): Data Selection for Silicon. PSI Technical Report TM-44-12-05, Paul Scherrer Institut, Villigen, Switzerland, 40 pp.
- Karpov I.K., Chudnenko K.V., Kulik D.A., Avchenko O.V., Bychinskii V.A. (2001). Minimization of Gibbs free energy in geochemical systems by convex programming. *Geochem. Internat.* 39, 1108-1119.
- Kulik D.A. (2011). Improving the structural consistency of C-S-H solid solution thermodynamic models. *Cement and Concrete Research* 41, 477-495.
- Kulik D.A., Kersten M. (2001). Aqueous solubility diagrams for cementitious waste stabilization systems: 2. End-member stoichiometries of ideal calcium silicate hydrate solid solutions. *J. Amer. Ceram. Soc.* 84, 3017-3026.
- Kulik D.A., Wagner T., Dmytrieva S.V., Kosakowski G., Hingerl F.F., Chudnenko K.V., Berner U. (2013). GEM-Selektor geochemical modeling package: revised algorithm and GEMS3K numerical kernel for coupled simulation codes. *Computat. Geosci.* 17, 1-24.
- L'Hopital E. (2014). Aluminium and alkali uptake in calcium silicate hydrates (C-S-H), PhD Thesis, EPFL, Oct.2, 2014.
- Lothenbach B., Winnefeld F. (2006). Thermodynamic modelling of the hydration of Portland cement. *Cement and Concrete Research* 36, 209-226.
- Lothenbach, B., Nonat, A., (2015). Calcium silicate hydrates: Solid and liquid phase composition. *Cem. Con. Res.* 78, Part A, 57-70.
- Miron G.D., Kulik D.A., Dmytrieva S.V., Wagner T. (2015). GEMSFITS: Code package for optimization of geochemical model parameters and inverse modeling. *Applied Geochemistry* 55, 28-45.

- Muller, A.C.A., Scrivener K.L., Gajewicz A.M., McDonald P.J. (2013). Use of bench-top NMR to measure the density, composition and desorption isotherm of C–S–H in cement paste. *Microporous and Mesoporous Materials*, 178, 99-103.
- Myers R.J., Bernal S.A., Provis J.L. (2014). A thermodynamic model for C-(N-)A-S-H gel: CNASH_{ss}. Derivation and validation. *Cement and Concrete Research* 66, 27-47.
- Pegado L., Labbez C., Churakov S.V. (2014). Mechanism of aluminium incorporation into C–S–H from ab initio calculations. *J. Mater. Chem. A* 2, 3477- 3483.
- Price J.G. (1985). Ideal site mixing in solid solutions, with an application to two-feldspar geothermometry. *Amer. Mineral.* 70, 696-701.
- Renaudin G., Russias J., Leroux F., Cau-Dit-Coumes C., Frizon F. (2009). Structural characterization of C–S–H and C–A–S–H samples - Part II: Local environment investigated by spectroscopic analyses. *J. Solid State Chemistry* 182, 3320-3329.
- Santschi, P.H. and Schindler, P.W. (1974). Complex formation in the ternary systems Ca-H₄SiO₄-H₂O and Mg-H₄SiO₄-H₂O. *Journal of the Chemical Society, Dalton Transactions*, 181-184.
- Sundman B., Ågren J. (1981). A regular solution model for phases with several components and sublattices, suitable for computer applications. *J. Phys. Chem. Solids* 42, 297-301.
- Thoenen, T., Hummel, W., Berner, U. and Curti, E. (2014). The PSI/Nagra Chemical Thermodynamic Database 12/07. Paul Scherrer Institut, Villigen PSI, Switzerland.
- Wagman D.D., Evans W.H., Parker V.B., et al. (1982). The NBS tables of chemical thermodynamic properties. Selected values for inorganic and C1 and C2 organic substances in SI units. *J. Phys. Chem. Ref. Data* 11, Suppl. 2.
- Wagner T., Kulik D.A., Hingerl F.F., Dmytrieva S.V. (2012). GEM-Selektor geochemical modeling package: TSolMod library and data interface for multicomponent phase models. *Canadian Mineralogist* 50, 1173-1195.
- Walker, C. S., Sutou, S., Oda, C., Mihara, M., Honda, A., (2016). Calcium silicate hydrate (C-S-H) gel solubility data and a discrete solid phase model at 25 °C based on two binary non-ideal solid solutions, *Cement and Concrete Research* 79, 1-30.
- Wood B.J., Nicholls J. (1978): The thermodynamic properties of reciprocal solid solutions. *Contrib. Mineral. Petrol.* 66, 389-400.

3. Internally consistent thermodynamic data for aqueous species in the system Na-K-Al-Si-O-H-Cl

George D. Miron^{a, c}, Thomas Wagner^b, Dmitrii A. Kulik^c, Christoph A. Heinrich^a

^aInstitute of Geochemistry and Petrology, ETH Zurich, Switzerland, dan.miron@erdw.ethz.ch

^bDepartment of Geosciences and Geography, University of Helsinki, Finland

^cLaboratory for Waste Management, Paul Scherrer Institut, 5232 Villigen PSI, Switzerland

Accepted: *Geochimica et Cosmochimica Acta*

Date: 18 April 2016

Abstract

A large amount of critically evaluated experimental data on mineral solubility, covering the entire Na-K-Al-Si-O-H-Cl system over wide ranges in temperature and pressure, was used to simultaneously refine the standard state Gibbs energies of aqueous ions and complexes in the framework of the revised Helgeson-Kirkham-Flowers equation of state. The thermodynamic properties of the solubility-controlling minerals were adopted from the internally consistent dataset of Holland and Powell (2002; Thermocalc dataset ds55). The global optimization of Gibbs energies of aqueous species, performed with the GEMSFITS code (Miron et al., 2015), was set up in such a way that the association equilibria for ion pairs and complexes, independently derived from conductance and potentiometric data, are always maintained. This was achieved by introducing reaction constraints into the parameter optimization that adjust Gibbs energies of complexes by their respective Gibbs energy effects of reaction, whenever the Gibbs energies of reactant species (ions) are changed. The optimized thermodynamic dataset is reported with confidence intervals for all parameters evaluated by Monte Carlo trial calculations. The new thermodynamic dataset is shown to reproduce all available fluid-mineral phase equilibria and mineral solubility data with good accuracy and precision over wide ranges in temperature (25 to 800°C), pressure (1 bar to 5 kbar) and composition (salt concentrations up to 5 molal). The global data optimization process adopted in this study can be readily repeated any time when extensions to new chemical elements and species are needed, when new experimental data become available, or when a different aqueous activity model or equation of state should be used. This work serves as a proof of concept that our optimization strategy is feasible and successful in generating a thermodynamic dataset reproducing all fluid-mineral and aqueous speciation equilibria in the Na-K-Al-Si-O-H-Cl system within their experimental uncertainties. The new dataset resolves the long-standing discrepancies between thermodynamic data of minerals and those of aqueous ions and complexes, by achieving an astonishing degree of consistency between a large number of fluid-mineral equilibrium data. All of this at the expense of changing the standard state properties of aqueous species, mainly the Gibbs energy of formation. Using the same strategy, the core dataset for the system Na-K-Al-Si-O-H-Cl can be extended with additional rock-forming elements such as Ca, Mg, Fe, Mn, Ti, S, C, B. In future, the standard-state properties of minerals and aqueous species should be simultaneously optimized, to create the next-generation of fully internally consistent data for fluid-mineral equilibria. Although we employ the widely used HKF equations for this study, the same computational approach can be readily applied to any other speciation-based equation of state for multicomponent aqueous solutions.

3.1. Introduction

Fluid-rock reactions play a key role in a wide range of geological processes such as mass transfer and hydrothermal convection at mid-ocean ridges, melting and fluid transfer in subduction zones, metamorphic devolatilization in compressional orogenic belts, the formation of hydrothermal ore deposits, and fluid circulation and permeability evolution in natural and engineered geothermal reservoirs. Detailed insight into fluid-rock reactions can be gained from quantitative field studies, high-temperature and -pressure laboratory experiments, and numerical geochemical and reactive transport simulations. Geochemical modeling combined with experimental studies of the equilibrium solubility of minerals and mineral assemblages are essential for constraining the transport capacity of natural aqueous fluids, for evaluating mass fluxes in fluid-rock systems, and for understanding reaction progress during hydrothermal alteration (e.g. Helgeson, 1969; Reed, 1982; Engi, 1992; Stefánsson, 2001; Zhu and Anderson, 2002; Anderson, 2005; Bénézech et al., 2009; Sverjensky, 2014).

Numerical reactive transport modeling is a powerful approach for simulating geochemical processes in natural fluid-rock systems (e.g. Lichtner et al., 1997; Xu et al., 2001; Steefel and Maher, 2009; Zheng et al., 2009; Xu et al., 2011; Leal et al., 2014; Zhang et al., 2015), which are inaccessible to direct field studies and too complex for controlled laboratory experimentation. Reactive transport models rely critically on the robustness of the geochemical models and, hence, on the availability, accuracy, precision and consistency of parameters such as standard state properties of minerals and aqueous species, equilibrium constants for solubility reactions, activity and equation of state parameters for non-ideal multicomponent phases (mineral solid-solutions, aqueous solutions, fluid and gas mixtures), and kinetic rate constants for mineral dissolution and precipitation (Engi, 1992; André et al., 2006; Schott et al., 2009; Thien et al., 2014).

Considerable progress in the thermodynamic description of minerals and their solid-solutions at high temperatures and pressures has been driven by the development of internally consistent thermodynamic datasets (Holland and Powell, 1985; Powell and Holland, 1985; Berman et al., 1986; Berman, 1988; Chatterjee et al., 1994; Gottschalk, 1997; Chatterjee et al., 1998; Holland and Powell, 1998; Holland and Powell, 2011). Typically, properties of minerals and fluids that are known from high-precision experiments or sufficiently accurate estimation techniques (Berman and Brown, 1985; Holland, 1989) such as heat capacity, molar volume, thermal expansion and compressibility, are accepted without further modification, and only enthalpies of formation (and sometimes entropies) as the most critical and least accurately known parameters are refined during the global fitting process.

If changes are applied to the formation Gibbs energies of mineral endmembers, adjustments of similar magnitude should be applied to the Gibbs energies of formation of the respective aqueous ions and complexes, to maintain the internal consistency. Adjustment of aqueous species data should be done in a simultaneous manner, by considering numerous mineral solubility experiments and always taking care that the complex electrolyte association equilibria known from conductance, electromotive force or spectroscopic experiments are maintained. However, aqueous electrolyte fluids at elevated temperatures and pressures have never been subject to any

simultaneous derivation of internally consistent data, because such fitting needs to combine very diverse types of experimental data including mineral solubility as well as direct fluid property measurements. Instead, all thermodynamic databases commonly used for aqueous geochemistry, such as SUPCRT92 (Johnson et al., 1992; Shock et al., 1997; Sverjensky et al., 1997), the LLNL database (Delany and Lundeen, 1990), and the FreeGs database (Bastrakov et al., 2005), are based on sequential evaluation of individual solubility equilibria or fitting of a few selected reactions (Pokrovskii and Helgeson, 1995, 1997a, b).

As a consequence, large discrepancies between modeled and experimentally determined mineral solubilities and speciation equilibria may persist in these datasets. Paradoxically, the situation is becoming worse, because the mineral data present in the geochemical databases have since been refined by new algorithms and simultaneous fitting against solid-solid phase equilibria experiments but without including mineral solubility (Holland and Powell, 1998; Holland and Powell, 2011). Prominent examples illustrating these discrepancies are the large mismatch between predicted and measured fluid compositions in the feldspar-mica-quartz system (Montoya and Hemley, 1975; Popp and Frantz, 1980; Gunter and Eugster, 1981; Sverjensky et al., 1991; Haselton et al., 1995), substantial disagreement between calculated and accurately measured carbonate mineral solubility products (Bénézech et al., 2009, 2011), and the poor description of ion association equilibria of major aqueous electrolytes such as HCl, KCl, NaOH, KOH and CaCl₂ (Tagirov et al., 1997; Ho and Palmer, 1996, 1997; Ho et al., 2001; Méndez de Leo and Wood, 2005). Reasons that have prevented developing internally consistent datasets for aqueous and hydrothermal geochemistry are the strong interrelation between standard state and activity model data (Helgeson et al., 1981), limitations in computational techniques and capacities required for the global fitting of very large datasets, and the uneven distribution of high-precision experimental data in temperature – pressure – composition space.

The body of experimental data for fluid-rock equilibria has grown considerably since the last concerted effort by Helgeson et al. (1981), Tanger and Helgeson (1988), Johnson et al. (1992), Sverjensky et al. (1997), and Shock et al. (1997). Of particular importance are high-precision experimental studies of electrolyte association using conductance methods. The experimental studies have covered most of the major aqueous electrolytes that are present in natural geofluids such as NaCl, KCl, HCl, NaOH, and KOH (Ho et al., 1994; 2000a, 2000b, 2001; Ho and Palmer, 1996, 1997). The experiments were conducted with modern high-precision static and flow-through conductance instruments using very dilute salt solutions, which makes the derived ion pair association constants largely independent of the aqueous activity model that was used. In addition, these studies used improved and theoretically sound conductance models for data processing, which resulted in much more reliable and accurate equilibrium constants (Sharygin et al., 2001, 2002). The speciation equilibria for the most important constituents of natural geofluids are now well constrained by high-quality experimental data that cover wide ranges in temperature and pressure.

Connecting the thermodynamic properties of aqueous species with those of the rock-forming minerals requires experimental data for mineral solubility in aqueous solutions. A large amount of

solubility measurements under crustal conditions at temperatures and pressures up to 600 °C and 10 kbar has been accumulated, including the solubility of rock-forming oxides, silicates, aluminosilicates and carbonates in pure water, aqueous salt solutions and H₂O-CO₂ mixtures. New solubility experiments of corundum and aluminum hydroxides (Bénézeth et al., 2001; Palmer et al., 2001), quartz (Manning, 1994; Newton and Manning, 2000; Shmulovich et al., 2001) and aluminosilicates (Shinohara and Fujimoto, 1994; Haselton et al., 1995; Manning et al., 2010; Wohlers et al., 2011) have become available. Most importantly, phase equilibria experiments have been performed in the multicomponent system Na-K-Al-Si-O-H-Cl at temperatures and pressures up to 650 °C and 2 kbar, involving the solubility of synthetic metapelite (K-feldspar, albite, aluminosilicate, quartz) in moderately saline aqueous solutions (Hauzenberger et al., 2001; Pak et al., 2003).

In summary, it is timely to develop a new approach to derive the first internally consistent thermodynamic dataset for fluid-rock equilibria that will resolve the discrepancies of the existing data. Our long-term vision is to develop a fully consistent dataset that covers at least the system Na-K-Ca-Fe-Mg-Mn-Al-Si-Ti-C-S-Cl-F-B-O-H, with possible extension to important ore metals and other trace elements. This dataset should simultaneously describe all experimentally determined mineral reaction equilibria, solubility measurements, spectroscopic data, and potentiometric and conductance constraints on aqueous speciation within experimental accuracy. As a first step towards that vision, we derive in this study an internally consistent dataset of the thermodynamic properties for aqueous species in the core system Na-K-Al-Si-O-H-Cl by simultaneously refining the standard state molal Gibbs energies of aqueous ions and complexes utilizing a large database of critically evaluated solubility, conductance and potentiometric experiments that cover a wide range in temperature, pressure and composition. The properties of the aqueous ions and complexes are derived using the Holland-Powell mineral dataset (Holland and Powell, 1998) as a given basis. The mineral properties from this dataset are assumed to be fully consistent and no adjustments were allowed to their thermodynamic properties. The dynamic approach to dataset regression makes it possible to repeat the procedure whenever new and improved experimental constraints become available or when more aqueous species and chemical elements are added.

3.2. Thermodynamic framework

The standard state convention for aqueous species adopted in this study is the ideal one molal solution referenced to infinite dilution. For water solvent, the standard state is pure water at any pressure and temperature, and water activity is based on the mole fraction concentration scale. For minerals, the standard state is unit activity of pure solids at any pressure or temperature (Oelkers et al., 1995). The standard partial molal Gibbs energies applied for aqueous species in this study are the apparent standard partial molal Gibbs energies, defined as (Helgeson et al., 1981):

$$\Delta G_{T,P}^0 = \Delta_f G_{T_r,P_r}^0 + (G_{T,P}^0 - G_{T_r,P_r}^0) \quad (3.1)$$

where $\Delta_f G_{T_r, P_r}^0$ represents the standard state partial molal Gibbs energy of formation (at reference temperature $T_r = 298.15$ K and reference pressure $P_r = 1$ bar) of the substance from the elements at their standard states at 298.15 K and 1 bar, and $(G_{T, P}^0 - G_{T_r, P_r}^0)$ represents the difference in the standard partial molal Gibbs energy of the substance at the temperature (T) and pressure (P) of interest and that at the reference temperature (T_r) and pressure (P_r).

The molar properties of minerals in this study were calculated from the Holland-Powell internally consistent thermodynamic dataset (Holland and Powell, 1998; updated Thermocalc 2002 dataset ds55) and the thermodynamic framework of this dataset. This dataset is referred to as HP02 in the remainder of this paper. The Gibbs energy of minerals at elevated temperatures and pressures is calculated by temperature integration of a 4-term heat capacity equation and pressure integration of a Murnaghan equation of state for molar volume. For phases with order-disorder transitions, a Landau model term is added (Holland and Powell, 1998). The following minerals were used during regression of solubility data: albite, andalusite, corundum, diaspore, kaolinite, kyanite, microcline, muscovite, nepheline, paragonite, pyrophyllite, quartz, sanidine, sillimanite, and topaz. The thermodynamic data for these minerals can be found in the electronic supplementary material (Table 3.EA1). Recently, a new updated mineral dataset has been published (Holland and Powell, 2011), but we have preferred to use the previous dataset because it is supported by comprehensive solid-solution models for all relevant rock-forming minerals (feldspars, micas, amphibole, chlorite, pyroxene, epidote etc.) and the data for key minerals of the system Na-K-Al-Si-O-H-Cl are more consistent with calorimetric constraints and the aqueous species data (Holland and Powell, 1998; Dolejs and Wagner, 2008). This results in smaller adjustments to the standard state properties of aqueous species during regression of the large body of experimental solubility data in this study.

Thermodynamic properties of water were calculated with the IAPS-84 equation of state (Kestin et al., 1984). The calculated Gibbs energies of H₂O liquid using this model were compared with the values calculated using the compensated Redlich-Kwong (CORK) model that is used in the HP02 dataset (Holland and Powell, 1991). The standard Gibbs energy per mole of H₂O calculated using the CORK model is slightly more positive than that calculated using IAPS-84 (in the range of 100-1000 °C and 1 bar to 5 kbar) with an average difference of 130 ± 90 J/mol. This difference is considerably smaller than the uncertainty of the experimental data that were used to derive both equations of state (Kestin et al., 1984; Holland and Powell, 1991) and thermodynamic properties predicted from both models are fully consistent with each other.

The properties of aqueous species were modeled within the framework of the revised Helgeson-Kirkham-Flowers (HKF) equation of state (Helgeson and Kirkham, 1974a, 1974b; Tanger and Helgeson, 1988; Shock et al., 1992). The HKF equation of state accounts for solvation and non-solvation properties of aqueous ions and complexes. The thermodynamic properties are calculated from $\Delta_f G_{298,1}^0$, $S_{298,1}^0$ and seven empirical coefficients ($a_1, a_2, a_3, a_4, c_1, c_2, \omega_0$), which describe the temperature and pressure dependence of partial molal volume and heat capacity. HKF equation of state parameters were derived for a large number of aqueous species by regression of experimentally determined equilibrium constants, volume and heat capacity data (Tanger and Helgeson, 1988; Shock and Helgeson, 1988; Shock et al., 1989; Shock et al., 1997; Sverjensky et

al., 1997; Sverjensky et al., 2014). Subsequently, empirical correlations between the partial molal properties were developed and used to predict the properties of a large number of aqueous species for which no or insufficient experimental data are available (Shock and Helgeson, 1988; Shock et al., 1989; Sassani and Shock, 1992; Shock et al., 1997; Sverjensky et al., 1997; Plyasunov and Shock, 2001; Sverjensky et al., 2014). These data were incorporated into the SUPCRT92 dataset (Johnson et al., 1992), which has become a de facto standard in geochemical modeling. We therefore use the SUPCRT92 dataset as a reference when comparing the calculations with our new dataset with experimental mineral solubility and phase stability data.

The activity coefficients for charged aqueous species were calculated with the extended Debye-Hückel equation (Helgeson et al., 1981):

$$\log_{10} \gamma_j = \frac{-A_\gamma z_j^2 \sqrt{I}}{1 + \overset{\circ}{a} B_\gamma \sqrt{I}} + b_\gamma I + \log_{10} \frac{n_{jw}}{n_w} \quad (3.2)$$

where A_γ and B_γ represent the Debye-Hückel solvent parameters, $\overset{\circ}{a}$ stands for the ion size parameter, b_γ is a semi-empirical extended term parameter, I represents the true ionic strength (corrected for ion pairing and complexing), and the last term represents the conversion from mole fraction to molality (with n_{jw} being the mole amount of water solvent, and n_w the total mole amount of the aqueous phase including water-solvent). In the model of Helgeson et al. (1981), $\overset{\circ}{a}$ and b_γ are common for all charged aqueous species in the predominant electrolyte. Revised models that account for the temperature and pressure dependence of b_γ for the four major background electrolytes (NaCl, KCl, NaOH, KOH) (Oelkers and Helgeson, 1990; Pokrovskii and Helgeson, 1995; Pokrovskii and Helgeson, 1997b; Pokrovskii and Helgeson, 1997a) were used in this study. In this model framework, the ion-size parameters are pressure and temperature dependent as well (Shock et al., 1992). The activity model is thought to be applicable for true ionic strengths up to 1-3 molal, but due to the formation of ion pairs with increasing temperature it can be used to total salt concentrations of up to 5 mol/kg (Oelkers and Helgeson, 1990; Sharygin et al., 2002; Dolejs and Wagner, 2008). For neutral species, the activity coefficient is assumed to be a linear function of the effective ionic strength:

$$\log_{10} \gamma_j = b_g I + \log_{10} \frac{n_{jw}}{n_w} \quad (3.3)$$

where b_g is the empirical Setchenow coefficient and is approximated to be equal to the common third parameter b_γ used for the charged species. The activity coefficient of water is calculated from the osmotic coefficient as in Helgeson et al. (1981):

$$\ln a_w = -\frac{\phi m_\Sigma}{55.508435} \quad (3.4)$$

where m_Σ is the sum of molalities of all aqueous species, and ϕ is the osmotic coefficient, calculated as in Helgeson et al. (1981).

An additional thermodynamic constraint was to retain the properties of the Cl^- ion as reported in Shock and Helgeson (1988). This was done because for each chemical element in an internally consistent thermodynamic dataset, one anchor substance is needed, whose thermodynamic

properties are accepted from calorimetric data (Holland and Powell 1990; 1998). Chlorine is a fluid volatile element and there are no chlorine-bearing silicate mineral phases in the HP02 dataset that would be suitable as anchor phases; the properties of halite (NaCl) in the HP02 dataset were adapted from Robie and Hemingway (1995) without being linked to other mineral phases by reaction equilibria. The standard state partial molal Gibbs energy, enthalpy, and entropy of Cl⁻ originate from the CODATA compilation (Cox et al., 1989) and were determined using electromotive force data at different temperatures (Bates and Kirschman, 1919; Bates and Bower, 1954; Cerquetti et al., 1968) and heat of solution data of gaseous hydrogen chloride (Vanderzee and Nutter, 1963). The values of the standard state partial molal heat capacity and volume of Cl⁻ were estimated by regressing standard partial molal volume, isothermal compressibility and isobaric heat capacity data (up to 100 °C) for aqueous HCl electrolyte solutions (Tanger and Helgeson, 1988), which were then used to derive the HKF parameters (Shock and Helgeson, 1988).

The H₂O dissociation constants calculated with the properties of the OH⁻ ion from the SUPCRT92 database differ by as much as 0.3-0.4 log units from those calculated from the density equation of Marshall and Franck (1981). However, the values for the H₂O dissociation constant calculated with the SUPCRT92 data are much closer to the data obtained from the new formulation by Bandura and Lvov (2006). This formulation is now recommended by the International Association for the Properties of Water and Steam as a replacement of the older formulation by Marshall and Franck (1981). The average deviation between the values calculated using the SUPCRT92 data for the OH⁻ ion and the formulation of Bandura and Lvov (2006) is better than 0.1 log units, which is well within the original experimental uncertainty. Consequently, we have retained the properties of the aqueous OH⁻ ion from the SUPCRT92 database.

3.3. Ion association properties of major electrolytes

Revision of the ion pair association constants for major electrolytes (NaCl, KCl, NaOH, KOH) was required due to many contradicting data and new high precision conductance experiments at high temperatures and pressures that became available since the major reviews by Sverjensky et al. (1997) and Shock et al. (1997). The partial molal standard state properties and HKF parameters of the neutral ion pairs NaCl⁰, KCl⁰, NaOH⁰, and KOH⁰ were refined using the OptimB optimization program (Shvarov, 2015), using equilibrium constants derived from recent conductance experiments. These experimental data have the advantage over the older datasets that the conductance was measured in very dilute solutions (Ho and Palmer 1997; Ho et al., 2000a, b; Ho et al., 2001; Sharygin et al., 2002; Zimmerman et al., 2007; Arcis et al., 2014) and that equilibrium constants were derived with more theoretically sound models for the conductivity of electrolyte solutions (Tagirov et al., 1997; Ho and Palmer 1997; Ho et al., 2000 a, b; Ho et al., 2001; Tagirov et al., 1997; Zimmerman et al., 2007; Plumridge et al., 2015). This makes the equilibrium constants retrieved from the conductance data largely independent from the aqueous activity model employed.

Table 3.1. Standard state properties (partial molal entropy, heat capacity and volume) and HKF parameters of neutral ion pairs derived from association constant data based on new conductance experiments.

Species	$S_{298,1}^0$ (J/mol·K)	$Cp_{298,1}^0$ (J/mol·K)	$V_{298,1}^0$ (J/bar)	$a_1 \cdot 10$ (cal/ mol/bar)	$a_2 \cdot 10^{-2}$ (cal/mol)	a_3 (cal·K /mol/bar)	$a_4 \cdot 10^{-4}$ (cal·K /mol)	c_1 (cal /mol/K)	$c_2 \cdot 10^{-4}$ (cal·K /mol)	$\omega_0 \cdot 10^{-5}$ (cal/mol)
⁽¹⁾ NaCl ⁰	110.8	47.5	2.4	5.0828	4.6290	3.9306	-2.9704	13.6339	-0.7212	0.0889
⁽¹⁾ NaOH ⁰	42.4	113.5	-0.022	1.7792	-3.4372	7.1010	-2.6369	22.8222	2.6543	0.1189
⁽¹⁾ KCl ⁰	182.16	33.32	2.99	5.8341	7.0550	2.9771	-3.0707	-5.7084	7.6228	0.1996
⁽¹⁾ KOH ⁰	90.6	41.46	1.41	3.7562	1.3900	5.2037	-2.8365	13.4990	-1.0192	0.1665
⁽²⁾ HCl ⁰	1.76	149.5	1.64	16.1573	-11.4311	-46.1866	-2.3036	46.4716	-5.2811	0.0000

⁽¹⁾ Optimized using association constant data.

⁽²⁾ Taken from Tagirov et al. (1997).

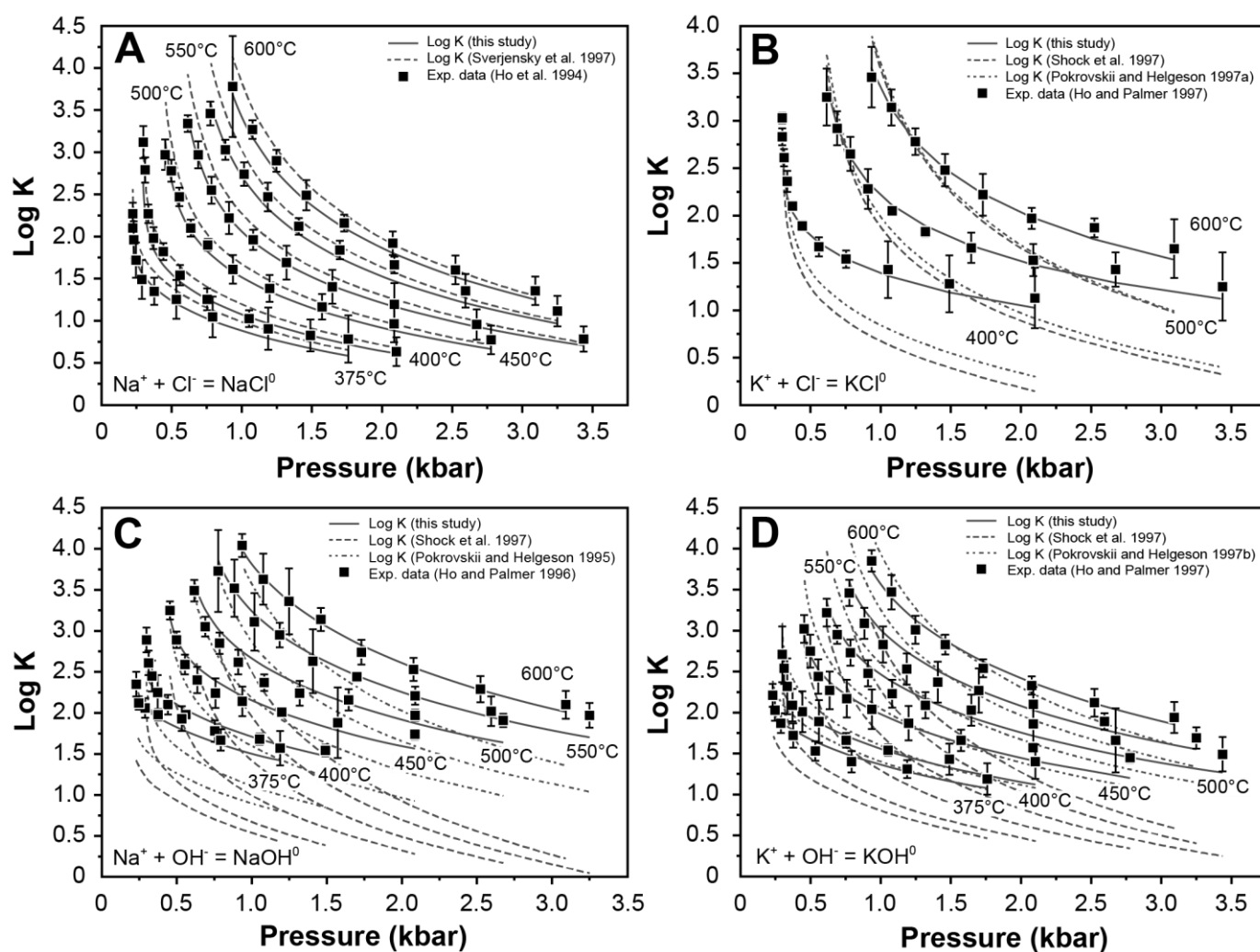


Figure 3.1. Comparison between calculated and experimentally determined (Ho et al., 1994; Ho and Palmer, 1996; Ho and Palmer, 1997) association constants for the major electrolytes (A) NaCl, (B) KCl, (C) NaOH and (D) KOH. Calculated association constants are from this study, the SUPCRT92 dataset (Shock et al., 1997; Sverjensky et al., 1997) and critical assessments of individual systems (Pokrovskii and Helgeson, 1995, 1997a, 1997b).

3.3.1. NaCl⁰ association constant

A considerable body of experimental data on the association constant of NaCl⁰ has become available that was not used in the data analysis by Sverjensky et al. (1997). The association constant of NaCl⁰ has been determined by high-precision conductance measurements of dilute aqueous NaCl solutions (with both a static and a flow-through cell) over wide ranges of temperature and pressure of 250-600 °C and 0.1-3.4 kbar (Ho et al., 1994, 2000a; Zimmermann et al., 1997; Gruskiewicz and Wood, 1997). In addition, the association constant has been derived from mean stoichiometric activity coefficients in the temperature interval 200-350 °C at saturated water vapor pressure (Plyasunov, 1988). We have obtained thermodynamic properties of NaCl⁰ from regression of the association constants based on the new conductance data only. The association constants calculated with the new thermodynamic properties of NaCl⁰ are fairly consistent with the ones derived in the supercritical region (400-800 °C, 0.5-4.0 kbar) by Oelkers and Helgeson (1988) from the older conductance data of Quist and Marshall (1969). Figure 3.1A shows a comparison

between the calculated values from this study, those calculated with the data from SUPCRT92 (Sverjensky et al., 1997), and the experimental data of Ho et al. (1994).

3.3.2. KCl^0 association constant

Substantial experimental datasets were published after the comprehensive data analysis presented by Sverjensky et al. (1997). The association constant of KCl^0 has been determined using high-precision conductance measurements (Ho and Palmer, 1997; Ho et al., 2000a) in the temperature range of 50-600 °C at pressures from saturated water vapor pressure (SWVP) to 3.4 kbar. In addition, association constants for KCl^0 were derived from mean stoichiometric activity coefficients in the temperature range 100-325 °C at saturated water vapor pressure (Pokrovskii and Helgeson, 1997a). The conductance data below 300 °C (Ho et al., 2000a) have a very large associated error and are inconsistent with those at higher temperatures. The association constants derived from mean stoichiometric activity coefficients at low temperatures were found to be inconsistent with the conductance data of Ho and Palmer (1997) and introduce larger errors in the properties of KCl^0 when included into the regression. Therefore, we have only considered dissociation constants derived from the conductance data above 300 °C for retrieving new thermodynamic properties of KCl^0 (Fig. 3.1B).

3.3.3. NaOH^0 association constant

The thermodynamic properties for NaOH^0 derived by Shock et al. (1997) are mainly based on few experiments at low temperatures and saturated water vapor pressure. Predictions of the association constants in the supercritical region at temperatures exceeding 400 °C are in gross disagreement with newer experimental data that extend to higher pressures and temperatures. The dissociation constant of NaOH^0 was recently determined using conductance measurements at temperatures of 100-600 °C and pressures of 0.1-3.1 kbar (Ho and Palmer, 1996; Ho et al., 2000b). Additional data were derived from mean stoichiometric activity coefficients in the temperature range 25-250 °C at saturation pressure (Pokrovskii and Helgeson, 1995) but, like in the case of KCl^0 , they introduce larger errors for the properties of NaOH^0 at supercritical conditions when fitted together with the conductance data. We have therefore retrieved thermodynamic properties of NaOH^0 from dissociation constants based on the conductance data above 300 °C (Fig. 3.1C).

3.3.4. KOH^0 association constant

The thermodynamic data for KOH^0 given by Shock et al. (1997) are essentially based on correlations and estimations. Pokrovskii and Helgeson (1997b) have obtained thermodynamic data for KOH^0 from regression of association constants that were derived from conductance measurements of Franck (1956) and Lukashov et al. (1975). The conductance models employed by Franck (1956) and Lukashov et al. (1975), which were used to extract the limiting equivalent conductance and association constants from the experiments, were shown to be very inaccurate compared to more recent studies (e.g., Ho et al., 2000b; Sharygin et al. 2001; Sharygin et al. 2002). Consequently, association constants in the supercritical region calculated with the models of Shock

et al. (1997) and Pokrovskii and Helgeson (1997b) are in considerable disagreement with the most recent experimental data. The association constants of KOH^0 were derived from high-precision conductance measurements in the temperature range 100-600 °C and at pressures of 0.14-3.4 kbar (Ho and Palmer 1997; Ho et al., 2000b). We have retrieved the thermodynamic properties of KOH^0 from regression of those new experimental data (Fig. 3.1D).

3.3.5. HCl^0 association constant

Based on the consideration of available datasets, we have concluded that the critical assessment of the properties of HCl^0 given by Tagirov et al. (1997) is the most consistent with the majority of experimental data, and we have accepted this dataset. The data that were derived by Tagirov et al. (1997) represent virtually all the experimental data available at the time when the evaluation was performed (e.g., Frantz and Marshall, 1984; Ruaya and Seward, 1987; Simonson et al., 1990; Sverjensky et al., 1991; Sretenskaya, 1992; Tagirov et al., 1997), except the experimental data points from Frantz and Marshall (1984) in the low-density region. Furthermore, the data from Tagirov et al. (1997) are in excellent agreement with recent potentiometric measurements by Reukov and Zotov (2006) and reasonably consistent with the new conductance measurements by Ho et al. (2001). Note that most of the experiments by Ho et al. (2001) were performed in the low-density region (350-400 °C, 0.26-0.31 kbar) where calculations using the revised HKF model are not accurate.

3.4. Selection of experimental solubility data

A large range of experimental mineral solubility datasets was reviewed prior to regression of the thermodynamic properties of aqueous species. Not all the experimental datasets could be used for fitting, because of mutual inconsistencies between different solubility datasets and, sometimes, insufficient documentation of the experimental conditions. The critical evaluation of experimental data was based on the following set of criteria:

(1) *Proof of attainment of equilibrium.* Preferred solubility experiments were the ones performed from both undersaturated and supersaturated conditions. In case where solubility equilibrium was only approached from undersaturated conditions, the documentation of the experimental conditions was carefully screened for sufficiently long run times and proper demonstration that indeed equilibrium solubility was measured.

(2) *Potential problems encountered during the experiments.* The documentation of the experimental conditions (where possible) was checked for possible reactions with the capsule or autoclave material, presence of contaminant phases or impurities in the reactants, or precipitation of mineral phases during quench.

(3) *Experimental and analytical methods.* The simplest way to perform solubility measurements is by the weight loss method, where only the weight loss of the reactant mineral is measured before and after the experiment (Morey et al., 1962; Manning, 1994). Using this method, it is impossible to demonstrate attainment of equilibrium from both undersaturated and

supersaturated conditions, but the problem is often addressed by investigating the required time for attainment of equilibrium or by comparison with reversed equilibrium experiments (Anderson and Burnham, 1965). The potentially largest source of error in weight loss experiments is mineral precipitation during the quench of the solutions (Manning, 1994). Therefore, experiments that use a fast quench method are preferred. Experimental settings that avoid problems due to quenching are the ones that extract the aqueous solution to be analyzed at run temperature and pressure. The analytical methods used for analyzing the elemental composition of the aqueous solutions can have a great impact on the accuracy of the measurements. Some elements, like aluminum, have very low concentrations under most experimental conditions studied. We have therefore preferred studies that demonstrate the reproducibility of measured dissolved element concentrations using different analytical techniques.

(4) *Consistency of the experiments.* The agreement between different independent measurements of the same quantity and the agreement between data obtained with different experimental methods served as an important selection criterion. In cases where many experimental studies have investigated one chemical system over the same range in pressure and temperature, it is critical that the reported values are consistent with each other within their stated uncertainty. However, the observation that several experimental datasets are consistent with each other while another dataset is not, is not a proof that the inconsistent dataset is the incorrect one. Therefore, our strategy was based on identifying at least one high quality dataset that would meet the strictest quality criteria (reversed equilibria, well documented experimental conditions and results, accurate analytical techniques) as a basis for evaluating the quality of other datasets. The high quality datasets would also need to show reasonably consistent trends in temperature, pressure and composition space and not a large scatter of the measured properties.

In a number of cases, the experimental uncertainty associated with the data is not specified, or it is difficult to assess. Commonly, the total error of the experiments does not account for the accuracy of the experimental conditions and the accuracy of the analytical methods. The selected high quality studies would always report the total errors, while others would not report them. For this reason, in our study the experimental errors could not be directly applied as weights in the optimization routine.

Due to the limitation of the revised HKF model (Tanger and Helgeson 1988) to pressures up to 5 kbar, only experiments at conditions equal or below 5 kbar were used during data regression (and experiments at pressures above 5 kbar are not considered in the following experimental data review). Sverjensky et al. (2014) proposed an extension of the HKF model to much higher pressures based on a different equation of state for water properties (Zhang and Duan, 2005) and an empirical expression for the dielectric constant of water valid up to 60 kbar. In their model, they used new correlations for the pressure dependence of the HKF parameters, as well as different speciation models for silica and aluminum including dimers and polymers that are needed for the high pressure systems. Understanding of the solubility and aqueous speciation of rock-forming elements at very high temperatures and pressures is still far from complete, and substantially more experimental data are needed to resolve some of the disagreements between different studies

(Audetat and Keppler, 2005; Antignano and Manning, 2008; Dolejs and Manning, 2010; Hayden and Manning, 2011; Mookherjee et al., 2014).

Because the extended Debye-Hückel activity model (Helgeson et al., 1981; Oelkers and Helgeson, 1990; Pokrovskii and Helgeson, 1995; Pokrovskii and Helgeson, 1997b; Pokrovskii and Helgeson, 1997a) used in our study is only valid up to salt concentrations of about 5 molal, experiments at higher concentrations (Sharygin et al., 2002) were excluded from the regression. A restriction of 2 and 3 molal for the calculated effective ionic strength was placed on experiments below and above 100 °C, respectively. Appelo et al. (2015) showed that the calculated activity coefficient for NaCl solutions starts to deviate from the measured values above 2 molal NaCl concentration at 25 °C. Nevertheless, we do compare the calculated mineral solubility data with their experimental counterparts at higher salt concentrations to evaluate the extrapolation capability of the thermodynamic model.

3.4.1. Quartz solubility

The solubility of quartz in water and salt solutions has been extensively studied over a wide range of pressure and temperature using various experimental methods and analytical techniques. A summary of the experimental datasets selected for the final database is presented in Table 3.2. These datasets were divided into three categories.

The first category contains experiments for which the authors demonstrated solubility equilibrium by approaching it both from undersaturated and supersaturated conditions (Morey et al., 1962; Crear and Anderson, 1971; Walther and Orville, 1983). These experiments involved the usage of pressure bombs or extraction-quench vessels and sampling of the solution in equilibrium with quartz at run conditions.

The second category of experiments were those where equilibrium was reached only from undersaturated conditions, but they employed (depending on the conditions) run times on the order of several days or even weeks (sufficient time to reach equilibrium). Equilibrated solution in these experiments was sampled at run conditions (Lier et al., 1960; Rimstidt, 1997) or for experiments above 100 °C after fast quenching (in less than 1 minute) (Siever, 1962; Hemley et al., 1980). Because of the slow dissolution rate of quartz, experiments at low temperatures require equilibration times on the order of many days, sometimes years (Rimstidt, 1997). Rimstidt (1997) studied the solubility of quartz at ambient conditions by analyzing the solution in equilibrium with quartz at 21 °C after more than 13 years. The thermodynamic data derived from these experiments are consistent with the ones obtained from amorphous silica solubility experiments widely investigated due to the technological importance for the glass manufacturing industry (Rimstidt, 1997). Rimstidt (1997) convincingly argued that the previously determined value for quartz solubility at ambient conditions (Morey et al., 1962) is incorrect because equilibrium was not attained.

The third category of experiments considered were those that used weight loss of a single quartz crystal and employed a very fast quenching procedure (less than 1 minute). This included the experiments from Manning (1994) and Newton and Manning (2000). Their approach

minimized the possibility of silica precipitation on the primary quartz crystal or on the capsule walls. All experimental data from categories 1 through 3 discussed above were included into the final experimental database.

Several studies determined quartz solubility using the weight loss method (Kennedy, 1950; Wyart and Sabatier, 1955; Kitahara, 1960; Weill and Fyfe, 1964; Novgorodov, 1975; Novgorodov, 1977) at conditions between 160 and 400 °C, from saturated water vapor pressure up to 2 kbar. Kennedy (1950) and Weill and Fyfe (1964) demonstrated the attainment of equilibrium by performing a series of dissolution rate experiments, thereby establishing the time required for obtaining a stable value for the concentration of dissolved silica. A drawback of their experimental procedure was the slow quench time used, increasing the risk of silica precipitation. Another important source of error was the determination of water present in the capsule at different conditions, which is essential for calculating the correct solubility (Weill and Fyfe, 1964). When compared with the preferred datasets reviewed above (Table 3.2), these experiments show systematically lower solubility. This most likely reflects problems related to silica precipitation during slow quenching, and we have therefore not included these data into the final experimental database.

A number of studies have measured quartz solubility by weight loss in perforated gold capsules containing quartz grains (Anderson and Burnham, 1965, 1967; Shmulovich et al., 2001, 2006). These capsules were enclosed in larger sealed gold capsules during the experiments. The difference in weight of the inner capsule after the completion of the runs was then taken as the amount of quartz dissolved in the solution of the outer capsule. Using this method, the fluid in the outer capsule is partially separated from the quartz in the inner capsule, preventing the precipitation of silica on the quartz crystal during quench (Anderson and Burnham, 1965). The authors approximated the time required to attain equilibrium by performing time series dissolution experiments (Anderson and Burnham, 1965) or by allowing relative large run times for equilibration (Shmulovich et al., 2001; Shmulovich et al., 2006). When compared with the datasets that employed a fast quench method or measured the solubility of quartz from both undersaturated and supersaturated conditions, the measured quartz solubility of these experiments is systematically lower. Manning (1994) reports on average about 10% higher quartz solubility for experiments above 600 °C compared to Anderson and Burnham (1965). One possible explanation for the lower solubility reported by Anderson and Burnham (1965) is the precipitation of quartz in the outer capsule during quench (Manning 1994). Shmulovich et al. (2001) report that in some of their experiments quartz could have precipitated on the cold end of the quartz crystal due to a small temperature gradient present in their capsules. These data were therefore not included into the final experimental database.

The dataset of Morey et al. (1962) shows considerably lower solubility at temperatures below 130 °C, compared to the trend of the data at higher temperatures. This most likely reflects that equilibrium was not attained in the lower temperature experiments. Therefore, the experimental data below 130 °C were not included into the final experimental database.

Experimental measurements of quartz solubility in NaOH solutions were performed by Crear and Anderson (1971) and agree with those done in pure H₂O when considering Si-Na complexation. The quartz solubility in KOH solutions reported by Cloke (1954) shows a large scatter of ± 1 log units, which is possibly due to corrosion of the experimental capsule. When compared with quartz solubility in pure water, the values reported by Anderson and Burnham (1967) and Pascal and Anderson (1989) for quartz solubility in KOH solutions are higher by 0.1 log units, indicating the presence of a K-Si complex. The quartz solubility experiments performed by Ostapenko et al. (1969) in NaOH solutions show better agreement with the selected data for quartz solubility in pure water. However, Ostapenko et al. (1969) used a slow quench method, which casts doubt on their results. The data of Ostapenko et al. (1969) were therefore not included into the final experimental database.

The solubility of quartz in NaCl solutions has been investigated in a number of studies (see review by Akinfiev and Diamond, 2009). The well-documented experiments of Fournier et al. (1982) were done using a gold bag hydrothermal apparatus. Equilibrium was reached both from undersaturated and supersaturated conditions, and the experimental solution was extracted at run conditions, quenched to below 80 °C and analyzed. This dataset also agrees with the experimental data for quartz solubility in H₂O and NaOH solutions reviewed above, and was therefore included into the final experimental database. A second dataset accepted for the final experimental database was that of Newton and Manning (2000), which was performed with the weight loss method but with a fast quench technique. The quartz solubility experiments in NaCl, KCl, and HCl solutions of Anderson and Burnham (1967) were not included into the final experimental database, because of the slow quench method used.

3.4.2. Corundum solubility

Corundum solubility in water and aqueous electrolyte solutions has been extensively studied and reviewed by Pokrovskii and Helgeson (1995, 1997b). There are several experimental studies of corundum solubility in pure water at elevated temperatures and pressures. The datasets included into the final experimental database are summarized in Table 3.2. Most of these experiments used the weight loss method (Anderson and Burnham, 1967; Burnham et al., 1973; Becker et al., 1983; Tropper and Manning, 2007). Ragnarsdóttir and Walther (1985) and Walther (1997) used an extraction-quench technique and measured the equilibrium concentration from both undersaturated and supersaturated conditions. The difference between these two datasets is around one order of magnitude. The solubility experiments of Walther (1997) yielded about 1.2-1.5 log units higher Al concentrations than those of Becker et al. (1983) and Tropper and Manning (2007). The experiments of Becker et al. (1983) and Tropper and Manning (2007) are in excellent agreement with each other and were used in several studies to model corundum solubility at high pressures and temperatures (Dolejs and Manning 2010; Sverjensky et al. 2014). Ragnarsdóttir and Walther (1985) report the presence of 0.3 wt.% of Na₂O impurity in their starting material. Although they discarded their first runs (yielding 2 orders of magnitude higher Al solubility than the subsequent

ones), even a small amount of Na₂O could dramatically influence the pH of the solution, the Al speciation and thus the total Al solubility.

The low solubility of corundum in water, as well as the very slow equilibration rates, result in generally rather poor reproducibility of dissolved aluminum concentrations in solubility experiments. The large scatter and the substantial disagreement between different datasets could be due to different grain sizes of the starting solid materials used, different sample treatment to remove contamination, or due to the formation of other stable phases during the experiments such as aluminum hydroxides which would substantially increase the solubility. The datasets of Walther (1997) and Ragnarsdóttir and Walther (1985) are in gross disagreement with other experiments and new high pressure experiments (Dolejs and Manning, 2010) and were therefore not included into the final experimental database.

The solubility of corundum in both KOH and NaOH solutions was studied by Barns et al. (1963), Anderson and Burnham (1967), and Pascal and Anderson (1989). Azaroual et al. (1996) studied corundum solubility in KOH solutions, and Yalman et al. (1960) and Yamaguchi et al. (1962) in NaOH solutions. All studies employed a weight loss method. The experiments of Yamaguchi et al. (1962) employed a very slow quench technique, making it likely that Al minerals precipitated during quench and that the measured solubility is lower than the equilibrium solubility. The corundum solubility data in NaOH solutions at 400 °C and 276 bars obtained by Yalman et al. (1960) are systematically lower by around 0.1 log units, compared with the other datasets. We suspect that equilibrium was not reached in their experiments. The solubility measurements of corundum in KOH solutions at 400 °C and 0.5-2.0 kbar performed by Azaroual et al. (1996) are somewhat lower (0.1 log units) than those predicted from the thermodynamic model of Pokrovskii and Helgeson (1997b). The calculated values using the model of Pokrovskii and Helgeson (1997b) reproduce the experimental data of Pascal and Anderson (1989), Anderson and Burnham (1967), and Barns et al. (1963) within their uncertainty. Therefore, we have selected only these data for the final experimental database.

Additional corundum solubility experiments were done by Walther (2001) in NaCl solutions and Korzhinskiy (1987) in HCl solutions. The resulting solubilities are much higher than in pure water, up to 2 log units in NaCl solutions (Walther, 2001) and up to 4 log units in HCl solutions (Korzhinskiy, 1987). To explain these elevated solubilities, the authors considered the possibility of chloro-aluminum complexes at their experimental conditions. Because the number of experimental data points was too small for refining the properties of Al-Cl species, we have not included these datasets into the final experimental database.

3.4.3. Gibbsite, boehmite and diaspore solubility

Several reviews of the solubility of aluminum hydroxide minerals have been published in the past decades (Apps et al., 1988; Apps and Neill, 1990; Hemingway et al., 1991; Verdes et al., 1992; Wesolowski, 1992; Pokrovskii and Helgeson, 1995; Pokrovskii and Helgeson, 1997b; Tagirov and Schott, 2001; Tutolo et al., 2014). Because of the intrinsic experimental difficulties related to measurement of Al solubility, new high quality studies have been performed quite

recently (Palmer et al., 2001; Bénézeth et al., 2001). Reflecting the availability of new data, we have performed a critical analysis of all available experimental datasets that report the solubility of aluminum hydroxide phases.

3.4.3.1. Gibbsite solubility

We selected a number of datasets that report the solubility of gibbsite in NaOH solutions for our final experimental database (Table 3.3). Gibbsite solubility was determined from both undersaturated and supersaturated sides by Ikkatai and Okada (1962) in NaOH solutions and by Wesolowski (1992) in NaOH, NaCl, KOH, and KCl solutions. Russell et al. (1955) collected a large consistent dataset allowing for very long run times (up to 11 days at 40 °C). Only the experiments above 120 °C were excluded because they reported decomposition of gibbsite to boehmite at these conditions. The experimental datasets of Tsirlina (1936) and Lyapunov et al. (1964) show rather close agreement with the results from the experimental studies discussed above. The dataset of Tsirlina (1936) was included while the one of Lyapunov et al. (1964) was excluded because of the high concentration of NaOH used in their study that exceeded the ion strength limit of 3 molal (where the activity model employed is considered appropriate). The gibbsite solubility data reported by Palmer and Wesolowski (1992) are in good agreement with the other selected datasets and thus were included into the final experimental database.

By contrast to the studies reviewed in the section above, the experimental results of Fricke and Jucaitis (1930) and Sato (1954) show systematically higher solubilities and were not included into the final experimental database (Fig. 3.2). The data of Berecz and Szita (1970) are in close agreement with other studies at lower temperatures, but show systematically higher solubilities at 50-60 °C, and therefore the dataset was not included. The experiments of Apps (1970) in dilute NaOH solutions show a large scatter and were discarded because of a suspected contamination of the run materials with bayerite (Apps et al., 1988). The experimental study of Hitch et al. (1980), although done from both undersaturated and supersaturated conditions, reports gibbsite solubilities that are higher by as much as 0.12 log units (Wesolowski, 1992). The systematically higher solubility could be due to the small grain size (<38 µm) used in their experiments, which can enhance the solubility due to surface energy effects (Wesolowski, 1992). Their dataset was therefore not included into the final database.

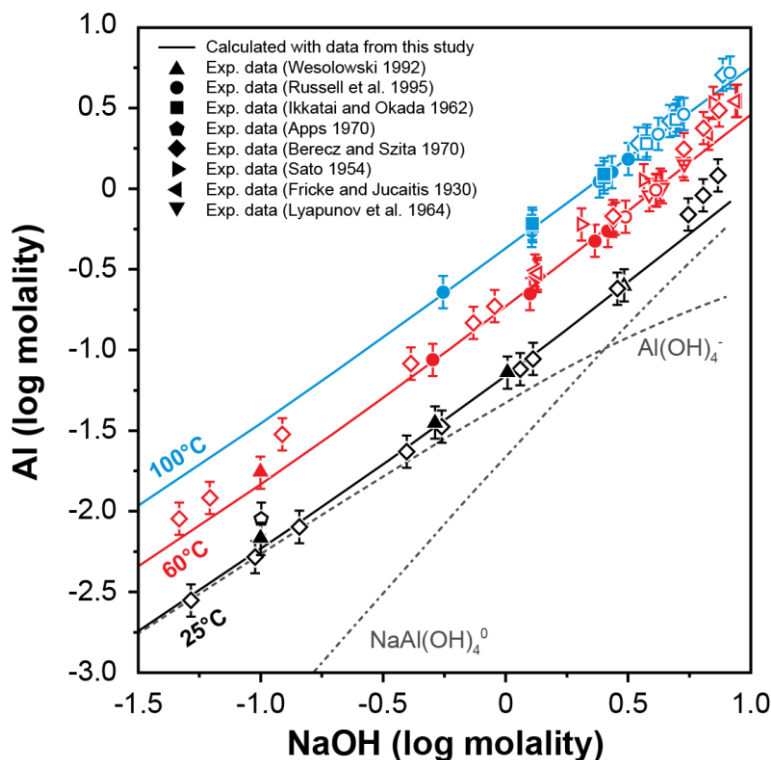


Figure 3.2. Comparison between calculated and experimental gibbsite solubility (Al concentration) data in NaOH solutions. Full symbols represent experimental datapoints which were used in the global data regression, while open symbols represent experimental datapoints which were not used. The grey dashed and dash-dotted lines show the relative contributions of the Al(OH)_4^- and NaAl(OH)_4^0 species to total solubility.

3.4.3.2. Boehmite solubility

Boehmite solubility experiments in H_2O -NaOH solutions were all performed from undersaturated conditions (Table 3.3). The datasets of Russell et al. (1955), Druzhinina (1955), Bernshtein and Matsenok (1961), Kuyunko et al. (1983), Diakonov et al. (1996), and Salvi et al. (1998) are all in good agreement with each other and show consistent trends with temperature and NaOH concentration. Therefore, they were included into the final experimental database. The data collected by Magarshak (1938) at 200 °C are in excellent agreement with those of Kuyunko et al. (1983) at the same temperature, but the experiments at 150 °C show a systematically higher solubility; thus the dataset was not selected. The experiments of Apps (1970) were also not selected due to large scatter and disagreement with the datasets discussed above. Castet et al. (1993) and Verdes et al. (1992) performed boehmite solubility experiments in mixed NaOH and NaCl solutions from both undersaturated and supersaturated conditions. Solubility experiments in acidic solutions were performed by Castet et al. (1993), Palmer et al. (2001) and Bénézech et al. (2001).

Both Palmer et al. (2001) and Bénézech et al. (2001) collected an extensive dataset of boehmite solubility over a wide range in pH conditions (2-10) between 100 and 290 °C at SWVP, and at 0.03, 0.1, 0.3, 1, and 5 molal NaCl concentration, from both undersaturated and supersaturated solutions. The measurements were performed in a hydrogen-electrode concentration cell, providing continuous in situ recording of hydrogen ion molality. The concentration of aluminum was measured from samples extracted at run conditions using ion chromatography and

spectrophotometry (Palmer et al., 2001). The boehmite solubility experiments measured by Bénézeth et al. (2001) at 0.03 molal NaCl concentration were all included into the final experimental database, with the exception of the data at 290 °C. We noted that when calculating the equilibrium aluminum concentration using thermodynamic properties of boehmite from Hemingway et al. (1991), the data from Bénézeth et al. (2001) above 250 °C are not in agreement with the trend obtained from the experimental results of Bénézeth et al. (2001) at lower temperatures. The experimental data above 250 °C were therefore not included into the final database. Palmer et al. (2001) measured the solubility of boehmite as function of increasing NaCl concentration, from 0.1 to 5 molal NaCl. Their calibration for determining the hydrogen ion concentration does not take into account the formation of the neutral species HCl^0 (Palmer et al., 2001). When the neutral ion pair HCl^0 is included in calculation of the equilibrium solubility and speciation, its proportion increases with increasing temperature and Cl concentration. The fraction of HCl^0 in 1 molal NaCl solutions is around 10% of the total dissolved hydrogen at 154 °C and around 30% at 203 °C. When calculating the total Al concentration for the complete datasets of Bénézeth et al. (2001) and Palmer et al. (2001), it was not possible to reproduce all data in the acidic to neutral pH range with one set of thermodynamic properties for the Al hydroxide species. This likely reflects differences in the calculation of hydrogen ion concentration between the experimental studies and our modeling, related to the effect of the HCl^0 ion pair formation. Our calculations predict different H^+ concentrations in the acidic region above 0.03 molal NaCl, compared to the values reported by Palmer et al. (2001). This problem was not observed for the data at alkaline pH, and we have therefore only included the experimental data above a pH value of 6 from the study of Palmer et al. (2001) into the final experimental database. From the data reported by Bénézeth et al. (2001) we included all experimental points with the exception of the experimental data above 250 °C.

3.4.3.3. Diaspore solubility

Solubility experiments of diaspore in dilute and concentrated NaOH and NaOH-NaCl solutions were performed from undersaturated conditions (Druzhinina, 1955; Bernshtein and Matsenok, 1965; Wefers, 1967; Chang et al., 1979; Apps et al., 1988; Verdes et al., 1992). The data above 150 °C are in fair agreement with each other with the exception of the dataset of Chang et al. (1979) which shows systematically lower Al concentrations (Pokrovskii and Helgeson, 1995). The experiments below 150 °C show a very large scatter, likely related to the low equilibration rate of the dissolution reaction and too short run times. The data of Chang et al. (1979) were therefore not considered. Table 3.3 summarizes the experimental datasets included into the final experimental database.

3.4.4. Solubility of feldspars, aluminosilicates, and silicate assemblages

Experimental solubility studies of aluminosilicates, feldspars and micas (and assemblages of several phases) are of particular importance, because they provide simultaneous constraints on the thermodynamic properties of several aqueous species. The experimental datasets that were included into the final database are summarized in Table 3.4.

3.4.4.1. Feldspar solubility

The solubility of feldspars has been investigated in a number of studies. Because of the incongruent dissolution of feldspars and difficulties in attaining equilibrium, these experiments are very challenging (Antignano and Manning, 2003; Azimov and Bushmin, 2007). Incongruent dissolution of feldspars can produce a number of different solid hydrolysis products that may include micas, aluminosilicates, corundum, leucite, and nepheline. Solubility experiments of albite and microcline were performed by Currie (1968) and Adcock (1985) using a dynamic flow through method. They reported that nepheline formed by incongruent dissolution of albite, which however is not in agreement with the measured ratios of dissolved element concentrations (Azimov and Bushmin, 2007). In the microcline solubility experiments, the reported Na concentrations are very close to those of K, probably due to the presence of Na in the natural microcline samples (up to 2.7 wt.% Na₂O). Even a very small albite component in microcline can have a large influence on the total solubility in this system, and the measured Na and K concentrations will reflect equilibrium with an albite-microcline solid-solution. To avoid such complications, we have only considered feldspar solubility studies where it was demonstrated that pure phases have been used.

Davis (1972) studied the solubility of albite in H₂O using a static tube-in-tube technique. Reflecting the incongruent dissolution behavior of albite, a residue of pragonite was found in experiments that were inside the paragonite stability field. These experiments show consistent pressure and temperature trends, and were done using both natural and synthetic albite samples. Where the experimental conditions of Davis (1972) overlap with the ones from Currie (1968), the latter show systematically lower solubility (Anderson and Burnham, 1983). The lower measured solubility in the experiments of Currie (1968) and Adcock (1985) could have been caused by reprecipitation, due to high flow rate in their experiments, or due to the formation of other secondary phases (nepheline) (Adcock, 1985). Therefore, we have only included the albite solubility experiments of Davis (1972) into our final database.

3.4.4.2. Aluminosilicate solubility

The solubility experiments involving aluminosilicates such as kyanite, andalusite and sillimanite (Brown and Fyfe, 1971; Ostapenko and Arapova, 1971; Ostapenko et al., 1978) are affected by incongruent dissolution behavior in a similar way as the feldspar experiments. This results in preferential transfer of silica into solution and precipitation of secondary corundum (Azimov and Bushmin, 2007). In all aluminosilicate solubility studies only the concentration of silica was determined, but not the concentration of aluminum. There is also a considerable scatter between different datasets, likely due to difficulties in reaching equilibrium (Azimov and Bushmin, 2007). Reflecting these issues, we have not included the aluminosilicate solubility experiments into the final database.

3.4.4.3. Solubility of silicate mineral assemblages

Solubility experiments in the system SiO₂-Al₂O₃-H₂O with two-mineral assemblages were conducted by Hemley et al. (1980). They used well-characterized pure natural minerals and a cold-

seal bomb quench method (30 seconds quench time to room temperature, followed by extraction and analysis of the solution). Their experiments were included into the final database.

When using three-mineral assemblages that buffer the composition of the solution, the uncertainties concerning the phase assemblages are eliminated and the solution is more likely to be in equilibrium with the solid phases (Azimov and Bushmin, 2007). Experiments containing potassium feldspar, muscovite and quartz were done by Walther and Woodland (1993), but the analyzed Na concentration in solution was similar to that of K or even higher, suggesting contamination by Na from the natural microcline sample used. Solubilities in the system $K_2O-Al_2O_3-SiO_2-H_2O$ were also studied by Anderson et al. (1987). They used natural mineral samples where the microcline had 97% orthoclase component and the corundum contained up to 1.2 wt.% Fe. Because of the presence of impurities, these datasets were not included into the final database.

Woodland and Walther (1987) determined the solubility of albite, paragonite and quartz in supercritical H_2O . The authors used relatively pure natural mineral samples and sampled the equilibrium solution at run conditions with an extraction-quench technique. Their experimental design should have provided for a reversal of solubility equilibrium based on the changes in element concentrations when going from one temperature-pressure state point to the next one (decrease in T would result in approach to equilibrium from supersaturation and increase from undersaturation). Although we could not identify any obvious issues in their experimental setup, the measured Si, Al, and Na concentrations show a substantial overlap between isotherms at pressures above 1-1.5 kbar. Furthermore, the trends with temperature and pressure displayed by the data are not in agreement with trends expected from thermodynamic relations. Therefore, we have not included these data into the final experimental database.

It is well known that the solubility and transport of many elements in crustal fluids is controlled by the chlorinity (Roedder, 1984; Yardley, 1997,). The solubility of silicate mineral assemblages in aqueous chloride solutions has therefore been determined by several experimental studies. Haselton et al. (1995) studied the stability of muscovite, andalusite, sanidine and quartz in 1 molal KCl solutions. Similar phase equilibria were studied by Haselton et al. (1988) but in topaz-bearing assemblages. Experiments investigating feldspar-mica-quartz equilibria in NaCl and KCl solutions were reported by Hemley (1959), Montoya and Hemley (1975), and Sverjensky et al. (1991). These studies used both synthetic and natural minerals. The experiments reported by Sverjensky et al. (1991) were done using extraction of the equilibrium solution at run conditions. This dataset is in good agreement with that of Montoya and Hemley (1975), who used a standard cold-seal vessel technique and sampled the solution after quench. The studies discussed above obtained reversed phase equilibrium by starting from Na- or K-rich solutions with lower HCl content than the equilibrium value, or from HCl concentrations higher than the equilibrium value. Except for the topaz-bearing assemblages (Haselton et al., 1988), these experimental data were all included into the final database.

Other experiments in similar systems were not included into the final dataset, but are shown in plots that compare solubilities and phase equilibria calculated with the final thermodynamic dataset with their experimental counterparts. These are the studies of Popp and Frantz (1980) and

Shinohara and Fujimoto (1994) in the system $\text{Na}_2\text{O}-\text{Al}_2\text{O}_3-\text{SiO}_2-\text{H}_2\text{O}-\text{HCl}$. Popp and Frantz (1980) used the Ag-AgCl buffer technique to control the activity of HCl, making the reproduction of the initial system composition technically impossible when using GEMS3. Shinohara and Fujimoto (1994) studied the composition of the vapor and liquid phases for NaCl concentrations from 0.05 to 1.0 molal at 600 °C and pressures 0.5 and 2 kbar. They determined HCl concentrations several times higher than those obtained by Popp and Frantz (1980) for very similar pressure-temperature conditions. A likely explanation could be the slow quench method used in their study, despite the fact that their results for different quench times were rather consistent. Other experimental data in the system $\text{K}_2\text{O}-\text{Al}_2\text{O}_3-\text{SiO}_2-\text{H}_2\text{O}-\text{HCl}$ that were not included into the final database were those by Gunter and Eugster (1981), Wintsch et al. (1980), and Shade (1974). Gunter and Eugster (1981) used the Ag-AgCl buffer technique to control the activity of HCl. Wintsch et al. (1980) performed the experiments in very dilute KCl solutions (0.02 molal), which introduced a large error when using the assumption that the ratio of K/H of the quench solution is the same as at the experimental pressure-temperature conditions. This is very different in experimental studies at 1 molal KCl concentrations (Haselton et al., 1995), because at low chlorinity the amount of total hydrogen at experimental conditions is sufficiently small to be affected by changes in the solution speciation during quench (Haselton et al., 1995). Shade (1974) used natural impure natural muscovite (with paragonite content of 10%) and potassium feldspar (with 10 % albite content) samples as starting materials.

High quality reversed solubility experiments at 600 and 650 °C and 2 kbar involving synthetic metapelite (assemblage potassium feldspar, albite, andalusite, and quartz) in moderately saline solutions were recently reported by Hauzenberger et al. (2001) and Pak et al. (2003). They used a rapid quench technique, accurate analytical methods and documented the experimental conditions very well. The four-mineral assemblage used was able to buffer all components in the system, and the concentrations of dissolved Na, K, Al and Si in the fluid were analyzed. We have specifically included their precise measurements of K/Na ratios in solution into the final experimental database.

3.5. Parameter optimization methods

The standard state Gibbs energies of aqueous species were regressed with the GEMSFITS code (Miron et al., 2015); <http://gems.web.psi.ch/GEMSFITS>, which uses the GEMS3K Gibbs energy minimization code (Kulik et al., 2013) and the TsoMod library of activity and equation of state models (Wagner et al., 2012). The chemical system definitions (lists of phases and species; initial thermodynamic properties of each species; bulk composition, pressure and temperature for each experimental data point) were prepared using the GEM-Selektor v.3 code (GEMS3) package (<http://gems.web.psi.ch/GEMS3>) and then exported into text files that can be read by GEMS3K and GEMSFITS codes (Miron et al., 2015). The starting composition of each experimental data point was specified in terms of the amounts of oxides, water and salts. If reported, the fluid/solid mass ratio in the experiment was specified as in the experimental studies; otherwise a fluid/mineral

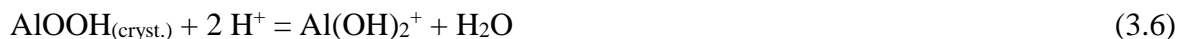
ratio of 0.1 was selected to make sure that the calculated equilibria would always remain mineral-buffered.

A weighted least-squares minimization method was used for the global fitting of the standard state molal Gibbs energies $\Delta_f G_{298,1}^0$ of several aqueous species. The standard state volume ($V_{298,1}^0$), entropy ($S_{298,1}^0$), heat capacity ($Cp_{298,1}^0$), and HKF parameters ($a_1, a_2, a_3, a_4, c_1, c_2, \omega_0$) were fixed to the values collected from several sources (Tables 3.1 and 3.5) or obtained from regression of equilibrium constants in this study. This mainly concerned the Al species $\text{Al}(\text{OH})_3^0$ and the neutral ion pairs $\text{NaCl}^0, \text{KCl}^0, \text{NaOH}^0, \text{KOH}^0$ and HCl^0 .

The weighting scheme was not directly retrieved from the experimental errors or the quality of the datasets. However, relative weights were used in order to obtain an accurate refinement of parameters and make the fit sufficiently sensitive to those experiments, which have only small contributions to the total sum of squared residuals. The relative and/or absolute change in the total sum of squared residuals from one fitting iteration to the next one can be small enough for the minimization algorithm to converge before accurately refining the properties of some minor but important species. For example, the number of experiments that constrain the properties of the KAlO_2^0 species is small compared to the total number of experiments processed in the global fit and hence the contribution of this species to the total sum of squared residuals is small. Consequently, the algorithm would converge before accurately refining the KAlO_2^0 properties to the desired precision. A solution to this problem was to increase the weight of those experiments that constrain the properties of the KAlO_2^0 species.

As stated in the thermodynamic framework section, the properties of the minerals are accepted from the Holland and Powell (1998) database as revised in the Thermocalc dataset ds55 (referred to as HP02). The standard state thermodynamic properties of boehmite and gibbsite are not part of this dataset, and were taken from Hemingway et al. (1991) and Robie and Hemingway (1995), respectively. Different thermodynamic data have been used for boehmite by Verdes et al. (1992), Castet et al. (1993), and Bénézech et al. (2001), when retrieving the thermodynamic properties of aluminum species. These studies used values for the standards state entropy and heat capacity of 48.4 J/(mol·K) and 65.6 J/(mol·K) (Shomate and Cook 1946; Takahashi et al. 1973) compared with 37.2 J/(mol·K) and 54.2 J/(mol·K) (Hemingway et al. 1991) selected for the present study. Verdes et al. (1992) attributed these differences to the possible presence of a small amount of excess water in the boehmite samples used by Shomate and Cook (1946) and Takahashi et al. (1973), while this contamination was not present in the samples studied calorimetrically by Hemingway et al. (1978). As highlighted by Tagirov and Schott (2001), there is no experimental evidence that gibbsite is converted to boehmite below 80 °C, but the existing thermodynamic data predict that boehmite is more stable than gibbsite below this temperature. One explanation for this could be that kinetic factors have affected the relative stability of gibbsite and boehmite in the experiments. The Ostwald step rule would predict that the formation of the mineral with the fastest crystallization rate (gibbsite) is favored, while the conversion to the thermodynamically stable phase (boehmite) can be extremely slow (Morse and Casey, 1988).

A substantial proportion of the experiments constraining aluminum solubility are those involving gibbsite and boehmite. They are not included into the HP02 mineral dataset, but offer essential information on the stability of aluminum speciation over the entire pH range. The solubility experiments on diaspore, corundum or other minerals present in the HP02 database are not sufficient to independently constrain the properties of all relevant aluminum species present under acidic to alkaline conditions. Therefore, we have adopted the following data refinement strategy for the Al species. In a first step, all hydrolysis constants of Al^{3+} were refined using the selected solubility experiments of gibbsite and boehmite (Table 3.3). The new hydrolysis constants were then subsequently used to independently refine the properties of Al^{3+} from experiments that involve the solubility of Al minerals in the HP02 dataset (diaspore, corundum). When refining the $\Delta_f G_{298,1}^0$ of Al^{3+} , we have included all Al hydroxide complexes in the speciation model and adjusted their $\Delta_f G_{298,1}^0$ based on the hydrolysis constants (and their temperature dependence) that were fixed to the values obtained from the gibbsite and boehmite solubility data. While the absolute values of $\Delta_f G_{298,1}^0$ of all aluminum species are dependent on the mineral properties, the aluminum hydrolysis constants are independent of the chosen mineral properties. This can be shown by the following set of chemical reactions for the species $\text{Al}(\text{OH})_2^+$, where the mineral properties obviously cancel out:



Optimization runs were first performed separately for the gibbsite and boehmite experiments, and subsequently for the remaining Al minerals present in the HP02 database. Finally, the data were refined in a global optimization run using all experimental data. This permitted to evaluate the level of consistency between the properties of gibbsite and boehmite and the aluminum minerals present in the HP02 database.

The $\Delta_f G_{298,1}^0$ values of several aqueous complexes were constrained using association constants derived from conductance and potentiometric experiments. The $\Delta_f G_{298,1}^0$ of these species were refined in the same way as discussed for the Al hydroxy species above. The independently regressed association constants were then used as reaction constraints. In this way, any change in $\Delta_f G_{298,1}^0$ from fitting solubility data is propagated to the related complexes using the $\Delta_r G_{298,1}^0$ of the reaction (e.g., for the reaction $\text{Na}^+ + \text{Cl}^- = \text{NaCl}^0$). At each optimization step, new $\Delta_f G_{298,1}^0$ values of the reaction constrained complexes are recalculated using the updated properties of the reactant species. The newly derived association constants from conductance measurements were used to constrain the properties of the neutral ion pairs (NaCl^0 , KCl^0 , NaOH^0 , KOH^0). Reaction constraints were also used for species which are not sensitive to the selected experiments (i.e., they do not form in significant amounts). Important examples are the complexes NaHSiO_3^0 and $\text{AlH}_3\text{SiO}_4^{2+}$, which are linked to simple species by the following reactions:





The association constants of these complexes were originally derived from quartz solubility experiments in borate solutions for the NaHSiO_3^0 (Seward, 1974) and from the silica injection experiments of Salvi et al. (1998) and potentiometric measurements of Pokrovskii et al. (1996) for $\text{AlH}_3\text{SiO}_4^{2+}$. An additional reaction constraint was imposed on the AlOH^{2+} species, because its properties are highly correlated with those of Al^{3+} , making it difficult to independently refine the $\Delta_f G_{298,1}^0$ of both species from solubility data alone. We accepted the association constants for AlOH^{2+} from the direct hydrolysis measurements of Palmer and Wesolowski (1993) (Figure 3.3).

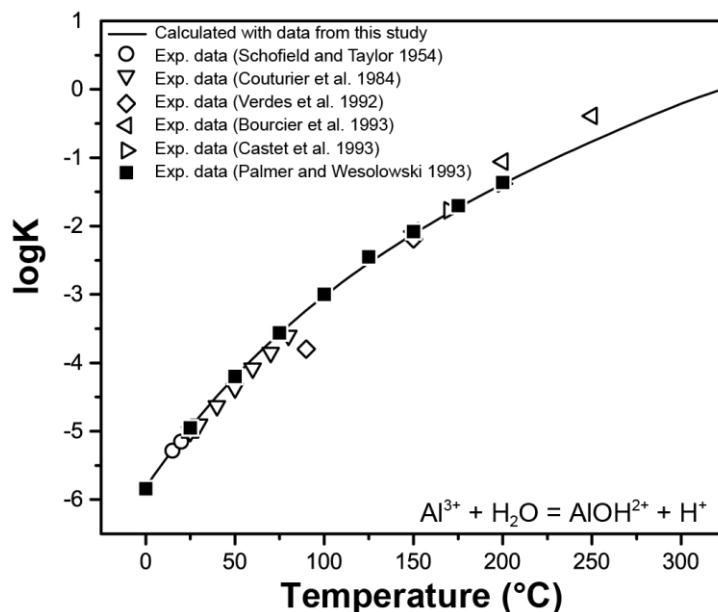


Figure 3.3. Comparison between calculated and reported literature values for the logK of the first hydrolysis reaction of Al^{3+} .

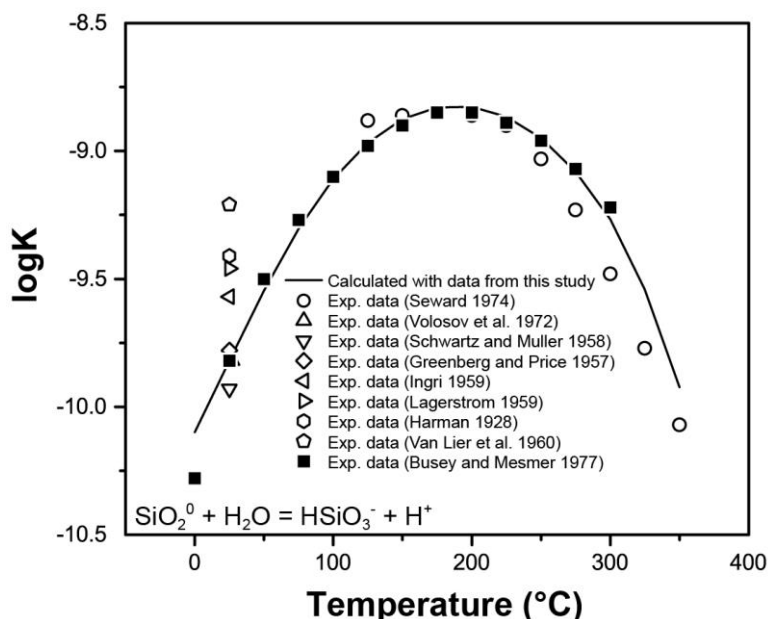


Figure 3.4. Comparison between calculated and reported literature values for the logK of the SiO_2^0 hydrolysis reaction to form HSiO_3^- .

The stability of the HSiO_3^- aqueous species was linked to SiO_2^0 through the reaction logK values determined from the potentiometric measurements (Figure 3.4) performed by Busey and Mesmer (1977):



In contrast, Sverjensky et al. (1997) selected to refine the standard state properties and parameters of HSiO_3^- using the logK data of Seward (1974) derived from quartz solubility in borate solutions. These results were criticized by Busey and Mesmer (1977) for being strongly dependent on the selected properties for aqueous borate speciation equilibria and the method of extrapolation to infinite dilution.

To reproduce those experiments where the actual bulk composition is not directly reported, the nested regression functionality of GEMSFITS was used. This makes it possible to iteratively adjust the input composition (e.g., amounts of HCl and NaOH) in such a way that reported output compositions (e.g., pH or amount of H^+) are reproduced. The iterative adjustment of the bulk composition was done before each iteration of the global fitting algorithm. In this way the temperature, pressure and also the pH conditions of the simulated experiments matched the reported values.

The uncertainties of the final regressed $\Delta_f G_{298,1}^0$ values were evaluated using Monte Carlo simulation of synthetic datasets generated from randomly sampled residuals added to the measured values for each dataset (Miron et al., 2015). The uncertainties of the reaction-constrained species were propagated from the independently fitted species and the average reported error on the reaction logK values. The uncertainties in the calculated standard state Gibbs energies at elevated temperatures and pressures are also affected by the uncertainties in the HKF parameters. If all errors of the HKF parameters would be added up, this would result in a maximum additional error of the $\Delta G_{T,p}^0$ between 2.4 kJ/mol at 500 °C and 2 kbar and 6.0 kJ/mol at 1000 °C and 5 kbar (Shock and Helgeson, 1988). More likely, these additional uncertainties should be typically below 2 kJ/mol (around 0.1 units in logK). This conclusion is supported by the generally good agreement between calculated and measured mineral solubilities, as will be discussed in the following section.

Table 3.2. Summary of the quartz and corundum solubility experiments selected for the global optimization.

Reference	System	Number of data points used (total number)	⁽¹⁾ Direction of equilibrium	Temperature range (deg. C)	^b Pressure range (kbar)	Dataset total error (Eq. 3.11)
Morey et al. (1962)	Quartz-H ₂ O	20 (41)	U+S	45 – 300	SWVP – 1.0	0.009
Crear and Anderson (1971)	Quartz-H ₂ O-NaOH	18 (38)	U+S	179 – 329	SWVP	0.028
Fournier et al. (1982)	Quartz-H ₂ O-NaCl	30 (35)	U+S	350	0.2 – 0.5	0.012
Walther and Orville (1983)	Quartz-H ₂ O	13 (20)	U+S	350 – 550	1 – 2	0.018
Lier et al. (1960)	Quartz-H ₂ O	5 (5)	U	65 – 100	SWVP	0.014
Siever (1962)	Quartz-H ₂ O	4 (16)	U	125 – 182	SWVP	0.015
Adcock (1985)	Quartz-H ₂ O	1 (1)	U	400	1.0	0.035
Manning (1994)	Quartz-H ₂ O	4 (52)	U	500 – 900	5 – 20	0.097
Rimstidt (1997)	Quartz-H ₂ O	5 (10)	U	21 – 96	SWVP	0.029
Newton and Manning (2000)	Quartz-H ₂ O	4 (10)	U	500 – 900	2 – 15	0.078
Becker et al. (1983)	Corundum-H ₂ O	10	U	670	2 – 20	0.053
Tropper and Manning (2007)	Corundum-H ₂ O	2	U	700 – 1100	5 – 20	0.041
Anderson and Burnham (1967)	Corundum-H ₂ O-KOH	6	U	600 – 900	2 – 6	0.081
Pascal and Anderson (1989)	Corundum-H ₂ O-NaOH-KOH	21	U	600 – 700	2 – 2.6	0.023
Barns et al. (1963)	Corundum-H ₂ O-NaOH-KOH	5	U	430 – 600	1.45	0.156

⁽¹⁾ U: equilibrium approached from undersaturation; S: equilibrium approached from supersaturation.

⁽²⁾ SWVP: Saturated water vapor pressure.

Table 3.3. Summary of gibbsite, boehmite and diaspore solubility experiments selected for the global optimization.

Reference	System	Number of data points used (total number)	⁽¹⁾ Direction of equilibrium	Temperature range (deg. C)	⁽²⁾ Pressure range (kbar)	Dataset total error (Eq. 3.11)
Ikkatai and Okada (1962)	Gibbsite-H ₂ O-NaOH	14	U+S	40 – 130	SWVP	0.133
Wesolowski et al. (1992)	Gibbsite-H ₂ O-NaOH-NaCl	28	U+S	25 – 80	0.001	0.021
Russell et al. (1955)	Gibbsite-H ₂ O-NaOH	34	U	40 – 120	SWVP	0.040
Tsirlina (1936)	Gibbsite-H ₂ O-NaOH	6	U	95	0.001	0.042
Palmer and Wesolowski (1992)	Gibbsite-H ₂ O-NaCl-HCl	51	U	30 – 70	0.001	0.051
Bénézech et al. (2001)	Boehmite-H ₂ O-NaOH-NaCl-HCl	392	U+S	100 – 290	SWVP	0.040
Palmer et al. (2001)	Boehmite-H ₂ O-NaOH-NaCl-HCl	108	U+S	100 – 290	SWVP	0.061
Castet et al. (1993)	Boehmite-H ₂ O-NaOH-NaCl-HCl	57	U+S	90 – 350	SWVP	0.053
Verdes et al. (1992)	Boehmite-H ₂ O-NaOH-NaCl	18	U	135 – 300	SWVP	0.031
Diakonov et al. (1996)	Boehmite-H ₂ O-NaOH-NaCl	16	U	125 – 350	SWVP	0.007
Salvi et al. (1998)	Boehmite-H ₂ O-NaOH	2	U	300	SWVP	0.017
Kuyunko et al. (1983)	Boehmite-H ₂ O-NaOH	8	U	200 – 250	SWVP	0.031
Bernshtein and Matsenok (1961)	Boehmite-H ₂ O-NaOH	6	U	250 – 300	SWVP	0.037
Russell et al. (1955)	Boehmite-H ₂ O-NaOH	33	U	80 – 170	SWVP	0.180
Druzhinina (1955)	Boehmite-H ₂ O-NaOH	4	U	200	SWVP	0.084
Verdes et al. (1992)	Diaspore-H ₂ O-NaOH-NaCl	26	U	135 – 300	SWVP	0.040
Wefers (1967)	Diaspore-H ₂ O-NaOH	19	U	250 – 330	SWVP	0.168
Bernshtein and Matsenok (1965)	Diaspore-H ₂ O-NaOH	4	U	250 – 300	SWVP	0.042
Druzhinina (1955)	Diaspore-H ₂ O-NaOH	5	U	200 – 220	SWVP	0.099

⁽¹⁾ U: equilibrium approached from undersaturation; S: equilibrium approached from supersaturation.

⁽²⁾ SWVP: Saturated water vapor pressure.

Table 3.4. Summary of aluminosilicate and Na-K-Al-Si mineral assemblage solubility experiments selected for the global optimization.

Reference	System	Number of data points used (total number)	⁽¹⁾ Direction of equilibrium	Temperature range (deg. C)	Pressure range (kbar)	Dataset property error (Eq. 3.11)
Davis (1972)	Albite-paragonite-H ₂ O	12	U	500 – 700	2 – 5	Si: 0.047 Al: 0.027 Na: 0.021
Hemley et al. (1980)	Pyrophyllite-kaolinite-andalusite-corundum-disapore-boehmite-H ₂ O	24	U	200 – 500	1 – 2	Si: 0.045
Hemley (1959)	Muscovite-K-feldspar-Quartz-H ₂ O-KCl	4	U	400 – 500	1	Log(K/H): 0.104
Sverjensky et al. (1991)	K-feldspar-muscovite-kaolinite-pyrophyllite-andalusite-quartz-H ₂ O-KCl	21	U+S	300 – 600	0.5 – 2	Log(K/H): 0.101
Haselton et al. (1995)	K-feldspar-muscovite-andalusite-quartz-H ₂ O-KCl	4	U+S	400 – 500	1	Log(K/H): 0.099
Montoya and Hemley (1975)	Albite-paragonite-andalusite-quartz-H ₂ O	3	U	300 – 500	1	Log(Na/H): 0.025
Hauzenberger et al. (2001)	K-feldspar-albite-andalusite-quartz-H ₂ O-KCl-NaCl	33	U+S	600	2	Na: 0.073 K: 0.057 K/Na: 0.147
Pak et al. (2003)	K-feldspar-albite-andalusite-quartz-H ₂ O-KCl-NaCl	22	U+S	650	2	Na: 0.072 K: 0.052 K/Na: 0.096

⁽¹⁾ U: equilibrium approached from undersaturation; S: equilibrium approached from supersaturation.

3.6. Results

The final regressed $\Delta_f G_{298,1}^0$ values of aqueous species generated by global optimization of all mineral solubility data selected for the final database (Tables 3.2, 3.3 and 3.4) are summarized in Table 3.6. This table also lists thermodynamic properties of species that were fixed during fitting, and those which were constrained from association reaction constants. The correlation coefficients between the freely optimized aqueous species are given in Table 3.7. The Electronic Supplementary Material lists values for the aluminum aqueous species obtained from fitting them only against gibbsite and boehmite solubility experiments (Table 3.EA2). The resulting properties (logK values) were then used as reaction constraints for the aluminum hydroxy species while the Gibbs energy of the Al^{3+} ion was fitted against the experimental corundum and diaspore solubility data (Table 3.EA3). The $\Delta_f G_{298,1}^0$ obtained for $\text{Al}(\text{OH})_4^-$ from independently fitting gibbsite and boehmite solubility was -1305.3 ± 0.3 kJ/mol, while fitting it using corundum and diaspore solubility along with the reaction constraints yielded -1305.2 ± 0.6 kJ/mol. The final value of -1305.1 ± 0.23 kJ/mol (Table 3.6) was obtained from the global optimization of all solubility experiments (including gibbsite, boehmite, corundum and diaspore solubility data) and is identical within errors with all other fitting results.

Selected experimental datasets that were used in the regression of Gibbs energies are plotted together with datasets that were not used, and are compared to calculations with the final aqueous species dataset in Figures 3.1 through 3.20. Filled symbols do always represent experimental data points used during fitting, while open symbols represent experimental data points which were not used. Solid curves represent calculated values using the final aqueous species dataset (Table 3.6), while dashed or dotted curves represent the values calculated with thermodynamic properties of aqueous species from SUPCRT92 (Shock and Helgeson, 1988; Shock et al., 1989; Johnson et al., 1992; Shock et al., 1997; Sverjensky et al., 1997) or other sources. Most importantly, the final aqueous species dataset is able to accurately reproduce the input experimental data largely within their uncertainty and without any systematic deviation. The overall quality of the fit for each individual experimental dataset is reported in Tables 3.2, 3.3 and 3.4 and defined by the normalized-root-mean-square-error (NRMSE):

$$NRMSE = \sqrt{\frac{\sum_i^N [y(i) - f(i)]^2}{\sum_i^N y(i)^2}} \quad (3.11)$$

where $y(i)$ represents the measured (experimental) value of a property (e.g. Si solubility), $f(i)$ is the calculated value of this property, and N the number of experiments in this dataset. This evaluation of the quality of the fit was performed after the GEMSFITS optimization and does not represent the minimized objective function.

The thermodynamic database presented in this study and future updates will be provided at the following web-address: <http://gems.web.psi.ch/>. The files are compatible with the GEM-Selektor geochemical modeling software (Kulik et al. 2013) and enable calculation of aqueous-mineral equilibria in the system Na-K-Al-Si-O-H-Cl at temperatures up to 1000 °C, pressures up to 5 kbar and salt concentrations up to 5 molal.

3.6.1. System Si-O-H-Cl

Figure 3.5 displays the quartz solubilities in pure H₂O over a wide range in temperature and from saturated water vapor pressure to 5 kbar. The calculated solubilities are in excellent agreement with the experimental data that were used in the data regression, but also in good agreement with experimental data that were not used. Figure 3.5B shows that the experimental data points from Xie and Walther (1993) are inconsistent with all other experimental datasets at the same conditions and that they have a different temperature trend. Other experimental datasets for quartz solubility show only minor differences between calculated and measured values.

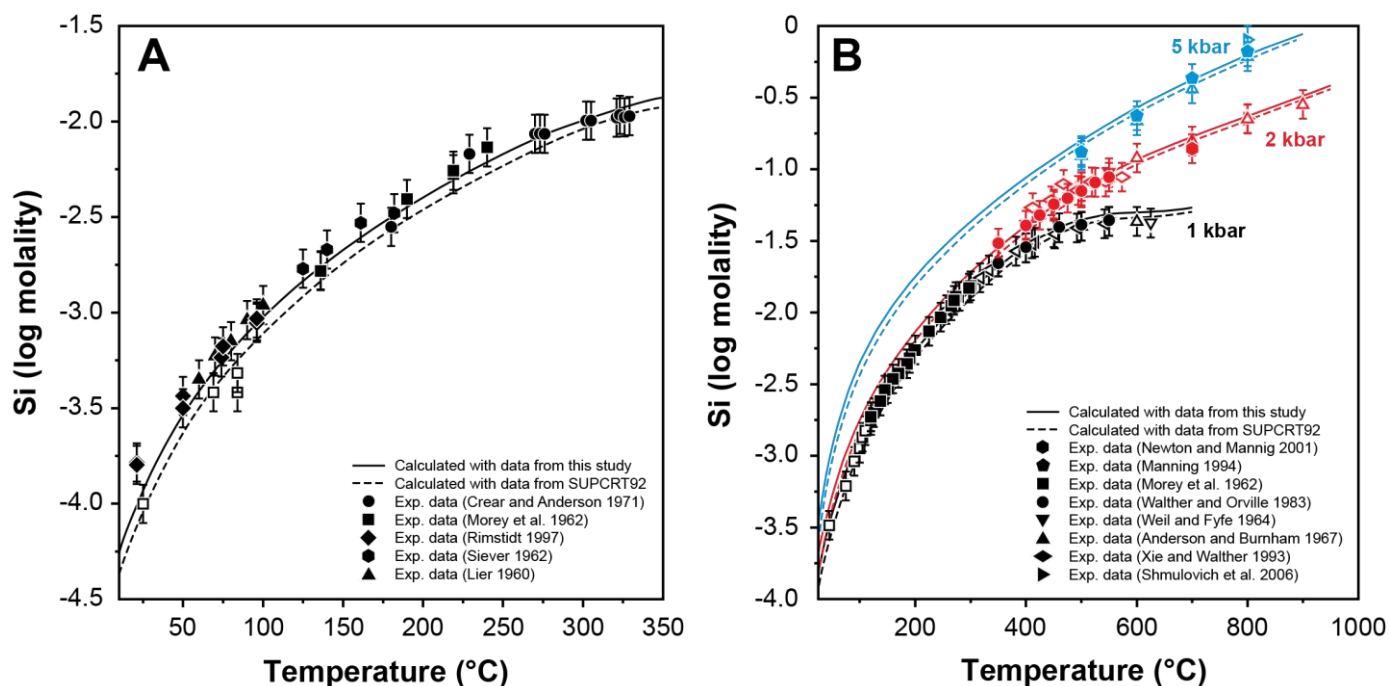


Figure 3.5. Comparison between calculated and experimentally measured quartz solubility (Si concentration) over a wide range in temperature and at several pressures up to 5 kbar. Full symbols represent experimental datapoints which were used in the global data regression, while open symbols represent experimental datapoints which were not used. (A) Data at SWVP. (B) Data at isobars of 1, 2 and 5 kbar.

3.6.2. System Al-O-H-Cl

In this section, we present results of the global optimization of all Al solubility data (including boehmite, gibbsite, corundum and diaspore solubility). The majority of experimental gibbsite and boehmite solubility data in acid, neutral and alkaline solutions and at different salt concentrations and temperatures are in good mutual agreement and are also in agreement with the diaspore solubility data. Calculated dissolved aluminum concentrations agree well with those determined from gibbsite solubility experiments at temperatures between 25 and 120 °C (Fig. 3.2). Very good

agreement is also observed with the experimental boehmite solubility in alkaline conditions (Fig. 3.6), especially with the large dataset of Bénézeth et al. (2001) that covers a wide range in temperature and solution pH (Fig. 3.7). Good agreement between calculations and experiments is also observed for the diaspore solubility in moderately concentrated alkaline solutions (Fig. 3.8A) and in very dilute solutions (Fig. 3.8B).

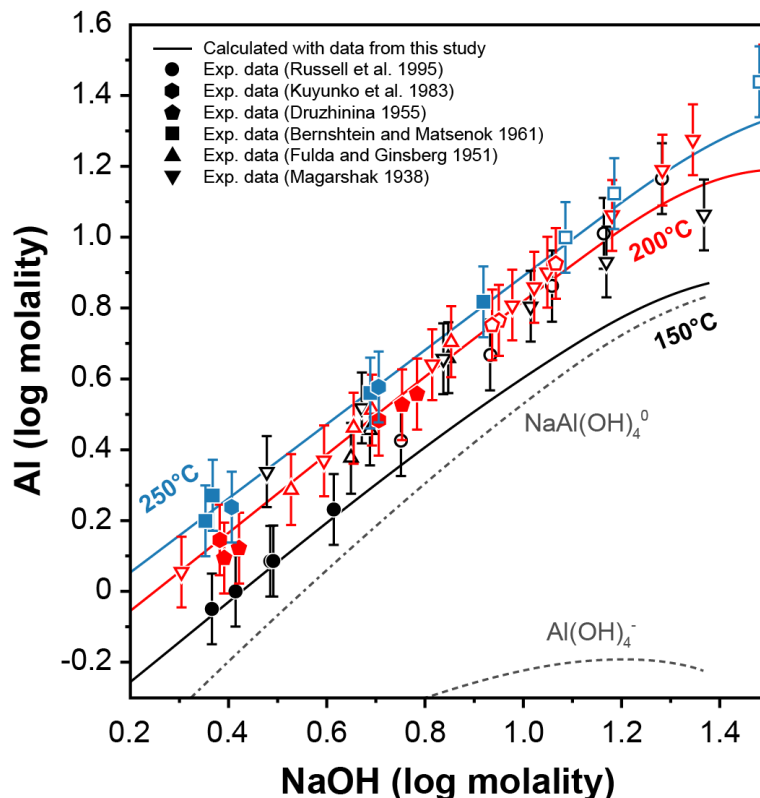


Figure 3.6. Comparison between calculated and experimentally determined boehmite solubility (Al concentration) as function of NaOH concentration. The data cover temperatures up to 250 °C at SWVP. Full symbols represent experimental datapoints which were used in the global data regression, while open symbols represent experimental datapoints which were not used.

The calculated aluminum concentrations using the new thermodynamic dataset (Table 3.6) are in very good agreement with the experimental data for corundum solubility in alkaline solutions at high temperatures and pressures (Fig. 3.9). The main impact on the calculated results comes from the greatly improved properties of the associated species KOH^0 and NaOH^0 taking advantage of the new high-quality conductance data. The calculated corundum solubilities are now in very good agreement with their experimental counterparts (Fig. 3.10). As expected, there is a considerable disagreement with some of the experimental corundum solubility data in H_2O (see discussion of experimental data above). Very good agreement between calculated and experimental corundum solubility is observed for the high-quality datasets of Becker et al. (1983) and Tropper and Manning (2007) when using the properties of $\text{Al}(\text{OH})_3^0$ derived in this study.

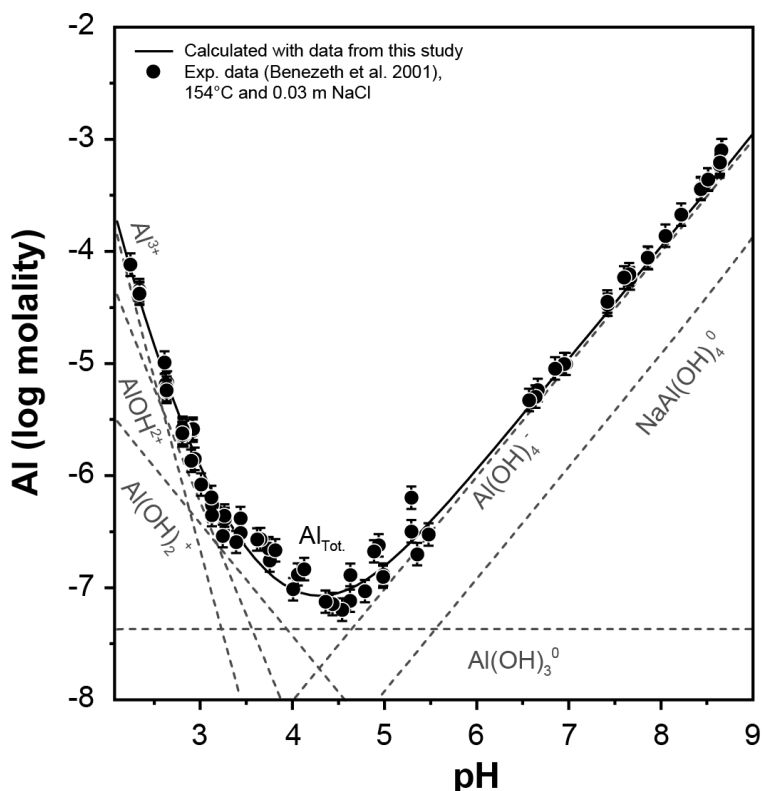


Figure 3.7. Comparison between calculated and experimentally measured boehmite solubility (Al concentration) as function of solution pH. The experimental data were obtained in 0.03 molal NaCl solutions (Bénézech et al., 2001).

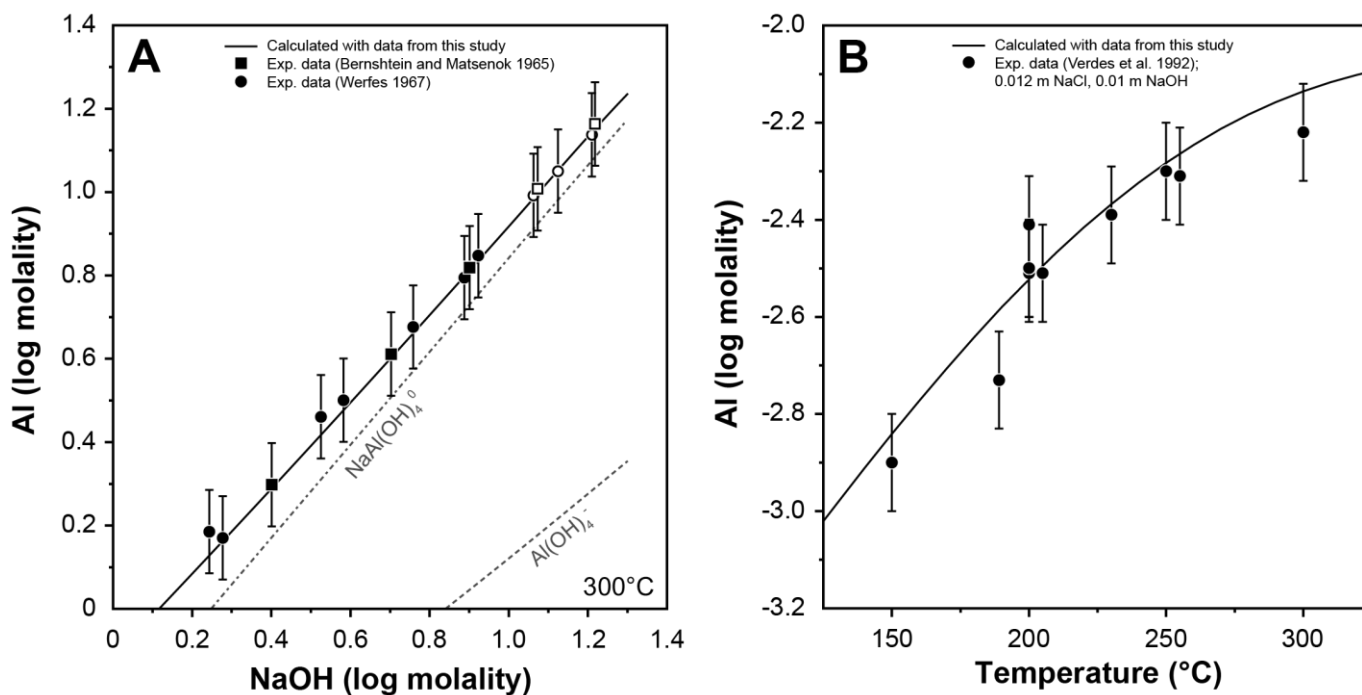


Figure 3.8. Comparison between calculated and experimentally determined diasporite solubility (Al concentration) as function of (A) NaOH concentration at 300 °C, and (B) as function of temperature. Full symbols represent experimental datapoints which were used in the global data regression, while open symbols represent experimental datapoints which were not used.

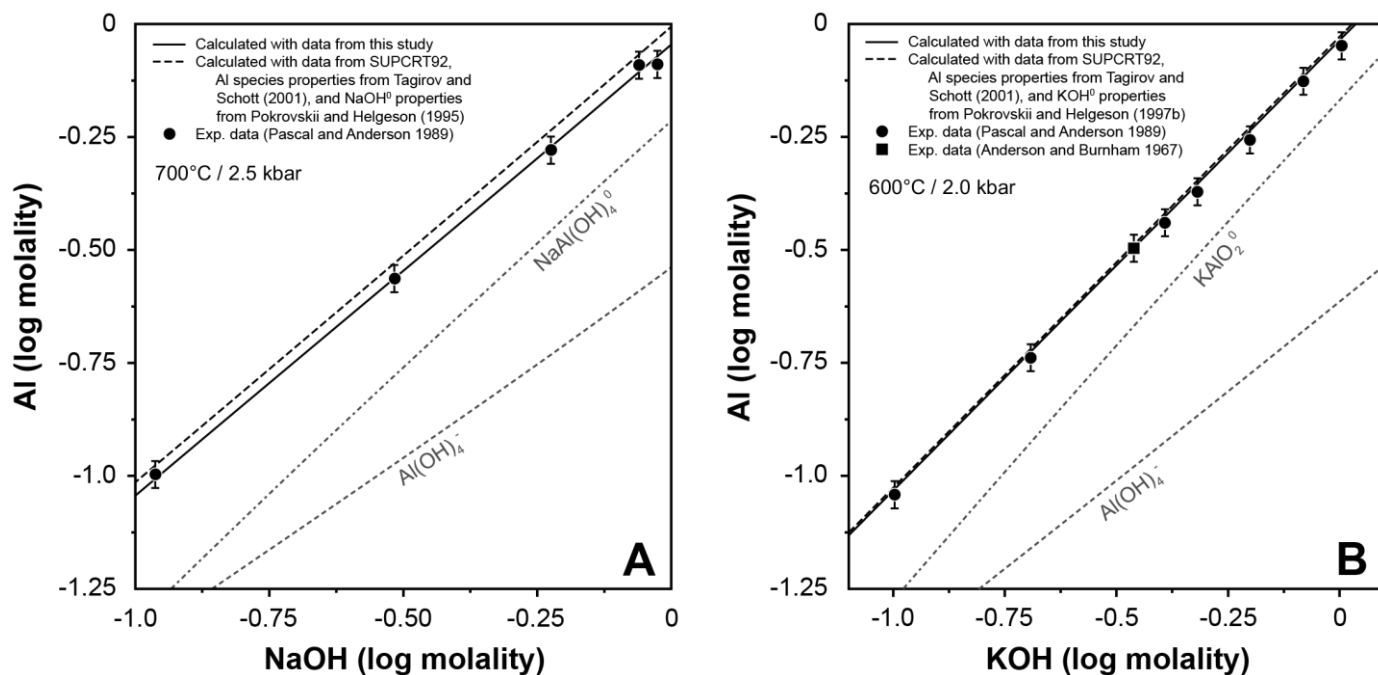


Figure 3.9. Comparison between calculated and experimentally determined corundum solubility (Al concentration) as function of (A) NaOH concentration (at 700°C and 2.5 kbar), and (B) KOH concentration (at 600°C and 2.0 kbar). The grey dashed and dash-dotted lines show the relative contributions of the $\text{Al}(\text{OH})_4^-$ species and alkali-aluminum ion pairs $\text{NaAl}(\text{OH})_4^0$ and KAlO_2^0 to total solubility.

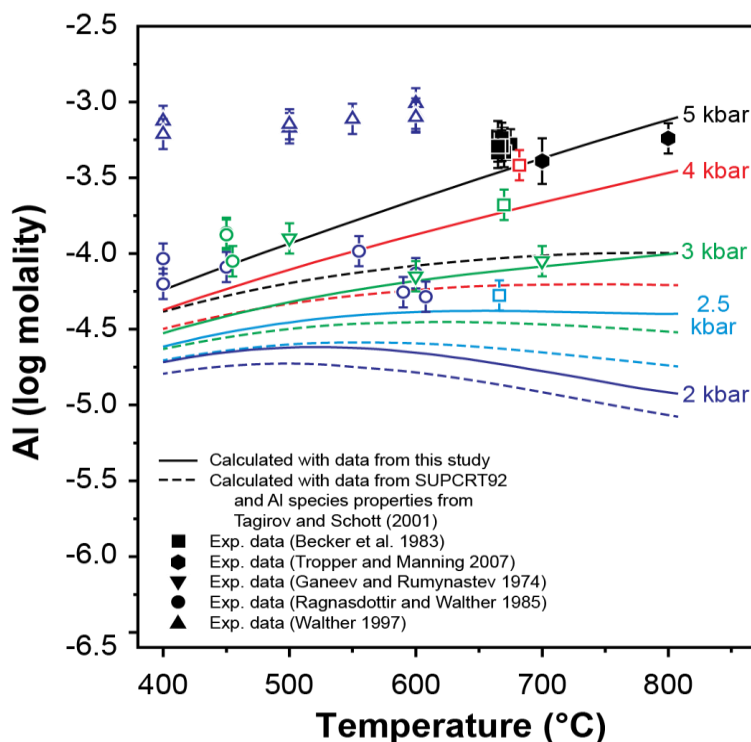


Figure 3.10. Comparison between calculated and measured corundum solubility (Al concentration) in supercritical water as function of temperature and at different pressures (2.0, 2.5, 3.0, 4.0 and 5.0 kbar). Full symbols represent experimental datapoints which were used in the global data regression, while open symbols represent experimental datapoints which were not used.

3.6.3. System Al-Si-O-H-Cl

There is a fairly good agreement between calculated and experimentally determined solubility data of aluminosilicate mineral pairs (Hemley et al. 1980). The phase equilibria pyrophyllite-kaolinite, pyrophyllite-andalusite and kaolinite-diaspore are mostly reproduced within their experimental uncertainty (Fig. 3.11). Only the calculated phase equilibria andalusite-corundum and andalusite-diaspore are slightly offset by a maximum value of 0.2 log units of the dissolved silica molality (Fig. 3.11).

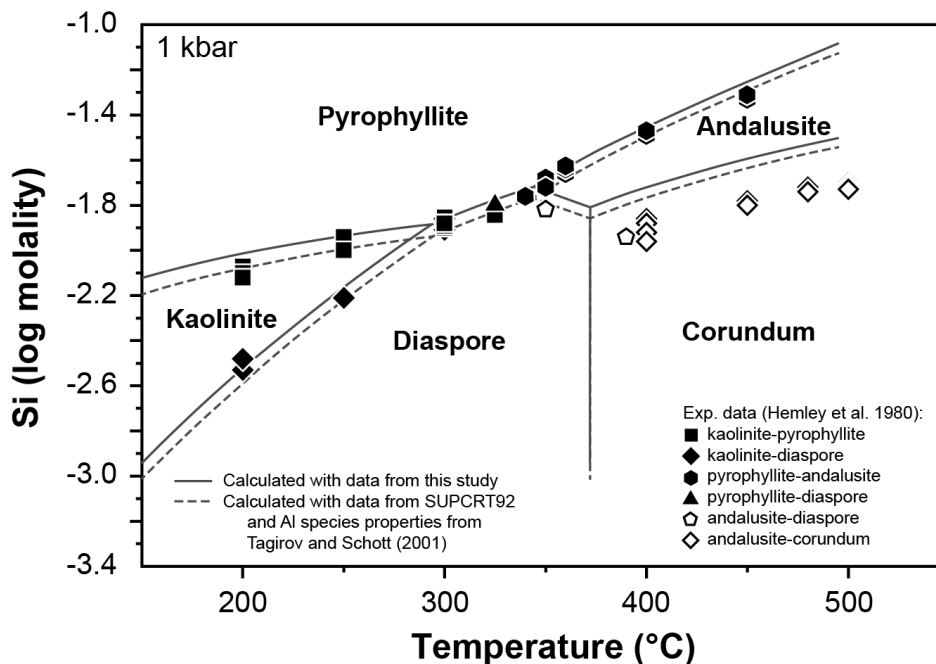


Figure 3.11. Comparison between calculated and experimentally determined phase equilibria and Si concentrations in the Si-Al-H-O system (Hemley et al., 1980) as function of temperature (and at 1 kbar pressure).

3.6.4. System K-Na-Al-Si-O-H-Cl

The only feldspar solubility experiments used for the global regression were those for albite reported by Davis (1972). The agreement between calculated and measured concentrations of Si, Na, and Al is generally very good (Fig. 3.12). There is not so good agreement with the albite-paragonite-quartz solubility data of Woodland and Walther (1987). While the calculated Si concentrations partly agree with the experimental ones, the Al and Na concentrations show substantial disagreement (Fig. 3.13). There is not only disagreement in terms of the absolute values of the Al and Na concentrations, but the calculated temperature and pressure trends do also diverge systematically from the experimental data. The experimental data at different pressures above 1.5 kbar appear to be overlapping within their uncertainties.

The new dataset is able to accurately reproduce the phase equilibria and $\log(\text{Na}/\text{H})$ values from the experimental study of Montoya and Hemley (1975) in the system albite-paragonite-quartz-fluid (Fig. 3.14). The calculated results are in better agreement with the absolute values of $\log(\text{Na}/\text{H})$ and their temperature trend than calculations using the SUPCRT92 dataset (Shock and Helgeson,

1988; Shock et al., 1989; Johnson et al., 1992; Shock et al., 1997; Sverjensky et al., 1997) and the HCl^0 properties from Tagirov et al. (1997). There is also fair agreement between calculated and experimental phase equilibria and $\log(\text{K}/\text{H})$ values (Hemley, 1959; Haselton et al., 1988; Sverjensky et al., 1991; Haselton et al., 1995) in the potassium system (Fig. 3.15). The agreement between calculated and experimental $\log(\text{K}/\text{H})$ values is not much improved with the new dataset for this system, but the temperature trends of the reaction boundaries are in better agreement with the experimental data. There is a systematic improvement in both the Na and K systems when the $\Delta_f G_{298,1}^0$ values for K^+ and Na^+ are included into the global regression. In the potassium system (Fig. 3.15), the only phase boundary that is still not too well reproduced is that of the pyrophyllite-muscovite reaction (Fig. 3.15). This could be due to possible changes in the structure of pyrophyllite during the experimental runs or some impurities in pyrophyllite or muscovite that would affect their stability.

Most importantly, calculations with the final aqueous species dataset are in very good agreement with the high-temperature solubility experiments in the four-mineral system albite+K-feldspar+andalusite+quartz (Hauzenberger et al., 2001; Pak et al., 2003). Especially the calculated Na and K concentrations are now exactly reproducing the experimental data (Figs. 3.16, 3.17 and 3.18). The Si and Al concentrations are also in good agreement with the experimental data, which are reproduced within their rather large uncertainties (Figs. 3.16 and 3.17). The experimental data for the Si and Al concentrations show a rather large scatter in the experimental dataset. This may reflect the fact that (unlike for the Na and K data), the Si and Al solubility data were not fully reversed in the experiments, and some values might therefore represent minimum concentrations.

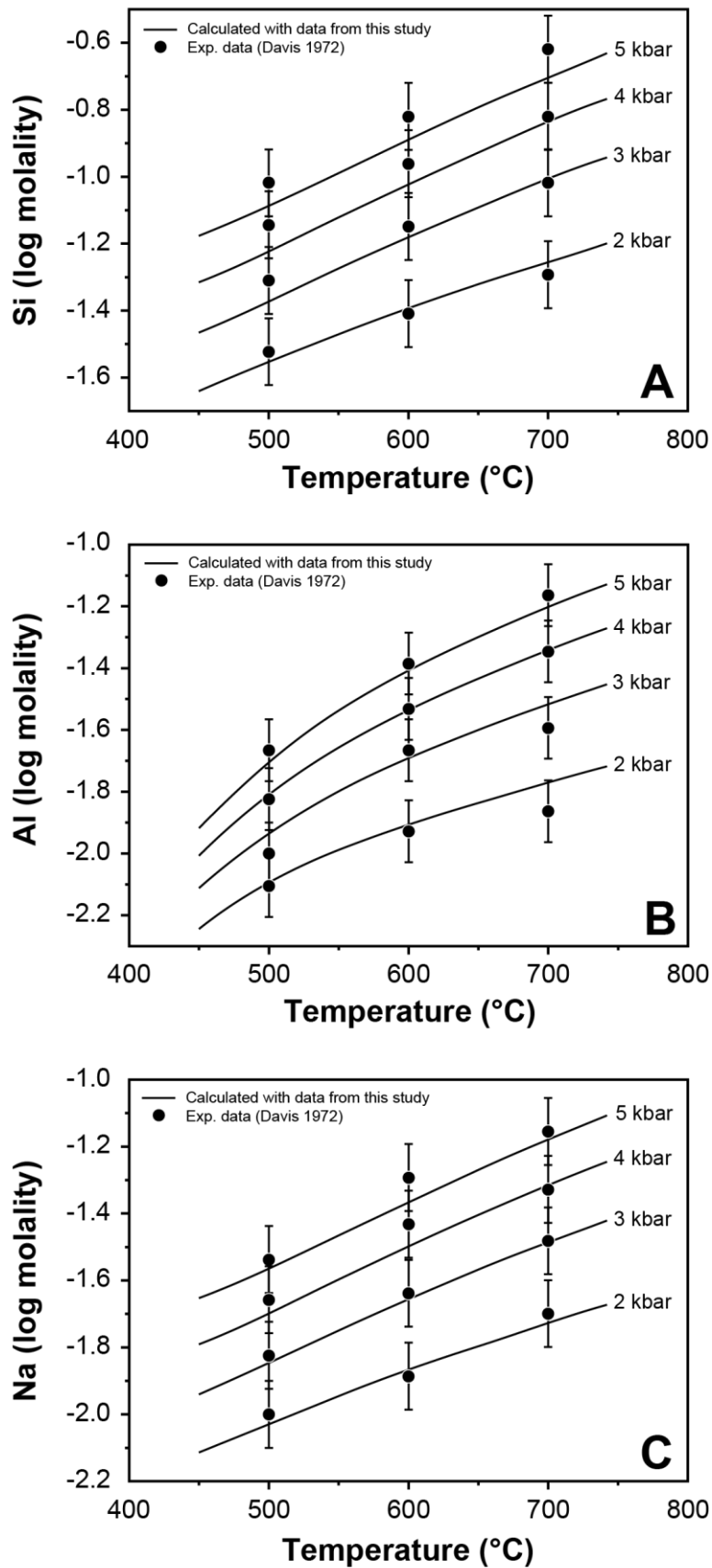


Figure 3.12. Comparison between calculated and experimentally determined albite solubility data (Davis, 1972) as function of temperature (and pressures of 2.0, 3.0, 4.0 and 5.0 kbar). (A) Si concentration. (B) Al concentration. (C) Na concentration.

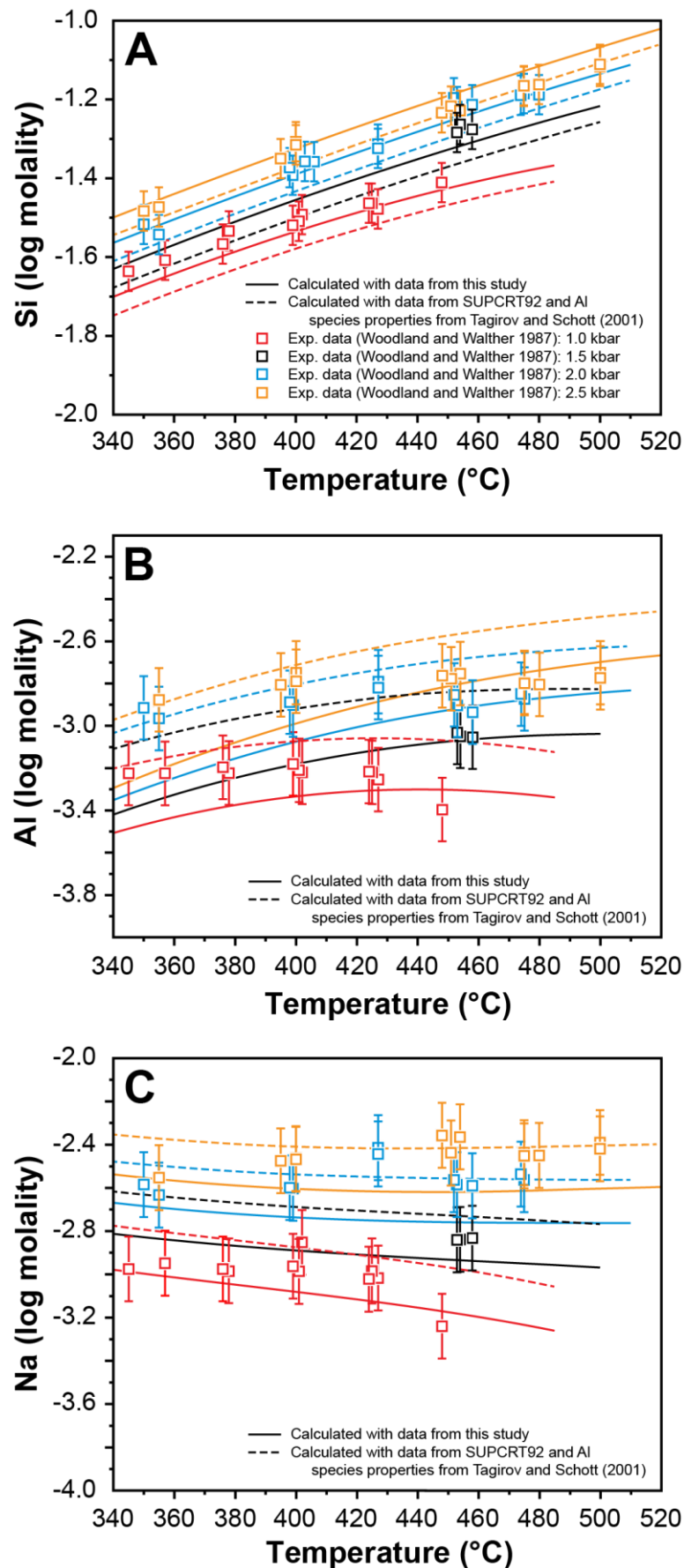


Figure 3.13. Comparison between calculated and experimentally determined solubility data in the albite-paragonite-quartz-water system (Woodland and Walther, 1987) as function of temperature (and pressures of 1.0, 1.5, 2.0 and 2.5 kbar). (A) Si concentration. (B) Al concentration. (C) Na concentration.

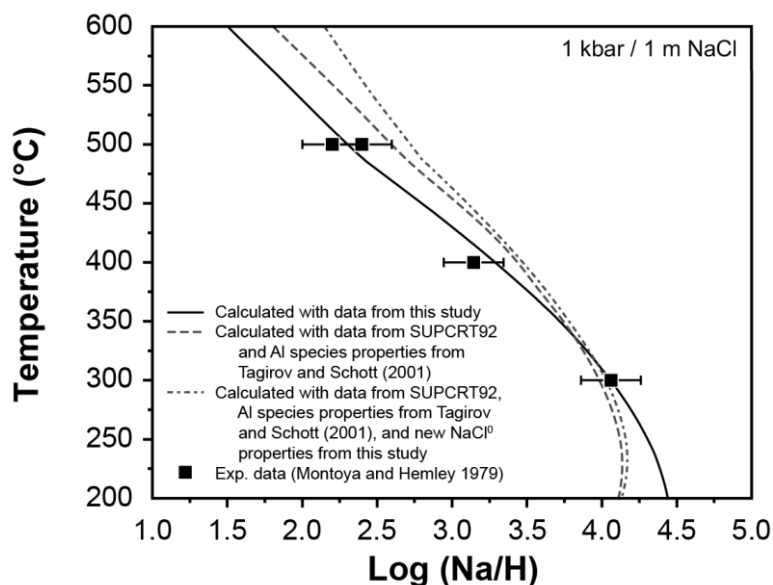


Figure 3.14. Comparison between calculated and experimentally determined $\log(\text{Na}/\text{H})$ values for the solubility of albite-paragonite-quartz assemblages (in 1 molal NaCl solution) as function of temperature (and at a pressure of 1 kbar).

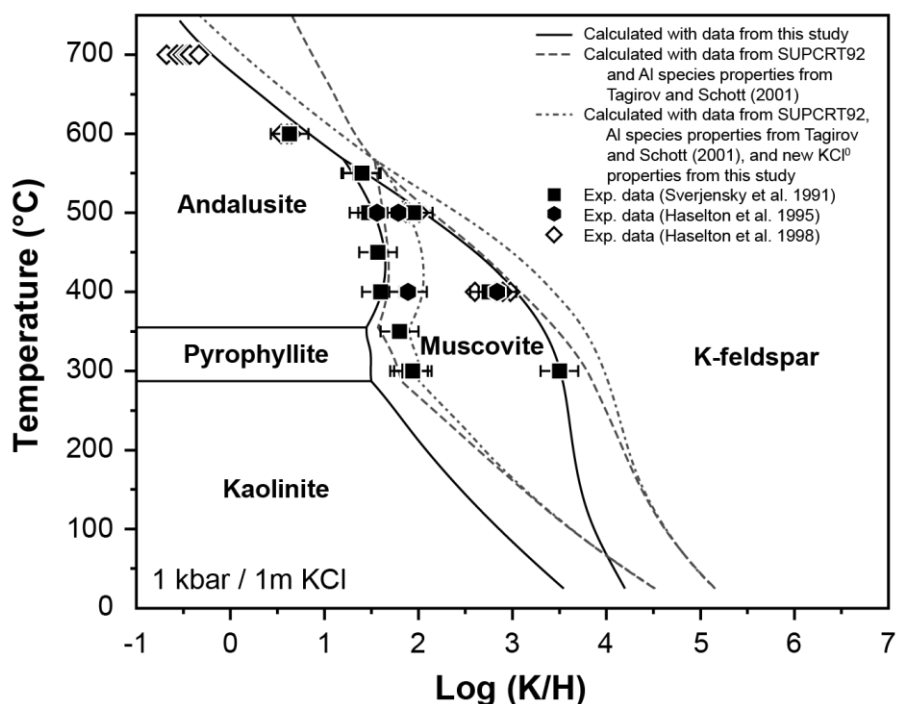


Figure 3.15. Comparison between calculated and experimentally determined phase equilibria and $\log(\text{K}/\text{H})$ values in the system Si-Al-K-OH-Cl (in 1 molal KCl solution) as function of temperature (and at a pressure of 1 kbar). Full symbols represent experimental datapoints which were used in the global data regression, while open symbols represent experimental datapoints which were not used.

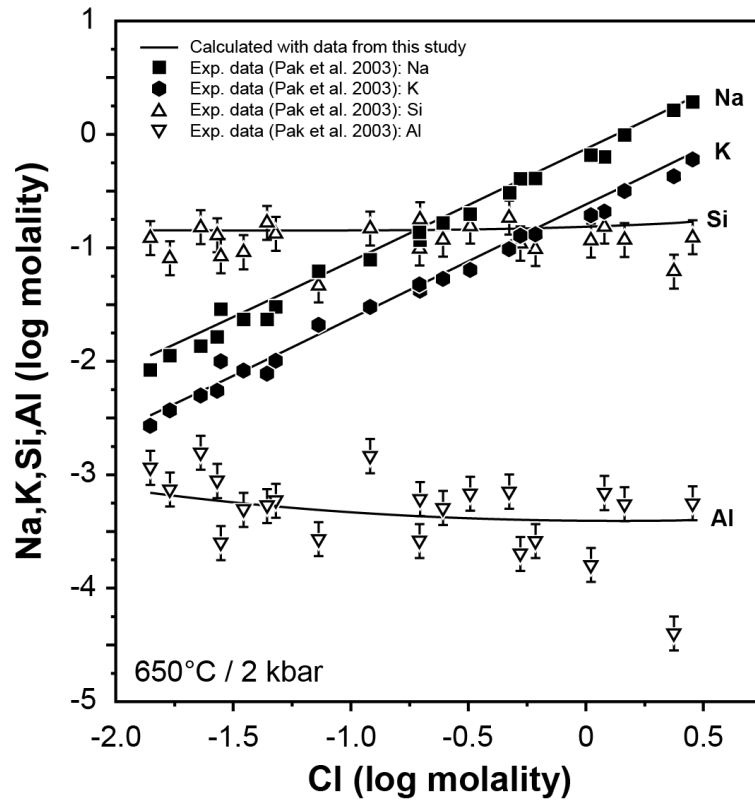


Figure 3.16. Comparison between calculated and experimentally determined (Pak et al., 2003) concentrations of Na, K Si and Al in a fluid in equilibrium with the mineral assemblage albite+K-feldspar+andalusite+quartz (at 650°C and 2.0 kbar), plotted as function of fluid chlorinity. The concentrations of Na and K in solution increase systematically with solution chlorinity, while the concentrations of Si and Al remain nearly constant.

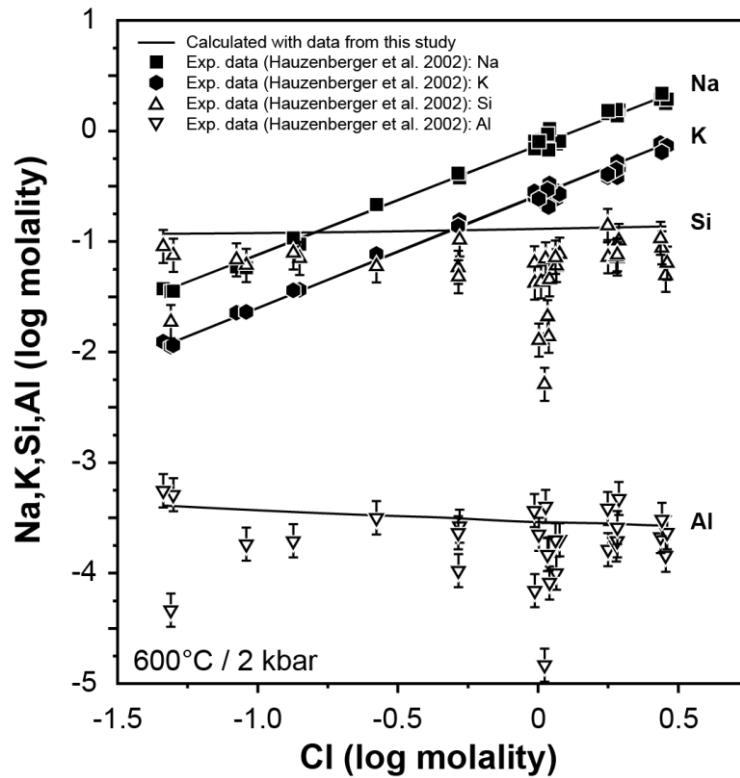


Figure 3.17. Comparison between calculated and experimentally determined (Hauzenberger et al., 2002) concentrations of Na, K Si and Al in a fluid in equilibrium with the mineral assemblage albite+K-feldspar+andalusite+quartz (at 600°C and 2.0 kbar), plotted as function of fluid chlorinity. The concentrations of Na and K in solution increase systematically with solution chlorinity, while the concentrations of Si and Al remain nearly constant.

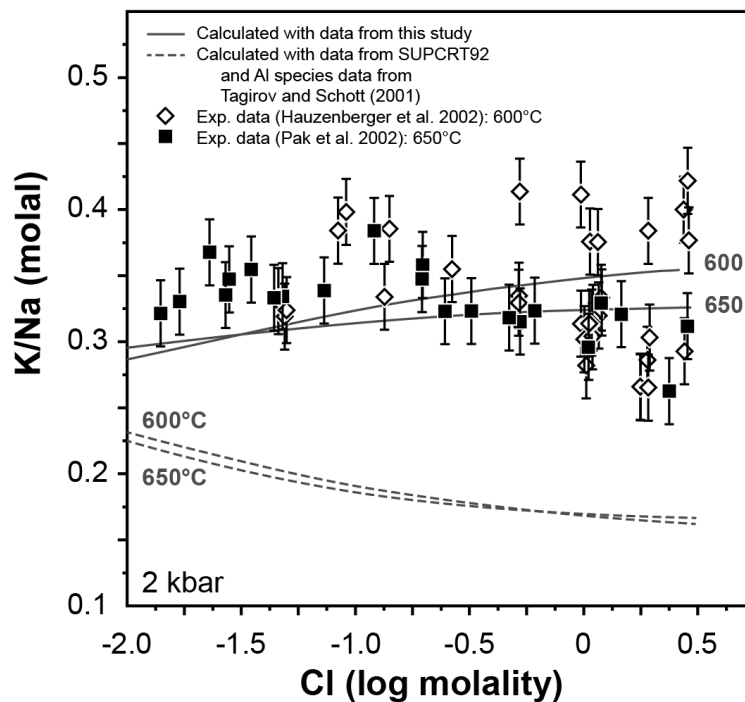


Figure 3.18. Comparison between calculated and measured molal (K/Na) ratios for the reversed solubility experiments in the system albite-K-feldspar-andalusite-quartz-fluid (Hauzenberger et al., 2002; Pak et al., 2003). The molal K/Na ratios are plotted as function of solution chlorinity.

Table 3.5. Standard state properties (partial molal entropy, heat capacity and volume) and HKF parameters of aqueous species used in this study. These values were not adjusted during the global optimization process but taken from their original references or from separate regression of association constant and solubility data.

Species	$S_{298,1}^0$ (J/mol·K)	$Cp_{298,1}^0$ (J/mol·K)	$V_{298,1}^0$ (J/bar)	$a_1 \cdot 10$ (cal/ mol/bar)	$a_2 \cdot 10^{-2}$ (cal/mol)	a_3 (cal·K /mol/bar)	$a_4 \cdot 10^{-4}$ (cal·K /mol)	c_1 (cal /mol/K)	$c_2 \cdot 10^{-4}$ (cal·K /mol)	$\omega_0 \cdot 10^{-5}$ (cal/mol)
⁽¹⁾ Al ³⁺	-339.74	-119.30	4.53	-3.3984	-16.0789	12.0699	-2.1143	14.4295	-8.8523	2.7403
⁽¹⁾ AlOH ²⁺	-181.13	-37.44	-2.06	-0.4532	-8.8878	9.2434	-2.4116	15.4131	-4.8618	1.5897
⁽¹⁾ Al(OH) ₂ ⁺	-27.55	40.84	0.386	2.4944	-1.6909	6.4146	-2.7091	16.7439	-1.0465	0.5324
⁽²⁾ Al(OH) ₃ ⁰	5.16	248.6	3.07	6.1977	8.2816	2.4950	-3.1214	71.1003	-1.0644	1.0461
⁽¹⁾ Al(OH) ₄ ⁻	103.55	96.54	4.63	8.4938	12.9576	0.6570	-3.3147	55.7265	-11.4047	1.0403
⁽¹⁾ NaAl(OH) ₄ ⁰	204.18	134.56	5.36	9.1270	14.3411	0.1121	-3.3719	60.7157	-14.0523	0.0000
⁽¹⁾ AlH ₃ SiO ₄ ²⁺	56.78	-300.66	1.393	0.1600	-7.2300	8.6100	-2.4800	37.0700	-49.6600	0.8800
⁽³⁾ KAlO ₂ ⁰	149.37	18.05	3.114	6.0070	6.8858	3.0436	-3.0637	1.3940	1.2120	-0.0500
⁽⁴⁾ K ⁺	101.04	8.28	0.906	3.559	-1.4730	5.4350	-2.7120	7.4000	-1.7910	0.1927
⁽⁴⁾ Na ⁺	58.41	37.91	-0.111	1.8390	-2.2850	3.2560	-2.7260	18.1800	-2.9810	0.3306
⁽⁵⁾ NaHSiO ₃ ⁰	41.84	102.95	1.273	3.4928	0.7500	5.4483	-2.8100	20.2395	1.9785	-0.0380
⁽⁶⁾ HSiO ₃ ⁻	19.7	-38.47	0.50	3.0900	-0.5201	5.9467	-2.7575	15.0000	-4.9202	1.5583
⁽⁷⁾ SiO ₂ ⁰	75.31	-318.45	1.61	1.9000	1.7000	20.0000	-2.7000	29.1000	51.2000	0.1291
⁽⁴⁾ Cl ⁻	56.74	123.18	1.779	4.0320	4.8010	5.5630	-2.8470	-4.4000	-5.7140	1.4560
⁽⁴⁾ OH ⁻	10.71	137.19	-0.418	1.2527	0.0738	1.8423	-2.7821	4.1500	-10.3460	1.7246
⁽⁴⁾ H ⁺	0	0	0	0	0	0	0	0	0	0

⁽¹⁾ Taken from Tagirov and Schott (2001).

⁽²⁾ Derived in this study using the standard state molar volume and heat capacity from Pokrovskii and Helgeson (1995), the boehmite solubility data from Benezeth et al. (2001) and the corundum solubility data at 5 kbar from Becker et al. (1983) and Tropper and Manning (2007).

⁽³⁾ Taken from Pokrovskii and Helgeson (1995).

⁽⁴⁾ Taken from Shock and Helgeson (1988).

⁽⁵⁾ Taken from Sverjensky et al. (1997).

⁽⁶⁾ Derived using the logK data from Busey and Mesmer (1977).

⁽⁷⁾ Taken from Shock et al. (1989)

Table 3.6. Final values of the standard-state molal Gibbs energy for aqueous species, obtained from the global optimization against experimental solubility datasets (Tables 3.2, 3.3 and 3.4). Gibbs energy values need to be combined with standard state entropy, volume, heat capacity and HKF parameters from Table 3.1 (ion pairs of main electrolytes) and Table 3.5 (other aqueous species). The standard deviation of parameters was calculated from 500 Monte Carlo simulation runs, and the 95% confidence interval - using the Student's t-distribution.

Species	$\Delta_f G_{298,1}^0$ (J/mol)	Standard deviation	95% confidence interval	Optimization mode
Al ³⁺	-486627	258	507	Optimized
AlOH ²⁺	-695574	543	1077	⁽¹⁾ Constrained
Al(OH) ₂ ⁺	-898295	1339	2627	Optimized
Al(OH) ₃ ⁰	-1105801	944	1852	Optimized
Al(OH) ₄ ⁻	-1305097	229	450	Optimized
NaAl(OH) ₄ ⁰	-1562121	944	1853	Optimized
AlH ₃ SiO ₄ ²⁺	-1782516	828	1547	⁽²⁾ Constrained
KAlO ₂ ⁰	-1100293	2423	4751	Optimized
K ⁺	-276893	643	1261	Optimized
KOH ⁰	-431656	-	-	⁽³⁾ Constrained
KCl ⁰	-402544	-	-	⁽³⁾ Constrained
Na ⁺	-256169	644	1263	Optimized
NaOH ⁰	-411594	-	-	⁽³⁾ Constrained
NaCl ⁰	-383091	-	-	⁽³⁾ Constrained
NaHSiO ₃ ⁰	-1283076	1820	3614	⁽⁴⁾ Constrained
HSiO ₃ ⁻	-1015237	-	-	⁽⁵⁾ Constrained
SiO ₂ ⁰	-834103	34	67	Optimized
Cl ⁻	-131290	-	-	⁽⁶⁾ Fixed
HCl ⁰	-127240	-	-	⁽⁷⁾ Fixed
OH ⁻	-157287	-	-	⁽⁶⁾ Fixed
H ⁺	0	-	-	⁽⁸⁾ Fixed
H ₂ O	-237183	-	-	⁽⁹⁾ Fixed

(1) Constrained to properties of Al³⁺ by the reaction: AlOH²⁺ + H⁺ = Al³⁺ + H₂O, using equilibrium constant values from Palmer and Wesolowski (1993).

(2) Constrained to properties of Al³⁺ and SiO₂⁰ by the reaction: Al³⁺ + 2 H₂O + SiO₂⁰ = AlH₃SiO₄²⁺ + H⁺, and equilibrium constants from Tagirov and Schott (2001), extracted from Pokrovskii et al. (1996) and Salvi et al. (1998).

(3) Constrained to properties of Na⁺, K⁺, OH⁻, and Cl⁻ using the equilibrium constants determined from the new standard state properties of ion pairs extracted from the conductance data (Table 3.1).

(4) Constrained to properties of Na⁺ and SiO₂⁰ by the reaction: Na⁺ + H₂O + SiO₂⁰ = NaHSiO₃⁰ + H⁺, using equilibrium constants from Sverjensky et al. (1997), extracted from Seward (1974).

(5) Constrained to properties of SiO₂⁰ by the reaction: SiO₂⁰ + H₂O = HSiO₃⁻ + H⁺, using equilibrium constants from Busey and Mesmer (1977)

(6) Taken from Shock and Helgeson (1988).

(7) Taken from Tagirov et al. (1997).

(8) Conventional value.

(9) Taken from Johnson et al. (1992).

Table 3.7. Correlation coefficients between the freely optimized aqueous species. They are calculated from the sensitivity analysis as outlined in Miron et al. (2015).

Species	Al(OH) ₂ ⁺	Al(OH) ₃ ⁰	Al(OH) ₄ ⁻	Al ³⁺	K ⁺	KAlO ₂ ⁰	Na ⁺	NaAl(OH) ₄ ⁰	SiO ₂ ⁰
Al(OH) ₂ ⁺	1.000	-0.604	0.049	-0.394	-0.004	-0.001	-0.004	-0.014	0.000
Al(OH) ₃ ⁰	-0.604	1.000	-0.109	0.175	0.003	0.004	0.003	0.027	0.000
Al(OH) ₄ ⁻	0.049	-0.109	1.000	-0.013	-0.009	-0.022	-0.010	-0.333	-0.002
Al ³⁺	-0.394	0.175	-0.013	1.000	0.005	-0.001	0.004	0.006	-0.001
K ⁺	-0.004	0.003	-0.009	0.005	1.000	0.062	0.791	0.684	-0.011
KAlO ₂ ⁰	-0.001	0.004	-0.022	-0.001	0.062	1.000	0.073	0.070	0.001
Na ⁺	-0.004	0.003	-0.010	0.004	0.791	0.073	1.000	0.864	-0.014
NaAl(OH) ₄ ⁰	-0.014	0.027	-0.333	0.006	0.684	0.070	0.864	1.000	-0.012
SiO ₂ ⁰	0.000	0.000	-0.002	-0.001	-0.011	0.001	-0.014	-0.012	1.000

3.7. Discussion

In the present study, we have adopted the strategy of refining the standard state Gibbs energies of aqueous ions and complexes by global regression of a large body of critically selected equilibrium solubility data for individual minerals and mineral assemblages. In this process, we have taken advantage of the availability of recent high-precision data for the association constants of aqueous complexes of major electrolytes (NaCl, KCl, NaOH, KOH, HCl) derived from conductance and potentiometric measurements. We have also accepted the thermodynamic properties of the minerals from the internally consistent database of Holland and Powell (1998), as given in the Thermocalc database ds55. This dataset is in very good agreement with the majority of the available calorimetric data and experimental phase equilibria brackets, and is widely used in a great number of petrological applications (e.g. Fabrichnaya et al., 2013; Lanari et al. 2014; Miron et al., 2013; Galvez et al., 2015; Tajčmanová et al. 2015). The Holland-Powell dataset is supported by a comprehensive suite of mineral solid-solution models that account for all essential crystal-chemical substitutions. Because we have accepted the thermodynamic properties of minerals as such, only the standard state thermodynamic properties of aqueous ions and complexes were allowed to adjust to bring them into agreement with the fluid-mineral equilibria experiments.

The problem of consistency between the standard state thermodynamic data of aqueous species and minerals in major geochemical-thermodynamic datasets has been addressed in a number of studies (Sverjensky et al., 1991; Zhu and Sverjensky, 1991; Holland and Powell, 1998; Tutolo et al., 2014). All studies concluded that there are major discrepancies between predictions from calculated fluid mineral-equilibria and experimental mineral solubility studies. Different strategies were then suggested for resolving these discrepancies. In most cases, the properties of aqueous species were accepted from different critical data compilations (e.g., CODATA), and the standard state Gibbs energies of the minerals were then adjusted to bring them into agreement with the experimental solubility data.

Sverjensky et al. (1991) resolved the discrepancies between calculated fluid-mineral equilibria and the respective experimental data by first adjusting the properties of minerals using a selected set of experiments, and then by refining the association constant data for HCl⁰. In this process, they retained the standard state thermodynamic properties and HKF parameters of all other aqueous ions and complexes. They adjusted the standard state Gibbs energies of selected minerals (paragonite, albite, muscovite, sanidine) using the thermodynamic datasets of Helgeson et al. (1978) and Berman (1988) as a basis. Zhu and Sverjensky (1991) extended the approach of Sverjensky et al. (1991) and determined the standard state properties of F- and Cl-bearing minerals using results of the F-Cl partitioning experiments between hydrous minerals and aqueous fluid.

The approach of Sverjensky et al. (1991) and Zhu and Sverjensky (1991) has a number of drawbacks. Firstly, the two mineral datasets (Helgeson et al., 1978; Berman, 1988) that were used as a basis for making the adjustments were not updated by taking advantage of more recent mineral phase equilibria experiments. The situation is fundamentally different for the mineral dataset of

Holland and Powell (1998), whose recent update (Thermocalc dataset ds55) has incorporated a large body of new experimental phase equilibria data. Secondly, the incremental adjustment to the standard state Gibbs energy of selected minerals breaks the internal consistency of the respective thermodynamic mineral dataset. Thirdly, the properties used for the ion pair association constants of major electrolytes (NaCl, KCl, NaOH, KOH, HCl) are not in agreement with the new conductance and potentiometric data. Fourthly, the choice to use a restricted set of experimental mineral solubility data for determining the magnitude of the Gibbs energy adjustments brings the data into better agreement with these particular experiments, but worsens the agreement with other mineral solubility data (as shown in the results section above).

Taking a different approach, Tutolo et al. (2014) proposed a method that is conceptually similar to the one proposed by Holland and Powell (1985) for producing an internally consistent mineral dataset. They refined the standard state Gibbs energy of some aluminum minerals against phase equilibria, calorimetric data, and also against selected solubility data. During the data optimization, they accepted the thermodynamic data for aqueous species from published sources. While the method used by Tutolo et al. (2014) ensures internal consistency for the system they have considered (they have chosen to adjust the properties of a few minerals in the aluminum system), this may break the thermodynamic consistency with experimental phase equilibria in other chemical systems where these minerals are involved into reactions. Although these authors noted a considerable improvement between calculated and experimental mineral solubility data, they nevertheless reported persisting discrepancies in modeling the Al-Si-Na-K-Cl-OH system using their adjusted mineral data. They further reported a substantial disagreement between the association constant data for the major electrolytes they used (Shock and Helgeson, 1988; Sverjensky et al., 1991) and the new experimental conductance data (Ho et al., 1994; Ho and Palmer, 1996; Ho and Palmer, 1997).

Holland and Powell (1998) presented a preliminary dataset for aqueous species together with their internally consistent database for minerals. They used an equation of state for aqueous species that is a modification of the density model (Anderson et al., 1991). The standard state properties of aqueous species were not refined as part of their simultaneous regression of the mineral thermodynamic data, but they have been collected from different sources and were processed separately. Holland and Powell (1998) compared the calculated fluid-mineral equilibria with the experimental data for a few selected examples, and demonstrated a reasonable agreement. However, they did not demonstrate that fluid-mineral equilibria calculated using their combined aqueous species and mineral data would be able to reproduce the large body of available mineral solubility data in the Na-K-Al-Si-O-H-Cl system. Furthermore, their data for aqueous ions and complexes are in disagreement with the association constants derived from the new conductance and potentiometric experiments.

Taken together, the previous attempts to address the large discrepancies between the calculated fluid-mineral equilibria and the experimental mineral solubility data have resulted in some improvements, but have not been able to fundamentally resolve the consistency issues in a general way. In our study, we have therefore used a very different approach by global regression of the

standard state Gibbs energies of aqueous ions and complexes against a large body of experimental mineral solubility data, while retaining the internally consistent thermodynamic data for minerals, and maintaining full consistency with the association constant data for aqueous complexes.

3.7.1. System Si-O-H-Cl

There are no major changes to the thermodynamic properties of the silica species, because this system was extensively studied and there is a large amount of high-quality experimental data available. The quartz solubility data in pure water over wide ranges of temperature and pressure are generally in good agreement with each other (with a few exceptions like the dataset of Xie and Walther, 1993) and can be well reproduced by model calculations. The quartz solubility data in KOH solutions (Anderson and Burnham, 1967; Pascal and Anderson, 1989) are systematically underpredicted by the speciation model that only accounts for the SiO_2^0 and HSiO_3^- species. This suggests that the KHSiO_3^0 complex may have formed in these experiments, similar to the better established complex NaHSiO_3^0 in the Na system, which would account for the difference between the calculated and measured quartz solubilities. More experimental data in the system $\text{SiO}_2\text{-H}_2\text{O-KOH}$ would be needed to evaluate the stability and standard state properties of the KHSiO_3^0 complex.

3.7.2. System Al-O-H-Cl

The experimental solubility data for gibbsite and boehmite were first used to retrieve the stability constants of Al hydroxide complexes AlOH^{2+} , Al(OH)_2^+ , Al(OH)_3^0 and Al(OH)_4^- . These were then used together with the experimental corundum and diaspore solubility data to refine the $\Delta_f G_{298,1}^0$ values of all Al species (Tables 3.5 and 3.6). When we initially fitted the corundum and diaspore solubility data separately, we noticed that the resulting $\Delta_f G_{298,1}^0$ for those Al species that are significant in the experiments were different by only a few hundred joules (but still within the 1 sigma error of the parameters), compared to the results obtained from the global fit that included the solubility data for all aluminum minerals. This suggests that the standard state properties of gibbsite and boehmite (Robie and Hemingway, 1995) are essentially consistent with the properties of corundum and diaspore in the HP02 dataset.

The extended Debye-Hückel aqueous activity model (Helgeson et al., 1981; Oelkers and Helgeson, 1990) is considered appropriate for aqueous solutions up to moderate salt concentrations. At higher salt concentration exceeding about 5 molal, the calculated activity coefficients start to deviate from experimental data (Sharygin et al., 2002; Hingerl et al., 2014; Appelo, 2015), resulting in a steeper increase in the calculated solubility compared to the experimentally measured values (Figs. 3.2, 3.5, and 3.6). We have, however, observed that the extended Debye-Hückel model is able to predict the experimental aluminum hydroxide solubilities in alkaline (NaOH and KOH) solutions reasonably well, even at higher salt concentrations. We attribute this to the predominance of associated neutral species at higher temperatures, which reduces the effective ionic strength to values within the applicability limits of the extended Debye-Hückel model.

Many studies have concluded that corundum solubility in water is controlled by the two species $\text{Al}(\text{OH})_3^0$ and $\text{Al}(\text{OH})_4^-$, with $\text{Al}(\text{OH})_3^0$ becoming predominant at temperatures exceeding 400 °C and pressures above 1.0 kbar (Pokrovskii and Helgeson, 1995; Tropper and Manning, 2007; Sverjensky et al., 2014). When using the thermodynamic properties for $\text{Al}(\text{OH})_3^0$ from Pokrovskii and Helgeson (1995), the calculated aluminum concentrations at near-neutral pH are about 1.5 orders of magnitude higher than those determined in the experiments (Tagirov and Schott, 2001). Using the thermodynamic data for Al species from Tagirov and Schott (2001) results in calculated corundum solubilities that are lower by around 0.7 log units than measured in the high-quality solubility experiments of Becker et al. (1983) and Tropper and Manning (2007). This most likely reflects that Tagirov and Schott (2001) derived the thermodynamic properties of $\text{Al}(\text{OH})_3^0$ only from boehmite solubility experiments up to 350 °C and SWVP. Therefore, calculated Al solubilities diverge increasingly from experimental ones at higher temperatures and pressures. To resolve this disagreement, we have refitted the standard state properties and HKF parameters of $\text{Al}(\text{OH})_3^0$ using both low- and high-temperature experiments. We accepted the standard state partial heat capacity and volume data of $\text{Al}(\text{OH})_3^0$ from Pokrovskii and Helgeson (1995) as initial values and then refined the $\Delta_f G_{298,1}^0$ in the global regression.

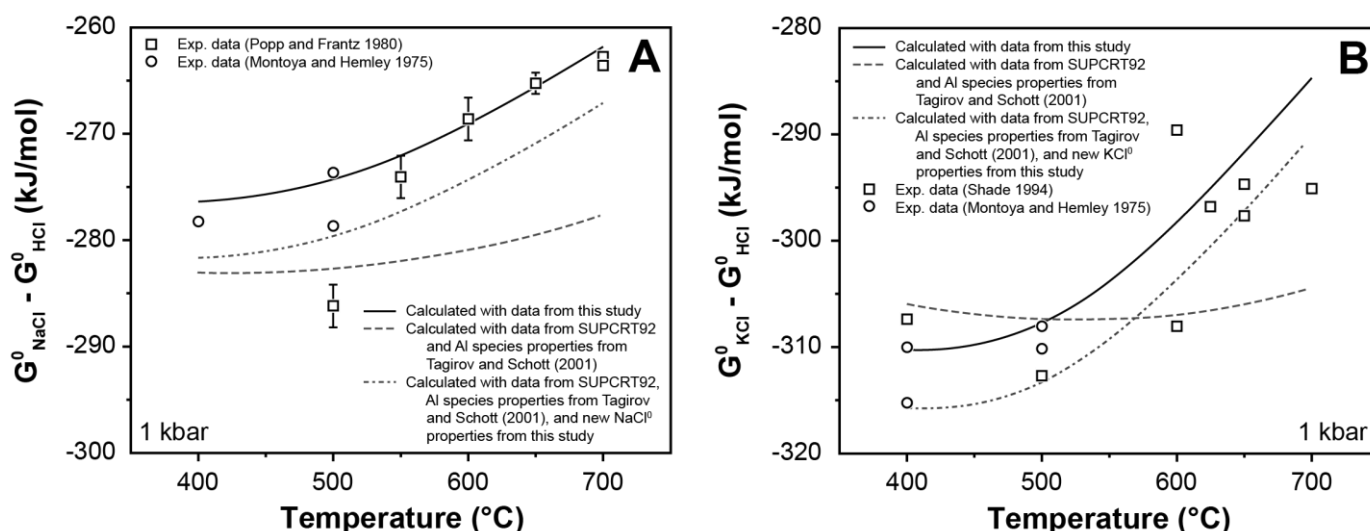


Figure 3.19. (A) Comparison between calculated ($G^0_{\text{NaCl}} - G^0_{\text{HCl}}$) values and their counterparts extracted from solubility experiments in the system Na-Al-Si-O-H-Cl (Montoya and Hemley, 1975; Popp and Frantz, 1980). The data are plotted as function of temperature (and at a pressure of 1 kbar). Popp and Franz (1980) suggest that their datapoint at 500°C is inconsistent with the remainder of their data. (B) Comparison between calculated ($G^0_{\text{KCl}} - G^0_{\text{HCl}}$) values and their counterparts extracted from solubility experiments in the system K-Al-Si-O-H-Cl (Montoya and Hemley, 1975; Shade 1994). The data are plotted as function of temperature (and at a pressure of 1 kbar).

3.7.3. System Al-Si-O-H-Cl

The discrepancies between the calculated and the experimentally determined Si concentrations in equilibrium with the assemblages corundum+andalusite and disapore+andalusite cannot be resolved by adjusting the standard state properties of the SiO_2^0 species (Fig. 3.11). We suspect that most likely additional Si-Al complexes that were not accounted for in our speciation model like AlSiO_4^- or HAlSiO_4^0 (Manning, 2007) have contributed to enhanced silica solubility. Because of insufficient data to constrain the thermodynamic properties of these species, we were not able to include them into our model.

3.7.4. System K-Na-Al-Si-O-H-Cl

The calculated $\log(\text{K}/\text{H})$, $\log(\text{Na}/\text{H})$ and K/Na ratios in chlorine bearing systems (Figs. 3.14, 3.15 and 3.18) are determined by the thermodynamic properties of Na^+ , K^+ , NaCl^0 , KCl^0 , HCl^0 , and those of the buffering minerals. Because we have adopted the strategy of using fixed thermodynamic properties of minerals, adjusting the properties of aqueous ions and complexes was the only possibility to bring the calculated fluid-mineral equilibria into agreement with the experimental solubility data. Because we wanted to maintain consistency with the association constant data NaCl^0 , KCl^0 and HCl^0 at elevated temperatures and pressures derived from conductance experiments, we had to adjust the thermodynamic properties of the Na^+ and K^+ ions. This was done by regressing their $\Delta_f G_{298,1}^0$ values against a large body of solubility data for Na-K-aluminosilicate mineral assemblages in chloride solutions (Montoya and Hemley, 1975; Haselton et al., 1988; Sverjensky et al., 1991; Haselton et al., 1995).

The calculated K/Na ratios are now in good agreement with the experimental data from Hauzenberger et al. (2001) and Pak et al. (2003). This is largely due to the improved thermodynamic properties of the KCl^0 and NaCl^0 species. This leads to the conclusion that during optimization of the $\Delta_f G_{298,1}^0$ values of the ions, every adjustment to K^+ must be accompanied by an adjustment to Na^+ of similar magnitude. This is essential for maintaining the agreement with the experimental K/Na partitioning data (Hauzenberger et al., 2001; Pak et al., 2003). This further leads to the prediction that an adjustment in the $\Delta_f G_{298,1}^0$ of K^+ and Na^+ of similar magnitude should then simultaneously improve the agreement between calculated and experimentally measured $\log(\text{K}/\text{H})$ and $\log(\text{Na}/\text{H})$ values. This is exactly what is observed as a key result from the final global data regression of this study. Figures 3.14 and 3.15 show that the agreement between calculated and experimentally measured data is considerably better in both the K- and the Na-system, while the good agreement with the experimental K/Na partitioning data is maintained (Figs. 3.16 and 3.17). This result can be further analyzed by looking at the relative Gibbs energy differences $(G_{\text{NaCl}}^0 - G_{\text{HCl}}^0)$ and $(G_{\text{KCl}}^0 - G_{\text{HCl}}^0)$ extracted by Popp and Frantz (1980) from experimental studies (Fig. 3.19). The agreement with the temperature trends is already greatly improved by using the KCl^0 and NaCl^0 association constant data from this study, but good

agreement with the absolute values is only achieved after optimization of the $\Delta_f G_{298,1}^0$ values of K^+ and Na^+ .

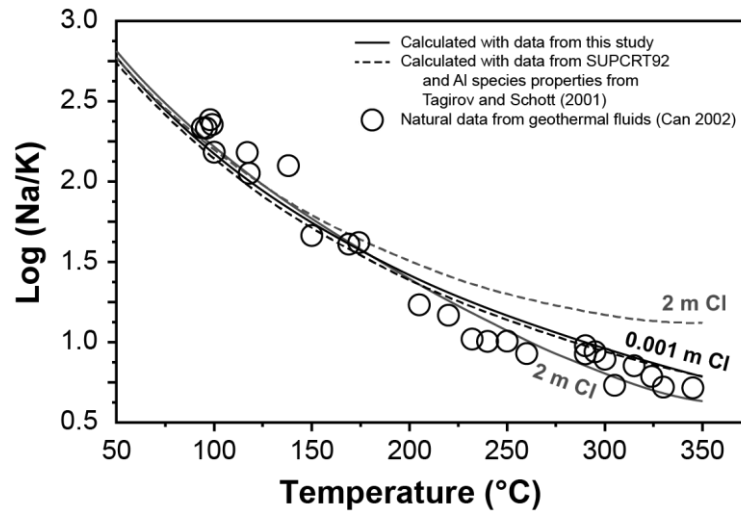


Figure 3.20. Comparison between calculated $\log(Na/K)$ ratios and those measured from natural geothermal fluids (Can, 2002), plotted as function of temperature (and at SWVP). The calculations were performed for fluid salinities of 0.001 and 2.0 molal NaCl, assuming equilibrium with the mineral assemblage K-feldspar+albite+muscovite+quartz.

An empirical test for the quality of the new thermodynamic dataset is provided by a comparison of calculated Na/K ratios for a fluid in equilibrium with the assemblage K-feldspar+albite+muscovite+quartz with the natural data from geothermal waters (Fig. 3.20). The calculated data are in excellent agreement with the natural Na/K ratios, which have been used by Can (2002) to develop an empirical solute thermometer for geothermal exploration.

3.7.5. Thermodynamics of the aqueous K^+ and Na^+ ions

The experiments that largely determine the adjustments to the $\Delta_f G_{298,1}^0$ values of the K^+ and Na^+ ions were performed at elevated temperature and pressure conditions. Therefore, it could be argued that a good agreement with the experimental data could have been achieved by adjusting the standard state entropy, volume, heat capacity or the HKF parameters for the ions. These properties were obtained using the framework of the HKF model by Tanger and Helgeson (1988). They used experimental standard partial molal volumes, isothermal compressibilities, and isobaric heat capacities of several aqueous electrolytes (e.g., HCl, NaCl, KCl, NaOH, KOH; Tanger and Helgeson, 1988) over a range in temperature. From those experimental data, they extracted the HKF equation of state parameters for the electrolytes. When performing regression of the partial molal entropy, volume, heat capacity and HKF equation of state coefficients for Na^+ and K^+ and other ions, they used the following thermodynamic constraint:

$$\Omega_k = \sum_j v_{j,k} \Omega_j \quad (3.12)$$

where Ω stands for the HKF equation of state coefficients of the j th aqueous ion and the k th aqueous electrolyte, and $v_{j,k}$ is the stoichiometry coefficient of the j th ion in the k th electrolyte.

This means that HKF coefficients for the aqueous ions are directly linked to the values of the corresponding coefficients for aqueous electrolytes. Therefore, any modification of the HKF coefficients of these ions that does not satisfy Eq. (3.12) will break the fundamental consistency of the HKF model. For example, if the values of some HKF coefficient for K^+ will be changed, this will result in an adjustment to the corresponding HKF coefficients of Cl^- . Because the HKF coefficients of Cl^- are also linked to those of $HCl(aq)$ through Eq. (3.12), this change in the HKF coefficients of Cl^- will then violate the fundamental convention that all properties of the H^+ ion are zero at any temperature and pressure.

Accepting these thermodynamic constraints, the only feasible strategy was to adjust the $\Delta_f G_{298,1}^0$ values of the K^+ and Na^+ ions. We will now discuss how this adjustment is justified in view of the sources for the $\Delta_f G_{298,1}^0$ values of K^+ and Na^+ that are found in the geochemical and chemical literature. The $\Delta_f G_{298,1}^0$ values of the Na^+ and K^+ ions used in most geochemical databases are accepted from CODATA (Cox et al., 1989). The sources for these values are ultimately calorimetric data for the heats of reaction and hydrolysis of solid Na and K metals with H_2O , and standard electrode potential measurements (Smith and Taylor 1940; Gunn and Green 1958; Cerquetti et al., 1968; Dill et al., 1968). These heats of reaction were combined with the heats of formation of $H_2O(aq)$, that of OH^- , the heats of dilution and the standard state entropies for the elements from the NBS tables (Wagman et al., 1982) to derive the heats of formation for the K^+ and Na^+ ions at infinite dilution. The standard state Gibbs energy of formation and the standard state entropy were calculated from standard electrode potential measurements (Smith and Taylor 1940; Dill et al., 1968). When reviewing the basic literature data on the electrode potential measurements related to Na^+ and K^+ , it becomes clear that the maximum error that could arise from the experimental measurements and the data processing should not exceed about 0.5 kJ/mol.

Another reason for adjustments of $\Delta_f G_{298,1}^0$ values of the Na^+ and K^+ ions could be our incomplete understanding of the speciation and activity coefficients of aqueous species in hydrothermal solutions. The HKF model parameters also introduce errors in the properties of the species, and the model itself has several limitations. While the HKF model was developed using the physically sound Born solvation theory for charged species, it was subsequently extended to nonelectrolytes and neutral species as well (Shock et al., 1989). However, it has been demonstrated theoretically and using experimental data that the Born-type model is not really suitable for calculating and predicting thermodynamic properties of neutral species, especially at near-critical and supercritical conditions (Akinfiev and Diamond, 2003; Plyasunov, 2015; Plyasunov and Shock, 2001).

3.7.6. Thermodynamics of Na- and K-bearing minerals

The overall success of the Holland-Powell mineral thermodynamic datasets (Holland and Powell, 1985, 1990, 1998, 2011) is based on their internal consistency and the close agreement with a large amount of phase equilibria experiments, rather than on the agreement of individual values for the standard enthalpies of formation with calorimetric data. This makes these datasets

extremely valuable and successful in petrological and geochemical applications where phase equilibria of complex rock-dominated systems are modeled. Favoring internal consistency rather than accuracy for individual enthalpy values is also the key reason, why subsequent versions of the database show large differences (up to ca. 7.0 kJ/mol and more) in standard enthalpies for some individual minerals. For example, the standard enthalpy of muscovite is 7.6 kJ/mol higher in Holland and Powell (2011) compared to Holland and Powell (1998), and that of paragonite is 3.4 kJ/mol higher. These differences do not have any visible impact when modeling phase equilibria for metamorphic rocks because essentially the same experimental dataset was used to refine the parameters in both versions of the database, and the agreement with these experimental data is very good. The changes in absolute values of enthalpies of formation for the minerals just reflect changes to the equations of state and phase transition models that were used, e.g. the new thermal equation of state and the symmetric formalism for modeling order-disorder in Holland and Powell (2011).

When optimizing the standard enthalpies of minerals, Holland and Powell (1998, 2011) have mainly used experimental phase equilibria data, but also mineral calorimetry data (Robie et al., 1979; Robie and Hemingway, 1995) as a set of rather loose constraints. The calorimetric constraints have a variable impact on the final regressed enthalpy values. In most cases, the mineral end-members with calorimetric constraints display the smallest change between different versions of the dataset. Most of the adjustments arising from the experimental phase equilibria data are assimilated by the standard enthalpies of mineral end-members without calorimetric constraints (e.g. muscovite, paragonite). As a result, the mineral end-members with no loose calorimetric constraints are typically those showing the largest differences between subsequent versions of the Holland-Powell database. For example, the substantial change in the standard enthalpy of microcline between Holland and Powell (1990) and Holland and Powell (1998) was due to a change in the calorimetric data that were used. In Holland and Powell (2011), the calorimetric constraint for microcline is retained, and the shift of the enthalpy value is just -280 J/mol compared to Holland and Powell (1998). By contrast, the difference in the standard enthalpy of muscovite, which did not have any calorimetric constraints, is -2.5 kJ/mol between Holland and Powell (1998) and Holland and Powell (1990), and 7.6 kJ/mol between Holland and Powell (2011) and Holland and Powell (1998). These substantial differences between versions of the Holland-Powell mineral dataset are also reflected by the rather large errors reported for the final values of the enthalpies of formation. These amount to 5.8, 6.1, 3.8 and 4.0 kJ/mol for microcline, muscovite, albite and paragonite, respectively (Holland and Powell, 1990, 1998, 2011).

Calorimetric values reported in compilations of Robie et al. (1979) and Robie and Hemingway (1995) do not come from direct measurements, but are based on calculation of thermochemical cycles using heats of reactions measured by HF dissolution or molten-salt calorimetry. The thermochemical cycle for calculating the standard enthalpy of formation of microcline, given in Hemingway and Haselton (1994), involves 13 reactions. Each reaction has an associated experimental error of several kJ/mol, and some reaction enthalpies may be affected by systematic errors as well. The change of 6.9 kJ/mol for microcline in Robie and Hemingway (1995) was

related to a systematic error in calorimetric measurements of the enthalpy of solution of aluminium chloride hexahydrate in HF. Considering that errors in calorimetric measurements of just one reaction are so large and that 13 reactions are involved in the thermochemical cycle, the uncertainty interval for the standard enthalpy of microcline and other rock-forming silicate minerals is at least of the order of 10 kJ/mol. This warrants adjustments to the enthalpies of formation of similar magnitude, when thermodynamic data for minerals are refined against experimental phase equilibria data via an internally-consistent data regression procedure.

In our study, we have selected the Holland-Powell mineral dataset as a hard constraint. Fitting the properties of the mineral end-members together with those of the aqueous species would have involved all the experimental phase equilibria data that were also used in optimizing the parameters in the Holland-Powell dataset. This formidable task was far beyond the scope of this study, because initially we did not see any need for refining the mineral properties, given that Holland and Powell (1990, 1998, 2011) have demonstrated that they are able to reproduce all available experimental phase equilibria data within their uncertainty brackets. The focus of our study was rather to model complex fluid-rock systems at hydrothermal conditions, taking advantage of the already refined and highly successful Holland-Powell database for minerals. We have therefore optimized the standard Gibbs energies for the aqueous species against the solubility experiments. We recognized that, in fact, the absolute values of standard enthalpies of formation for the K- and Na-bearing minerals are much less constrained than those for the Na⁺ and K⁺ ions. However, we accepted that as a consequence of our approach, the Gibbs energies of formation for the K⁺ and Na⁺ ions had to be adjusted to bring about a good agreement between calculated and experimentally determined fluid-mineral equilibria data.

3.7.7. Internally consistent thermodynamic database

Internally consistent thermodynamic data are not necessarily in best agreement with all of the experimental solubility data or with other types of data such as calorimetric or electromotive force measurements. Because the equations of state and thermodynamic models used in calculations have associated errors and because the data fixed during the regression process (e.g. equilibrium constants for complexes derived from conductance data, the thermodynamic data for minerals) contribute additional errors, the accumulated discrepancies are assimilated by the adjustable parameters i.e. standard Gibbs energies of the aqueous species in this work. Therefore, internally consistent datasets may actually show significant differences between modeled and measured properties of individual substances. The major advantage of an internally consistent dataset is the ability to reproduce a large range of experimental data and to model complex natural systems in a robust and accurate way, in contrast with plain compilations of thermodynamic data collected from different sources, which may have been derived from individual experiments using vastly different assumptions and models. While some of these data compilations (e.g. CODATA) may be in good agreement with selected precisely measured thermodynamic properties, they are clearly not fully consistent with the large body of experimental solubility, conductance and calorimetric data and can therefore not be used directly to model complex geochemical fluid-mineral equilibria.

This clearly highlights that it is not sensible to model complex geochemical systems at hydrothermal conditions using thermodynamic properties of minerals and aqueous species assembled from several data sources that are not linked to each other by a consistent data treatment procedure. The only feasible approach for overcoming these limitations is to derive thermodynamic data through an internally consistent regression procedure, as performed in this study. The resulting values may not be the most accurate ones for each and every specific chemical system, and the refined properties of some aqueous species may differ from the values accepted in major compilations like CODATA. Nevertheless, the new dataset can be successfully used to model complex multi-component, multi-phase geochemical systems, including mineral solubility and aqueous speciation, at a level of confidence and accuracy that was hardly possible before.

3.7.8. Agreement with CODATA for Na⁺ and K⁺ ions

Because we have adopted the strategy to keep the thermodynamic properties of minerals fixed during the global regression of solubility data, the discrepancies between calculated and experimentally determined fluid-mineral equilibria were translated into adjustments to the values of the standard state Gibbs energy of formation aqueous species including those of the Na⁺ and K⁺ ions. This has the result that their $\Delta_f G_{298,1}^0$ values are not any more in agreement with the CODATA recommended values. However, even if we would have included the $\Delta_f G_{298,1}^0$ of minerals along with those of aqueous species into the regression process (and fitting them against mineral solubility data and mineral reaction phase equilibria), this would not guarantee the outcome that the refined $\Delta_f G_{298,1}^0$ values of K⁺ and Na⁺ ions would be equal to those from CODATA. Acknowledging that many aqueous and hydrothermal geochemists consider the agreement with CODATA values as highly important, we have generated an alternative converted thermodynamic dataset where the $\Delta_f G_{298,1}^0$ values of K⁺ and Na⁺ from CODATA were retained, but the properties of the K- and Na-bearing minerals were shifted accordingly (Table 3.EA-4). This was done by adjusting the $\Delta_f G_{298,1}^0$ values of all K- and Na-bearing minerals by 5569 and 5712 J per mole of K and Na in their formula, respectively. A similar adjustment method was proposed by Sverjensky et al. (1991). This alternative dataset provides the same level of internal consistency and quality in terms of the agreement with experimental solubility and fluid-mineral equilibria data. This is because the reaction equilibrium constants between any K and/or Na-bearing aqueous ions, species, and minerals in the two datasets are not affected. The alternative dataset represents a workaround for matching the recommended CODATA values of Na⁺ and K⁺ aqueous ions. We, nevertheless, recognize the shortcomings of this formal conversion, and suggest that the next generation of internally consistent thermodynamic datasets for fluid-rock interaction should take advantage of both experimental mineral reaction brackets and fluid-mineral equilibria data. The properties of aqueous species and mineral end-members should be simultaneously refined, but the properties of the basic ions such as K⁺ and Na⁺ should be used as anchors, because they are well-constrained from highly accurate experiments.

3.8. Conclusions and outlook

- (1) A large amount of critically evaluated experimental solubility data covering the entire Na-K-Al-Si-O-H-Cl system over a wide range in temperatures and pressures was used to simultaneously refine, in an internally consistent way, the standard state Gibbs energies of aqueous ions and complexes. An astonishing degree of consistency with a large body of fluid-mineral equilibria data is obtained. This is achieved by adjusting the standard state Gibbs energies of the aqueous species.
- (2) The global optimization of standard state Gibbs energies of aqueous species was set up in such a way that the association equilibria for ion pairs and complexes independently derived from conductance and potentiometric data are always maintained. This was achieved by introducing reaction constraints into the optimization problem, which adjust the standard state Gibbs energies of complexes by their respective Gibbs energy of reaction whenever the properties of the reactant species (ions) are changed. Optimized parameters can therefore be reported with calculated parameter confidence intervals and correlation coefficients.
- (3) The new dataset is inherently consistent with the Holland and Powell (1998) mineral dataset (Thermocalc dataset ds55) and with all experimental mineral phase equilibria used to derive these data, as well as with experimental constraints on aqueous speciation equilibria. The dataset reproduces all available fluid-mineral phase equilibria and mineral solubility data with good accuracy over a wide range in temperature, pressure and composition (25 to 800 °C; 1 bar to 5 kbar; salt concentrations up to 5 molal).
- (4) This work serves as a proof of concept for the optimization strategy that is feasible and successful in generating a thermodynamic dataset reproducing all fluid-mineral and aqueous speciation equilibria essentially within their experimental uncertainties. The core dataset in the system Na-K-Al-Si-O-H-Cl can be further extended using the same strategy to include additional rock-forming elements such as Ca, Mg, Fe, Mn, Ti, S, C and B. Work is currently in progress to incorporate Ca, Mg and C into the dataset, taking advantage of new experimental data for the solubility of Ca and Mg carbonate and silicate minerals.
- (5) The global data optimization process implemented for this study can be repeated when an extension to new chemical elements and species is needed, when new experimental data become available, or when different aqueous activity models should be used. From a conceptual point of view, it is desirable that in the future also mineral phase equilibria and stability data and mineral partitioning data would be added to the experimental database. Then the standard-state properties of minerals and aqueous species could be simultaneously optimized to create a next-generation internally consistent dataset for fluid-mineral equilibria.
- (6) The new geochemical-thermodynamic dataset for fluid-mineral equilibria, which resolves the existing data discrepancies, will help dramatically improve the quality and robustness of the next generation of geochemical and reactive transport models. This is a crucial step in gaining in-depth understanding of fluid-rock reaction processes such as formation of hydrothermal ore deposits, evolution of natural and engineered geothermal reservoirs, and fluid chemistry in compressional orogenic belts, subduction zones, and mid-ocean ridges.

(7) Simultaneous parameter fitting in multicomponent and P-T space provides a clear guide to future experimentation, by highlighting the most sensitive gaps in fluid-mineral phase equilibria experiments. The thermodynamic database for aqueous species can be further improved when new solubility experiments become available, such as those involving feldspar and aluminosilicate assemblages in pure water but also in salt solutions. Experimental data on the solubilities of minerals at hydrothermal conditions are still needed to resolve some of the persisting discrepancies between available studies. New data on the speciation in the hydrothermal fluids especially on the association properties of species like AlSiO_4^- , HAlSiO_4^0 , and KSiOH_3^0 are also needed to improve the agreement between calculations and experiments.

Acknowledgements

The authors would like to acknowledge D. J. Wesolowski and an anonymous reviewer for their constructive reviews. We would also like to thank the associate editor Jean-Francois Boily for handling the manuscript.

This project was supported by funding from ETH Zurich, ETHIRA grant number ETH-19 11-2.

Supplementary tables

Table 3.EA1. Standard state properties (Gibbs energy of formation, partial molal entropy, heat capacity and volume) for mineral end members used in this study. The values were taken as such from Holland and Powell database (dataset ds55 2002). These values were not optimized during the global optimization.

	$Cp^0 = a_0 + a_1 \cdot T + a_2 \cdot T^{-2} + a_3 \cdot T^{-0.5} + a_4 \cdot T^2$									
	$\Delta_f G_{298,1}^0$	$S_{298,1}^0$	$Cp_{298,1}^0$	$V_{298,1}^0$	a_0	$a_1 \cdot 10^5$	a_2	a_3	a°	κ
	(J/mol)	(J/mol·K)	(J/mol·K)	(J/bar)	(kJ/K)	(kJ/K ²)	(kJ·K)	(kJ/K ^{0.5})	(K ⁻¹)	(kbar)
albite	-3711996	210.1	207.725	10.006	0.4520	-1.3364	-1275.9	-3.9536	4.56	593
albite high	-3706202	223.4	204.694	10.109	0.4520	-1.3364	-1275.9	-3.9536	4.56	593
analcite (analcime)	-3091093	232	211.729	9.740	0.6435	-1.6067	9302.3	-9.1796	5.00	400
andalusite	-2441050	92.7	122.594	5.153	0.2773	-0.6588	-1914.1	-2.2656	4.11	1334
coesite	-850864	40.8	45.0974	2.064	0.0965	-0.0577	-448.8	-0.7982	1.80	1000
crystalobalite	-853084	46.5	44.919	2.610	0.0979	-0.3350	-626.2	-0.7740	0.81	600
corundum	-1581808	50.9	79.4529	2.558	0.1395	0.5890	-2460.6	-0.5892	4.19	2520
diaspore	-920825	35	53.4369	1.776	0.1451	0.8709	584.4	-1.7411	7.97	2300
jadeite	-2849218	133.5	159.915	6.040	0.3011	1.0143	-2239.3	-2.0551	4.66	1284
kalsilite	-2006218	134	118.477	6.040	0.2420	-0.4482	-859.8	-1.9358	5.76	590
kaolinite	-3801669	203.7	224.553	9.934	0.4367	-3.4295	-4055.9	-2.6991	5.10	645
kyanite	-2442617	83.5	121.564	4.414	0.2794	-0.7124	-2055.6	-2.2894	4.04	1590
leucite	-2866366	200	162.794	8.828	0.3698	-1.6332	684.7	-3.6831	3.67	630
microcline	-3750316	216	204.267	10.892	0.4488	-1.0075	-1007.3	-3.9731	3.35	574
muscovite	-5603884	292	321.881	14.083	0.7564	-1.9840	-2170	-6.9792	5.96	490
nepheline	-1980505	124.4	114.290	5.419	0.2727	-1.2398	0	-2.7631	8.10	600
paragonite	-5565263	276	323.97	13.211	0.8030	-3.1580	217	-8.1510	7.74	550
pyrophyllite	-5266775	239.4	293.738	12.810	0.7845	-4.2948	1251	-8.4959	7.50	525
quartz	-856433	41.5	44.8909	2.2688	0.1107	-0.5189	0	-1.1283	0.65	750
sanidine	-3744340	230	204.367	10.900	0.4488	-1.0075	-1007.3	-3.9731	3.35	574
sillimanite	-2438765	95.5	124	4.986	0.2802	-0.6900	-1375.7	-2.3994	2.21	1320
shistovite	-816165	24.5	42.8835	1.401	0.0681	0.6010	-1978.2	-0.0821	2.50	3160

topaz-OH	-2690013	100.5	159.093	5.339	0.3877	-0.7120	-857.2	-3.7442	4.04	1315
tridymite	-853665	46.1	44.919	2.700	0.0979	-0.3350	-636.2	-0.7740	0.50	450
¹ boehmite	-918400	37.19	54.2399	1.954	0.205721	-3.4921	1026.66	-2.63527	-	-
¹ gibbsite	-1154900	68.4	91.7203	3.196	0.0546974	17.0272	-1221.73	0	-	-

(1) Taken from Robie d Hemingway (1995), heat capacity polynomial coefficients for gibbsite from Pokrovskii and Helgeson (1995). a° is the thermal expansion parameter; κ is the bulk modulus (incompressibility) at 298K.

Table 3.EA2. The values for the standard state molal Gibbs free energy for the aluminium aqueous species which resulted after the optimization against gibbsite and boehmite solubility experiments.

Species	$\Delta_f G_{298,1}^0$ (J/mole)	Standard Deviation	95% confidence	Optimization mode
Al ³⁺	-486513	352	691	Optimized
AlOH ²⁺	-695460	652 ⁽²⁾	3749	⁽¹⁾ Constrained
Al(OH) ₂ ⁺	-898674	486	955	Optimized
Al(OH) ₃ ⁰	-1105180	1923	3775	Optimized
Al(OH) ₄ ⁻	-1305337	343	673	Optimized
NaAl(OH) ₄ ⁰	-1567809	1103	2165	Optimized

(1) Constrained to Al³⁺ by the reaction: AlOH⁺² + H⁺ = Al³⁺ + H₂O, and the logK values from Palmer and Wesolowski (1993)

(2) Calculated using the error for the Al³⁺ and the reported error for the logK at 298.15 K of about 0.05

Table 3.EA3. Values of the standard state molal Gibbs energy for the aqueous species, which resulted after the optimization against the solubility experiments for minerals present in the HP02 database, but with the values for aluminium hydrolysis species constrained through reactions using logK values (Table S1) derived from fitting those for aluminium species against gibbsite and boehmite solubility experiments.

Species	$\Delta_f G_{298,1}^0$ (J/mole)	Standard Deviation	95% confidence	Optimization mode
Al ³⁺	-486338	282	554	Optimized
AlOH ²⁺	-695153	934	1858	(1)Constrained
Al(OH) ₂ ⁺	-898500	768	1509	(1)Constrained
Al(OH) ₃ ⁰	-1105006	2205	4329	(1)Constrained
Al(OH) ₄ ⁻	-1305163	625	1227	(1)Constrained
NaAl(OH) ₄ ⁰	-1561967	1984	3895	(1)Constrained
AlH ₃ SiO ₄ ²⁺	-1782276	916	1720	(2)Constrained
KAlO ₂ ⁰	-1100302	932	1831	(3)Constrained
K ⁺	-276768	650	1277	Optimized
KOH	-431534			(4)Constrained
KCl	-393258			(4)Constrained
Na ⁺	-256212	599	1176	Optimized
NaOH	-411737			(4)Constrained
NaCl	-383234			(4)Constrained
NaHSiO ₃ ⁰	-1283195	1805	3586	(5)Constrained
HSiO ₃ ⁻	-1018600	314	616	Optimized
SiO ₂ ⁰	-834063	64	126	Optimized
Cl ⁻	-131290			(6)Fixed
HCl ⁰	-127240			(7)Fixed
OH ⁻	-157287			(6)Fixed
H ₂ O(aq)	-237183	(8)100		(8)Fixed

(1) Constrained to Al³⁺ by the following reactions: (a) AlOH²⁺ + H⁺ = Al³⁺ + H₂O; (b) Al(OH)₂⁺ + H⁺ = AlOH²⁺ + H₂O; (c) Al(OH)₃⁰ + H⁺ = Al(OH)₂⁺ + H₂O; (d) Al(OH)₄⁻ + H⁺ = Al(OH)₃⁰ + H₂O; (e) NaAl(OH)₄⁰ = Al(OH)₄⁻ + Na⁺; and the logK values calculated using the values in Table S1 and their corresponding HKF parameters and other standard state properties for the values at elevated temperatures and pressures

(2) Constrained to Al³⁺ and SiO₂⁰ by the reaction: Al³⁺ + 2 H₂O + SiO₂⁰ = AlH₃SiO₄⁰ + H⁺, and the logK from Tagirov and Schott (2001), extracted from Pokrovskii et al. (1996) and Salvi et al. (1998)

(3) Constrained to K⁺ and Al₃⁺ by the reaction: K⁺ + Al₃⁺ + 2 H₂O = KAlO₂⁰ + 4 H⁺

(4) Constrained to Na⁺, K⁺, OH⁻, and Cl⁻ using the logK determined from the new standard state properties properties of the ion pairs extracted from conductance data (Table 1)

(5) Constrained to Na⁺ and SiO₂⁰ by the reaction: Na⁺ + H₂O + SiO₂⁰ = NaHSiO₃⁰ + H⁺, and the logK from Sverjensky et al. (1997), extracted from Seward (1974)

(6) Shock and Helgeson (1988)

(7) Tagirov et al. (1997)

(8) Johnson et al. (1992)

Table 3.EA4. Alternative thermodynamic dataset for aqueous species and minerals, converted to restore the CODATA recommended $\Delta_f G_{298,1}^0$ values for Na⁺ and K⁺ aqueous ions.

Aqueous Species	$\Delta_f G_{298,1}^0$ (J/mol)	Mineral end-members	$\Delta_f G_{298,1}^0$ (J/mol)
Al ³⁺	-486627	⁽³⁾ albite	-3706284
AlOH ²⁺	-695574	⁽³⁾ albite high	-3700490
Al(OH) ₂ ⁺	-898295	⁽³⁾ analcite (analcime)	-3085381
Al(OH) ₃ ⁰	-1105801	andalusite	-2441050
Al(OH) ₄ ⁻	-1305097	boehmite	-918400
⁽¹⁾ NaAl(OH) ₄ ⁰	-1567833	coesite	-850864
AlH ₃ SiO ₄ ²⁺	-1782516	cristobalite	-853084
⁽²⁾ KAlO ₂ ⁰	-1105862	corundum	-1581808
Al(OH) ₄ ⁻	-1305097	diaspore	-920825
⁽²⁾ K ⁺	-282462	gibbsite	-1154900
⁽²⁾ KOH ⁰	-437225	⁽³⁾ jadeite	-2843506
⁽²⁾ KCl ⁰	-408113	⁽⁴⁾ kalsilite	-2000649
⁽¹⁾ Na ⁺	-261881	kaolinite	-3801669
⁽¹⁾ NaOH ⁰	-417306	kyanite	-2442617
⁽¹⁾ NaCl ⁰	-388803	⁽³⁾ leucite	-2860654
⁽¹⁾ NaHSiO ₃ ⁰	-1288788	⁽⁴⁾ microcline	-3744747
HSiO ₃ ⁻	-1015237	⁽⁴⁾ muscovite	-5598315
SiO ₂ ⁰	-834103	⁽³⁾ nepheline	-1974793
Cl ⁻	-131290	⁽³⁾ paragonite	-5559551
HCl ⁰	-127240	pyrophyllite	-5266775
OH ⁻	-157287	quartz	-856433
H ⁺	0	⁽⁴⁾ sanidine	-3738771
H ₂ O	-237183	sillimanite	-2438765
		shistovite	-816165
		topaz-OH	-2690013
		tridymite	-853665

(1) $\Delta_f G_{298,1}^0$ (Table 6) -5712; (2) $\Delta_f G_{298,1}^0$ (Table 6) -5569; (3) $\Delta_f G_{298,1}^0$ (HP98, ds55 2002) +5712; (4) $\Delta_f G_{298,1}^0$ (HP98, ds55 2002) +5569. The standard Gibbs energy values for Na⁺ and K⁺ aqueous ions and species, reported in Table 6 (main text), were adjusted by adding -5712 and -5569 J/mol, respectively. The standard Gibbs energy values for Na and K-bearing minerals from Holland and Powell (1998) database (ds55), reported in Table EA1, were adjusted with +5712 and +5569 J/mol per mol of Na and K in the mineral formula. The remaining (unchanged) thermodynamic properties and HKF parameters of the aqueous species are reported in Tables 1 and 5 in the manuscript; those of minerals (unchanged) are reported in Table EA1 of the electronic supplementary material. The reaction constants between any K and Na aqueous ions, species, and minerals in this database remain the same as in the database reported in the main text (Table 6 for aqueous species and Table AE1 for minerals).

References

- Adcock, S.W., 1985. The solubility of some aluminosilicate minerals in supercritical water - An experimental and thermodynamic study. Ph.D. thesis, Dep. of Geol., Carleton University, Ottawa, Ontario, 337 pp.
- Akinfiyev, N.N., Diamond, L.W., 2003. Thermodynamic description of aqueous nonelectrolytes at infinite dilution over a wide range of state parameters. *Geochim. Cosmochim. Acta* 67, 613-629.
- Akinfiyev, N.N., Diamond, L.W., 2009. A simple predictive model of quartz solubility in water-salt-CO₂ systems at temperatures up to 1000 °C and pressures up to 1000 MPa. *Geochim. Cosmochim. Acta* 73, 1597-1608.
- André, L., Spycher, N., Xu, T., Vuataz F.D., Pruess, K., 2006. Modeling brine-rock interactions in an enhanced geothermal system deep fractured reservoir at Soultz-Sous-Forets (France): a joint approach using two geochemical codes: FRACHEM and TOUGHREACT. Technical report, Center of Geothermal Research, Switzerland, 71 pp.
- Anderson, G.M., 2005. *Thermodynamics of Natural Systems*, Second Ed., Cambridge University Press, Cambridge, 648 pp.
- Anderson, G. M., Burnham, C.W., 1965. The solubility of quartz in super-critical water. *Amer. J. Sci.* 263, 494-511.
- Anderson, G.M., Burnham, C.W., 1967. Reactions of quartz and corundum with aqueous chloride and hydroxide solutions at high temperatures and pressures. *Amer. J. Sci.* 265, 12-27.
- Anderson, G.M., Burnham, C.W., 1983. Feldspar solubility and the transport of aluminum under metamorphic conditions. *Amer. J. Sci.* 283A, 283-297.
- Anderson, G.M., Castet, S., Schott, J., Mesmer R.E., 1991. The density model for estimation of thermodynamic parameters of reactions at high temperatures and pressures. *Geochim. Cosmochim. Acta* 55, 1769-1779.
- Anderson, G.M., Pascal, M.L., Rao, J., 1987. Aluminum speciation in metamorphic fluids. In *Chemical Transport in Metasomatic Processes* (ed. Helgeson H.), Springer Netherlands, 297-321.
- Antignano, A., Manning, C.E., 2003. Solubility of albite + paragonite ± quartz in H₂O at 1 GPa, 580° C: Implications for metamorphic fluids. *AGU Fall Meeting Abstracts* 01/2003.
- Audetat, A., Keppler, H., 2005. Solubility of rutile in subduction zone fluids, as determined by experiments in the hydrothermal diamond anvil cell. *Earth Planet. Sci. Lett.* 232, 393-402.
- Appelo, C.A.J., 2015. Principles, caveats and improvements in databases for calculating hydrogeochemical reactions in saline waters from 0 to 200 °C and 1 to 1000 atm. *Appl. Geochem.* 55, 62-71.
- Apps, J.A., 1970. The Stability field of analcime. Ph.D. Thesis, Harvard University, 347 pp.
- Apps, J.A., Neill, J.M., 1990. Solubilities of aluminum hydroxides and oxihydroxides in alkaline solutions. Correlation with thermodynamic properties of Al(OH)₄⁻. In: *Chemical Modelling of Aqueous Systems II*, 414-428.
- Apps, J.A., Neill, J.M., Jun, C.H., 1988. Thermochemical properties of gibbsite, bayerite, boehmite, diaspore, and the aluminate ion between 0 and 350 °C. Technical Report, Lawrence Berkeley National Laboratory, 350 pp.
- Arcis, H., Zimmerman, G.H., Tremaine, P.R., 2014. Ion-pair formation in aqueous strontium chloride and strontium hydroxide solutions under hydrothermal conditions by AC conductivity measurements. *Phys. Chem. Chem. Phys.* 16, 17688-17704.
- Azaroual, M., Pascal, M.L., Roux, J., 1996. Corundum solubility and aluminum speciation in KOH aqueous solutions at 400°C from 0.5 to 2.0 kbar. *Geochim. Cosmochim. Acta* 60, 4601-4614.
- Azimov, P., Bushmin, S., 2007. Solubility of minerals of metamorphic and metasomatic rocks in hydrothermal solutions of varying acidity: Thermodynamic modeling at 400-800°C and 1-5 kbar. *Geochem. Internat.* 45, 1210-1234.
- Bandura, A.V., Lvov, S.N., 2006. The ionization constant of water over wide ranges of temperature and density. *J. Phys. Chem. Ref. Data* 35, 15-30.
- Barns, R.L., Laudise, R.A., Shields, R.M., 1963. The solubility of corundum in basic hydrothermal solvents. *J. Phys. Chem.* 67, 835-839.
- Bastrakov, E., Shvarov, Y., Girvan, S., Cleverley, J., McPhail, D., Wyborn, L.A.I., 2005. FreeGs: A web-enabled thermodynamic database for geochemical modelling. *Geochim. Cosmochim. Acta*, 69 (Suppl. 1), A845.

- Bates, R.G., Bower, V.E., 1954. Standard potential of the silver-silver-chloride electrode from 0° to 95° C and the thermodynamic properties of dilute hydrochloric acid solutions. *J. Res. National Bureau Standards* 53, 283-290.
- Bates, S.J., Kirschman, H.D., 1919. The vapor pressures and free energies of the hydrogen halides in aqueous solution; the free energy of formation of hydrogen chloride. *J. Amer. Chem. Soc.* 41, 1991-2001.
- Becker, K.H., Cemic, L., Langer, K., 1983. Solubility of corundum in supercritical water. *Geochim. Cosmochim. Acta* 47, 1573-1578.
- Bénézech, P., Palmer, D.A., Wesolowski, D.J., 2001. Aqueous high-temperature solubility studies. II. The solubility of boehmite at 0.03 m ionic strength as a function of temperature and pH as determined by in situ measurements. *Geochim. Cosmochim. Acta* 65, 2097-2111.
- Bénézech, P., Dandurand, J.L., Harrichoury, J.C., 2009. Solubility product of siderite (FeCO₃) as a function of temperature (25–250 °C). *Chem. Geol.* 265, 3-12.
- Bénézech, P., Saldi, G.D., Dandurand, J.L., Schott, J., 2011. Experimental determination of the solubility product of magnesite at 50 to 200°C. *Chem. Geol.* 286, 21-31.
- Berecz, E., Szita, L., 1970. Electrochemical method for the solubility and dissolution of solid compounds. Some thermodynamic properties of the system Al(OH)₃-NaOH-H₂O. *Electrochim. Acta* 15, 1407-1419.
- Berman, R.G., Brown, T.H., 1985. Heat capacity of minerals in the system Na₂O-K₂O-CaO-MgO-FeO-Fe₂O₃-Al₂O₃-SiO₂-TiO₂-H₂O-CO₂: representation, estimation, and high temperature extrapolation. *Contrib. Mineral. Petrol.* 89, 168-183.
- Berman, R.G., 1988. Internally-consistent thermodynamic data for minerals in the system Na₂O-K₂O-CaO-MgO-FeO-Fe₂O₃-Al₂O₃-SiO₂-TiO₂-H₂O-CO₂. *J. Petrol.* 29, 445-522.
- Berman, R.G., Engi, M., Greenwood, H.J., Brown, T.H., 1986. Derivation of internally-consistent thermodynamic data by the technique of mathematical programming: a review with application the System MgO-SiO₂-H₂O. *J. Petrol.* 27, 1331-1364.
- Bernshtein, V.A., Matsenok, Y.A., 1965. Equilibrium in the interaction of diasporite with solutions of sodium hydroxide at temperatures of 250 and 300 °C. *J. Appl. Chem. USSR* 38, 1898-1901.
- Bernshtein, V.A., Matsenok, Y.A., 1961. Solubility of boehmite in alkaline solution at 250 and 300°C. *Zhurnal Prikladnoi Khimii* 34, 982-986 (in Russian).
- Bourcier, W.L., Knauss, K.G., Jackson, K.J., 1993. Aluminum hydrolysis constants to 250°C from boehmite solubility measurements. *Geochim. Cosmochim. Acta* 57, 747-762.
- Brown, G.C., Fyfe, W.S., 1971. Kyanite-andalusite equilibrium. *Contrib. Mineral. Petrol.* 33, 227-231.
- Burnham, C.W., Ryzhenko, B.N., Schitl, D., 1973. Water solubility of corundum at 500-800°C and 6 kbar. *Geochem. Intern.* 10 (6), 1374.
- Busey, R.H. and Mesmer, R.E. (1977) Ionization equilibria of silicic acid and polysilicate formation in aqueous sodium chloride solutions to 300 °C. *Inorg. Chem.* 16, 2444-2450.
- Can, I. (2002) A new improved Na/K geothermometer by artificial neural networks. *Geothermics* 31, 751-760.
- Castet, S., Dandurand, J.L., Schott, J., Gout, R., 1993. Boehmite solubility and aqueous aluminum speciation in hydrothermal solutions (90-350°C): Experimental study and modeling. *Geochim. Cosmochim. Acta* 57, 4869-4884.
- Cerquetti, A., Longhi, P., Mussini, T., 1968. Thermodynamics of aqueous hydrochloric acid from the emf. of hydrogen-chlorine cells. *J. Chem. Eng. Data* 13, 458-461.
- Chang, B.T., Pak, L.H., Li, Y.S., 1979. Solubilities and rates of dissolution of diasporite in NaOH aqueous solutions. *Bull. Chem. Soc. Japan* 52, 1321-1326.
- Chatterjee, N., Miller, K., Olbricht, W., 1994. Bayes estimation: A novel approach to derivation of internally consistent thermodynamic data for minerals, their uncertainties, and correlations. Part II: Application. *Phys. Chem. Miner.* 21, 50-62.
- Chatterjee, N.D., Krüger, R., Haller, G., Olbricht, W., 1998. The Bayesian approach to an internally consistent thermodynamic database: theory, database, and generation of phase diagrams. *Contrib. Mineral. Petrol.* 133, 149-168.

- Cloke, P.L., 1954. Quartz solubility in potassium hydroxide solutions under elevated pressures and temperatures with some geological applications. Ph.D. Thesis, Massachusetts Institute of Technology, 87 pp.
- Couturier, Y., Michard, G., Sarazin, G., 1984. Constantes de formation des complexes hydroxydés de l'aluminium en solution aqueuse de 20 a 70°C. *Geochim. Cosmochim. Acta* 48, 649-659.
- Cox, J.D., Wagman, D.D., Medvedev, V.A., 1989. CODATA Key Values for Thermodynamics. Hemisphere Publishing Company, New York.
- Crear, D.A., Anderson, G.M., 1971. Solubility and solvation reactions of quartz in dilute hydrothermal solutions. *Chem. Geol.* 8, 107-122.
- Currie, K.L., 1968. On the solubility of albite in supercritical water in the range of 400 degrees to 600 degrees C and 750 to 3500 bars. *Amer. J. Sci.* 266, 321-341.
- Davis, N.F., 1972. Experimental studies in the system NaAlSi₃O₈-H₂O. Ph.D. Thesis, Pennsylvania State University, 319 pp.
- Delany, J.M., Lundeen, S.R., 1990. The LLNL thermochemical database. Lawrence Livermore National Laboratory, Report UCRL-21658.
- Diakonov, I., Pokrovski, G., Schott, J., Castet, S., Gout, R., 1996. An experimental and computational study of sodium-aluminum complexing in crustal fluids. *Geochim. Cosmochim. Acta* 60, 197-211.
- Dill, A.J., Itzkowitz, L.M., Popovych, O., 1968. Standard potentials of potassium electrodes and activity coefficients and medium effects of potassium chloride in ethanol-water solvents. *J. Phys. Chem.* 72, 4580-4586.
- Dolejs, D., Manning, C.E., 2010. Thermodynamic model for mineral solubility in aqueous fluids: theory, calibration and application to model fluid-flow systems. *Geofluids* 10, 20-40.
- Dolejs, D., Wagner, T., 2008. Thermodynamic modeling of non-ideal mineral-fluid equilibria in the system Si-Al-Fe-Mg-Ca-Na-K-H-O-Cl at elevated temperatures and pressures: Implications for hydrothermal mass transfer in granitic rocks. *Geochim. Cosmochim. Acta* 72, 526-553.
- Druzhinina, N.K., 1955. Solubility of diaspore in aluminate solutions. *Tsvetnyye Metally* 1, 54-56 (in Russian).
- Engi, M., 1992. Thermodynamic data for minerals: a critical assessment, In: Price, G., Ross, N. (Eds.), *The Stability of Minerals*. Springer Netherlands, 267-328.
- Fabrichnaya, O., Saxena, S.K., Richet, P., Westrum, E.F., 2013. Thermodynamic data, models, and phase Diagrams in multicomponent oxide systems: an assessment for materials and planetary scientists based on calorimetric, volumetric and phase equilibrium data. Springer, Berlin, 198 pp.
- Fournier, R.O., Rosenbauer, R.J., Bischoff, J.L., 1982. The solubility of quartz in aqueous sodium chloride solution at 350°C and 180 to 500 bars. *Geochim. Cosmochim. Acta* 46, 1975-1978.
- Franck, E.U., 1956. Hochverdichteter Wasserdampf. III. Ionendissoziation von HCl, KOH und H₂O in überkritischem Wasser. *Z. Phys. Chem.* 8, 192-206.
- Frantz, J.D., Marshall, W.L., 1984. Electrical conductances and ionization constants of salts, acids, and bases in supercritical aqueous fluids. I. Hydrochloric acid from 100 °C to 700 °C and at pressures to 4000 bars. *Amer. J. Sci.* 284, 651-667.
- Fricke, R., Jucaitis, P., 1930. Untersuchungen über die Gleichgewichte in den Systemen Al₂O₃-Na₂O-H₂O and Al₂O₃-K₂O-H₂O. *Z. Anorg. Allgem. Chem.* 191, 129-149.
- Galvez, M.E., Manning, C.E., Connolly, J.A.D., Rumble D., 2015. The solubility of rocks in metamorphic fluids: A model for rock-dominated conditions to upper mantle pressure and temperature. *Earth and Planetary Science Letters*, In Press. <http://dx.doi.org/10.1016/j.epsl.2015.06.019>
- Gottschalk, M., 1997. Internally consistent thermodynamic data for rock-forming minerals in the system SiO₂-TiO₂-Al₂O₃-CaO-MgO-FeO-K₂O-Na₂O-H₂O-CO₂. *Eur. J. Mineral.* 9, 175-223.
- Greenberg S. A., Price E. W., 1957. The solubility of silica in solutions of electrolytes. *J. Phys. Chem.* 61, 1539-1541.
- Gruskiewicz, M.S., Wood, R.H., 1997. Conductance of dilute LiCl, NaCl, NaBr, and CsBr solutions in supercritical water using a flow conductance cell. *J. Phys. Chem. B* 101, 6549-6559.
- Gunn, S.R., Green, L.G., 1958. The heats of formation at 25° of the crystalline hydrides and deuterides and aqueous hydroxides of lithium, sodium and potassium. *J. Am. Chem. Soc.* 80, 4782-4786.

- Gunter, W.D., Eugster, H.P., 1981. Mica-feldspar equilibria in supercritical alkali chloride solutions. *Contrib. Mineral. Petrol.* 75, 235-250.
- Harman R. W., 1928. Aqueous solutions of sodium silicates: Part VIII. *J. Phys. Chem.* 32, 44-60.
- Haselton, H.T., Cygan, G.L., and D'Angelo, W.M., 1988. Chemistry of aqueous solutions coexisting with fluoride buffers in the system $K_2O-Al_2O_3-SiO_2-H_2O-F_2O_1$ (1 kbar, 400 °C - 700 °C). *Econ. Geol.* 83,163-173.
- Haselton, H.T., Cygan, G.L., Jenkins, D.M., 1995. Experimental study of muscovite stability in pure H_2O and 1 molal KCl-HCl solutions. *Geochim. Cosmochim. Acta* 59 429-442.
- Hauzenberger, C.A., Baumgartner, L.P., Pak, T.M., 2001. Experimental study on the solubility of the "model"-pelite mineral assemblage albite + K-feldspar + andalusite + quartz in supercritical chloride-rich aqueous solutions at 0.2 GPa and 600 °C. *Geochim. Cosmochim. Acta* 65, 4493-4507.
- Hayden, L.A., Manning, C.E., 2011. Rutile solubility in supercritical $NaAlSi_3O_8-H_2O$ fluids. *Chem. Geol.* 284, 74-81.
- Helgeson, H.C., 1969. Thermodynamics of hydrothermal systems at elevated temperatures and pressures. *Amer. Jour. Sci.* 267, 729-804.
- Helgeson, H.C., Kirkham, D.H., 1974a. Theoretical prediction of the thermodynamic behavior of aqueous electrolytes at high pressures and temperatures. I. Summary of the thermodynamic/electrostatic properties of the solvent. *Amer. J. Sci.* 274, 1089-1198.
- Helgeson, H.C., Kirkham, D.H., 1974b. Theoretical prediction of the thermodynamic behavior of aqueous electrolytes at high pressures and temperatures. II. Debye-Huckel parameters for activity coefficients and relative partial molal properties. *Amer. J. Sci.* 274, 1199-1261.
- Helgeson, H.C., Kirkham, D.H., Flowers, G.C., 1981. Theoretical prediction of the thermodynamic behavior of aqueous electrolytes by high pressures and temperatures. IV. Calculation of activity coefficients, osmotic coefficients, and apparent molal and standard and relative partial molal properties to 600 °C and 5kb. *Amer. J. Sci.* 281, 1249-1516.
- Helgeson, H.C., Delaney, J.M., Nesbitt, H.W., Bird, D.K., 1978. Summary and critique of the thermodynamic properties of rock-forming minerals. *Amer. J. Sci.* 278A, 1-229.
- Hemingway, B.S., Haselton Jr, H.T., 1994. A reevaluation of the calorimetric data for the enthalpy of formation of some K- and Na-bearing silicate minerals. U.S. Geological Survey, 33 pp.
- Hemingway, B.S., Robie, R.A., Kittrick, J.A., 1978. Revised values for Gibbs free-energy of formation of $Al(OH)_4(aq)$, diaspore, boehmite and bayerite at 298.15 K and 1 bar, thermodynamic properties of kaolinite to 800 K and 1 bar, and heats of solution of several gibbsite samples. *Geochim. Cosmochim. Acta* 42, 1533-1543.
- Hemingway, B.S., Robie, R.A., Apps, J.A., 1991. Revised values for the thermodynamic properties of boehmite, $AlOOH$ and related species and phases in the system Al-H-O. *Amer. Mineral.* 76, 445-457.
- Hemley, J.J., 1959. Some mineralogical equilibria in the system $K_2O-Al_2O_3-SiO_2-H_2O$. *Amer. J. Sci.* 257, 241-270.
- Hemley, J.J., Montoya, J.W., Marinenko, J.W., Luce, R.W., 1980. Equilibria in the system $Al_2O_3-SiO_2-H_2O$ and some general implications for alteration/mineralization processes. *Econ. Geol.* 75, 210-228.
- Hingerl, F.F., Wagner, T., Kulik, D.A., Thomsen, K., Driesner, T., 2014. A new aqueous activity model for geothermal brines in the system Na-K-Ca-Mg-H-Cl-SO₄-H₂O from 25 to 300 °C. *Chem. Geol.* 381, 78-93.
- Hitch, B.F., Mesmer, R.E., Baes, C.F., Sweeton, F.H., 1980. The solubility of Gibbsite ($\alpha-Al(OH)_3$) in 1 molal NaCl as a function of pH and temperature. Oak Ridge National Laboratory Report ORNL-5623, 35 pp.
- Ho, P., Bianchi, H., Palmer, D.A., Wood, R., 2000a. Conductivity of dilute aqueous electrolyte solutions at high temperatures and pressures using a flow cell. *J. Solut. Chem.* 29, 217-235.
- Ho, P.C., Palmer, D.A., Wood, R.H., 2000. Conductivity measurements of dilute aqueous LiOH, NaOH, and KOH solutions to high temperatures and pressures using a flow-through cell. *J. Phys. Chem. B* 104, 12084-12089.
- Ho, P., Palmer, D.A., 1996. Ion association of dilute aqueous sodium hydroxide solutions to 600°C and 300 MPa by conductance measurements. *J. Solut. Chem.* 25, 711-729.
- Ho, P., Palmer, D.A., Mesmer, R., 1994. Electrical conductivity measurements of aqueous sodium chloride solutions to 600°C and 300 MPa. *J. Solut. Chem.* 23, 997-1018.

- Ho, P.C., Palmer, D.A., 1997. Ion association of dilute aqueous potassium chloride and potassium hydroxide solutions to 600°C and 300 MPa determined by electrical conductance measurements. *Geochim. Cosmochim. Acta* 61, 3027-3040.
- Ho, P.C., Palmer, D.A., Gruszkiewicz, M.S., 2001. Conductivity measurements of dilute aqueous HCl solutions to high temperatures and pressures using a flow-through cell. *J. Phys. Chem. B* 105, 1260-1266.
- Holland, T.J.B., 1989. Dependence of entropy on volume for silicate and oxide minerals; a review and predictive model. *Amer. Mineral.* 74, 5-13.
- Holland, T.J.B., Powell, R., 1985. An internally consistent thermodynamic dataset with uncertainties and correlations. 2. Data and results. *J. Metam. Geol.* 3, 343-370.
- Holland, T.J.B., Powell, R., 1990. An enlarged and updated internally consistent thermodynamic dataset with uncertainties and correlations: the system $K_2O-Na_2O-CaO-MgO-MnO-FeO-Fe_2O_3-Al_2O_3-TiO_2-SiO_2-C-H_2O_2$. *Journal of Metamorphic Geology* 8, 89-124.
- Holland, T.J.B., Powell, R., 1991. A compensated-Redlich-Kwong (CORK) equation for volumes and fugacities of CO_2 and H_2O in the range 1 bar to 50 kbar and 100-1600 °C. *Contrib. Mineral. Petrol* 109, 265-273.
- Holland, T.J.B., Powell, R., 1998. An internally consistent thermodynamic data set for phases of petrological interest. *J. Metam. Geol.* 16, 309-343.
- Holland, T.J.B., Powell, R., 2011. An improved and extended internally consistent thermodynamic dataset for phases of petrological interest, involving a new equation of state for solids. *J. Metam. Geol.* 29, 333-383.
- Ikkatai, T., Okada, N., 1962. Viscosity, specific gravity and equilibrium concentrations of sodium aluminate solutions. In: Gerhard, G., Stroup, P.T. (Eds.) *Extractive Metallurgy of Aluminum*. New York, Interscience Publishers, pp. 159-173.
- Ingri N., 1959. Equilibrium studies of polyanions IV. Silicate ions in NaCl medium. *Acta Chem. Scand.* 13, 758-775.
- Johnson, J.W., Oelkers, E.H., Helgeson, H.C., 1992. SUPCRT92: A software package for calculating the standard molal thermodynamic properties of minerals, gases, aqueous species, and reactions from 1 to 5000 bar and 0 to 1000 °C. *Comp. Geosci.* 18, 899-947.
- Kennedy, G.C., 1950. A portion of the system silica-water. *Econ. Geol.* 45, 629-653.
- Kestin, J., Sengers, J.V., Kamgar-Parsi, B., Levelt-Sengers, J.H.M., 1984. Thermophysical properties of fluid H_2O . *J. Phys. Chem. Ref. Data* 13, 175-183.
- Kitahara, S., 1960. The solubility of quartz in water at high temperatures and high pressures. *Review Phys. Chem. Japan* 30, 109-114.
- Korzinskiy, M.A., 1987. The solubility of corundum in HCl fluid and forms taken by Al. *Geochem. Intern.* 24, 105-110.
- Kulik, D.A., Wagner, T., Dmytrieva, S.V., Kosakowski, G., Hingerl, F.F., Chudnenko, K.V., Berner, U., 2013. GEM-Selektor geochemical modeling package: revised algorithm and GEMS3K numerical kernel for coupled simulation codes. *Computat. Geosci.* 17, 1-24.
- Kuyunko, N.S., Malinin, S.D., Khodakovskiy, I.L., 1983. An experimental study of aluminum ion hydrolysis at 150, 200, and 250 °C. *Geochem. Intern.* 20, 76-86.
- Lagerström G., 1959. Equilibrium studies of polyanions III. Silicate ions in $NaClO_4$ medium. *Acta. Chem. Scand.* 13, 722-736.
- Lanari, P., Wagner, T., Vidal, O., 2014. A thermodynamic model for di-trioctahedral chlorite from experimental and natural data in the system $MgO-FeO-Al_2O_3-SiO_2-H_2O$: applications to P-T sections and geothermometry. *Contrib. Mineral. Petrol.* 167, 1-19.
- Leal, A.M.M., Blunt, M.J., LaForce, T.C., 2014. Efficient chemical equilibrium calculations for geochemical speciation and reactive transport modelling. *Geochim. Cosmochim. Acta.* 131, 301-322.
- Lichtner, P.C., Steefel, C.I., Oelkers, E.H., 1997. Reactive transport in porous media. *Rev. Mineral. Geochem.* 34, 448 pp.
- Lier, J.A.V., Bruyn, P.L.D., Overbeek, J.T.G., 1960. The solubility of quartz. *J. Phys. Chem.* 64, 1675-1682.

- Lukashov, Y.M., Komissarov, K.B., Golubev, B.P., Smirnov, S.N., Svistunov, E.P., 1975. An experimental investigation of the electrolytic properties of uni-univalent electrolytes at high parameters of state. *Thermal Eng.* 22, 79-82.
- Lyapunov, A.N., Khodakova, A.G., Galkina, Z.G., 1964. Solubility of hydrargillite in NaOH solutions, containing soda or sodium chloride, at 60°C and 95°C. *Tsvetnyye Metally* 38, 48-51.
- Magarshak, G.K., 1938. Polytherms in the $\text{Al}_2\text{O}_3\text{-Na}_2\text{O-H}_2\text{O}$ System at 30-200°C. *Legkiye Metally* 7, 12-16 (in Russian).
- Manning, C.E., 1994. The solubility of quartz in H_2O in the lower crust and upper mantle. *Geochim. Cosmochim. Acta* 58, 4831-4839.
- Manning, C.E., 2007. Solubility of corundum + kyanite in H_2O at 700°C and 10 kbar: evidence for Al-Si complexing at high pressure and temperature. *Geofluids* 7, 258-269.
- Manning, C.E., Antignano, A., Lin, H.A., 2010. Premelting polymerization of crustal and mantle fluids, as indicated by the solubility of albite-paragonite-quartz in H_2O at 1 GPa and 350-620 °C. *Earth Planet. Sci. Lett.* 292, 325-336.
- Marshall, W.L., Franck, E.U., 1981. Ion product of water substance, 0-1000 °C, 1-10,000 bars, new international formulation and its background. *J. Phys. Chem. Ref. Data* 10, 295-304.
- Méndez De Leo, L.P., Wood, R.H., 2005. Conductance study of association in aqueous CaCl_2 , $\text{Ca}(\text{CH}_3\text{COO})_2$, and $\text{Ca}(\text{CH}_3\text{COO})_2 \cdot n\text{CH}_3\text{COOH}$ from 348 to 523 K at 10 MPa. *J. Phys. Chem. B* 109, 14243-24250.
- Miron, G.D., Kulik, D.A., Dmytrieva, S.V., Wagner, T., 2015. GEMSFITS: Code package for optimization of geochemical model parameters and inverse modeling. *Appl. Geochem.* 55, 28-45.
- Miron, G.D., Wagner, T., Wälle, M., Heinrich, C.A., 2013. Major and trace-element composition and pressure-temperature evolution of rock-buffered fluids in low-grade accretionary-wedge metasediments, Central Alps. *Contrib. Mineral. Petrol* 165, 981-1008.
- Montoya, J.W., Hemley, J.J., 1975. Activity relations and stabilities in alkali feldspar and mica alteration reactions. *Econ. Geol.* 70, 577-583.
- Mookherjee, M., Keppler, H., Manning, C.E., 2014. Aluminum speciation in aqueous fluids at deep crustal pressure and temperature. *Geochim. Cosmochim. Acta* 133, 128-141.
- Morey, G.W., Fournier, R.O., Rowe, J.J., 1962. The solubility of quartz in water in the temperature interval from 25° to 300° C. *Geochim. Cosmochim. Acta* 26, 1029-1043.
- Morse, J.W., Casey, W.H., 1988. Ostwald processes and mineral paragenesis in sediments. *Amer. J. Sci.* 288, 537-560.
- Newton, R.C., Manning, C.E., 2000. Quartz solubility in $\text{H}_2\text{O-NaCl}$ and $\text{H}_2\text{O-CO}_2$ solutions at deep crust-upper mantle pressures and temperatures: 2-15 kbar and 500-900 °C. *Geochim. Cosmochim. Acta* 64, 2993-3005.
- Novgorodov, P.G., 1975. Solubility of quartz in $\text{H}_2\text{O-CO}_2$ mixtures at 700 °C and pressures of 3 and 5 kbar. *Geochem. Internat.* 12, 122-126.
- Novgorodov, P.G., 1977. On the solubility of quartz in $\text{H}_2\text{O} + \text{CO}_2$ and $\text{H}_2\text{O} + \text{NaCl}$ at 700 °C and 1.5 kb pressure. *Geochem. Internat.* 14, 191-193.
- Oelkers, E.H., Helgeson, H.C., 1988. Calculation of the thermodynamic and transport properties of aqueous species at high pressures and temperatures: Aqueous tracer diffusion coefficients of ions to 1000 °C and 5 kb. *Geochim. Cosmochim. Acta* 52, 63-85.
- Oelkers, E.H., Helgeson, H.C., 1990. Triple-ion anions and polynuclear complexing in supercritical electrolyte solutions. *Geochim. Cosmochim. Acta* 54, 727-738.
- Oelkers, E.H., Helgeson, H.C., Shock, E.L., Sverjensky, D.A., Johnson, J.W., Pokrovskii, V.A., 1995. Summary of the apparent standard partial molal Gibbs free energies of formation of aqueous species, minerals, and gases at pressures 1 to 5000 bars and temperatures 25 to 1000 °C. *J. Phys. Chem. Ref. Data* 24, 1401-1560.
- Ostapenko, G.T., Khetchikov, L.N., Balitskiy, V.S., 1969. Hydrolysis of aqueous solutions of sodium sulfide and solubility of quartz in these solutions. *Geochem. Internat.* 6, 22-28.
- Ostapenko, G.T., Arapova, M.A., 1971. Solubility of kyanite, corundum, quartz and amorphous silica in aqueous hydrochloric acid solutions at 285 °C and 485 bars. *Geochem. Internat.* 8, 482-488.

- Ostapenko, G.T., Timoshkova, L.P., Tsybal, S.N., 1978. Gibbs energy of sillimanite from data on its solubility in water at 530 °C and 1300 bars. *Intern. Geol. Review* 20, 864-866.
- Pak, T.M., Hauzenberger, C.A., Baumgartner, L.P., 2003. Solubility of the assemblage albite+K-feldspar+andalusite+quartz in supercritical aqueous chloride solutions at 650 °C and 2 kbar. *Chem. Geol.* 200, 377-393.
- Palmer, D.A., Bénéžeth, P., Wesolowski, D.J., 2001. Aqueous high-temperature solubility studies. I. The solubility of boehmite as functions of ionic strength (to 5 molal, NaCl), temperature (100-290°C), and pH as determined by in situ measurements. *Geochim. Cosmochim. Acta* 65, 2081-2095.
- Palmer, D.A., Wesolowski, D.J., 1992. Aluminum speciation and equilibria in aqueous solution: II. The solubility of gibbsite in acidic sodium chloride solutions from 30 to 70 °C. *Geochim. Cosmochim. Acta* 56, 1093-1111.
- Palmer, D.A., Wesolowski, D.J., 1993. Aluminum speciation and equilibria in aqueous solution: III. Potentiometric determination of the first hydrolysis constant of aluminum(III) in sodium chloride solutions to 125 °C. *Geochim. Cosmochim. Acta* 57, 2929-2938.
- Pascal, M.L., Anderson, G.M., 1989. Speciation of Al, Si, and K in supercritical solutions: Experimental study and interpretation. *Geochim. Cosmochim. Acta* 53, 1843-1855.
- Plumridge, J., Arcis, H., Tremaine, P.R., 2015. Limiting conductivities of univalent cations and the chloride ion in H₂O and D₂O under hydrothermal conditions. *J. Solut. Chem.* 44, 1062-1089.
- Plyasunov, A.V., 1988. Estimation for dissociation constants for symmetrical electrolytes on the basis of stoichiometric activity coefficients. *Russ. J. Phys. Chem.* 62, 622-625.
- Plyasunov, A.V., 2015. Correlation and prediction of thermodynamic properties of nonelectrolytes at infinite dilution in water over very wide temperature and pressure ranges (2000 K and 10 GPa). *Geochim. Cosmochim. Acta* 168, 236-260.
- Plyasunov, A.V., Shock, E.L., 2001. Correlation strategy for determining the parameters of the revised Helgeson-Kirkham-Flowers model for aqueous nonelectrolytes. *Geochim. Cosmochim. Acta* 65, 3879-3900.
- Pokrovskii, G.S., Schott, J., Harrichoury, J.C., Sergeev, A.S., 1996. The stability of aluminum silicate complexes in acidic solutions from 25 to 150 °C. *Geochim. Cosmochim. Acta* 60, 2495-2501.
- Pokrovskii, V.A., Helgeson, H.C., 1995. Thermodynamic properties of aqueous species and the solubilities of minerals at high pressures and temperatures; the system Al₂O₃-H₂O-NaCl. *Amer. J. Sci.* 295, 1255-1342.
- Pokrovskii, V.A., Helgeson, H.C., 1997a. Calculation of the standard partial molal thermodynamic properties of KCl⁰ and activity coefficients of aqueous KCl⁰ at temperatures and pressures to 1000 °C and 5 kbar. *Geochim. Cosmochim. Acta* 61, 2175-2183.
- Pokrovskii, V.A., Helgeson, H.C., 1997b. Thermodynamic properties of aqueous species and the solubilities of minerals at high pressures and temperatures: the system Al₂O₃-H₂O-KOH. *Chem. Geol.* 137, 221-242.
- Popp, R.K., Frantz, J.D., 1980. Mineral-solution equilibria. III. The system Na₂O-Al₂O₃-SiO₂-H₂O-HCl. *Geochim. Cosmochim. Acta* 44, 1029-1037.
- Powell, R., Holland, T.J.B., 1985. An internally consistent thermodynamic dataset with uncertainties and correlations: 1. Methods and a worked example. *J. Metam. Geol.* 3, 327-342.
- Quist, A.S., Marshall, W.L., 1969. Electrical conductances of some alkali metal halides in aqueous solutions from 0 to 800 °C and at pressures to 4000 bars. *J. Phys. Chem.* 73, 978-985.
- Ragnarsdóttir, K.V., Walther, J.V., 1985. Experimental determination of corundum solubilities in pure water between 400-700 °C and 1-3 kbar. *Geochim. Cosmochim. Acta* 49, 2109-2115.
- Reed, M.H., 1982. Calculation of multicomponent chemical equilibria and reaction processes in systems involving minerals, gases and an aqueous phase. *Geochim. Cosmochim. Acta* 46, 513-528.
- Reukov, V.V., Zotov, A.V., 2006. Determination of the HCl dissociation constant at a temperature of 350°C and 200 bars of pressure by the potentiometric method using a ceramic electrode. *Geol. Ore Depos.* 48, 144-150.
- Rimstidt, J.D., 1997. Quartz solubility at low temperatures. *Geochim. Cosmochim. Acta* 61, 2553-2558.
- Robie, R.A., Hemingway, B.S., Fisher, J.R., 1979. Thermodynamic Properties of Minerals and Related Substances at 298.15 K and 1 Bar (10⁵ Pascals) Pressure and at Higher Temperatures, U.S. Geological Survey Bulletin, Washington, 452 pp.

- Robie, R.A., Hemingway, B.S., 1995. Thermodynamic Properties of Minerals and Related Substances at 298.15 K and 1 Bar (10^5 Pascals) Pressure and at Higher Temperatures. U.S. Geol. Survey Bull. 2131, 461 pp.
- Roedder, E., 1984. Fluid inclusions. *Rev. Mineral. Geochem.* 12, 464 pp.
- Ruaya, J.R., Seward, T.M., 1987. The ion-pair constant and other thermodynamic properties of HCl up to 350°C. *Geochim. Cosmochim. Acta* 51, 121-130.
- Russell, A.S., Edwards, J.D., Taylor, C.S., 1955. Solubility and density of hydrated alumina in NaOH solutions. *Journal of Metals* 7, 1123-1128.
- Salvi, S., Pokrovski, G.S., Schott, J., 1998. Experimental investigation of aluminum-silica aqueous complexing at 300°C. *Chem. Geol.* 151, 51-67.
- Sassani, D.C., Shock, E.L., 1992. Estimation of standard partial molal entropies of aqueous ions at 25°C and 1 bar. *Geochim. Cosmochim. Acta* 56, 3895-3908.
- Sato, T., 1954. Hydrolysis of sodium aluminate solution. XIII. Effect of decomposition temperature. *J. Chem. Soc. Japan Ind. Chem. Sect.* 57, 805-808.
- Schofield, R.K., Taylor, A.W., 1954. The hydrolysis of aluminium salt solutions. *Journal of the Chemical Society (Resumed)*, 4445-4448.
- Schott, J., Pokrovsky, O.S., Oelkers, E.H., 2009. The link between mineral dissolution/precipitation kinetics and solution chemistry. *Rev. Mineral. Geochem.* 70, 207-258.
- Schwarz, R., Müller, W.D., 1958. Zur Kenntnis der Kieselsäuren. XIV. Die wasserlösliche Monokieselsäure. *Z Anorg Allg Chem* 296, 273-279.
- Seward, T.M., 1974. Determination of the first ionization constant of silicic acid from quartz solubility in borate buffer solutions to 350°C. *Geochim. Cosmochim. Acta* 38, 1651-1664.
- Shade, J.W., 1974. Hydrolysis reactions in the SiO₂-excess portion of the system K₂O-Al₂O₃-SiO₂-H₂O in chloride fluids at magmatic conditions. *Econ. Geol.* 69, 218-228.
- Sharygin, A.V., Mokbel, I., Xiao, C.B., Wood, R.H., 2001. Tests of equations for the electrical conductance of electrolyte mixtures: Measurements of association of NaCl(aq) and Na₂SO₄(aq) at high temperatures. *J. Phys. Chem. B* 105, 229-237.
- Sharygin, A.V., Wood, R.H., Zimmerman, G.H., Balashov, V.N., 2002. Multiple ion association versus redissociation in aqueous NaCl and KCl at high temperatures. *J. Phys. Chem. B* 106, 7121-7134.
- Shinohara, H., Fujimoto, K., 1994. Experimental study in the system albite-andalusite-quartz-NaCl-HCl-H₂O at 600°C and 400 to 2000 bars. *Geochim. Cosmochim. Acta* 58, 4857-4866.
- Shmulovich, K., Graham, C., Yardley, B., 2001. Quartz, albite and diopside solubilities in H₂O-NaCl and H₂O-CO₂ fluids at 0.5-0.9 GPa. *Contrib. Mineral. Petrol* 141, 95-108.
- Shmulovich, K.I., Yardley, B.W.D., Graham, C.M., 2006. Solubility of quartz in crustal fluids: experiments and general equations for salt solutions and H₂O-CO₂ mixtures at 400-800°C and 0.1-0.9 GPa. *Geofluids* 6, 154-167.
- Shock, E.L., Helgeson, H.C., 1988. Calculation of the thermodynamic and transport properties of aqueous species at high pressures and temperatures: Correlation algorithms for ionic species and equation of state predictions to 5 kb and 1000°C. *Geochim. Cosmochim. Acta* 52, 2009-2036.
- Shock, E.L., Helgeson, H.C., Sverjensky, D.A., 1989. Calculation of the thermodynamic and transport properties of aqueous species at high pressures and temperatures: Standard partial molal properties of inorganic neutral species. *Geochim. Cosmochim. Acta* 53, 2157-2183.
- Shock, E.L., Oelkers, E.H., Johnson, J.W., Sverjensky, D.A., Helgeson, H.C., 1992. Calculation of the thermodynamic properties of aqueous species at high pressures and temperatures. Effective electrostatic radii, dissociation constants and standard partial molal properties to 1000 °C and 5 kbar. *J. Chem. Soc. Faraday Trans.* 88, 803-826.
- Shock, E.L., Sassani, D.C., Willis, M., Sverjensky, D.A., 1997. Inorganic species in geologic fluids: Correlations among standard molal thermodynamic properties of aqueous ions and hydroxide complexes. *Geochim. Cosmochim. Acta* 61, 907-950.
- Shomate, C.H., Cook, O.A., 1946. Low-temperature heat capacities and high-temperature heat contents of Al₂O₃·3H₂O and Al₂O₃·H₂O. *J. Amer. Chem. Soc.* 68, 2140-2142.

- Shvarov, Y., 2015. A suite of programs, OptimA, OptimB, OptimC, and OptimS compatible with the Unitherm database, for deriving the thermodynamic properties of aqueous species from solubility, potentiometry and spectroscopy measurements. *Appl. Geochem.* 55, 17-27.
- Siever, R., 1962. Silica solubility, 0-200° C, and the diagenesis of siliceous sediments. *J. Geol.* 70, 127-150.
- Simonson, J.M., Holmes, H.F., Busey, R.H., Mesmer, R.E., Archer, D.G., Wood, R.H., 1990. Modeling of the thermodynamics of electrolyte solutions to high temperatures including ion association. Application to hydrochloric acid. *J. Phys. Chem.* 94, 7675-7681.
- Smith, E.R., Taylor, J.K., 1940. Standard electrode potential of sodium. *J. Res. National Bureau Standards* 25, 731-744.
- Sretenskaya, N.G., 1992. The dissociation constant of hydrochloric acid from the electrical conductance data for HCl solutions in water-dioxane mixtures. *Geochem. Internat.* 29, 447-453.
- Steeffel, C.I., Maher, K., 2009. Fluid-rock interaction: a reactive transport approach. *Rev. Mineral.* 70, 485-532.
- Stefánsson, A., 2001. Dissolution of primary minerals of basalt in natural waters: I. Calculation of mineral solubilities from 0°C to 350°C. *Chem. Geol.* 172, 225-250.
- Sverjensky, D., Shock, E.L., Helgeson, H.C., 1997. Prediction of the thermodynamic properties of aqueous metal complexes to 1000°C and 5 kb. *Geochim. Cosmochim. Acta* 61, 1359-1412.
- Sverjensky, D.A., Harrison, B., Azzolini, D., 2014. Water in the deep Earth: The dielectric constant and the solubilities of quartz and corundum to 60kb and 1200°C. *Geochim. Cosmochim. Acta* 129, 125-145.
- Sverjensky, D.A., Hemley, J.J., D'Angelo, W.M., 1991. Thermodynamic assessment of hydrothermal alkali feldspar-mica-aluminosilicate equilibria. *Geochim. Cosmochim. Acta* 55, 989-1004.
- Tajčmanová, L., Vrijmoed, J., Moulas, E., 2015. Grain-scale pressure variations in metamorphic rocks: implications for the interpretation of petrographic observations. *Lithos* 216-217, 338-351.
- Tagirov, B.R., Schott, J., 2001. Aluminum speciation in crustal fluids revisited. *Geochim. Cosmochim. Acta* 65, 3965-3992.
- Tagirov, B.R., Zotov, A.V., Akinfiyev, N.N., 1997. Experimental study of dissociation of HCl from 350 to 500°C and from 500 to 2500 bars: Thermodynamic properties of HCl°(aq). *Geochim. Cosmochim. Acta* 61, 4267-4280.
- Takahashi, Y., Yamada, K., Fukunaga, T., Mukaibo, T., 1973. Heat capacity of hydrated and crystalline aluminas. *Denki Kagaku* 41, 287-290.
- Tanger, J.C., Helgeson, H.C., 1988. Calculation of the thermodynamic and transport properties of aqueous species at high pressures and temperatures; revised equations of state for the standard partial molal properties of ions and electrolytes. *Amer. J. Sci.* 288, 19-98.
- Thien, B.M.J., Kulik, D.A., Curti, E., 2014. A unified approach to model uptake kinetics of trace elements in complex aqueous - solid solution systems. *Appl. Geochem.* 41, 135-150.
- Tropper, P., Manning, C.E., 2007. The solubility of corundum in H₂O at high pressure and temperature and its implications for Al mobility in the deep crust and upper mantle. *Chem. Geol.* 240, 54-60.
- Tsirlina, S.M., 1936. The solubility of aluminum hydroxides in sodium hydroxide solutions. (System Al(OH)-NaOH-H₂O). *Legkiye Metally* 5, 10.
- Tutolo, B.M., Kong, X.Z., Seyfried, W.E., Saar, M.O., 2014. Internal consistency in aqueous geochemical data revisited: Applications to the aluminum system. *Geochim. Cosmochim. Acta* 133, 216-234.
- Vanderzee, C.E., Nutter, J.D., 1963. Heats of solution of gaseous hydrogen chloride and hydrogen bromide in water at 25°C. *J. Phys. Chem.* 67, 2521-2523.
- Verdes, G., Gout, R., Castet, S., 1992. Thermodynamic properties of the aluminate ion and of bayerite, boehmite, diaspre and gibbsite. *Eur. J. Mineral.* 4, 767-792.
- Volosov A.G., Khodakovskiy I.L., Ryzhenko B.N., 1972. Equilibria in the system SiO₂-H₂O at elevated temperatures along the lower three-phase curve. *Geochem. Intl.* 9, 362-377
- Wagman, D.D., Evans, W.H., Parker, V.B., Schumm, R.H., Halow, I., Bailey, S.M., Churney, K.L. Nuttal, R.L., 1982, The NBS tables of chemical thermodynamic properties. Selected values for inorganic and C1, and C2 organic substances in SI units. *J. Phys. Chem. Ref. Data* 11 (Suppl. 2), 392 pp.

- Wagner, T., Kulik, D.A., Hingerl, F.F., Dmytrieva, S.V., 2012. GEM-Selektor geochemical modeling package: TSolMod library and data interface for multicomponent phase models. *Can. Mineral.* 50, 1173-1195.
- Walther, J.V., Orville, P.M., 1983. The extraction-quench technique for determination of the thermodynamic properties of solute complexes: application to quartz solubility in fluid mixtures. *Amer. Mineral.* 68, 731-741.
- Walther, J.V., 1997. Experimental determination and interpretation of the solubility of corundum in H₂O between 350 and 600°C from 0.5 to 2.2 kbar. *Geochim. Cosmochim. Acta* 61, 4955-4964.
- Walther, J.V., 2001. Experimental determination and analysis of the solubility of corundum in 0.1 and 0.5 m NaCl solutions between 400 and 600°C from 0.5 to 2.0 kbar. *Geochim. Cosmochim. Acta* 65, 2843-2851.
- Walther, J.V., Woodland, A.B., 1993. Experimental determination and interpretation of the solubility of the assemblage microcline, muscovite, and quartz in supercritical H₂O. *Geochim. Cosmochim. Acta* 57, 2431-2437.
- Wefers, K., 1967. Zur chemischen Technologie des Bauxitaufschlusses. Teil 1: Das System N₂Q-Al₂O₃-H₂O. *Metallography* 21, 1-10.
- Weill, D.F., Fyfe, W.S., 1964. The solubility of quartz in H₂O in the range 1000-4000 bars and 400-550°C. *Geochim. Cosmochim. Acta* 28, 1243-1255.
- Wesolowski, D.J., 1992. Aluminum speciation and equilibria in aqueous solution: I. The solubility of gibbsite in the system Na-K-Cl-OH-Al(OH)₄ from 0 to 100°C. *Geochim. Cosmochim. Acta* 56, 1065-1091.
- Wintsch, R.P., Merino, E., Blakely, R.F., 1980. Rapid-quench hydrothermal experiments in dilute chloride solutions applied to the muscovite-quartz-sanidine equilibrium. *Amer. Mineral.* 65, 1002-1011.
- Wohlert, A., Manning, C.E., Thompson, A.B., 2011. Experimental investigation of the solubility of albite and jadeite in H₂O, with paragonite-quartz at 500 and 600°C, and 1-2.25 GPa. *Geochim. Cosmochim. Acta* 75, 2924-2939.
- Woodland, A.B., Walther, J.V., 1987. Experimental determination of the solubility of the assemblage paragonite, albite, and quartz in supercritical H₂O. *Geochim. Cosmochim. Acta* 51, 365-372.
- Wyart, J., Sabatier, G., 1955. Nouvelles mesures de la solubilité du quartz, de la tridymite et de la cristobalite dans l'eau sous pression au-dessus de la température critique. *Compt. Rendus Acad. Sci.* 240, 1905-1907.
- Xie, Z., Walther, J.V., 1993. Quartz solubilities in NaCl solutions with and without wollastonite at elevated temperatures and pressures. *Geochim. Cosmochim. Acta* 57, 1947-1955.
- Xu, T., Sonnenthal, E., Spycher, N., Pruess, K., Brimhall, G., Apps, J., 2001. Modeling multiphase non-Isothermal fluid flow and reactive geochemical transport in variably saturated fractured rocks: 2. Applications to supergene copper enrichment and hydrothermal flows. *Amer. J. Sci.* 301, 34-59.
- Xu, T., Spycher, N., Sonnenthal, E., Zhang, G., Zheng, L., Pruess, K., 2011. TOUGHREACT Version 2.0: A simulator for subsurface reactive transport under non-isothermal multiphase flow conditions. *Comp. Geosci.* 37, 763-774.
- Yalman, R.G., Shaw, E.R., Corwin, J.F., 1960. The effect of pH and fluoride on the formation of aluminum oxides. *J. Phys. Chem.* 64, 300-303.
- Yamaguchi, G., Yanagida, H., Soejima, S., 1962. On the solubility and the velocity of dissolution of corundum under hydrothermal conditions. *Bull. Chem. Soc. Japan* 35, 1789-1794.
- Yardley, B.W.D., 1997. The evolution of fluids through the metamorphic cycle. In: Jamtveit, B., Yardley, B.W.D. (Eds.) *Fluid Flow and Transport in Rocks*, pp. 139-147.
- Zhang, Z., Duan, Z., 2005. Prediction of the PVT properties of water over wide range of temperatures and pressures from molecular dynamics simulation. *Phys. Earth Planet. Inter.* 149, 335-354.
- Zhang, L., Soong, Y., Dillmore, R., Lopano, C. (2015) Numerical simulation of porosity and permeability evolution of Mount Simon sandstone under geological carbon sequestration conditions. *Chem. Geol.* 403, 1-12.
- Zheng, L., Apps, J.A., Zhang, Y., Xu, T., Birkholzer, J.T., 2009. On mobilization of lead and arsenic in groundwater in response to CO₂ leakage from deep geological storage. *Chem. Geol.* 268, 281-297.
- Zhu, C., Sverjensky, D.A., 1991. Partitioning of F-Cl-OH between minerals and hydrothermal fluids. *Geochim. Cosmochim. Acta* 55, 1837-1858.
- Zhu, C., Anderson, G., 2002. *Environmental Applications of Geochemical Modeling*, Cambridge University Press, 300 pp.

- Zimmermann, R., Gottschalk, M., Heinrich, W., Franz, G., 1997. Experimental Na-K distribution between amphiboles and aqueous chloride solutions, and a mixing model along the richterite – K-richterite join. *Contrib. Mineral. Petrol.* 126, 252-264.
- Zimmerman, G.H., Scott, P.W., Greynolds, W., 2007. A new flow instrument for conductance measurements at elevated temperatures and pressures: Measurements on NaCl(aq) to 458 K and 1.4 MPa. *J. Solut. Chem.* 36, 767-786.

4. Extension of internally consistent thermodynamic dataset for aqueous species to the system Ca-Mg-Na-K-Al-Si-O-H-C-Cl

George D. Miron^a, Thomas Wagner^b, Dmitrii A. Kulik^c

^aInstitute of Geochemistry and Petrology, ETH Zurich, Switzerland, dan.miron@erdw.ethz.ch

^bDepartment of Geosciences and Geography, University of Helsinki, Finland

^cLaboratory for Waste Management, Paul Scherrer Institut, 5232 Villigen PSI, Switzerland

In preparation to be submitted to a peer-reviewed journal

Abstract

This study represents an extension with calcium, magnesium and carbon, of the previous core dataset (Miron et al. 2016), now covering the Ca-Mg-Na-K-Al-Si-O-H-C-Cl system. Critically evaluated experimental data on Ca, Mg, and C mineral solubility in water and electrolyte solutions over wide ranges in temperature and pressure, was added to the previous experimental data collection (Miron et al. 2016), and was used to simultaneously refine the standard state Gibbs energies of aqueous ions and complexes in the framework of the revised Helgeson-Kirkham-Flowers equation of state. The thermodynamic properties of the solubility controlling minerals were adopted from the internally consistent dataset of Holland and Powell (2002; Thermocalc dataset ds55). The association equilibria of important complexes and ion pairs forming in the system was critically reviewed and their standard state properties and HKF parameters were independently derived from experimentally derived logK data from conductance, potentiometric and exceptionally from solubility measurements. The global optimization of the Gibbs energies of aqueous species, performed with the GEMSFITS code (Miron et al., 2015), was set up in such a way that the association equilibria for ion pairs and complexes are always maintained. The new thermodynamic dataset reproduces all available fluid-mineral phase equilibria and mineral solubility data with good accuracy and precision over wide ranges in temperature, pressure and composition (25 to 800°C; 1 bar to 5 kbar; salt concentrations up to 5 molal). The method used allowed the identification of gaps and inconsistencies in the available experimental data. From this study it resulted that more experimental data is needed to retrieve the stability of calcium, magnesium chloride and hydroxide species at supercritical conditions. More research is needed for a better identification of the presence of complexes such as calcium and magnesium silicate species, and higher order associated species, and for determining their thermodynamic properties. Using the same strategy, the dataset can be further extended with more major and also trace and ore elements, and the optimization can be repeated when improved speciation and equation of state for multicomponent aqueous solutions becomes available.

4.1. Introduction

Thermodynamic modeling is an important approach for gaining fundamental understanding of chemical processes in natural and engineered geochemical systems such as formation of hydrothermal ore deposits, mass transfer and hydrothermal convection at mid-ocean ridges, fluid transfer and release in subduction zones, fluid release during crystallization of igneous intrusions, fluid circulation in geothermal reservoirs, and carbon dioxide sequestration in deep geological formations. The results of geochemical-computational models rely critically on the robustness of the geochemical models and, hence, on the availability, quality and consistency of parameters such as standard state properties of minerals, gases and aqueous species, equilibrium constants for solubility reactions, activity and equation of state parameters for non-ideal multicomponent phases

(mineral solid-solutions, aqueous solutions, fluid and gas mixtures), and kinetic rate constants for mineral dissolution and precipitation (Engi, 1992; André et al., 2006; Thien et al., 2015).

Calcium and magnesium are major components of carbonate and calc-silicate rocks, and together with carbon and iron, they play an important role in regional metamorphic processes (Baumgartner and Ferry, 1991; Miron et al., 2012; Miron et al., 2013). Calcite and dolomite are the major components in carbonate-bearing rocks, thus playing a key role in geological environments such as the deep Earth carbon cycle (Dasgupta and Hirschmann, 2010), sediment-hosted hydrothermal ore deposits (Baker et al., 2004; Meinert et al., 2003), carbonate alteration of basalts in geothermal systems (e.g. Alfredsson et al., 2008), diagenesis and dolomitization of carbonate platforms (e.g. Wilson et al., 2001) and geochemical reactions related to cementitious systems in nuclear waste repositories (Berner, 1992; Kulik and Kersten, 2001; Lothenbach and Winnefeld, 2006; Lothenbach et al., 2012).

At elevated temperatures and pressures, crustal fluids become enriched in carbon bearing species, which impacts the solvation behavior of aqueous ions and affects the mobility of rock-forming elements and trace ore metals (Kyser and Hiatt, 2003; Dasgupta and Hirschmann, 2010; Galvez et al., 2013). Carbon is initially taken up by rocks via reaction processes such as weathering or submarine alteration of oceanic basalts which can increase their carbon concentration from below 0.2 wt.% up to 3 wt.% (Staudigel, 2003). Metamorphic pressure-temperature gradients during regional metamorphism or subduction-related high-pressure metamorphism result in dehydration and decarbonation of the carbonated rocks. This causes the release of a fluid phase rich in water and carbon components (Plank and Langmuir, 1998), while part of the carbon is being transported into the mantle and fixed as graphite or diamond (Frezzotti et al., 2011; Galvez et al., 2013). The fluids released from the subducting slab cause metasomatism of the overlying mantle wedge. The carbon present in fluids in these environments has a major impact on the melting behavior of the rocks, element transport and fluid properties, and on the amount of carbon released during volcanic eruptions (Manning et al., 2013). A large source of carbon is buried organic material found in sedimentary rocks (Sephton and Hazen, 2013).

Quantitative modeling of the behavior of calcium, magnesium and carbon in a wide range of geological systems and at elevated temperatures and pressures requires a high-quality internally-consistent thermodynamic model for the solubility and aqueous speciation of these elements. In a previous study (Miron et al. 2016), we have developed a strategy for generating an internally consistent thermodynamic dataset for aqueous species in the system Na-K-Al-Si-O-H-Cl over wide ranges of temperature and pressure up to 600 °C and 5 kbar. A large amount of critically evaluated experimental mineral solubility data was used to refine the standard state Gibbs energies of aqueous ions and complexes while maintaining a close agreement with the association equilibria for ion pairs and complexes as independently derived from the conductance and potentiometric data. In this study, we use the same strategy as in Miron et al. (2016) to extend the chemical system coverage, by addition of calcium, magnesium, and carbon. The existing experimental data on the solubility of calcium, magnesium, and carbon minerals (silicates, hydroxides, carbonates) in water and different electrolyte solutions was critically assessed. Based on the experimental data, a

speciation model that accounts for chloride, hydroxide and carbonate complexes has been developed. Properties of aqueous ions and complexes in the system Ca-Mg-Na-K-Al-Si-O-H-Cl were then globally optimized against a large collection of experimental data covering a wide range of conditions. The resulting thermodynamic dataset is able to represent the majority of experimental solubility data within their uncertainty. The results do also reveal important gaps and limitations in the available experimental fluid-mineral equilibria data, and provide some guidance for key future experimental studies.

4.2. Thermodynamic framework

The thermodynamic framework used in this study is the same as the one used in the previous study (Miron et al., 2016). The standard state convention for aqueous species adopted is the ideal one molal solution referenced to infinite dilution. For water solvent, the standard state is pure water at any pressure and temperature, and water activity is based on the mole fraction concentration scale. For minerals, the standard state is unit activity of pure solids at any pressure or temperature (Oelkers et al., 1995). For gases, the standard state is that of a hypothetical pure ideal gas at the standard pressure of 10^5 Pa (1 bar). The standard Gibbs energies for aqueous species, solids and gas species in this study are apparent standard Gibbs energies in Benson-Helgeson convention (Helgeson et al., 1981).

The properties of minerals in this study were calculated from the Holland-Powell internally consistent thermodynamic dataset (Holland and Powell, 1998; updated Thermocalc dataset ds55) and the related thermodynamic framework. This dataset is referred to as HP02 in the remainder of this paper. In addition to the minerals used in the previous dataset optimization, the present study included the following pure mineral end-members: anorthite, anthophyllite, antigorite, aragonite, brucite, calcite, chrysotile, enstatite, forsterite, magnesite, pyrophyllite, talc, tremolite, and wollastonite. The remaining Ca and Mg oxides, silicates, and carbonates present in the HP02 database are also consistent with the current dataset, but were not used in the study because no experimental solubility data are available for them. Portlandite is not included in the HP02 database and, although it was not used in the global optimization, it was an essential mineral in this study for constraining the calcium speciation model. The standard state properties for portlandite came from the compilation of Robie and Hemingway (1995) and Thoenen et al. (2014). The thermodynamic data for portlandite were employed in such a way that the final values for the Gibbs free energies of the aqueous species are not dependent on them (see discussion below).

The properties of aqueous species were modeled within the framework of the revised Helgeson-Kirkham-Flowers (HKF) equation of state (Helgeson and Kirkham, 1974a, 1974b; Tanger and Helgeson, 1988; Shock et al., 1992). The activity coefficients for charged aqueous species were calculated with an extended Debye-Hückel equation (Helgeson et al., 1981). For the solubility experiments done in CaCl_2 and MgCl_2 solutions, the extended Debye-Hückel parameters were taken from Helgeson et al. (1981). The ion size parameters \hat{a} are 4.32 and 4.11, while the

extended term parameters b_γ are 0.077 and 0.106 (assumed constant at any temperature and pressure) for CaCl_2 and MgCl_2 , respectively.

The standard state properties and fugacity coefficients of pure gases in the gas phase (for modeling CO_2 solubility in water and NaCl solutions) were calculated using the compensated Redlich-Kwong (CORK) model, which is consistent with the HP02 dataset (Holland and Powell, 1991). Fugacity and activity coefficients for gas mixtures were calculated using the asymmetric formalism (Holland and Powell, 2003). These calculations were performed within the GEM-Selektor package and the GEMS3K library (Kulik et al., 2013; Wagner et al., 2012; gems.web.psi.ch).

4.3. Carbon dioxide solubility in water

Carbon dioxide dissolves in aqueous solutions according to the initial reaction:



The solubility of CO_2 in pure water and electrolyte solutions has been extensively studied over the years. Recent reviews on the existing models and experimental data were made by Diamond and Akinfiev (2003), Duan and Sun (2003) and De Visscher et al. (2012). The CO_2 solubility experiments in water are used to extract Henry's law solubility constants, but these constants are highly dependent on the aqueous model used to evaluate the data (Plummer and Busenberg, 1982). Besides analytical problems, the extracted reaction constants are influenced by the calculation of the activity coefficient of $\text{CO}_2(\text{aq})$ in the aqueous phase (diverges from 1.0 at above about 2 mol.% dissolved CO_2), the estimation of the CO_2 mole fraction in the gas phase, and the dissociation of $\text{CO}_2(\text{aq})$ which was not considered in all studies (Plummer and Busenberg, 1982; Diamond and Akinfiev, 2003; De Visscher et al., 2012).

Several models have been developed to calculate the solubility of CO_2 in water and electrolyte solutions. Akinfiev and Diamond (2003) proposed a virial-like equation of state (EOS) for calculating the thermodynamic properties of aqueous nonelectrolytes over a wide range of conditions. Their EOS is compatible with the HKF model for electrolytes. Duan and Sun (2003) proposed a model that combines the EOS for gaseous CO_2 from Duan et al. (1992) with the Pitzer ion interaction model (Pitzer, 1973) for calculating the chemical potential of CO_2 in the aqueous phase. The HKF model (Tanger and Helgeson, 1988) developed for calculating the standard chemical potentials of ionic species was also extended for calculating standard state properties of aqueous nonelectrolytes (Shock and Helgeson, 1990; Shock et al., 1989). However, recent experimental data for the standard partial molar volume and heat capacity of nonelectrolytes have demonstrated that the HKF model fails to correctly predict the standard state properties of nonelectrolytes close to the critical point of water but also in the supercritical region (Plyasunov and Shock, 2001; Schulte et al., 2001; Akinfiev and Diamond, 2003; Plyasunov, 2015). Schulte et al. (2001) and Plyasunov and Shock (2001) have revised the HKF parameters of $\text{CO}_2(\text{aq})$ to

accurately reproduce the recent measurements (Hnědkovský and Wood, 1997) of partial molal heat capacity and partial molal volume of $\text{CO}_2(\text{aq})$.

Fig. 4.1 shows a comparison of different thermodynamic models and experimental determinations of the CO_2 solubility constants in water from 0 to 360 °C at saturated water vapor pressure (SWVP). Properties of the gas phase were calculated with the CORK model (Holland and Powell, 1991). The agreement between different experimental datasets and model predictions is quite good below 100 °C, with slightly larger differences in data and their trends for the higher temperatures. The maximum discrepancy is less than 0.1 log units.

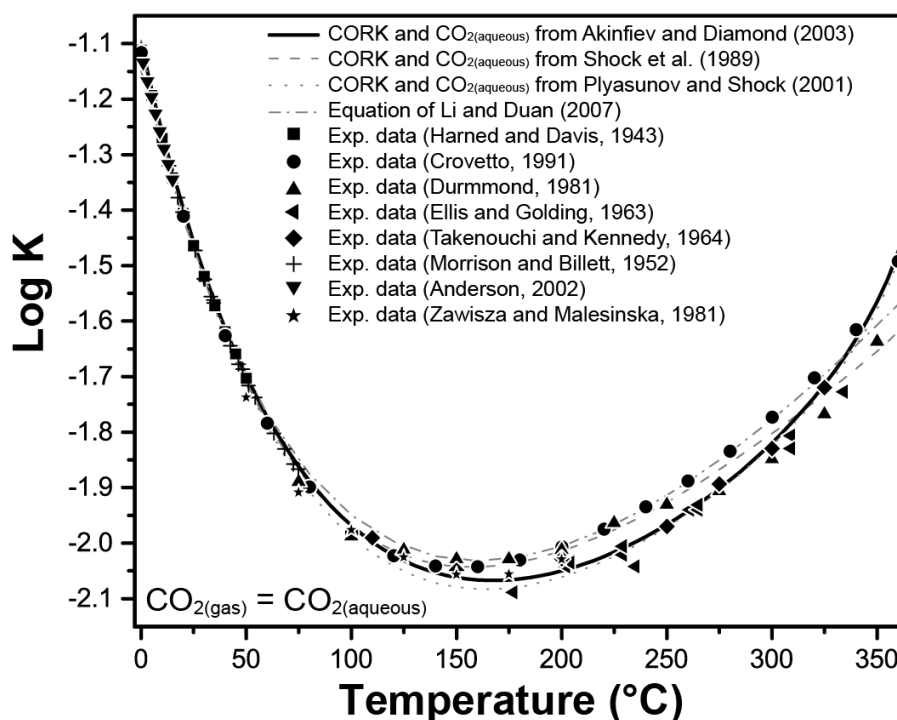


Figure 4.1. Comparison between calculated values using the standard state properties of $\text{CO}_2(\text{aqueous})$ from different sources and experimentally determined solubility constants of $\text{CO}_2(\text{gas})$ in H_2O . The CORK (Holland and Powell, 1991) model was used for the gas phase.

We have made a comparison between the experimentally measured dissolved aqueous CO_2 concentrations and calculated values using different sources for the thermodynamic properties of the $\text{CO}_2(\text{aq})$ species at different total pressures (Fig. 4.2). Both experiments performed in pure water and in NaCl solutions were included. A more detailed review of the experimental data can be found in Duan and Sun (2003). In our calculations, the activity coefficient of $\text{CO}_2(\text{aq})$ is approximated to be 1.0 which is a good approximation up to around 2 wt.% dissolved CO_2 (equivalent to 1 mol/kg). It can be seen in Figs. 4.1 and 4.2 that there is a rather good agreement between different sources for the properties of $\text{CO}_2(\text{aq})$. The best agreement between modeled and experimental CO_2 solubility data is achieved when using the model of Akinfiev and Diamond (2003). We have therefore selected this model for calculating the properties for $\text{CO}_2(\text{aq})$ in this study.

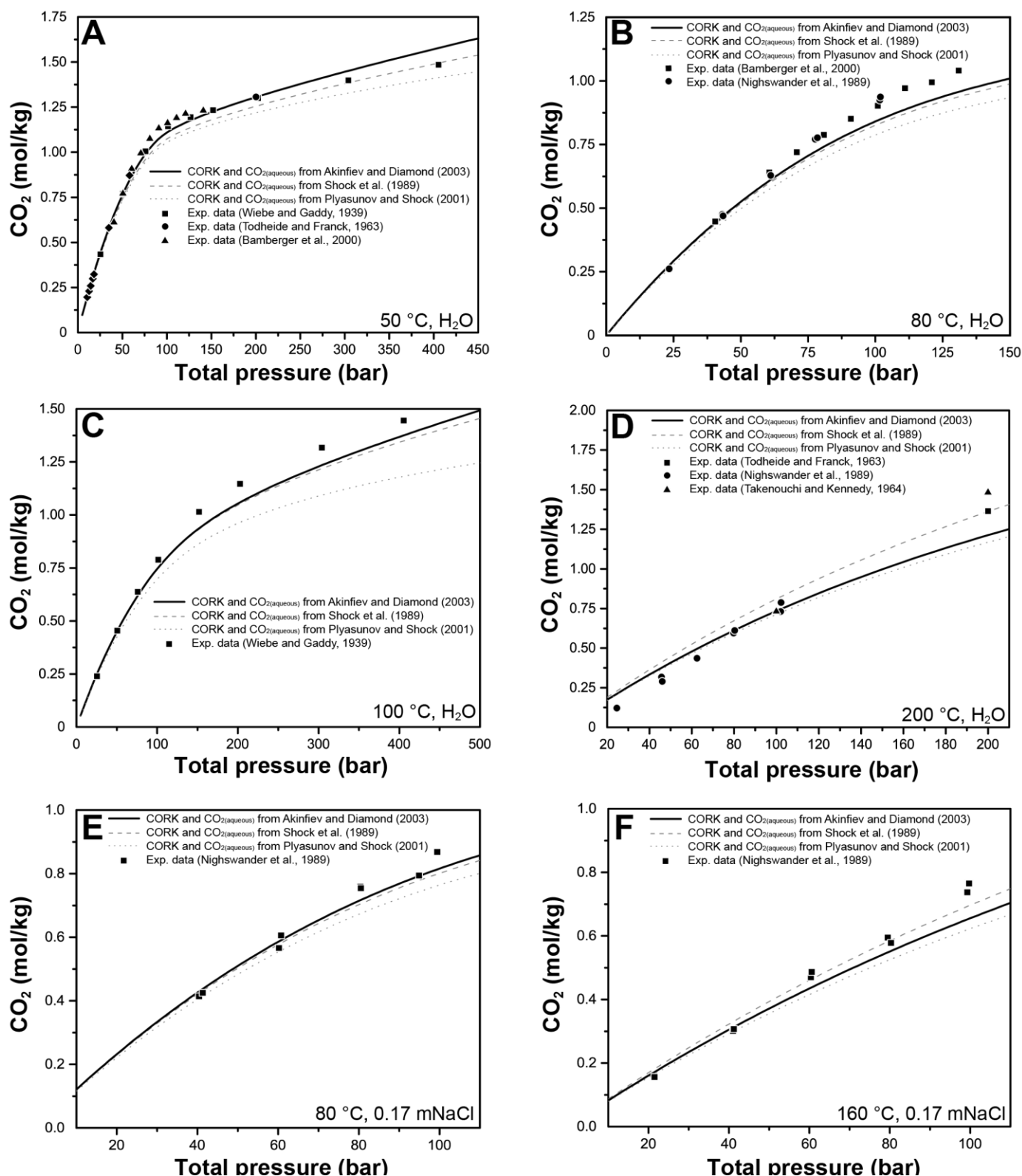


Figure 4.2. Comparison between calculated values using the standard state properties of CO₂(aq) from different sources and experimentally determined solubility of CO₂(gas) in H₂O (A, B, C, D) and in NaCl solutions (E, F) at different temperatures with increasing pressure.

4.4. Carbon species

The CO₂ solubility in aqueous solution increases as a function of the CO₂(g) partial pressure (Diamond and Akinfiyev, 2003; Duan and Sun, 2003). The CO₂ that dissolves in an aqueous solution will partially dissociate into HCO₃⁻ and CO₃²⁻ according to two stepwise reactions:



Both reactions are strongly dependent on pH, and increase in pH will shift them to the right-hand side. At ambient pressure-temperature conditions, the formation of the bicarbonate complex is only favored at low pH. In a closed fluid-rock system controlled by equilibria with carbonate minerals at temperatures below 200 °C, HCO₃⁻ is the dominant species, and above this temperature, CO₂(aq) becomes dominant. Both the bicarbonate and carbonate species can form stable complexes with various metal cations.

4.4.1. Carbonate and bicarbonate

The values of the first dissociation constant reported in the literature were recently reviewed (Li and Duan, 2007; De Visscher et al., 2012; Stefánsson et al., 2013). There is a fairly good agreement between the experimental data and thermodynamic models at pressures of 1 bar and SWVP and at temperatures from 25 °C up to the critical point of water (Fig. 4.3A). The only high-pressure experimental studies on the dissociation constant were done by Ellis (1959a) up to 3000 bar and 65 °C and by Read (1975) up to 2000 bar and 250 °C using conductance methods. When comparing the available models with the experimental data at high-pressures (Figs. 4.3C and 4.3D), there is an increasing disagreement with increasing pressure and temperature between the predicted values and the experimental data of Read (1975). Read (1975) used KCl and KHCO₃ solutions for the experiments, but did not consider the possibility that potassium carbonate species would form. Although in concentrated chlorine bearing solutions these species have insignificant concentrations, they become more important in solutions with lower chlorinity. The HKF parameters for HCO₃⁻ were refined in this study to better represent the high pressure data of Read (1975) and Ellis (1959a), but keeping the standard state properties ($\Delta_f G_{298,1}^0$, $S_{298,1}^0$, $Cp_{298,1}^0$, $V_{298,1}^0$) from Shock and Helgeson (1988).

The second dissociation constant of aqueous CO₂ was only investigated experimentally at pressures of 1 bar and at SWVP (Fig. 4.3B). The agreement between different experimental studies is very good up to 125 °C (Stefánsson et al., 2013), but at higher temperatures the differences increase up to 0.5 log units. It is important to note that many studies considered only the HCO₃⁻ and CO₃²⁻ species for data processing. For example, Patterson et al. (1982, 1984) performed potentiometric measurements in NaCl solutions up to 5 molal concentration, but did not consider the formation of sodium carbonate species, which can affect the determination of the stability constant at low NaCl concentrations. Data on the high pressure stability (> 10 kbar) of the bicarbonate complex was obtained from in situ Raman measurements (Facq et al., 2014), but the

P-T conditions are outside the permissible range of the HKF model used in this study. The bicarbonate species is predicted to be important in aqueous solutions at very high pressures exceeding 30 kbar (Facq et al., 2014). The $Cp_{298,1}^0$ for CO_3^{2-} was previously determined by Shock and Helgeson (1988) based on the data of Patterson et al. (1982). In this study, we have refined the $Cp_{298,1}^0$ using the new data of Stefánsson et al. (2013), Stefánsson et al. (2014), and the data of Patterson et al. (1982) below 125 °C. The $S_{298,1}^0$ of CO_3^{2-} was adopted from the calorimetric measurements of Berg and Vanderzee (1978), while other standard state properties were taken from Shock and Helgeson (1988).

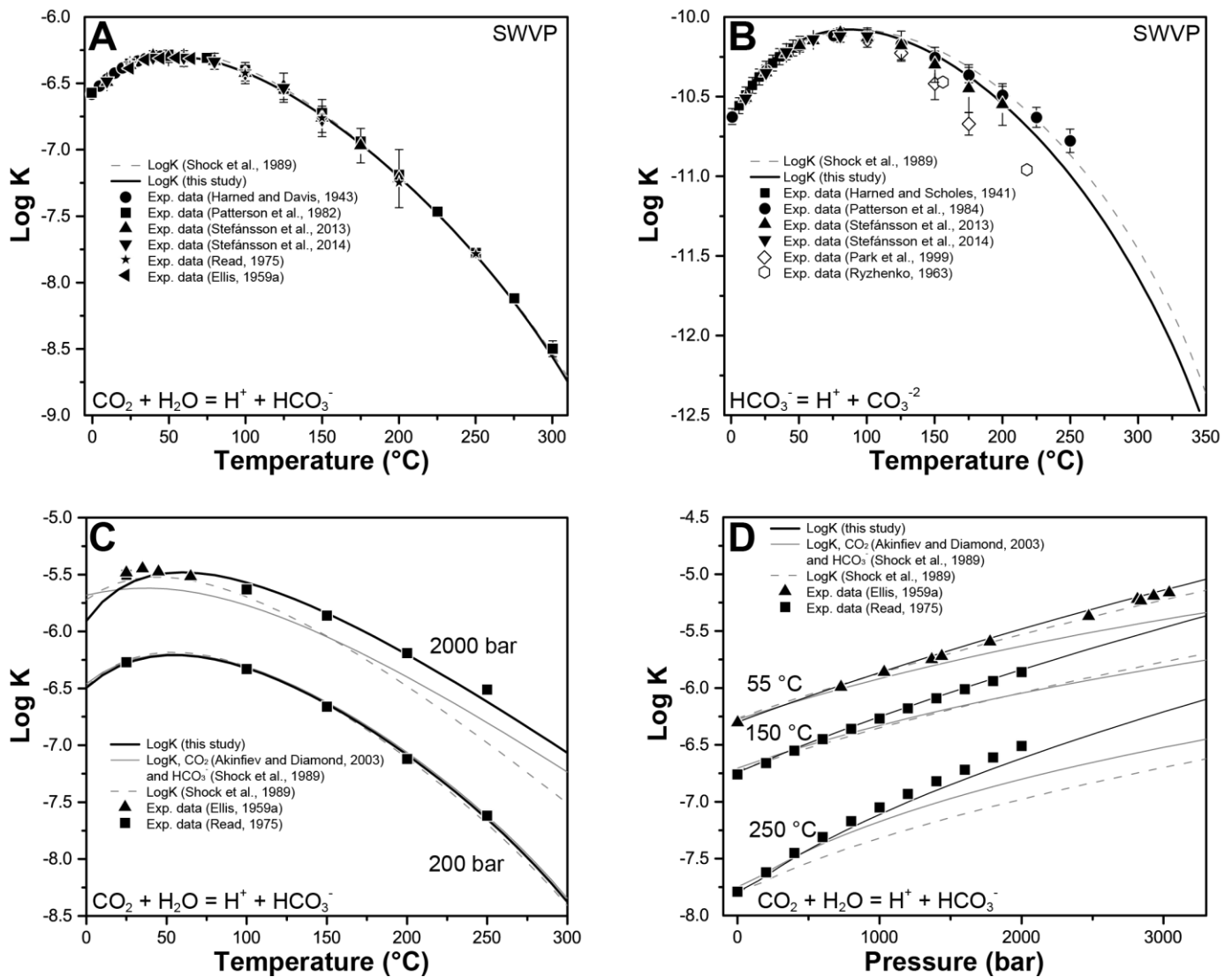
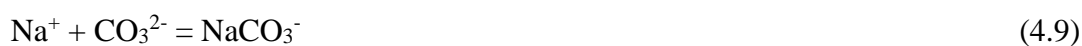


Figure 4.3. Comparison between calculated and experimentally determined stability constants of carbonate and bicarbonate complexes. (A) HCO_3^- at SWVP; (B) CO_3^{2-} at SWVP; (C) HCO_3^- at different pressures with increasing temperature; (D) HCO_3^- at different temperatures with increasing pressure.

4.4.2. Metal-bicarbonate and -carbonate complexes

While the metal-carbonate complexes are only significant at extremely low CO₂ partial pressure and at elevated pH, the metal-bicarbonate ion pairs have significant influence on carbonate mineral solubility their dependence on CO₂ partial pressure at all conditions (De Visscher et al., 2012). The existence of alkali metal bicarbonate and carbonate species has been confirmed by Raman spectroscopy (Capewell et al., 1999; Sipos et al., 2000) and atomistic simulations studies (Demichelis et al., 2011). The stability constants derived from experimental solubility data are largely dependent on the speciation model used, which in turn also affects the calculation of ionic strength and pH (Turner et al., 1981).

The speciation model of this study considers the first bicarbonate and carbonate complexes of the earth alkaline and alkali metals Ca, Mg, Na and K. The association reactions are:



4.4.2.1. Ca complexes

The calcium complexes CaHCO₃⁺ and CaCO₃⁰ were clearly identified by Raman measurements and by atomistic calculations (Demichelis et al., 2011). Caciagli and Manning (2003) suggested that at the pressure-temperature conditions (6-16 kbar, 500-800 °C) of their experiments CO₂(aq) was the predominant species and CO₃²⁻, CaHCO₃⁺, and CaCO₃⁰ were negligible (<1%). Facq et al. (2014) concluded that CaHCO₃⁺ would be more stable at pressures <30 kbar, while CaCO₃⁰ becomes more stable at higher pressures. They also noted that at high-pressure conditions, both carbonate and bicarbonate are the major carbonate species, which also form complexes with calcium. With increasing pressure (above 5 kbar), CO₂(aq) is replaced by HCO₃⁻ and finally by CO₃²⁻ as the dominant species. With the exception of high-pressure studies, all other experiments were done at pressures of 1 bar and at SWVP. There is a considerable disagreement concerning the stability of CaHCO₃⁺, and the reported logK values range from 0.29 to 1.29 at 25 °C 1 bar. There is reasonable agreement between two experimental studies, which are the conductance measurements of Jacobson and Langmuir (1974) and the aragonite and calcite solubility data of Plummer and Busenberg (1982). By contrast, the study of Martynova et al. (1974), which used an ion-selective electrode method over the temperature range 22-98 °C, resulted in logK data that are in disagreement with the two studies mentioned above (Fig. 4.4A).

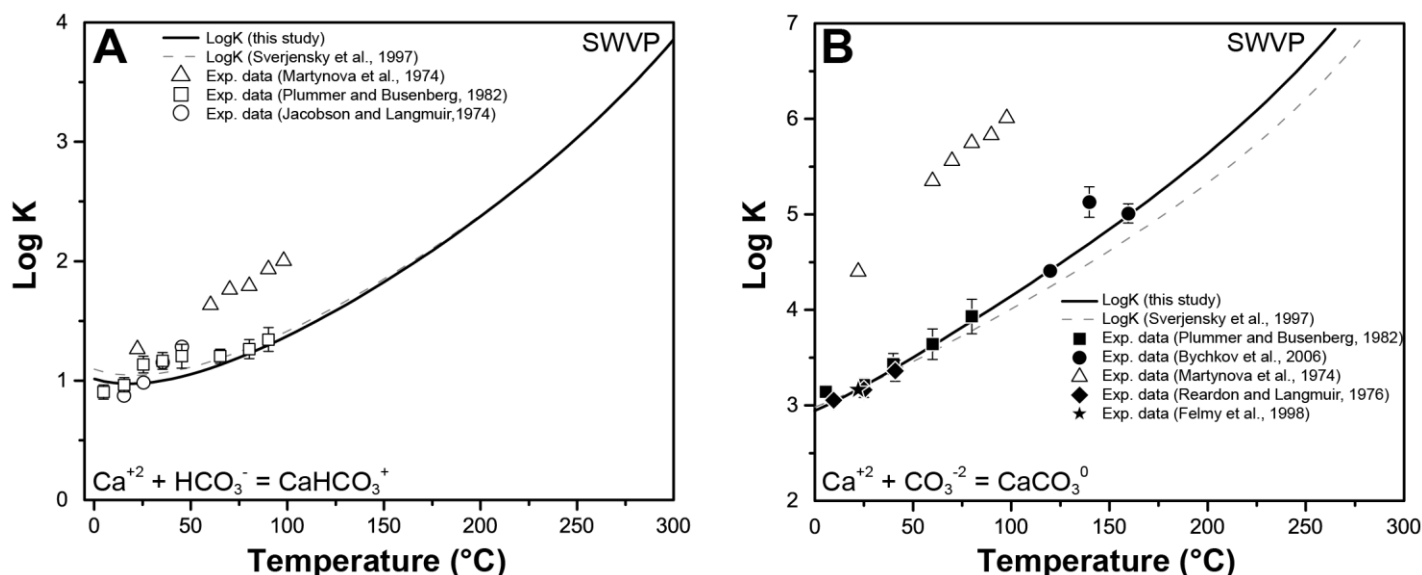


Figure 4.4. Comparison between calculated and experimentally determined stability constants of calcium carbonate and calcium bicarbonate complexes. (A) CaHCO_3^+ at SWVP; (B) CaCO_3^0 at SWVP.

Stability constants for Ca bicarbonate and carbonate species derived from solubility data depend on the values used for the first and second dissociation constant of $\text{CO}_2(\text{aq})$. This should not affect the data from Plummer and Busenberg (1982) much, because their experiments were performed below 90 °C, where the agreement between different datasets for the dissociation constants of $\text{CO}_2(\text{aq})$ is good. For CaCO_3^0 , there is reasonable agreement between the potentiometric study of Reardon and Langmuir (1974) and the data derived by Plummer and Busenberg (1982) from the pH of $\text{CaCl}_2/\text{K}_2\text{CO}_3$ solutions. The ion-selective electrode measurements of Martynova et al. (1974) are again in disagreement with the other two studies (Fig. 4.4B).

For CaHCO_3^+ , we selected the standard state properties from the study of Duan and Li (2008), which are derived from both low and high pressure calcite solubility experiments at saturated CO_2 conditions. The $S_{298,1}^0$ of CaCO_3^0 was refined based on the reported logK values of Reardon and Langmuir (1974), Plummer and Busenberg (1982), Felmy et al. (1998) and Bychkov et al. (2006). The remaining standard state properties and HKF parameters were accepted from Sverjensky et al. (1997).

4.4.2.2. Mg complexes

Since the extensive review of De Visscher et al. (2012), data for the association constants for Mg complexes MgHCO_3^+ and MgCO_3^0 were retrieved by Stefánsson et al. (2014) from new potentiometric and spectrophotometric measurements. Their data are in good agreement with the potentiometric measurements of Siebert and Hostetler (1977) for both complexes and also with the potentiometric measurements of Reardon and Langmuir (1974) for MgCO_3^0 (Fig. 4.5). The data analysis of Stefánsson et al. (2014) considered also the presence of MgOH^+ , MgCl^+ , NaHCO_3^0 and NaCO_3^- . They concluded that MgCl^+ , NaHCO_3^0 and NaCO_3^- are present in insignificant amounts

at their experimental conditions. Other reported values for the association constants of MgHCO_3^+ and MgCO_3^0 are in disagreement with the above mentioned studies.

We have therefore refined the $S_{298,1}^0$ of MgHCO_3^+ based on the logK values from Siebert and Hostetler (1977) and Stefánsson et al. (2014). The remaining standard state properties and the HKF parameters for this complex were taken from Sverjensky et al. (1997). For MgCO_3^0 , we have refined the $S_{298,1}^0$ against the data of Siebert and Hostetler (1977) and Stefánsson et al. (2014), while accepting the remaining properties from Sverjensky et al. (1997).

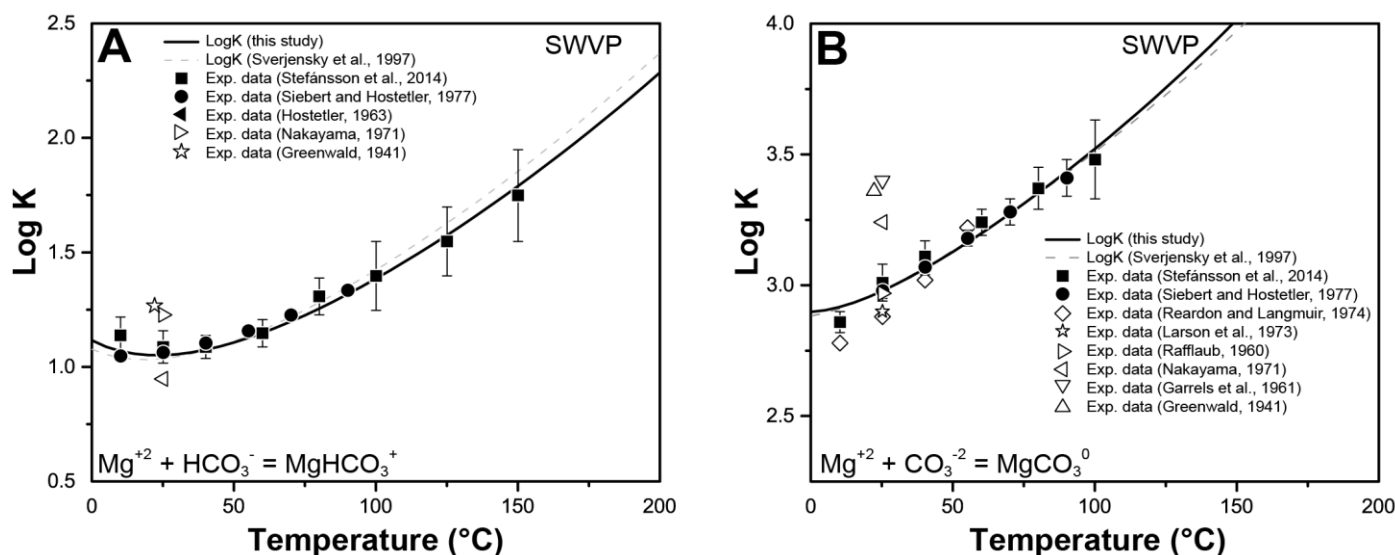


Figure 4.5. Comparison between calculated and experimentally determined stability constants of magnesium carbonate and magnesium bicarbonate complexes. (A) MgHCO_3^+ at SWVP; (B) MgCO_3^0 at SWVP.

4.4.2.3. Na complexes

The presence of the NaCO_3^- and NaHCO_3^0 complexes has been identified by Raman spectroscopy studies (Capewell et al., 1999; Sipos et al., 2000). The only high temperature studies (at SWVP) that would constrain the stability of these complexes are the potentiometric and spectrophotometric measurements of Stefánsson et al. (2013) that cover temperatures from 80 to 200 °C, and the data of Bychkov et al. (2007) as reported by Stefánsson et al. (2013) from 100 to 160 °C. For 25 °C and 1 bar, Capewell et al. (1999) calculated a logK value of 0.98 for NaCO_3^- from Raman spectroscopic data, while Wimberley et al. (1985) calculated logK values for both NaCO_3^- and NaHCO_3^0 of 0.92 and -0.143 at 25 °C and 1 bar from ion selective electrode measurements (Fig. 4.6). These values agree within their uncertainties with extrapolations to 25 °C using the data of Stefánsson et al. (2013). We have accepted the $\Delta_f G_{298,1}^0$ values for NaCO_3^- and NaHCO_3^0 derived from the study of Wimberley et al. (1985). Subsequently, we have obtained the other standard state properties and HKF parameters of both species using the estimation methods from Sverjensky et al. (1997). Then the $S_{298,1}^0$ values were regressed against the logK values reported by Wimberley et al. (1985), Bychkov et al. (2007) and Stefánsson et al. (2014).

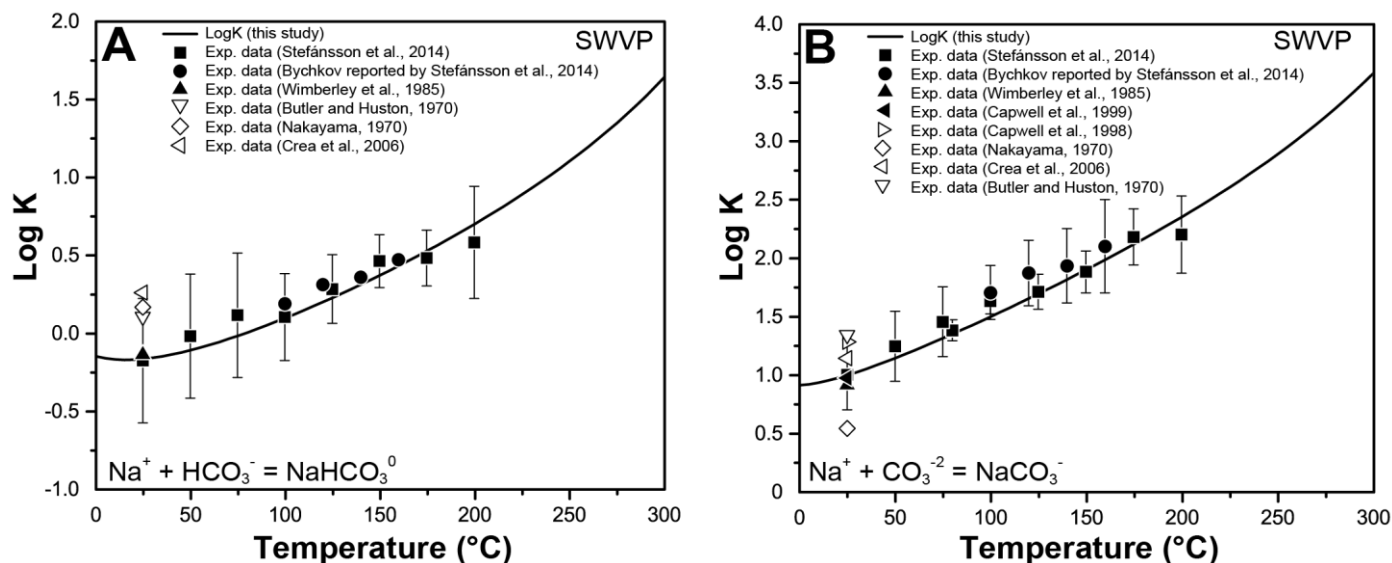


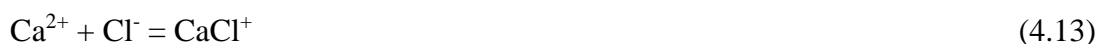
Figure 4.6. Comparison between calculated and experimentally determined stability constants of sodium carbonate and sodium bicarbonate complexes. (A) NaHCO_3^0 at SWVP; NaCO_3^- at SWVP.

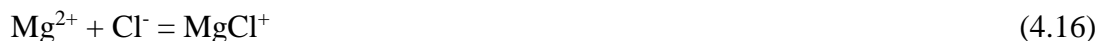
4.4.2.4. K complexes

The possible presence of KHCO_3^0 and KCO_3^- complexes was identified in the Raman spectroscopic study of Sipos et al. (2000), but the inferred stability of both species was lower than that of their Na counterparts. Wimberley et al. (1985) derived values for the association constants of KCO_3^- and KHCO_3^0 as 1.025 and -0.26 at 25 °C and 1 bar, using measurements with an ion selective electrode. To our knowledge, there are currently no experimental constraints on the stability of potassium bicarbonate and carbonate complexes at elevated temperatures and pressures. We have therefore accepted the $\Delta_f G_{298,1}^0$ values for KCO_3^- and KHCO_3^0 derived from the study of Wimberley et al. (1985) and estimated the remaining standard state properties and HKF parameters using the correlation methods of Sverjensky et al. (1997).

4.5. Ion association properties of Ca and Mg with hydroxide and chlorine

The standard state properties and HKF parameters of Ca and Mg hydroxy and chloride species were derived from the experimental data, where preference was given to conductance and potentiometric measurements in aqueous solutions with low concentrations of dissolved Ca and Mg. Most datasets are restricted to subcritical conditions, and there is a clear lack of experimental data at supercritical temperatures and high pressures. The speciation model of this study considers a hydroxide complex and the first and second chloride complex of Ca and Mg. The association reactions are:





4.5.1. Hydroxide species

While the concentrations of Ca and Mg hydroxide species are negligible at low temperatures and slightly alkaline pH (De Visscher et al., 2012), they become more important as temperature increases (Walther, 1986; Seewald and Seyfried, 1991), and at pH >12. The properties of CaOH^+ and MgOH^+ in the SUPCRT92 dataset are solely based on predictions using correlations between the standard state properties of the ions and that of the hydroxide species. They were refined in this study taking into account the new experimental data that constrain their stability.

4.5.1.1. CaOH^+ association constant

Experimental data on the stability of CaOH^+ are only available at temperatures below 100 °C (Fig. 4.7A) and at SWVP. These studies include potentiometric measurements by Bates et al. (1959), electromotive force measurements by Gimblett and Monk (1954) and measurements using ion-selective electrodes by Martynova et al. (1974). Additional studies that permit to derive the stability constant of CaOH^+ are portlandite solubility experiments. Felmy et al. (1998) derived a logK value of -12.93 at 22 °C from portlandite solubility, while Baes and Mesmer (1981) report a value of -12.85 at 25 °C. Both values are in excellent agreement with the value of -12.86 at 25 °C that was reported by Bates et al. (1959). Gimblett and Monk (1954) report a logK values of -12.63, which is in disagreement with all other studies. At elevated temperatures and pressures, the stability of CaOH^+ species was exclusively retrieved from portlandite solubility measurements (Fig. 4.7B). At temperatures between 100 and 350 °C and at 500 bar pressure, CaOH^+ stability constants have been extracted from the experiments by Seewald and Seyfried (1991). For processing their data at low concentrations, they employed the extended Debye-Hückel model from Helgeson and Kirkham (1974b), which is consistent with the activity model used in this study. Walther (1986) studied the solubility of portlandite from 300 to 600 °C and from 1 to 3 kbar. The possible formation of CaOH^+ was not considered in the data treatment, and agreement between calculated and measured solubility was achieved by adjusting the $\Delta_f G_{298,1}^0$ of the Ca^{2+} ion. Seewald and Seyfried (1991) reinterpreted the data from Walther (1986) taking into account the formation of CaOH^+ . They extracted logK values up to 425 °C from solubility data, but could not obtain them for higher temperature due to the lack of high-temperature heat capacity data for portlandite. We have refined the standard state properties and HKF parameters of CaOH^+ using the low temperature data of Bates et al. (1959) and the portlandite solubility data of Seewald and Seyfried (1991) and Walther (1986).

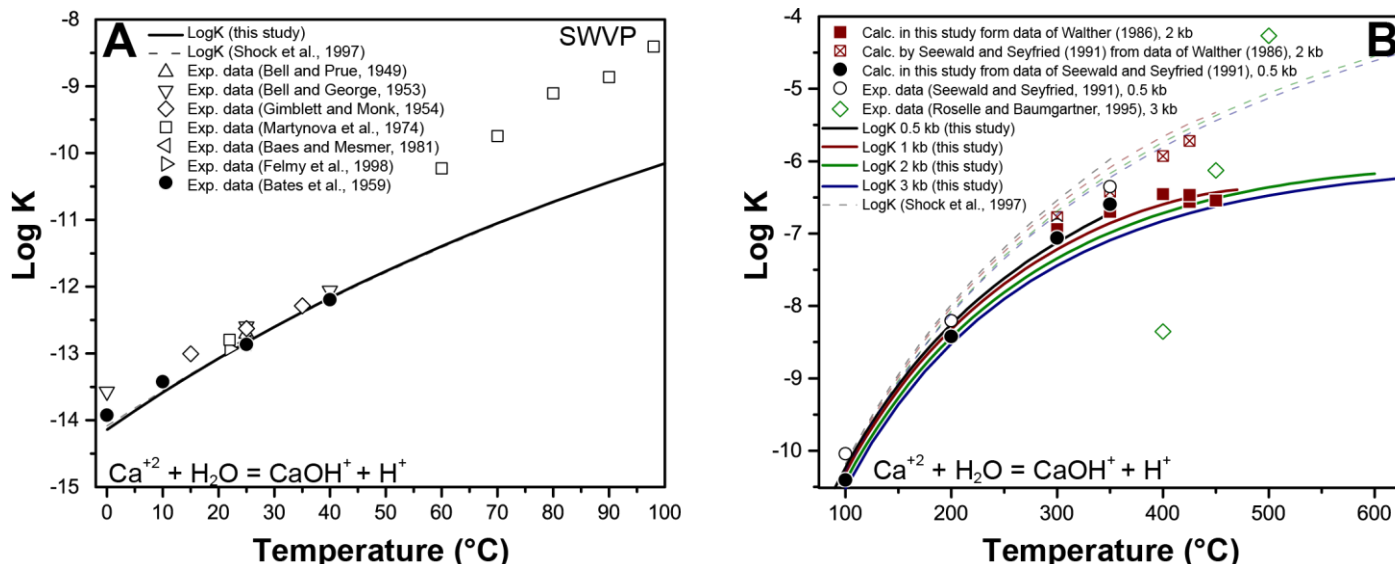


Figure 4.7. Comparison between calculated and experimentally determined association constants of calcium hydroxide complex. (A) at SWVP; (B) at different pressures with increasing temperature.

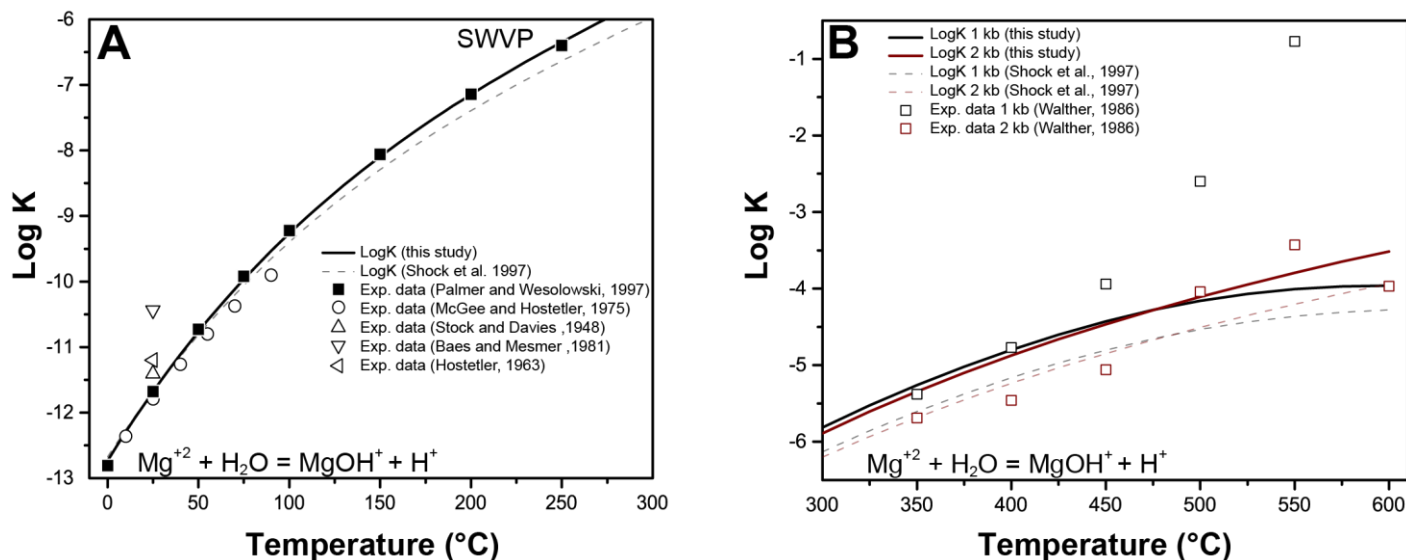


Figure 4.8. Comparison between calculated and experimentally determined association constants of magnesium hydroxide complex. (A) at SWVP; (B) at 1 and 2 kbar with increasing temperature.

4.5.1.2. MgOH^+ association constant

The stability of MgOH^+ has been studied using the potentiometric method by McGee and Hostetler (1975) from 10 to 90 °C and Palmer and Wesolowski (1997) from 25 to 250 °C and at SWVP (Fig. 4.8A). Both datasets have a slightly different trend with temperature and start to diverge above 60 °C, with a maximum difference of around 0.4 log units at 90 °C. At high temperatures and pressures, the logK values of MgOH^+ have been derived from brucite solubility measurements by Walther (1986) assuming that MgOH^+ is the dominant species (Fig. 4.8B). The thermodynamic properties of brucite used by Walther (1986) were those from Helgeson et al. (1978). We have refined the $S_{298,1}^0$ and the HKF parameters of MgOH^+ based on the accurate potentiometric data of Palmer and Wesolowski (1997). The pressure and temperature trends of the stability constant of MgOH^+ calculated with the properties from Shock et al. (1997) and this study

are substantially different from those of Walther (1986). The brucite solubility experiments of Walther (1986) were not explicitly used to extract the stability constants of MgOH^+ , but they were used in the global regression of all mineral solubility data (see below).

4.5.2. Ca and Mg chloride species

The standard state properties and HKF parameters of Ca and Mg chloride species present in the SUPCRT92 database were derived from a limited number of experimentally determined stability constants below 100 °C and from correlations between aqueous metal complexes (Sverjensky et al., 1997). The properties for both CaCl^+ and MgCl^+ were derived from the potentiometric measurements of Majer and Štulík (1982). As already noted by Méndez De Leo and Wood (2005) and Arcis et al. (2014), the logK values reported by Majer and Štulík (1982) were not extrapolated to infinite dilution. This results in a systematic error for the properties of CaCl^+ and MgCl^+ reported by Sverjensky et al. (1997). The same applies to the properties of the complexes SrCl^+ , BaCl^+ , MgF^+ , CaF^+ , BaF^+ , and SrF^+ , which are also based on the data of Majer and Štulík (1982). The logK values for CaCl^+ and CaCl_2^0 at 25 °C and 1 bar that were derived from the study of Ramette (1986) were also not corrected to infinite dilution. Ramette (1986) derived the association constants of CaCl^+ , CaCl_2^0 and CaCl_3^- from solubility experiments performed at constant ionic strength of 5 molal. Ruaya (1988) employed an isocoulombic approach to estimate the properties of the Ca chloride complexes but also used the original logK values of Majer and Štulík (1982). Rard and Clegg (1997) reviewed of the properties of aqueous CaCl_2 solutions and identified large inconsistencies between different data for the association constants of calcium chloride complexes at low temperatures.

Frantz and Marshall (1982) derived the ionization constants for magnesium and calcium chloride species (the first and second association constants for both elements) from electrical conductance measurements from 400 to 600 °C and 1 to 4 kbar in solutions of low total concentrations (0.001-0.005 molal). They did not account for the formation of the hydroxide species CaOH^+ and MgOH^+ in their data treatment, which introduced systematic errors in the association constants for the chloride ion pairs. While hydroxide species are rather insignificant in moderately to highly concentrated chloride solutions, they form in appreciable amounts in solutions with low electrolyte concentrations. Calculating the equilibrium speciation of a fluid with 0.001 CaCl_2 or MgCl_2 (using the Ca and Mg species properties from this study) at 400 to 600 °C and pressures of 1000 to 4000 bars demonstrates that the Ca and Mg hydroxide species are not negligible. CaOH^+ accounts for 3 to 8 % of the total dissolved calcium and MgOH^+ accounts for 5 to 16 % of the total dissolved magnesium.

4.5.2.1. CaCl^+ and CaCl_2^0 association constants

The stability of the CaCl^+ complex was studied at subcritical conditions by various experimental techniques. This included potentiometric measurements from 15 to 85 °C (Majer and Štulík 1982), flow calorimetric measurements from 250 to 325 °C and SWVP (Gillespie et al. 1992), enthalpy of dilution measurements from 300 to 325 °C and SWVP (Oscarson et al. 2001), and by conductance measurements (Méndez De Leo and Wood 2005). The association constants

from Oscarson et al. (2001) are systematically lower than the ones reported by Gillespie et al. (1992) at the same conditions (Fig. 4.9A). At supercritical conditions (Fig. 4.9B), the association constants of calcium chloride were derived from electrical conductance measurements from 400 to 600 °C and 1 to 4 kbar by Frantz and Marshall (1982). Williams-Jones and Seward (1989) extracted the values for the first (at 150 °C only) and second association constant from solubility measurements of AgCl in HCl-CaCl₂ solutions from 0.3 to 3 molal, for temperatures of 100 to 360 °C at SWVP. Their association constants depend highly on the values used for the properties of silver chloride complexes, the solubility product of AgCl(s) and the properties of the HCl⁰ ion. Their result may also be affected by the activity model used (Helgeson et al., 1981) to calculate the mean activity for mixed HCl-CaCl₂ solutions.

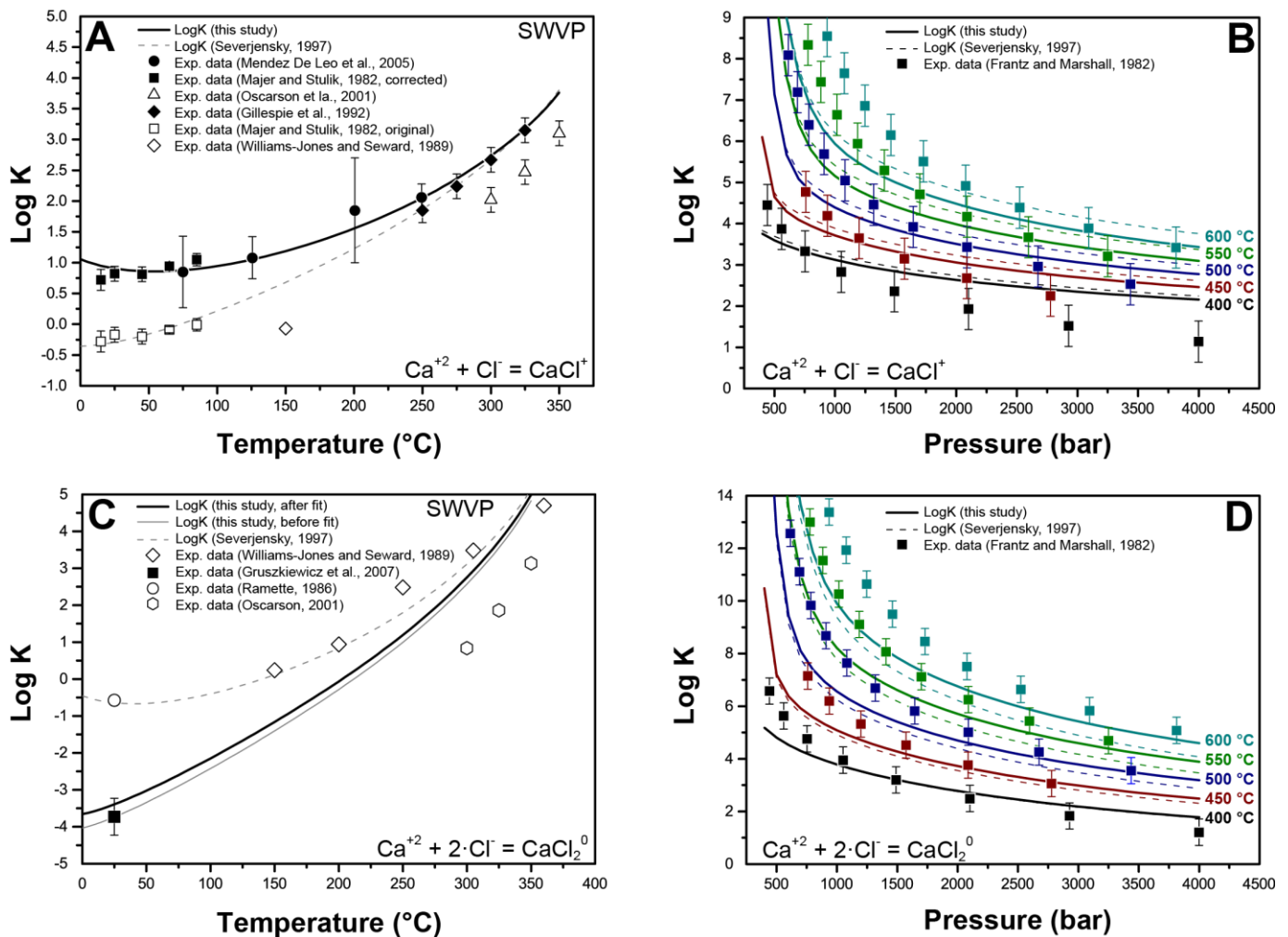


Figure 4.9. Comparison between calculated and experimentally determined first and second association constants of calcium chloride complexes. (A) CaCl⁺ and (C) CaCl₂⁰ at SWVP; (B) CaCl⁺ and (D) CaCl₂⁰ at different temperatures with increasing pressure, compared with the logKs derived from conductance measurements.

When regressing the experimental data above 150 °C, Williams-Jones and Seward (1989) assumed that CaCl^+ was present in insignificant amounts and that CaCl_2^0 was the only species that need to be considered. Reflecting the large discrepancies between different dataset for the relative stability of both CaCl^+ and CaCl_2^0 , this assumption is valid for one particular set of thermodynamic properties of the Ca chloride only. This is straightforwardly demonstrated by comparing the species distribution in a 1 molal chloride solution obtained from their thermodynamic data and the one obtained from the data of Sverjensky et al. (1997) at 150 °C and SWVP (Fig. 4.10).

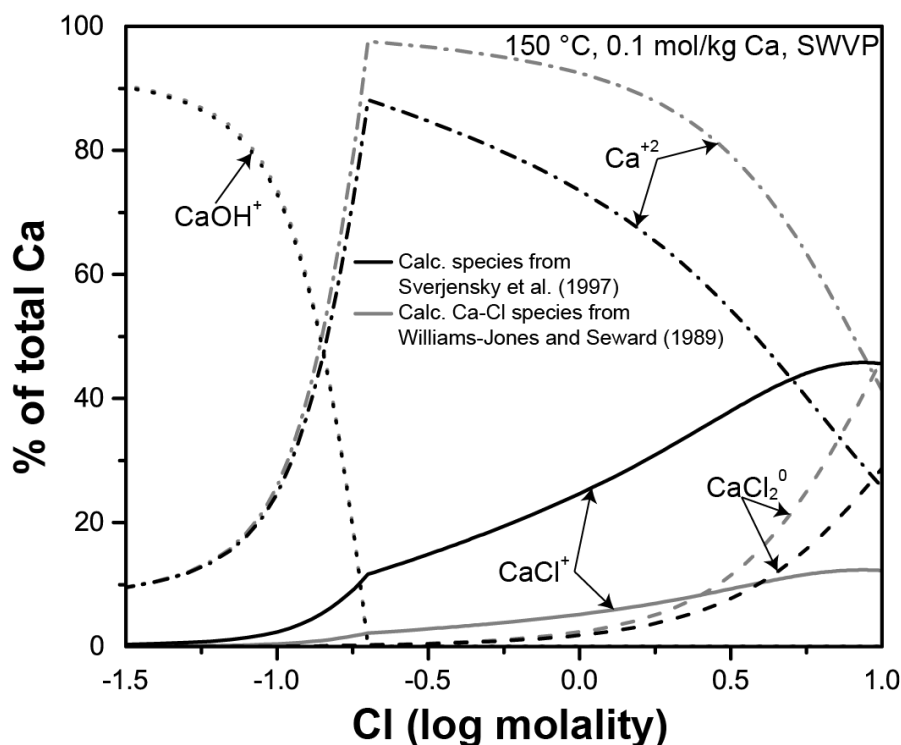


Figure 4.10. Calculated percentage from total calcium of different calcium species present in a 1 molal Ca solution with increasing chlorinity.

The association constants of CaCl_2^0 were also determined by Popp and Frantz (1979) from solubility experiments of quartz+wollastonite in $\text{CaCl}_2\text{-HCl}$ solutions at supercritical conditions (425 to 600 °C, 1 to 2 kbar) using the Ag-AgCl buffer technique. Their results strongly depend on the properties used for the HCl^0 species and the calibration of the Ag-AgCl buffer. They also calculated the difference between the standard state Gibbs free energies of CaCl_2^0 and HCl^0 , which is as such independent of the absolute properties used. However, they only considered CaCl_2^0 as the major Ca species and ignored the presence of CaCl^+ at the conditions of their experiments.

To overcome the large inconsistencies between different datasets for the Ca chloride species, we have re-fitted the standard state Gibbs energy, entropy, and HKF parameters of CaCl^+ using carefully evaluated experimental data. These include the data of Majer and Štulík (1982) corrected to infinite dilution, the data from the high-precision conductance experiments of Méndez De Leo and Wood (2005), and the data from the calorimetric measurements of Gillespie et al. (1992). The $Cp_{298,1}^0$ and $V_{298,1}^0$ values were adopted from Sverjensky et al. (1997). Reflecting the fact that only few data are available for CaCl_2^0 , we accepted the Gibbs energy and entropy of this complex from

the recent study of Gruszkiewicz et al. (2007). They used isopiestic measurements of concentrated CaCl_2 and mixed electrolyte solutions and extracted the thermodynamic properties using a well-calibrated Pitzer activity coefficient model. The association constants of CaCl_2^0 calculated with the data from this study result in a considerable disagreement with the data of Frantz and Marshall (1982) at supercritical conditions (Fig. 4.9D). Similar discrepancies have been observed when comparing the association constants of HCl_0 from the critical review of Tagirov et al. (1997) with the data reported by Frantz and Marshall (1984). However, as will be shown below, the new association constant data for CaCl^+ and CaCl_2^0 , in conjunction with the association constant data for CaOH^+ that are based on robust experiments, are able to simultaneously represent all experimental calcite and Ca-silicate solubility data.

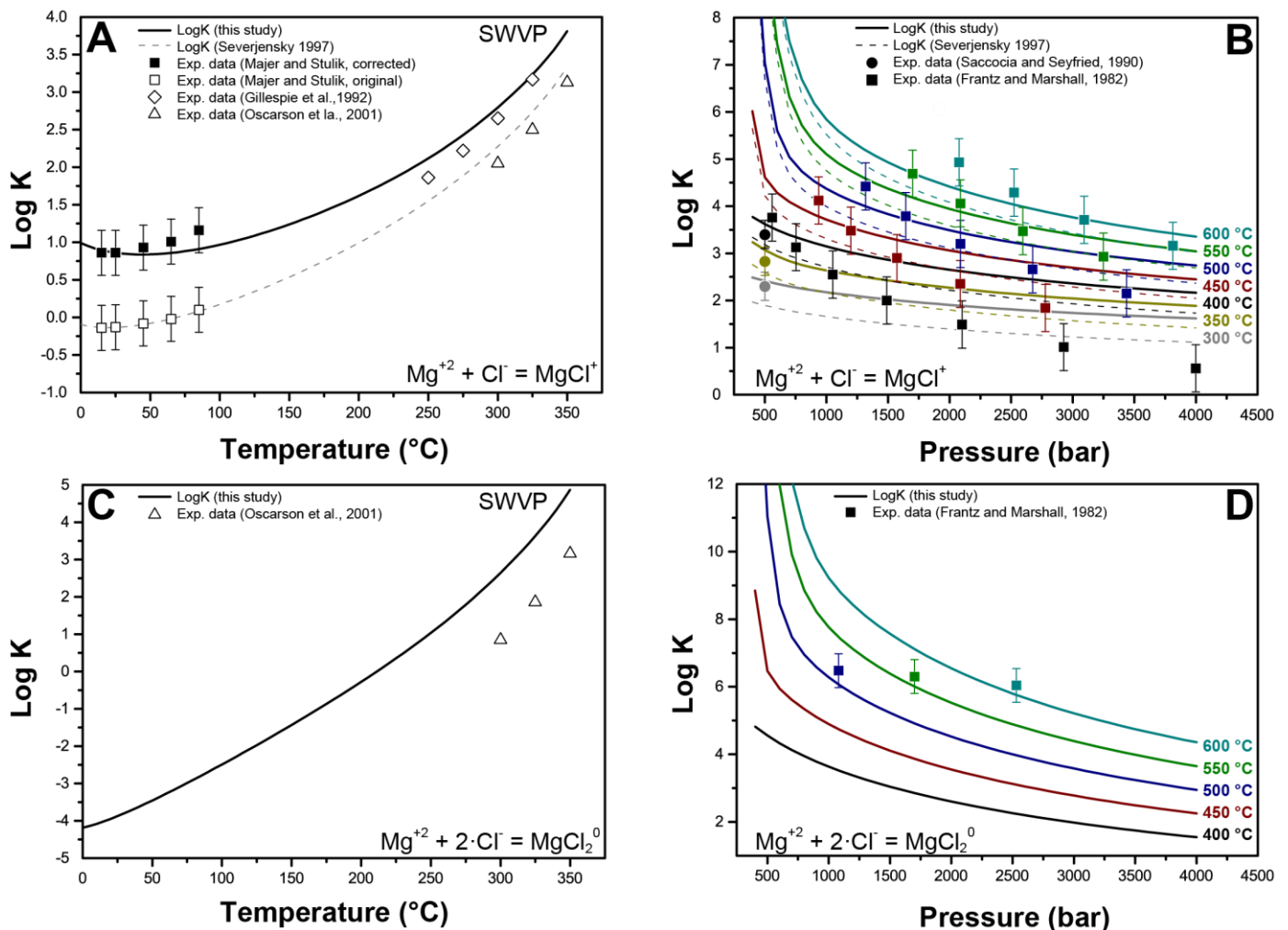


Figure 4.11. Comparison between calculated and experimentally determined first and second association constants of magnesium chloride complexes. (A) MgCl^+ and (C) MgCl_2^0 at SWVP; (B) MgCl^+ and (D) MgCl_2^0 at different temperatures with increasing pressure, compared with the logKs derived from conductance measurements.

4.5.2.2. MgCl^+ and MgCl_2^0 association constants

The association constant of the MgCl^+ complex was studied using a potentiometric method by Majer and Štulík (1982) from 15 to 85 °C (Fig. 4.11A). They did not correct their results to infinite dilution. We have approximated the logK values at infinite dilution by applying a correction of

similar magnitude that was used by Méndez De Leo and Wood (2005) to correct the CaCl⁺ data to infinite dilution. This approach is justified because the same background electrolyte and ionic strengths were used by Majer and Štulík (1982) in the experiments in Mg and Ca chloride solutions. At supercritical conditions, the association constants of Mg chloride species were derived from electrical conductance measurements from 400 to 600 °C and 1 to 4 kbar by Frantz and Marshall (1982) (Figs. 4.11B and 4.11D). Saccocia and Seyfried (1990) extracted the stability constants of MgCl⁺ from solubility measurements of talc and quartz in NaCl-MgCl₂ solutions (300-400 °C, 500 bar). They assumed that MgCl₂⁰ is insignificant at their experimental conditions, and they used the properties for HCl⁰ from Frantz and Marshall (1984). The association constants of MgCl₂⁰ were extracted by Frantz and Popp (1979) from quartz+talc solubility experiments in MgCl₂-HCl solutions (400 to 650 °C, 1 to 2 kbar) using the Ag-AgCl buffer technique. Their results depend strongly on the calibration of the Ag-AgCl buffer used. They assumed that MgCl₂⁰ was the only chloride species present, which was subsequently demonstrated to be incorrect (Frantz and Popp, 1981). They also calculated the difference between the standard state Gibbs free energy of MgCl₂⁰ and HCl⁰, which is independent of the absolute properties of both species.

In this study, we derived a new $\Delta_f G_{298,1}^0$ for MgCl⁺ to bring it into agreement with the corrected logK value at 25 °C and 1 bar from Majer and Štulík (1982). The $Cp_{298,1}^0$ and $V_{298,1}^0$ were accepted from Sverjensky et al. (1997) and the $S_{298,1}^0$ is essentially identical to the one derived by Sverjensky et al. (1997), because the temperature dependence at 15-85 °C of the logK values corrected to infinite dilution is approximately the same as that of the uncorrected data. When comparing the association constants of MgCl⁺ and CaCl⁺ calculated with the properties from this study, they agree within 0.1 log units and show identical temperature and pressure trends. This led to the conclusion that there should be a similar agreement between the temperature and pressure trends of the association constants for MgCl₂⁰ and CaCl₂⁰. We have therefore re-fitted the standard state properties and the HKF parameters of MgCl₂⁰ based on this assumption. The results of Frantz and Marshall (1982) in the MgCl₂ system suffer from the same issues as in the CaCl₂ system (see above and discussion below).

4.6. Ca and Mg silicate species

The speciation model in this study considers the silicate complexes of Ca and Mg. The association reactions are:



The standard state properties and HKF parameters for the calcium and magnesium hydrosilicate species are reported by Sverjensky et al. (1997). They adopted the $\Delta_f G_{298,1}^0$ of CaHSiO_3^+ and MgHSiO_3^+ from the compilation of Turner et al. (1981), which are in very good agreement with those reported in the recent critical evaluation of Thoenen et al. (2014). Sverjensky et al. (1997) estimated the $S_{298,1}^0$, $Cp_{298,1}^0$ and $V_{298,1}^0$ from correlations that involve metal ions and complexes with chemically similar ligands. Because there are no new experimental data that would constrain the stability of Ca and Mg silicate complexes, we accepted the data from Sverjensky et al. (1997). There are no experimentally based standard state properties and HKF parameters for CaSiO_3^0 and MgSiO_3^0 available. The available information about the stability of these species at ambient conditions and elevated temperature and pressure is scarce (Walker et al., 2016). These species can become important at ambient conditions and elevated pH (Walker et al., 2016) but can also play a role in systems at high temperature buffered by calcium and magnesium silicates. Due to the relevance of these species in these systems we have made rough estimates on their thermodynamic properties and HKF parameters (Table 4.1). The Gibbs energy of formation and standard state entropy of CaSiO_3^0 was taken from the study of Walker et al. (2016). The authors used the solubility calcium-silicate-hydrate to constrain the species at ambient conditions. The $Cp_{298,1}^0$ was subsequently adjusted to reproduce the increase in wollastonite+quartz solubility above 500 °C from the experiments of Xie and Walther (1993b). The HKF parameters were estimated from correlations (Sverjensky et al., 1997). Because there is no data available for the stability of MgSiO_3^0 , it was assumed that its stability constant is the same as for CaSiO_3^0 which were subsequently used to regress values for its thermodynamic standard state properties and HKF parameters. These species were not considered in the global optimization until more constraints on their stability at different conditions become available.

4.7. Selection of experimental solubility data

The available experimental solubility datasets that would constrain the stability of Ca and Mg aqueous species are much smaller in number than for the previously evaluated system Na-K-Al-Si-Cl-O-H (Miron et al., 2016). Priority was given to the experiments that demonstrated the attainment of equilibrium, used experimental techniques that were not affected by quenching problems, and sampled the aqueous solutions at the equilibrium conditions.

4.7.1. System Ca-Mg-Al-Si-O-H

Fluid-mineral equilibria in the system Mg-Si-O-H in a wide range of temperatures and pressures of 1 and 2 kbar were studied by Hemley et al. (1977a) and Hemley et al. (1977b). They used cold-seal pressure vessels with a rapid quench method for their experiments. The equilibrium was established by approaching it from different initial silica concentrations; they used both synthetic and natural minerals. For the same experimental temperature-pressure conditions, the results using synthetic and natural mineral samples agree within their experimental uncertainty.

They also investigated the possible loss of dissolved silica by precipitation during quench, but concluded that it did not occur.

Walther (1986) determined the solubility of brucite in water between 300 and 600 °C and at pressures of 1 to 3 kbar. The experiments were performed using an extraction quench hydrothermal apparatus. The aqueous phase was equilibrated with synthetic brucite, and the final material was analyzed optically and by X-ray diffraction to confirm that brucite was the only mineral phase present in the run products. Equilibrium was considered to be approached from supersaturation if the Mg concentration decreased by more than 10% from the previous step, and from undersaturation, if the concentration of Mg increased by more than 10%. The solubility of brucite at low temperatures in different electrolyte solutions has been extensively reviewed by Lambert and Clever (1992a). The solubility product of brucite is rather small and thus difficult to measure with sufficiently good precision (Lambert and Clever, 1992a).

Xie and Walther (1993b) studied the solubility of the assemblage wollastonite+quartz in water and NaCl solutions. The experiments in pure H₂O were performed at temperatures of 250 to 600 °C and pressures of 1 to 2 kbar. They used an extraction quench hydrothermal apparatus similar to what was used by Walther (1986) for brucite solubility experiments. The authors used natural wollastonite samples, and they did not report the chemical composition of the mineral. They approached equilibrium from both undersaturated and supersaturated conditions by increasing or decreasing the concentration of Ca between different experiments. Wollastonite solubility experiments at very high pressures were done by Fockenberg et al. (2006), but the experimental conditions are outside the permissible range of the HKF model for aqueous species used in this study.

Portlandite solubility experiments at hydrothermal conditions were performed by Seewald and Seyfried (1991) and Walther (1986). Seewald and Seyfried (1991) measured portlandite solubility in water and acetate solutions from 100 to 350 °C at 500 bars. Walther (1986) conducted solubility experiments between 300 and 600 °C and pressures of 1 to 3 kbar. They report results that approached equilibrium from both undersaturated and supersaturated conditions based on the change in concentration of the sampled solution in one set of experiments (increase or decrease by 10%). The experimental technique in both studies employed sample extraction at run conditions, thus avoiding possible errors related to quenching. The solubility of portlandite at low temperatures and in different electrolyte solutions has been reviewed by Lambert and Clever (1992b).

4.7.2. System Ca-Mg-Al-Si-Cl-O-H

The most comprehensive study in the Ca-Mg-Si-Cl-O-H system has been conducted by Luce et al. (1985). The studied fluid-mineral equilibria comprise the mineral assemblages talc+quartz, tremolite+talc+quartz, diopside+tremolite+quartz, wollastonite+diopside+quartz and wollastonite+quartz. The experiments were done between 500 and 700°C, at a pressure of 2 kbar and chloride concentrations from 0.03 to 6.0 molal. The solubility data of this study are important for constraining the stability of calc-silicates in the framework of metasomatic skarn reactions. The experiments were done in cold-seal pressure vessels and the solutions were analyzed after fast

quench. They used both natural and synthetic minerals as starting materials. They derived the concentration of HCl in their experiments using pH calibration curves, which were determined from known HCl concentrations in solutions with variable CaCl₂ and MgCl₂ concentrations. The experimental dataset of Luce et al. (1985) was used as a reference dataset in this study, because it provides a great number of constraints on the stability of the key aqueous species.

Roselle and Baumgartner (1995) studied the solubility of the assemblage anorthite+andalusite+quartz in supercritical chloride solutions. They used the experimental results to derive the anorthite-andalusite phase equilibrium, evaluate the stability of higher order calcium chloride species CaCl₃⁻ and CaCl₄²⁻ and determine the stability constant of Ca(OH)⁺. They used a cold-seal pressure vessel method that is comparable to the one used by Hemley (1959). The actual H⁺ concentration was derived using a calibration method of the pH electrode that accounts for salt and electrode specific effects. Synthetic anorthite and natural andalusite and quartz were used as starting materials. The equilibrium constants derived from their experiments depend strongly on the values they used for the association constants of H₂O, HCl⁰, CaCl⁺, and CaCl₂⁰. They used a different set of association constants than was used in this study.

Xie and Walther (1993a) studied the solubility of quartz+wollastonite in pure water and in NaCl solutions using an extraction quench method. They extracted association constants for CaCl⁺, and CaCl₂⁰ from their experiments in NaCl solutions, using the properties of HCl⁰ from Frantz and Marshall (1984). The resulting association constants for CaCl₂⁰ are around 2 log units lower than the ones from Frantz and Marshall (1982) at similar conditions.

Saccocia and Seyfried (1990) studied the solubility of the assemblage talc+quartz between 300 and 400 °C and at 500 bars in NaCl-MgCl₂ solutions. They employed a hydrothermal apparatus and extracted the solutions at run conditions. They performed experiments from both undersaturated and supersaturated conditions by changing the concentration of MgCl₂. They measured the pH of the extracted solutions at 25 °C. They derived the association constant for MgCl⁺ while using the properties of HCl⁰ from Frantz and Marshall (1984) and not considering the formation of MgCl₂⁰. Their results are in disagreement with extrapolated data from Frantz and Marshall (1982), but in reasonable agreement with the results of Luce et al. (1985).

Several studies of the solubility of calcium and magnesium silicates have been performed using the Ag(s)-AgCl(s) acid buffer technique. This method allows to control the activity of HCl at the experimental conditions, but it is highly dependent on the calibration of the method and on the thermodynamic properties of Ag(s), AgCl(s), the aqueous species and oxygen fugacity buffers. The Ag(s)-AgCl(s) buffer method was re-calibrated in several studies (Frantz and Popp, 1979; Luce et al., 1985). The method has been employed in a number of studies, including the solubility of wollastonite+quartz in supercritical chloride solutions by Gunter and Eugster (1978) and Popp and Frantz (1979) and the solubility of talc+quartz in supercritical chloride solutions by Frantz and Popp (1979) and Grabman and Popp (1991). Grabman and Popp (1991) used NaCl-MgCl₂ solutions in their experiments and suggest that higher order Mg chloride and mixed Na-Mg chloride species may form at temperatures above 500 °C. They concluded that at temperatures above 500 °C, higher-order chloride species are needed to explain their data.

4.7.3. System Ca-Mg-Cl-O-H-C

The most extensive reviews of the solubility of alkaline-earth metal carbonates in water and electrolyte solutions was presented by Duan and Li (2008), De Visscher et al. (2012), and De Visscher and Vanderdeelen (2012). The majority of carbonate solubility data was done at temperatures up to 100 °C and in the three-phase system (solid carbonate, aqueous solution and CO₂-rich gas-phase). A large number of calcite and aragonite solubility measurements below 100 °C over a range in CO₂ partial pressure were performed by Plummer and Busenberg (1982). Segnit et al. (1962) measured the solubility of calcite from 75 to 200 °C and at CO₂ partial pressures of 6 to 63 bars. Ellis (1959b) measured the solubility of calcite from 100 to 302 °C and at CO₂ partial pressures of 1 to 63 bars. The solubility of calcite at temperatures above 100 °C in dilute NaCl solutions was measured by Ellis (1963) at CO₂ partial pressure of 12.16 bar. Bychkov et al. (2007) evaluated the solubility of calcite from pH measurements in NaCl solutions from 120 to 160 °C with varying CO₂ partial pressure (2-50 bar). Their values are in good agreements with SUPCRT92 calculated solubility and the authors concluded that the calcium carbonate species play no role in the calcite solubility at these conditions. Calcite solubility in brines at different CO₂ concentration was also measured by Malinin and Kanukov (1971) between 200 and 600 °C. Their measurements were done mostly at high CO₂ concentrations where the assumption of the activity coefficient of CO₂(aq) being equal to 1 is not valid. Experiments with only aqueous solution and a carbonate mineral are very challenging, because even a small external contamination with CO₂ can have a large impact on the measured solubility. This explains why the experimentally determined calcite solubility data below 100 °C show a large scatter (Fig. 4.12). These data were not included into the final experimental database that was used for global regression of aqueous species thermodynamic data.

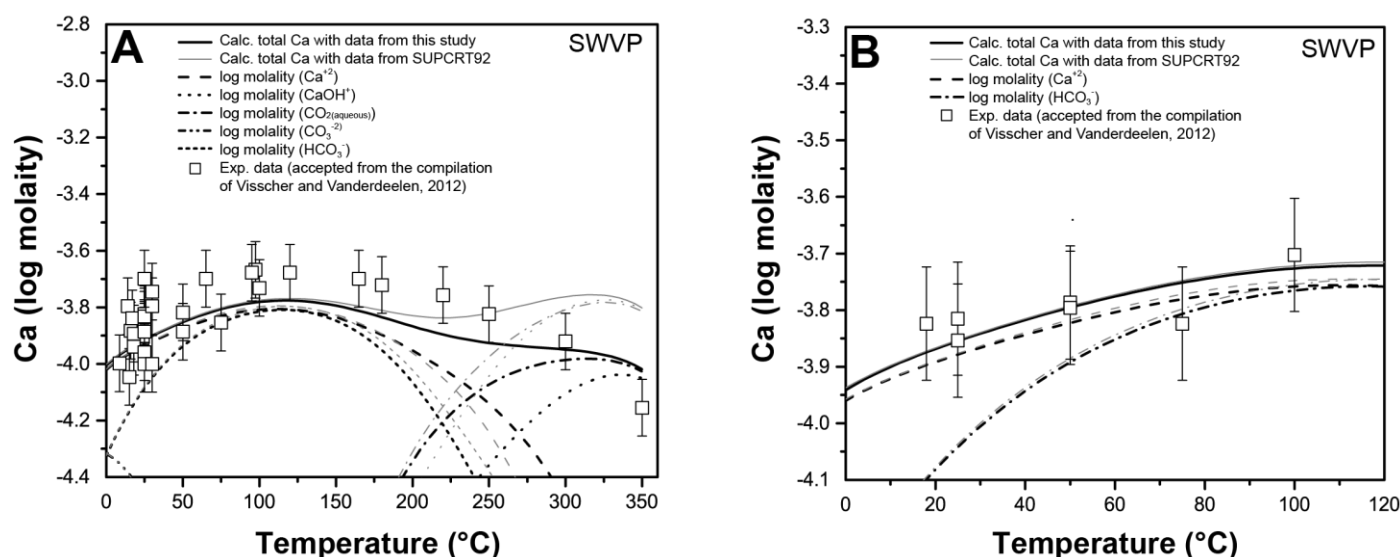


Figure 4.12. Comparison between calculated and experimentally determined calcite (A) and aragonite (B) solubility in CaCO₃-H₂O system, at different temperatures, SWVP.

At supercritical conditions, there are only three studies that determined the solubility of calcite in water and aqueous electrolyte solutions. The solubility experiments of Walther and Long (1986)

were done at 300 to 600 °C and 1000 to 3000 bars. Fein and Walther (1989) measured the solubility of calcite in water and in HCl-NaCl solutions at 2000 bars and temperatures up to 600 °C. Their calcite solubility data in water are systematically higher than the ones reported by Walther and Long (1986). Fein and Walther (1987) measured the calcite solubility in H₂O-CO₂ fluids at conditions above 2 mol% CO₂ dissolved in the aqueous phase where the assumption that the activity coefficient of CO₂ aqueous species is close to one is not valid anymore. Datasets of experiments performed at more than 2 mol% CO₂ were not considered in our evaluation. Caciagli and Manning (2003) and Newton and Manning (2002) studied the calcite solubility in H₂O and NaCl solutions at deep crust and mantle pressures which exceed the applicability of the HKF equation of state that was used in this study.

A review on magnesite solubility under subcritical conditions was done by De Visscher et al. (2012). Their review shows that the data in the system open to CO₂, pure water, in electrolyte solutions, is scarce and inconsistent, mostly given as approximate. Bénézeth et al. (2011) measured the solubility of magnesite from 50 to 200 °C in 0.1 mol/kg NaCl solutions under different CO₂ partial pressures using the hydrogen electrode concentration cell and a batch Ti-reactor. Based on carbon and magnesium species properties from the literature and their measured data, they generated the solubility products of magnesite and the standard state properties of magnesite at 25 °C, 1 bar.

4.8. Parameter optimization methods

We used the same global optimization method and settings that were applied in the previous study addressing the thermodynamic data in the Na-K-Al-Si-O-H-Cl system (Miron et al. 2016). The standard state Gibbs energies of aqueous species were regressed with the GEMSFITS code (Miron et al., 2015), which uses the GEMS3K Gibbs energy minimization code (Kulik et al., 2013) and the TsolMod library of activity and equation of state models (Wagner et al., 2012). The chemical system definitions (lists of phases and species, initial thermodynamic properties of each species, bulk composition, pressure and temperature for each experimental data point) were prepared using the GEM-Selektor v.3 code package (<http://gems.web.psi.ch/GEMS3>) and then exported into text files that can be read by GEMS3K and GEMSFITS codes (Miron et al., 2015). The final parameter values for the aqueous species in the system Na-K-Al-Si-O-H-Cl from the previous study (Miron et al., 2016) were used as starting values for the new global optimization. The starting values for the aqueous species related to calcium, magnesium and carbon were taken from Shock and Helgeson (1988), Shock et al. (1989), Sverjensky et al. (1997), Shock et al. (1997), and Stefánsson et al. (2014).

The standard state properties and the HKF parameters (other than $\Delta_f G_{298,1}^0$) for the aqueous species were taken from several sources or were separately optimized in this study as shown in Tables 4.1 and 4.2 (details in section 4.4 and 4.5). These parameters were not refined during the global regression of mineral solubility data and only the values of the $\Delta_f G_{298,1}^0$ of the aqueous

species were optimized. The program OptimB (Shvarov, 2015) was used for optimizing the HKF parameters of several aqueous complexes based on the critically evaluated datasets of association constants discussed above.

The critically evaluated experimental dataset for the system Na-K-Al-Si-O-H-Cl (Miron et al., 2016) was accepted in this study and only the new experimental data for solubility of Ca-Mg silicate and carbonate assemblages were added. In addition to the freely optimized $\Delta_f G_{298,1}^0$ values (Na^+ , K^+ , SiO_2^0 , HSiO_3^- , Al_3^+ , $\text{Al}(\text{OH})_2^+$, $\text{Al}(\text{OH})_3^0$, $\text{Al}(\text{OH})_4^-$, $\text{NaAl}(\text{OH})_4^0$, KAlO_2^0) parameters that were considered when addressing the system Na-K-Al-Si-O-H-Cl (Miron et al., 2016), we added to the global optimization the $\Delta_f G_{298,1}^0$ values of Ca^{+2} , Mg^{+2} , CaCl_2^0 , and MgCl_2^0 . Other calcium, magnesium and carbonate species considered in the extended system Ca-Mg-Na-K-Al-Si-O-H-C-Cl were either adjusted through reaction constraints or accepted from carefully evaluated datasets. There are only very limited and partly contradicting data available that would constrain the stability and standard state thermodynamic properties of CaCl_2^0 , and MgCl_2^0 . As long as no new high-quality conductance experiments become available, the values of CaCl_2^0 , and MgCl_2^0 need to be included into the regression in order to achieve a sufficiently good representation of the experimental Ca and Mg silicate and carbonate solubility data.

The overall quality of the fit for each individual experimental dataset related to Ca-Mg silicate and carbonate solubility is reported in Table 4.3 and defined by the normalized-root-mean-square-error (NRMSE):

$$NRMSE = \sqrt{\frac{\sum_i^N [y(i) - f(i)]^2}{\sum_i^N y(i)^2}} \quad (4.22)$$

This evaluation of the quality of the fit by the NRMSE is done after the GEMSFITS optimization and is not equivalent to the objective function that is used by the optimization algorithm.

4.9. Results

The experimental solubility data are compared with their calculated counterparts in Figs. 4.13 through 23. In these figures, full symbols do always denote experimental data points used in the global optimization, while open symbols denote data points that were not used.

Final regressed $\Delta_f G_{298,1}^0$ values of the aqueous species obtained from the global optimization of all mineral solubility data, including refined data for the species included in the earlier study of the system Na-K-Al-Si-O-H-Cl (Miron et al., 2016), are summarized in Tables 4.4 and 4.5. These tables also list all thermodynamic properties of the species that were fixed during fitting, and those which were constrained using association reaction constants.

Table 4.1. Standard state properties (partial molal entropy, heat capacity and volume), HKF, and Akinfiev and Diamond (2003) model parameters of CO₂(aq) used in this study. These values were not adjusted but taken from their original references.

Species	$S_{298,1}^0$ (J/mol)	$Cp_{298,1}^0$ (J/mol)	$V_{298,1}^0$ (J/bar)	$a_1 \cdot 10$ (cal/mol/bar)	$a_2 \cdot 10^{-2}$ (cal/mol)	a_3 (cal·K/mol/bar)	$a_4 \cdot 10^{-4}$ (cal·K/mol)	c_1 (cal/mol/K)	$c_2 \cdot 10^{-4}$ (cal·K/mol)	$\omega_0 \cdot 10^{-5}$ (cal/mol)
⁽¹⁾ Ca ⁺²	-56.48	-30.92	-1.84	-0.1947	-7.2520	5.2966	-2.4792	9.00000	-2.5220	1.2366
⁽¹⁾ Mg ⁺²	-138.07	-21.662	-2.2	-0.8217	-8.5990	8.3900	-2.3900	20.8000	-5.8920	1.5372
⁽²⁾ CaHSiO ₃ ⁺	-8.33	137.8	-0.67	1.0647	-5.1787	7.7785	-2.5649	30.8048	3.6619	0.5831
⁽²⁾ MgHSiO ₃ ⁺	-99.5	158.65	-1.08	0.6289	-6.2428	8.1967	-2.5209	36.7882	4.6702	0.9177

	$Cp^0 = a_0 + a_1 \cdot T + a_2 \cdot T^{-2} + a_3 \cdot T^{-0.5} + a_4 \cdot T^2$					Empirical parameters					
	$a_0 \cdot 10^{-1}$	$a_1 \cdot 10^2$	$a_2 \cdot 10^{-5}$	$a_3 \cdot 10^{-2}$	$a_4 \cdot 10^6$	ξ	a (cm ³ /g)	b (cm ³ ·K ^{0.5} /g)			
⁽³⁾ CO ₂ (aq)	119.29	209.75	3.27	6.56823	1.11973	2.80403	-5.99129	-3.92	-0.085	-8.8321	11.2684

⁽¹⁾ Taken from Shock et al. (1997)

⁽²⁾ Taken from Sverjensky et al. (1997).

⁽³⁾ Taken from the model of Akinfiev and Diamond (2003). The molal thermodynamic properties of the species in the ideal gas state are calculated through standard heat capacity integration, and the hydration properties are then added as a pressure correction. The Gibbs energy of hydration is calculated using the Akinfiev and Diamond (2003) model.

Table 4.2. Standard state properties (partial molal entropy, heat capacity and volume) and HKF parameters of aqueous species derived in this study from conductance, literature logKs, and solubility (protlandite) data. For details on how the properties and parameters were generated see Section 4.4 and 4.5.

Species	$S_{298,1}^0$	$Cp_{298,1}^0$	$V_{298,1}^0$	$a_1 \cdot 10$	$a_2 \cdot 10^{-2}$	a_3	$a_4 \cdot 10^{-4}$	c_1	$c_2 \cdot 10^{-4}$	$\omega_0 \cdot 10^{-5}$
	(J/mol)	(J/mol)	(J/bar)	(cal/mol/bar)	(cal/mol)	(cal·K/mol/bar)	(cal·K/mol)	(cal/mol/K)	(cal·K/mol)	(cal/mol)
CaOH ⁺	36.47	-78.41	1.096	3.9385	-1.1019	6.1831	-2.7334	-9.5888	-2.6253	0.4190
CaCl ⁺	-2.97	73.33	0.556	2.7406	-1.0897	6.1783	-2.7340	21.5880	0.5240	0.5626
CaCl ₂ ⁰	67.73	129.52	3.265	6.2186	7.4024	2.8406	-3.0850	23.9609	3.2720	-0.0380
CaHCO ₃ ⁺	66.27	234.27	1.328	3.7000	1.2579	5.2520	-2.8310	43.1120	7.7228	0.3113
CaCO ₃ ⁰	20.11	-123.86	-1.565	-0.3907	-8.7325	9.1753	-2.4179	-11.5309	-9.0641	-0.0380
MgOH ⁺	-67.36	129.1	0.166	2.2937	-2.1809	6.6072	-2.6888	31.5415	3.2394	0.7950
MgCl ⁺	-79.5	104.96	0.125	2.2809	-2.3585	6.6770	-2.6815	28.5471	2.0579	0.8389
MgCl ₂ ⁰	-11.57	170.77	2.825	5.6165	5.9323	3.4184	-3.0242	29.7395	5.2804	-0.0380
MgHCO ₃ ⁺	-19.11	254.69	0.934	3.3000	0.1608	5.6868	-2.7875	47.5204	9.3524	0.6204
MgCO ₃ ⁰	-102.57	-114.64	-1.827	-0.7355	-9.5745	9.5062	-2.3831	-9.8914	-8.6160	0.0000
NaCO ₃ ⁻	56.09	-83.31	-0.152	2.0000	-2.3350	6.6714	-2.6825	7.7693	-7.1095	1.4265
NaHCO ₃ ⁰	158.66	201.84	3.182	6.1192	7.1597	2.9359	-3.0750	34.4381	6.7919	0.0000
KCO ₃ ⁻	76.32	-112.85	0.829	3.4128	0.5540	5.5266	-2.8018	2.7390	-8.5569	1.3525
KHCO ₃ ⁰	208.74	134.95	4.319	7.6623	10.9298	1.4497	-3.2307	24.7193	3.5355	-0.0380
CO ₃ ⁻²	-50	-322.65	-0.606	2.8524	-3.9844	6.4142	-2.6143	-7.9872	-18.8139	3.3914
HCO ₃ ⁻	96.62	-34.85	2.421	2.9936	4.9787	23.5905	-2.9848	12.994	-4.7579	1.2792
CaSiO ₃ ⁰	-20.54	-179	1.57	3.1272	-10.5859	42.3257	-2.3414	61.9110	-51.1046	0.0935
MgSiO ₃ ⁰	-102	-169.9	1.21	0.8426	-11.069	52.9604	-2.3216	68.7194	-53.9981	-0.0445

Table 4.3. Summary of solubility experimental datasets selected for the global optimization.

Reference	System	Number of data points used	⁽¹⁾ Direction of equilibrium	Temperature range (deg. C)	Pressure range (kbar) / Partial pressure gas (bar)	Dataset total error (Eq. 4.22)
Hemley et al. (1977a)	talc-chrysotile-forsterite-H ₂ O	38	U	90 – 600	1bar – 2.0	Si: 0.035
Hemley et al. (1977b)	talc-forsterite-antophyllite-enstatite-H ₂ O	55	U	300-720	1.0 – 2.0	Si: 0.064
Walther (1986)	brucite-H ₂ O	39	U-S?	350-630	1.0-2.9	Mg: 0.045
Luce et al (1985)	talc-wollastonite-diopside-tremolite-quartz-MgCl ₂ -CaCl ₂ -H ₂ O	68	U	500-700	2.0	Log(Ca/Mg): 0.086 Log(Ca/H ²): 0.032 Log(Mg/H ²): 0.125
Fein and Walther (1989)	calcite-H ₂ O-HCl-NaCl	65	U	400-600	2.0	Ca: 0.031
Plummer and Busenberg (1982)	calcite-H ₂ O-CO ₂	141	U	0-90	1 / ⁽²⁾ PCO ₂ 1 – <0.01	Ca: 0.019
Plummer and Busenberg (1982)	aragonite-H ₂ O-CO ₂	205	U	1-90	1 / PCO ₂ 1 – <0.01	Ca: 0.017
Ellis (1959b)	calcite-H ₂ O-CO ₂	59	U	98-302	⁽³⁾ SWVP / PCO ₂ 1 – 62	Ca: 0.021
Bénézech et al. (2011)	magnesite-H ₂ O-NaCl-CO ₂	34	U	50-202	SWVP / PCO ₂ 13 – 30	Mg: 0.078

⁽¹⁾ U: equilibrium approached from undersaturation; S?: was considered that the equilibrium was approached from supersaturation if the measured concentration decreased by 10% from previous measurements (in a continuous series of varying conditions).

⁽²⁾ PCO₂: partial pressure of carbon dioxide gas.

⁽³⁾ SWVP: Saturated water vapor pressure.

Table 4.4. Final values of the standard-state molal Gibbs energy for aqueous species related to calcium, magnesium, and carbon, which were optimized using the experimental datasets presented in this study (Table 4.3). Gibbs energy values need to be combined with standard state entropy, volume, heat capacity, and HKF parameters from Tables 4.1 and 4.2. The standard deviation of optimized parameters was calculated from 500 Monte Carlo simulation runs, and the 95% confidence interval - using the Student's t-distribution.

Species	$\Delta_f G_{298,1}^0$ (J/mol) this study	Standard deviation	95% confidence interval	Optimization mode
Ca ⁺²	-552821	50	100	Optimized
CaOH ⁺	-716750	-	-	⁽¹⁾ Constrained
CaCl ⁺	-689297	-	-	⁽¹⁾ Constrained
CaCl ₂ ⁰	-795990	985	1933	Optimized
CaHCO ₃ ⁺	-1145214	-	-	⁽¹⁾ Constrained
CaCO ₃ ⁰	-1099084	-	-	⁽¹⁾ Constrained
CaHSiO ₃ ⁺	-1575097	-	-	⁽²⁾ Constrained
CaSiO ₃ ⁰	-1515154	-	-	⁽¹⁾ Constrained
Mg ⁺²	-456005	519	1019	Optimized
MgOH ⁺	-626503	-	-	⁽¹⁾ Constrained
MgCl ⁺	-592204	-	-	⁽¹⁾ Constrained
MgCl ₂ ⁰	-696566	957	1879	Optimized
MgHCO ₃ ⁺	-1048857	-	-	⁽¹⁾ Constrained
MgCO ₃ ⁰	-1000992	-	-	⁽¹⁾ Constrained
MgHSiO ₃ ⁺	-1479708	-	-	⁽²⁾ Constrained
MgSiO ₃ ⁰	-1418335	-	-	⁽¹⁾ Constrained
NaCO ₃ ⁻	-789833	-	-	⁽¹⁾ Constrained
NaHCO ₃ ⁰	-842065	-	-	⁽¹⁾ Constrained
KCO ₃ ⁻	-810746	-	-	⁽¹⁾ Constrained
KHCO ₃ ⁰	-862284	-	-	⁽¹⁾ Constrained
CO ₃ ⁻²	-527983	-	-	⁽³⁾ Fixed
HCO ₃ ⁻	-586855	-	-	⁽⁴⁾ Fixed
CO _{2(aqueous)}	-386030	-	-	⁽⁵⁾ Fixed

⁽¹⁾ Constrained to properties of the respective ions by the reactions presented in Section 4 consistent with the standard state properties and HKF parameters from Tables 4.1 and 4.2.

⁽²⁾ Constrained to properties of Ca⁺², Mg⁺², and SiO₂⁰ by the reaction: Ca⁺² + H₂O + SiO₂⁰ = CaHSiO₃⁺ + H⁺, Mg⁺² + H₂O + SiO₂⁰ = MgHSiO₃⁺ + H⁺ and equilibrium constants consistent with the standard state properties and HKF parameters from Table 4.1 taken from Sverjensky et al. (1997).

⁽³⁾ Taken from Shock et al. (1997).

⁽⁴⁾ Refined in this study against literature logK values, -586940 reported by Shock et al. (1997).

⁽⁵⁾ Taken from model of Akinfiev and Diamond (2003).

Table 4.5. Final values of the standard-state molal Gibbs energy for aqueous species that were previously refined in Miron et al. (2016), and the new optimized values obtained using the experimental datasets from Miron et al. (2016) and from this study (Table 4.3). Gibbs energy values need to be combined with standard state entropy, volume, heat capacity and HKF parameters from Table 4.1 (ion pairs of main electrolytes) and Table 4.5 (other aqueous species) from Miron et al. (2016). The standard deviation of parameters was calculated from 500 Monte Carlo simulation runs, and the 95% confidence interval - using the Student's t-distribution.

Species	$\Delta_f G_{298,1}^0$ (J/mol) Miron et al. (2016)	$\Delta_f G_{298,1}^0$ (J/mol) this study	Δ 2016-this study	Standard deviation	95% confidence interval	Optimization mode
Al ³⁺	-486627	-486594	-33	258	507	Optimized
AlOH ²⁺	-695574	-695541	-33	543	1077	⁽¹⁾ Constrained
Al(OH) ₂ ⁺	-898295	-898292	-3	1339	2627	Optimized
Al(OH) ₃ ⁰	-1105801	-1105813	12	944	1852	Optimized
Al(OH) ₄ ⁻	-1305097	-1305097	0	229	450	Optimized
NaAl(OH) ₄ ⁰	-1562121	-1562083	-38	944	1853	Optimized
AlH ₃ SiO ₄ ²⁺	-1782516	-1782421	-95	828	1547	⁽²⁾ Constrained
KAlO ₂ ⁰	-1100293	-1100134	-159	2423	4751	Optimized
K ⁺	-276893	-276870	-23	643	1261	Optimized
KOH ⁰	-431656	-431633	-23	-	-	⁽³⁾ Constrained
KCl ⁰	-402544	-393521	-23	-	-	⁽³⁾ Constrained
Na ⁺	-256169	-256142	-27	644	1263	Optimized
NaOH ⁰	-411594	-411567	-27	-	-	⁽³⁾ Constrained
NaCl ⁰	-383091	-383064	-27	-	-	⁽³⁾ Constrained
NaHSiO ₃ ⁰	-1283076	-1282987	-89	1820	3614	⁽⁴⁾ Constrained
HSiO ₃ ⁻	-1015237	-1015175	-62	303	594	Optimized
SiO ₂ ⁰	-834103	-834041	-62	34	67	Optimized
Cl ⁻	-131290	-131290	0	-	-	⁽⁵⁾ Fixed
HCl ⁰	-127240	-127240	0	-	-	⁽⁶⁾ Fixed
OH ⁻	-157287	-157287	0	-	-	⁽⁵⁾ Fixed
H ⁺	0	0	0	-	-	⁽⁷⁾ Fixed
H ₂ O	-237183	-237183	0	-	-	⁽⁸⁾ Fixed

⁽¹⁾ Constrained to properties of Al³⁺ by the reaction: AlOH²⁺ + H⁺ = Al³⁺ + 2 H₂O, using equilibrium constant values from Palmer and Wesolowski (1993).

⁽²⁾ Constrained to properties of Al³⁺ and SiO₂⁰ by the reaction: Al³⁺ + 2 H₂O + SiO₂⁰ = AlH₃SiO₄²⁺ + H⁺, and equilibrium constants from Tagirov and Schott (2001), extracted from Pokrovskii et al. (1996) and Salvi et al. (1998).

⁽³⁾ Constrained to properties of Na⁺, K⁺, OH⁻, and Cl⁻ using the equilibrium constants determined from the new standard state properties of ion pairs extracted from the conductance data (Table 4.1).

⁽⁴⁾ Constrained to properties of Na⁺ and SiO₂⁰ by the reaction: Na⁺ + H₂O + SiO₂⁰ = NaHSiO₃⁰ + H⁺, using equilibrium constants from Sverjensky et al. (1997), extracted from Seward (1974).

⁽⁵⁾ Taken from Shock and Helgeson (1988).

⁽⁶⁾ Taken from Tagirov et al. (1997).

⁽⁷⁾ Conventional value.

⁽⁸⁾ Taken from Johnson et al. (1992).

4.9.1. System Ca-Mg-Al-Si-O-H

There is a fairly good agreement between the calculated and the measured silica concentration data for fluid-mineral equilibria experiments in the system Mg-Si-O-H (Fig. 4.13A). There are some small differences for experiments involving talc+antigorite (Fig. 4.13B), enstatite+forsterite and talc+anthophyllite assemblages. Considering the good agreement with all the other experimental data involving Ca and Mg silicates, these differences could be at least partly related to thermodynamic properties of minerals which were accepted from the Holland-Powell mineral dataset (Holland and Powell, 1998), or to some issues with the experiments.

Calculated Mg concentrations for brucite solubility equilibrium at different temperatures and pressures are in reasonably good agreement with the experimental data (Fig. 4.14) from Walther (1986). The agreement between calculated and measured data is better for the dataset from this study compared to calculations using the aqueous species from Shock et al. (1997).

The calculated wollastonite solubility using data from Shock et al. (1997) underestimates the experimentally measured solubility in pure water by around 0.3 log units. Calculating the wollastonite solubility with the data from this study results in underestimation of the experimental solubility as well (Fig. 4.15). The discrepancy between calculated and measured solubility increases with temperature.

The refined thermodynamic properties of CaOH^+ result in a good agreement between the calculated portlandite solubility and the experimental data from Walther (1986) and Seewald and Seyfried (1991) for temperatures between 100 and 500 °C and pressures of 0.5 and 1.0 kbar (Fig. 4.16). The agreement is much better than for calculations that use the CaOH^+ properties from Shock et al. (1997). There remains, however, a disagreement between calculated and experimentally measured portlandite solubility for 2.0 and 3.0 kbar. While the experimental results of Walther (1986) at these two pressures may not be necessarily incorrect, they are discrepant with their data at lower pressures and the results of the study of Seewald and Seyfried (1991). It is not possible to reconcile these discrepancies within the thermodynamic framework of this study.

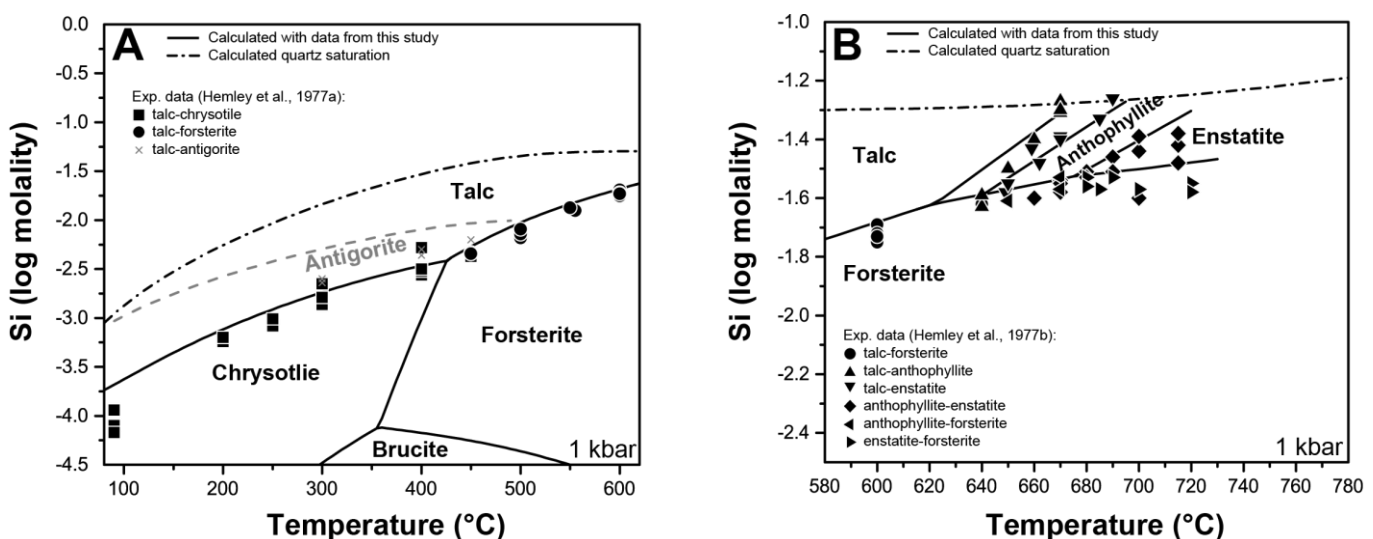


Figure 4.13. Comparison between calculated and experimentally determined phase equilibria and Si concentrations in the Si-Al-Mg-H-O system (Hemley et al., 1977a; Hemley et al., 1977b) as function of temperature at 1 kbar pressure.

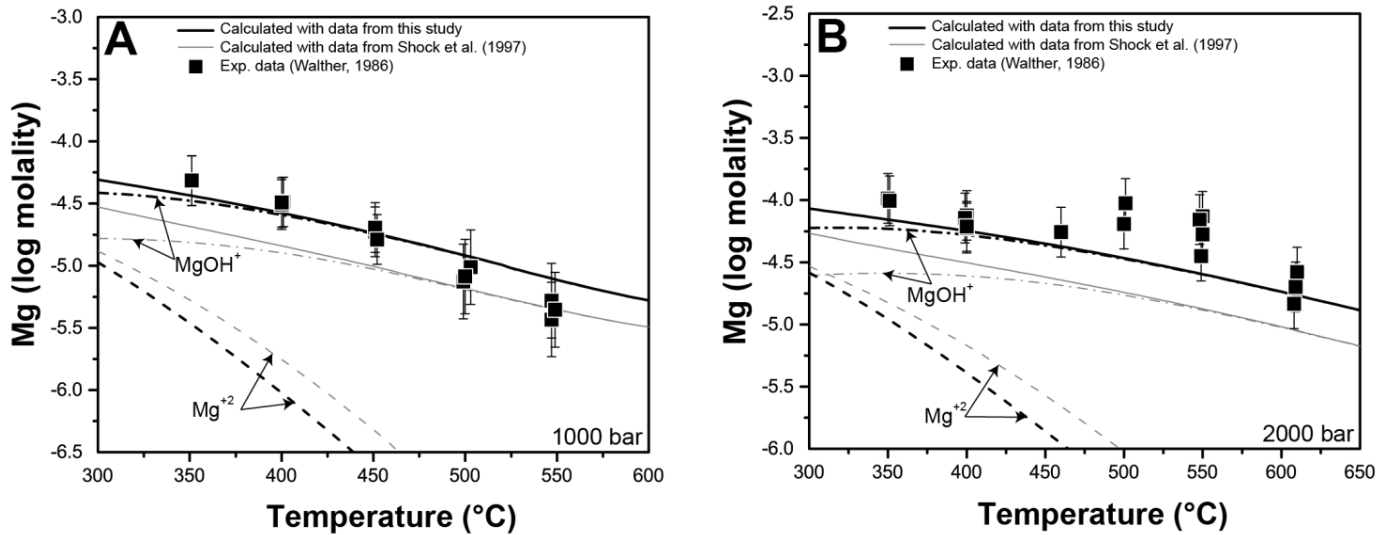


Figure 4.14. Comparison between calculated and experimentally determined brucite solubility in water (Walther, 1986), with increasing temperature: (A) at 1 kbar; (B) at 2 kbar.

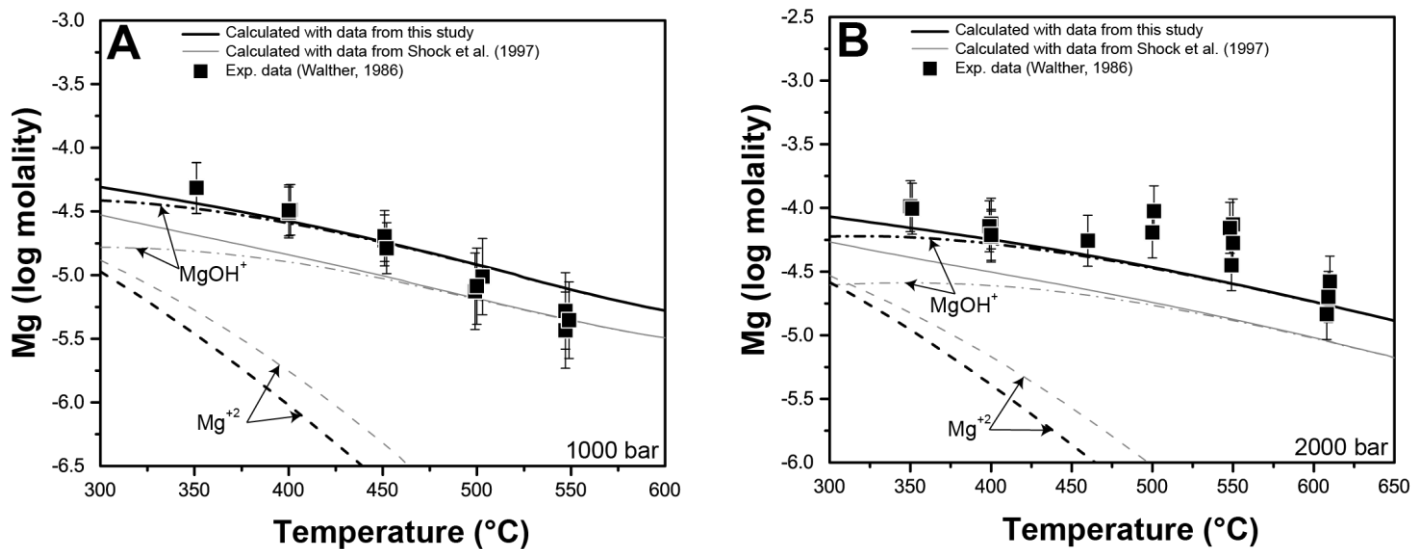


Figure 4.15. Comparison between calculated and experimentally determined wollastonite-quartz solubility in water (Xie and Walther, 1993b), with increasing temperature at 2 kbar. (A) Calculated with the species properties from this study and from SUPCRT92. (B) Calculated by assuming an increase in the stability of the CaHSiO_3^+ by 20 kJ/mol and the presence of CaSiO_3^0 with a $\log K (\text{Ca}^{+2} + \text{H}_2\text{O} + \text{SiO}_2 = \text{CaSiO}_3^0 + 2\text{H}^+)$ at 25 °C of -19.07, $\Delta_r S_{298,1}^0 = -109.27 \text{ J/K}\cdot\text{mol}$, and a refined $\Delta_r C_p_{298,1}^0 = 95 \text{ J/K}\cdot\text{mol}$, to agree with the experimental points.

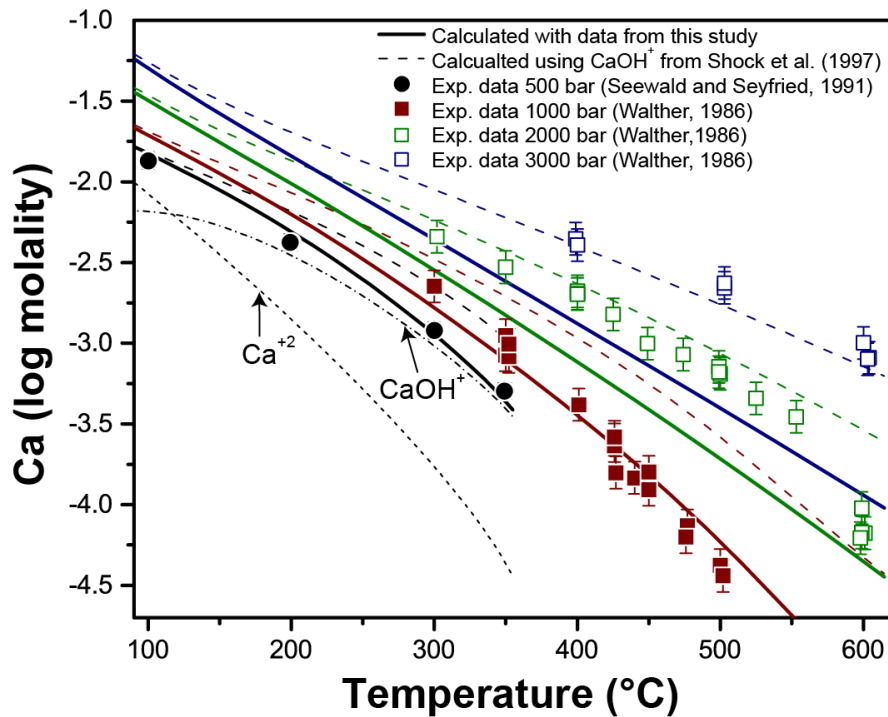


Figure 4.16. Comparison between calculated and experimentally determined portlandite solubility in water (Walther 1986; Seewald and Seyfried 1991), at different pressures with increasing temperature. Full symbols represent experimental datapoints which were used to constrain the properties of CaOH^+ species, while open symbols represent experimental datapoints which were not used.

4.9.2. System Ca-Mg-Al-Si-Cl-O-H

The calculated total calcium to hydrogen ratios, $\log(\text{Ca}^{2+}/(\text{H}^+)^2)$, for fluid-mineral equilibria involving different Ca and Mg silicate assemblages are in good agreement (Fig. 4.17) with the experimental data from Luce et al. (1985) at all temperatures. By contrast, calculations with the aqueous species data from SUPCRT92 show only good agreement with the experimental data from Luce et al. (1985) at 600 °C (Fig. 4.17). The agreement between the calculated total magnesium to hydrogen ratios, $\log(\text{Mg}^{2+}/(\text{H}^+)^2)$, and their experimental counterparts (Luce et al., 1985) is good for the data at 600 and 700 °C, but not as good for the data at 500 °C.

The wollastonite+quartz solubility experiments by Xie and Walther (1993b) in NaCl solutions are not well reproduced by calculations with the data from this study (Fig. 4.18). There is disagreement in terms of the absolute Ca concentration data, but also in terms of the temperature dependence at different NaCl concentrations. Interestingly, at 1.0 kbar pressure (and NaCl concentration of 0.83 molal), the measured Ca concentration is overestimated, while at 2.0 kbar total Ca is underestimated by the calculations. This would imply that the pressure dependence of the solubility is not well reproduced by the thermodynamic properties of the aqueous species. The calculated total calcium values in equilibrium with anorthite+andalusite+quartz, are in good agreement with their measured counterparts from the solubility experiments of Roselle and Baumgartner (1995).

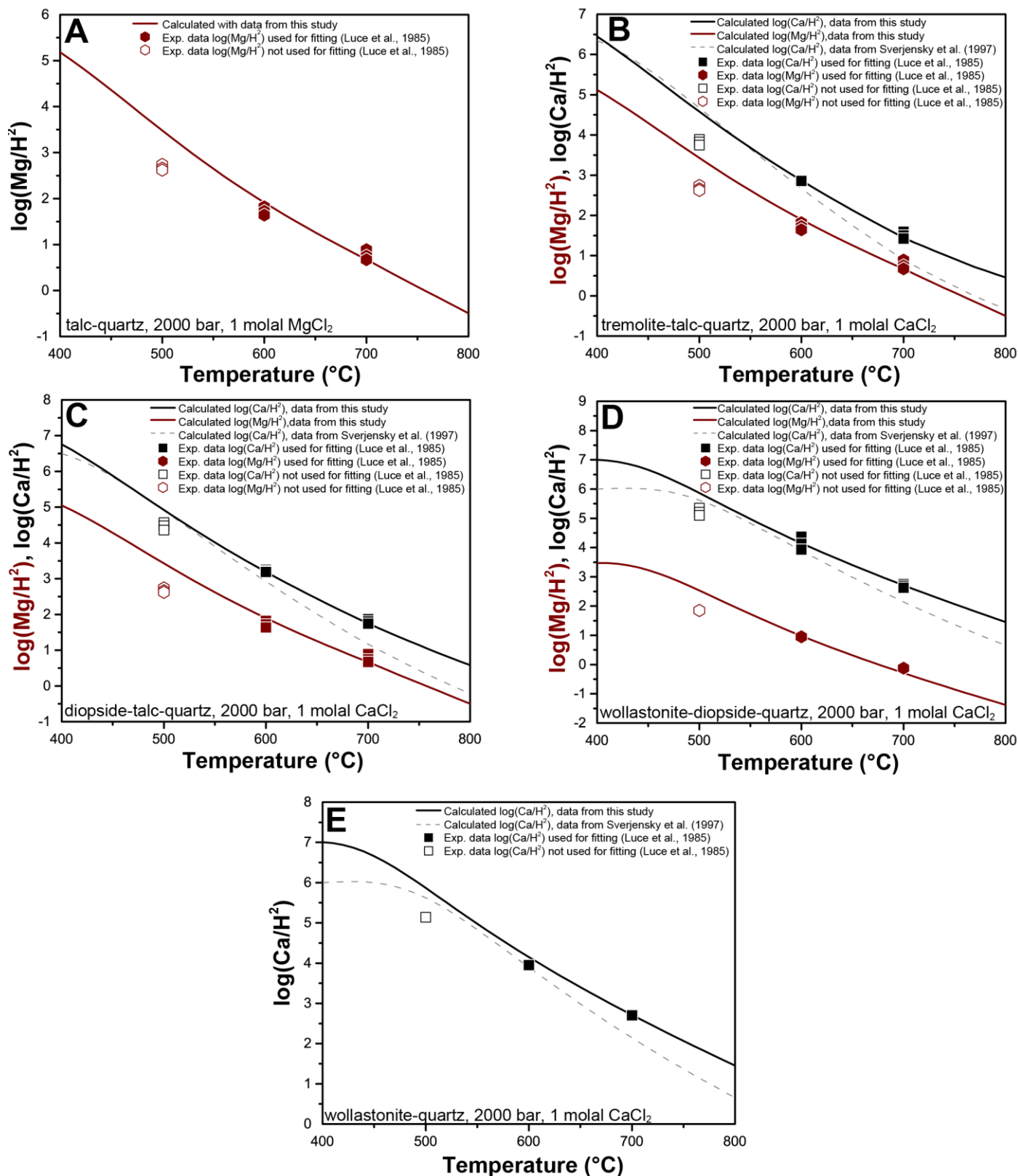


Figure 4.17. Comparison between calculated and experimentally determined $\log(Ca/H^2)$ and $\log(Mg/H^2)$ values in the system Ca-Mg-Si-Al-OH-Cl (in 1 molal $CaCl_2$ or $MgCl_2$ solutions) as function of temperature (and at a pressure of 1 kbar). (A) talc-quartz; (B) tremolite-talc-quartz; (C) diopside-talc-quartz; (D) wollastonite-diopside-quartz; (E) wollastonite-quartz. Full symbols represent experimental datapoints which were used in the global data regression, while open symbols represent experimental datapoints which were not used.

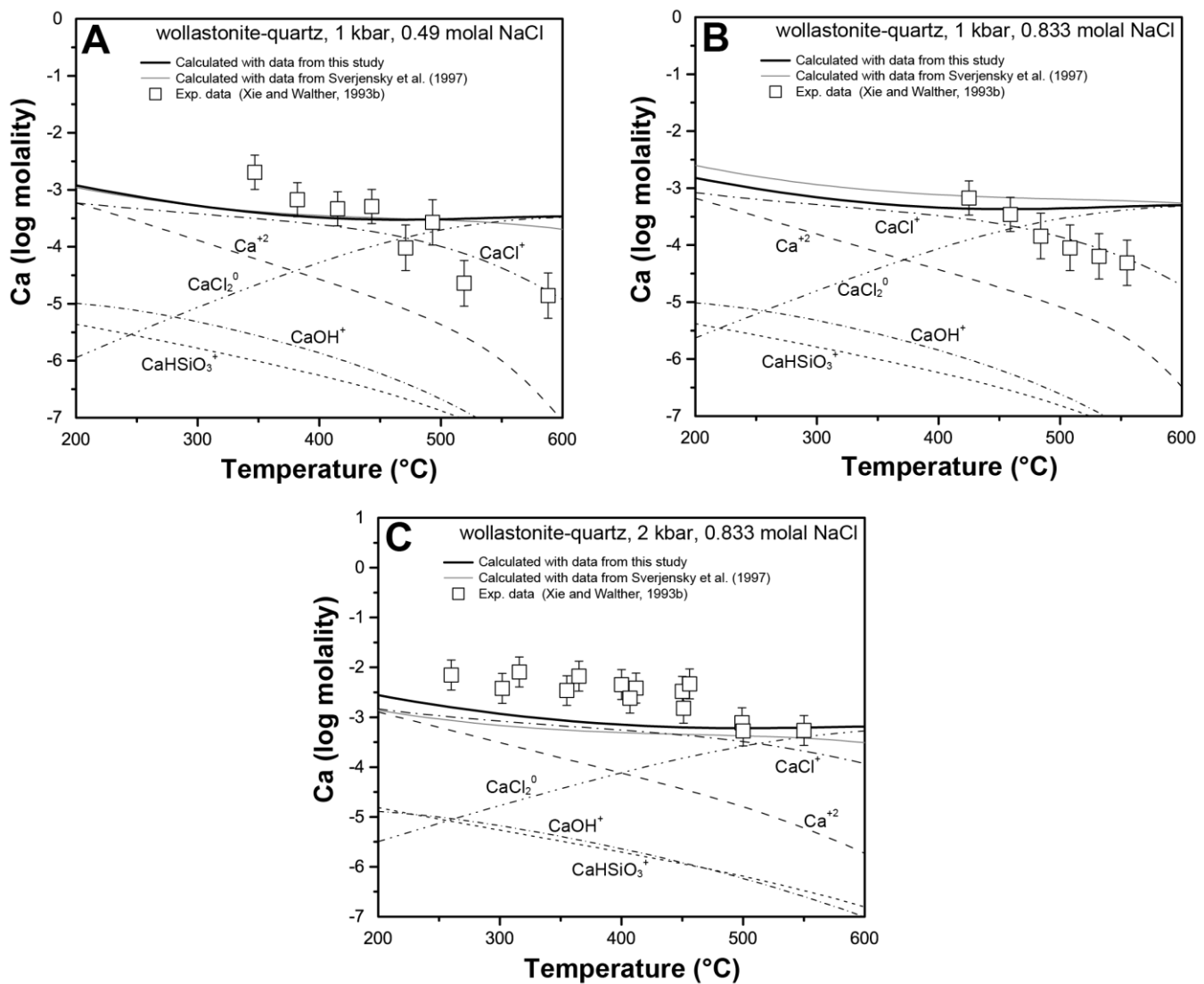


Figure 4.18. Comparison between calculated and experimentally determined wollastonite-quartz solubility in NaCl solutions of different concentrations (Xie and Walther 1993b): (A) 0.49 molal NaCl, (B) and (C) 0.833 molal NaCl, at 1 and 2 kbar with increasing temperature.

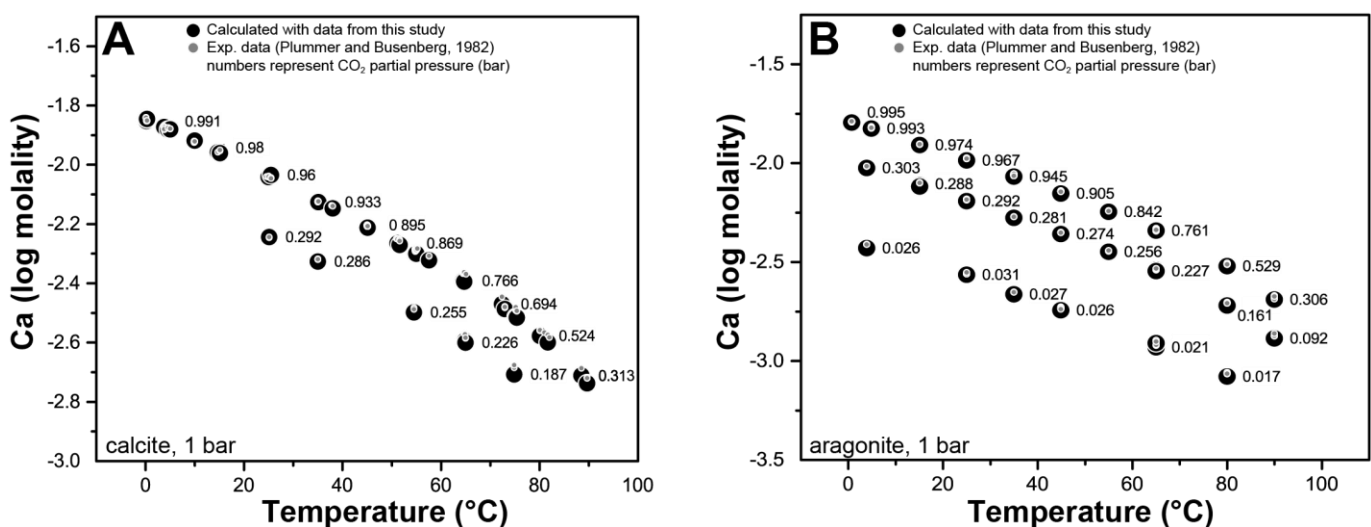


Figure 4.19. Comparison between calculated and experimentally determined calcite (A) and aragonite (B) solubility in $\text{CaCO}_3\text{-H}_2\text{O-CO}_2$ system, at temperatures $<100^\circ\text{C}$, 1 bar total pressure and different CO_2 partial pressures (Plummer and Busenberg, 1982).

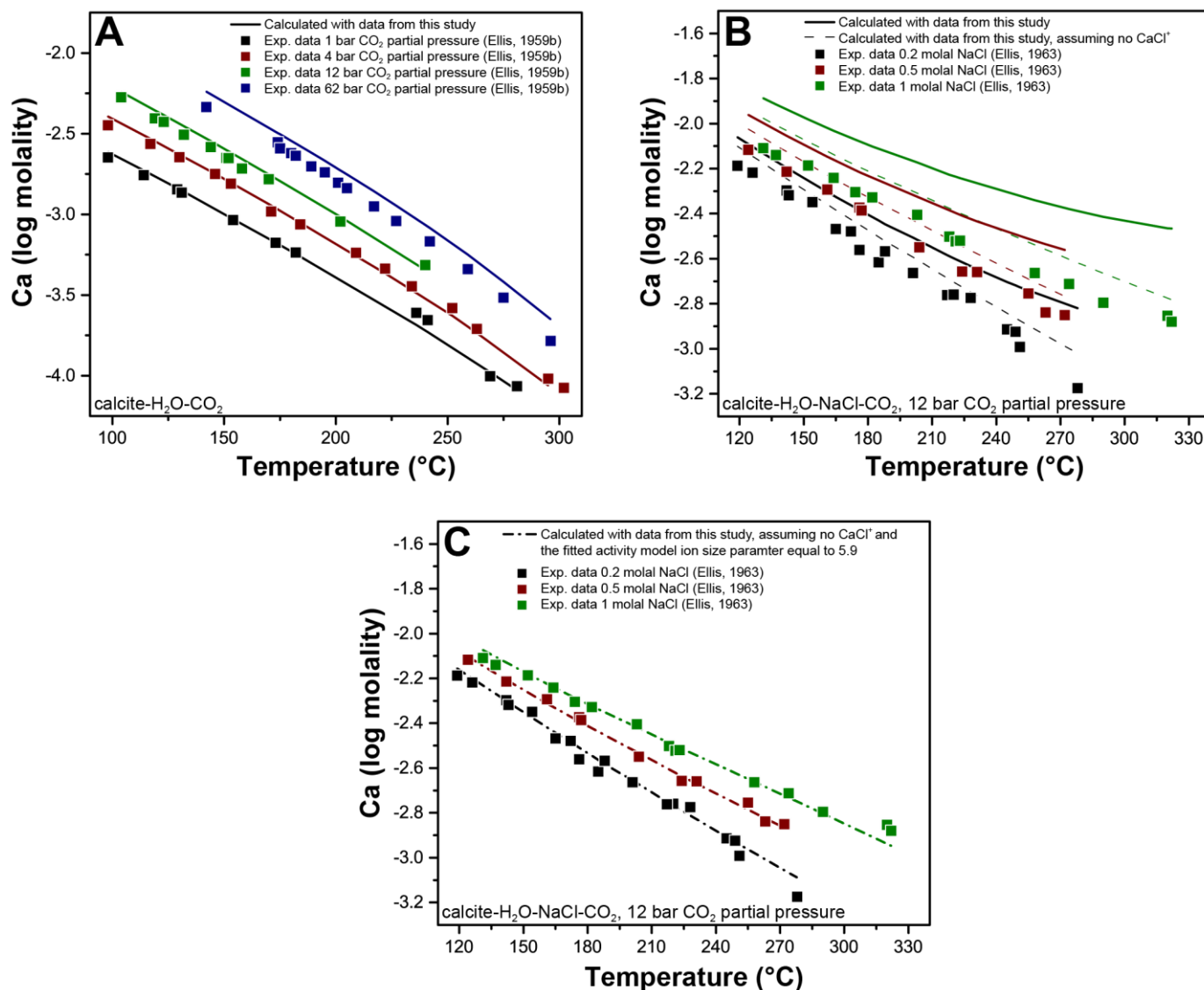


Figure 4.20. Comparison between calculated and experimentally determined calcite solubility: (A) CaCO₃-H₂O-CO₂ system at different CO₂ partial pressures, with increasing temperature; (B) CaCO₃-NaCl-H₂O-CO₂ system at 12 bar CO₂ partial pressure, with increasing temperature and different salt concentrations; (C) same as (B), but the calculated values resulted from using a fitted ion size activity model parameter of 5.9 and suppressing the formation of CaCl⁺ species.

4.9.3. System Ca-Mg-Cl-O-H-C

There is a very good agreement between calculated calcite and aragonite solubility and the experimental data from Plummer and Busenberg (1982). The agreement is good for all experimental data points over a considerable range of CO₂ partial pressure (Fig. 4.19). The calculations do also show a good agreement with the calcite solubility experiments in water at different CO₂ partial pressures at temperatures of 100 to 300 °C (Ellis 1959b). The calculated solubility slightly overestimates the measured one at a CO₂ partial pressure of 63 bar and this could be due to activity coefficient effects of CO₂(aq) becoming important (Fig. 4.20A). The calcite solubilities in NaCl solutions from Ellis (1963) are overestimated by the calculations using the thermodynamic dataset of this study. The difference amounts to about 0.1 log units in 0.2 molal

NaCl solution at 120 °C and 0.4 log units in 1 molal NaCl solution at 320 °C (Fig. 4.20B). We note that the experimental data of Ellis (1963) were not included into the final experimental database and global optimization of the $\Delta_f G_{298,1}^0$ of the aqueous species.

At higher temperatures and pressures, the calculated calcite solubilities in water are systematically higher than those experimentally determined by Walther and Long (1986). It is important to note that the experimental data of Walther and Long (1986) are also in disagreement with the subsequent calcite solubility study of Fein and Walther (1989), and some experimental problems in Walther and Long (1986) have been discussed by Fein and Walther (1989). There is a fairly good agreement between the calculated and the measured calcite solubility data in water from 400 to 600 °C and at 2.0 kbar (Fein and Walther, 1989), obtained using the properties of calcium and carbonate species from this study (Fig. 4.21). The agreement between calculations and experiments is much better than with the thermodynamic data from SUPCRT92, including calcite solubility in pure H₂O and in NaCl solutions (Fig. 4.22).

There is a good agreement between the calculated and the experimentally determined magnesite solubility data from Bénézeth et al. (2011). The agreement is good for all experimentally studied temperatures from 50 to 200 °C and at SWVP (Fig. 4.23). Unfortunately, there are no experimental magnesite solubility data available for supercritical conditions and predictions using the thermodynamic data from this study cannot be tested at higher temperatures and pressures.

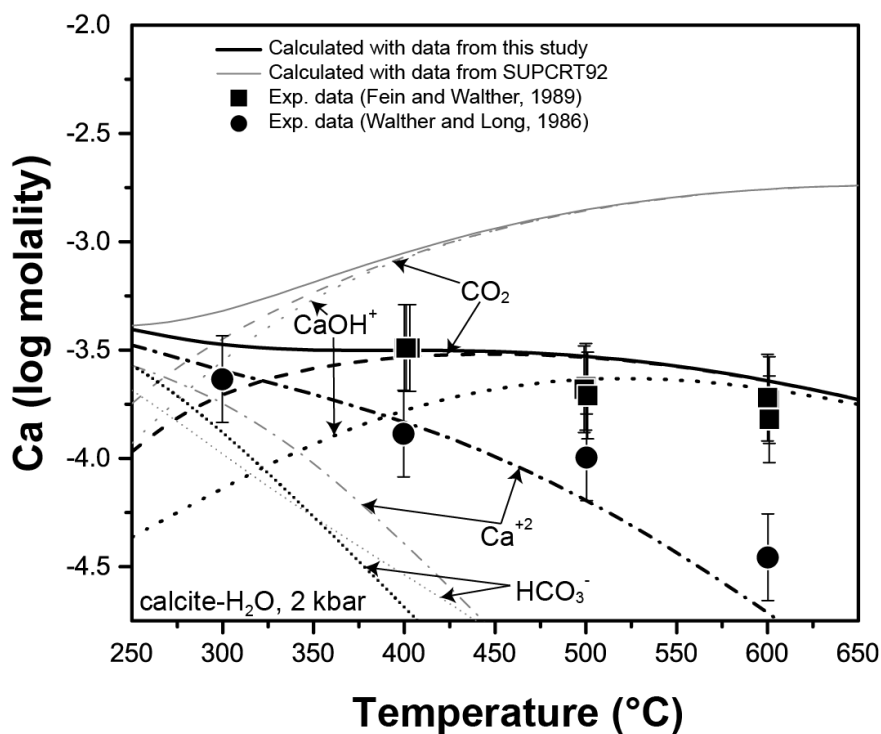


Figure 4.21. Comparison between calculated and experimentally determined calcite solubility in the CaCO₃-H₂O system at 2 kbar and different temperatures.

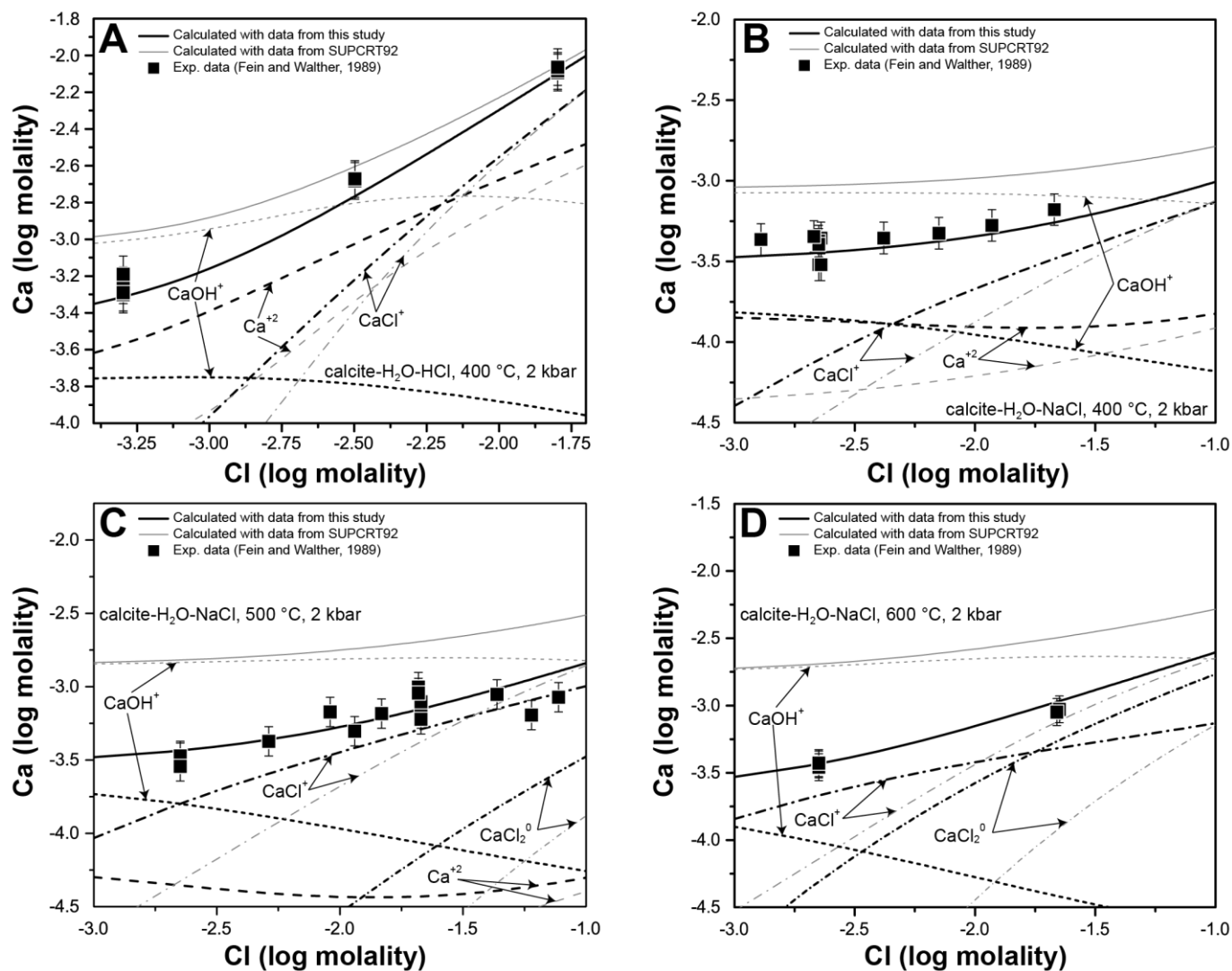


Figure 4.22. Comparison between calculated and experimentally measured calcite solubility in: (A) CaCO₃-HCl-H₂O system, at 400 °C; (B), (C), (D) CaCO₃-NaCl-H₂O system, at 400, 500, 600 °C.

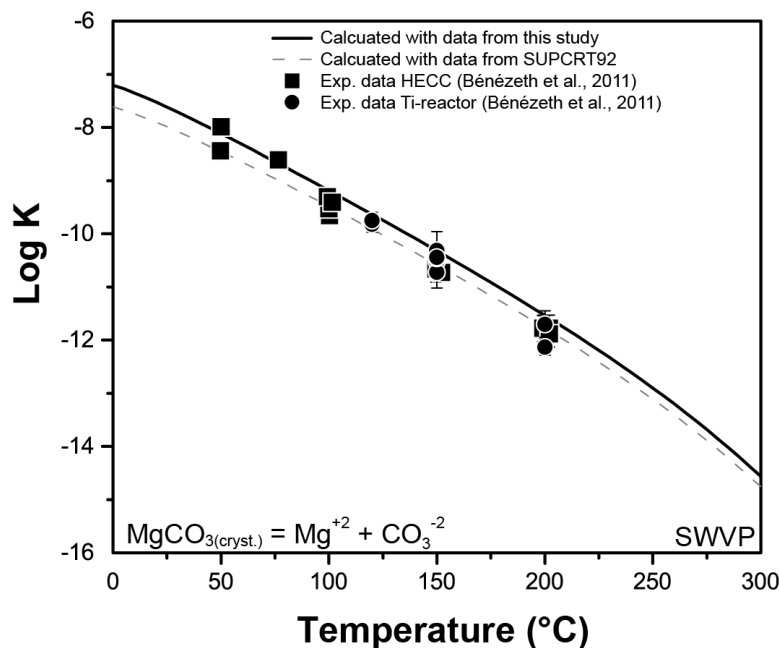


Figure 4.23. Comparison between calculated and experimentally determined magnesite solubility constants from the magnesite solubility experiments reported by Bénézech et al. (2011).

4.10. Discussion

4.10.1. System Ca-Mg-Al-Si-O-H

The CaOH^+ complex becomes increasingly important with increasing temperature at alkaline pH (Seewald and Seyfried, 1991). The existing standard state properties and HKF parameters for CaOH^+ are only based on correlations and low temperature association constant data ($< 50\text{ }^\circ\text{C}$) and have a rather large uncertainty. Because portlandite is not included in the Holland-Powell thermodynamic database, the portlandite solubility experiments were not used in the global optimization process. Rather, the data from the two experimental datasets (Walther, 1986; Seewald and Seyfried, 1991) at 0.5 and 1.0 kbar were used to independently retrieve the association constant of CaOH^+ . In the absence of other experimental constraints, these values were subsequently used to refine the standard state properties and HKF parameters of CaOH^+ .

There are differences between the reported values for the $\Delta_f G_{298,1}^0$ of portlandite. Walther reports a $\Delta_f G_{298,1}^0$ value of -898.4 kJ/mol, whereas the data compilation of Robie and Hemingway (1995) gives a value of -898.0 kJ/mol. Thoenen et al. (2014) report a value of -897.0 kJ/mol, which is consistent with the logarithm of the solubility product of 22.8 at 25 °C and 1 bar ($\text{Ca}(\text{OH})_{2(\text{cryst.})} + 2\text{H}^+ = \text{Ca}^{2+} + 2\text{H}_2\text{O}$). This value for the logarithm of the solubility product is based on a number of critical data evaluations and compilations (Baes and Mesmer, 1976; Duchesne and Reardon, 1995; Nordstrom, 2013). Using the $\Delta_f G_{298,1}^0$ of portlandite from Robie and Hemingway (1995) and the $\Delta_f G_{298,1}^0$ values of Ca^{2+} and H_2O from Cox et al. (1989), the logarithm of the solubility product is calculated as 22.55. In order to maintain consistency with the generally accepted value for the solubility product of portlandite, we have accepted the $\Delta_f G_{298,1}^0$ value from Thoenen et al. (2014). The standard state entropy, volume, and heat capacity of portlandite were adopted from Robie and Hemingway (1995). Fig. 4.16 compares the solubility product of portlandite, calculated with the thermodynamic data of this study, with the experimental data at elevated temperatures and pressures. This highlights the strong interdependence of the thermodynamic properties used for all the aqueous species, complexes and solid phases involved in the solubility model.

The calculated solubility of wollastonite+quartz assemblages in water is somewhat underestimated with the thermodynamic data of this study (Fig. 4.15). This may reflect that the standard state properties and HKF parameters of the calcium silicate complex (CaHSiO_3^+) are not well constrained by independent experiments (Sverjensky et al., 1997). If the stability of CaHSiO_3^+ would be increased by about 20 kJ/mol, this would result in better agreement between calculated and experimental wollastonite+quartz solubility up to 500 °C. Discarding possible issues with the wollastonite+quartz experiments, the measured calcium concentrations above 500 °C can only be accounted for if an additional higher-order Ca silicate species becomes important at the highest temperatures. A likely candidate would be the neutral calcium silicate complex CaSiO_3^0 . If included in the speciation model, this complex will bring the calculated solubility of wollastonite+quartz in a good agreement with the experimental data (Fig. 4.15B). However,

because there are no independent solubility data (on minerals present in the HP database) that could constrain the stability of the calcium silicate complex CaSiO_3^0 , we have not included this species into the final speciation model and have not used the wollastonite+quartz solubility data in the global data regression.

Altmaier et al. (2003) suggest that the logarithm of the solubility product of brucite ($\log K=16.3$, Fig. 4.24) calculated with the thermodynamic data from SUPCRT92 is inconsistent with the results of several solubility studies. The logarithm of the solubility product derived in their study is 17.1 ± 0.2 at 25 °C and 1 bar and agrees very well with the values of 17.11 ± 0.16 and 17.05 ± 0.2 reported by McGee and Hostetler (1977) and Xiong (2008) derived from solubility experiments. It also agrees very well with the value of 17.13 reported by Brown et al. (1996) obtained by extrapolation of high-temperature potentiometric titration. In contrast, Thoenen et al. (2014) report the logarithm of the brucite solubility product as 16.84 at 25 °C and 1 bar. The calculated logarithm of the brucite solubility product is 16.3 when using the thermodynamic data from SUPCRT92 and 16.48 when using the properties of H_2O and Mg^{2+} from SUPCRT92 but the $\Delta_f G_{298,1}^0$ of brucite from the Holland-Powell database. This suggests that either the $\Delta_f G_{298,1}^0$ of Mg^{2+} or the one of brucite are inconsistent with the experimentally determined solubility constant at 25 °C. Fig. 4.24 compares the brucite solubility products obtained from experimental studies (McGee and Hostetler, 1977; Brown et al., 1996) with calculations from different thermodynamic datasets. The difference between calculated and measured data can be accommodated by an adjustment of the $\Delta_f G_{298,1}^0$ of Mg^{2+} of around 3 to 4 kJ/mol or by a change in the properties of brucite. After the global optimization performed in this study, the refined $\Delta_f G_{298,1}^0$ value of Mg^{2+} is 2 kJ/mol more negative, resulting in a logarithm of the solubility product of brucite of 16.85 which is in reasonably good agreement with the experimental data.

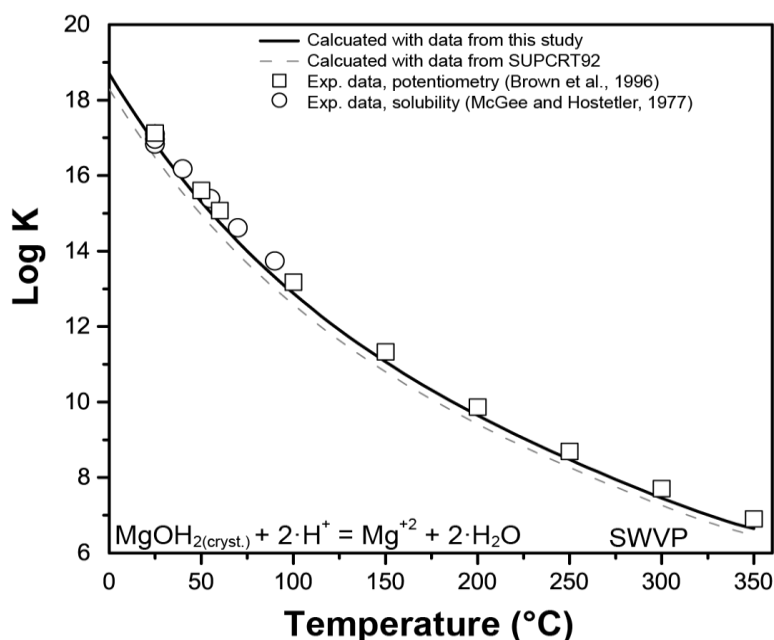


Figure 4.24. Comparison between calculated and experimentally determined brucite solubility constants from potentiometric measurements (Brown et al., 1996) and solubility experiments (McGee and Hostetler, 1977).

4.10.2. System Ca-Mg-Al-Si-Cl-O-H

There is a good agreement between the calculated and the experimental mineral solubility data in chloride solutions of Luce et al. (1985) at temperatures above 500 °C, while the agreement is not as good at 500 °C and below. The disagreement at lower temperatures could be related to the thermodynamic properties of the calcium and magnesium chloride complexes, in particular to the HKF parameters that define the temperature and pressure dependence of the standard state Gibbs free energies. This issue could also affect the observed disagreement between calculated and experimentally determined $\log(\text{Ca}/\text{H}^2)$ and $\log(\text{Mg}/\text{H}^2)$, total concentration ratios).

There is no clear explanation for the disagreement between the calculated and the measured Ca concentrations from the wollastonite+quartz solubility experiments in NaCl solutions (Xie and Walther, 1993b). Close inspection of the experimental data reveals a considerable scatter, with even measured Ca concentrations for P-T-X conditions that are very close to each other varying by as much as 0.5 log units (Fig. 4.18). Another feature of the data of Xie and Walther (1993b) is the very large pressure dependence of the solubility. Increasing the experimental pressure from 1 to 2 kbar results in an increase in the dissolved Ca concentration by one order of magnitude. Such a strong pressure dependence has not been reported from any other silicate mineral solubility study. Considering the large variations in the measured Ca concentrations for approximately similar state points, the unreasonably high pressure dependence and the absence of a clear temperature trend suggests that at least some of the experimental results of Xie and Walther (1993b) did not obtain equilibrium.

A major problem in the chlorine-bearing systems relates to the insufficient constraints on the stability of the aqueous Ca and Mg chloride complexes. Despite substantial efforts, it was not possible to reconcile the association constants from the conductance study of Frantz and Marshall (1982) with those from conductance experiments at lower temperatures (Méndez De Leo and Wood, 2005). The association constants for CaCl^+ and CaCl_2^0 from Frantz and Marshall (1982) are also discrepant with the temperature and pressure trends predicted by Sverjensky et al. (1997) and with trends shown by other well-studied electrolyte solutions. Most likely, the discrepancies relate to the method that was used for extracting the association constants from the conductance experiments of Frantz and Marshall (1982). The values for the limiting equivalent conductance of the CaCl_2 and MgCl_2 electrolytes and the method used for extracting molar conductance appear to be correct, in view of the fact that the limiting equivalent conductance for CaCl_2 from Frantz and Marshall (1982) agrees well with the results of molecular dynamics simulations by Lee (2004).

Retrieving association constants from the conductance data in the Ca and Mg chloride systems depends largely on the speciation model employed. Frantz and Marshall (1982) assumed that only the first and the second chloride complex would form in their experiments, but ignored the possible formation of the hydroxide species CaOH^+ and MgOH^+ and of higher-order chloride complexes such as CaCl_3^- . Considering that the conductance measurements were performed at rather low

chlorinity (0.001-0.005 molal), it is not very likely that higher-order chloride complexes were significant. The data reduction method used by Frantz and Marshall (1982) may have also resulted in large errors for the association constants of the chloride complexes. When retrieving association constants from the experiments in the $\text{CaCl}_2\text{-H}_2\text{O}$ system, they first modeled the measured molar conductance data assuming that only Ca^{2+} and Cl^- , and then separately only CaCl^+ and Cl^- would be present. Subsequently, they assumed that all measured conductance values lying between these two end-member cases would contain Ca^{2+} , CaCl^+ , and Cl^- ions. Only for conductance values below the one modeled for the end-member case with CaCl^+ and Cl^- present, they assumed that the solutions would contain CaCl^+ , Cl^- , and CaCl_2^0 but not Ca^{2+} . Actually, they never modeled any of their experiments with a full speciation model that would include Ca^{2+} , CaCl^+ , CaCl_2^0 and Cl^- . This potentially resulted in underestimation of the relative stability of CaCl_2^0 compared to that of the CaCl^+ complex.

In Fig. 4.25, the measured $\log(\text{Ca}/\text{H}^2)$ and $\log(\text{Mg}/\text{H}^2)$ are compared with their calculated counterparts using association constants for the Ca and Mg chloride species from Frantz and Marshall (1984) and the HCl^0 association constants from Frantz and Marshall (1984). The experimental values are poorly reproduced by the modeled data, but when the $\log(\text{Ca}/\text{H}^2)$ and $\log(\text{Mg}/\text{H}^2)$ values are calculated with a speciation model that only accounts for CaCl^+ and MgCl^+ , the calculated data agree very well with the experimental ones. This strongly supports the conclusion that the data reduction method used by Frantz and Marshall (1982) has resulted in incorrect association constant data for the Ca and Mg chloride species, by underestimating the relative stability of CaCl_2^0 compared to that of the CaCl^+ complex.

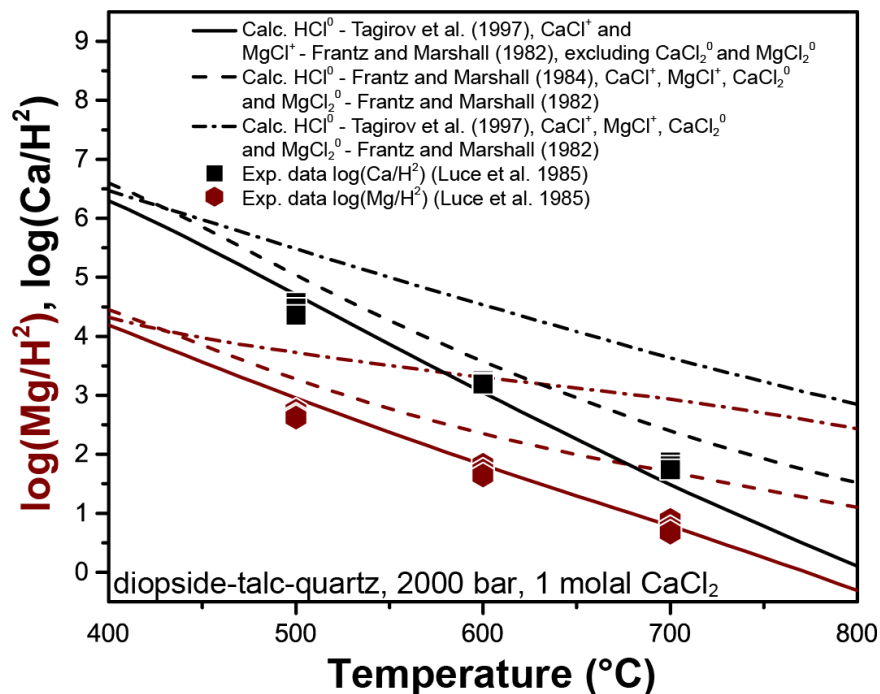


Figure 4.25. Comparison between experimentally determined $\log(\text{Ca}/\text{H}^2)$ values in the system diopside-talc-quartz, and values calculated using the association constants for calcium chloride species and HCl neutral ion pair from different sources.

4.10.3. System Ca-Mg-Cl-O-H-C

Refining the thermodynamic properties of the CaOH^+ complex has brought the calculated and experimentally determined calcite solubility data in water and chloride solutions into very good agreement. The improvement is substantial compared to calculations with the properties of CaOH^+ from Shock et al. (1997). Their data predict much larger stability of CaOH^+ , which has a strong impact on the calculated calcite solubility. This outcome highlights that regression of the standard state properties and HKF parameters of aqueous complexes should also take advantage of available solubility data. This particularly applies to cases such as CaOH^+ where no independent experimental information such as conductance or potentiometric data is available.

The solubility of calcite and magnesite in sodium chloride solutions at saturated CO_2 conditions is somewhat overestimated by the thermodynamic data of this study. This could be related to an overestimation of the stability of some of the Ca complexes or the activity coefficient model employed. With increasing NaCl concentration, the calculated stability of CaCl^+ for the experiments of Ellis (1963) increases and it becomes the predominant Ca complex in 1 molal solutions above 140 °C. If calcite solubility is calculated without including the Ca chloride complexes into the speciation model, the modeled Ca concentrations are still higher than the experimentally determined values (Fig. 4.20B). At these conditions, the stability of the CaCl^+ complex is in agreement with association constants derived from the experiments of Majer and Štulík (1982), Gillespie et al. (1992) and Méndez De Leo and Wood (2005). We have investigated the relative impact of the activity coefficient model by regressing the calcite solubility data for different values of the ion size parameter. The results show that the agreement between calculated and experimental data becomes very good if the ion size parameter is increased to a value of 5.9 (Fig. 4.20C). We also investigated the effect of the extended term parameter of the Debye-Hückel model, but it is very insensitive to the calcite solubility data. It was not possible to arrive at realistic values for the ion size parameter (<20) when the CaCl^+ complex was included into the speciation model. Until more experimental data become that would constrain the activity coefficients and association constants in the $\text{CaCl}_2\text{-H}_2\text{O-CO}_2$ system, we suggest to maintain the standard state properties of calcium carbonate and chloride species as presented in this study.

Calculating the magnesite solubility in water and NaCl solutions at saturated CO_2 conditions results in a moderate underestimation of the experimentally determined values (Bénézech et al., 2011). We note that the experiments that were performed in a hydrogen electrode concentration cell containing no CO_2 saturating gas phase are better modeled by the thermodynamic data of this study. The same overestimation effect was observed when modeling the magnesite solubility experiments in CO_2 saturated conditions and NaCl solution reported by Bénézech et al. (2011). The experiments on magnesite solubility done in the hydrogen electrode concentration cell, which contain no CO_2 saturated gas phase, do not show the systematic overestimation of the calculated values when compared with the measured ones.

A possible explanation for the disagreement between calculated and measured calcite solubility could be that the extended Debye-Hückel model (Helgeson et al., 1981) is inadequate for the aqueous carbonate species in systems saturated with CO_2 . The activity coefficient of $\text{CO}_2(\text{aq})$ and

of other neutral complexes is assumed to be close to unity (only the solution concentration effect is accounted for). The activity coefficients for the charged species are calculated by the extended Debye-Hückel model using the parameters for the NaCl background electrolyte for all species. This approach may not be suitable for electrolyte solutions that contain large concentrations of CO₂(aq) buffered by a CO₂-rich gas phase. Resolving the remaining disagreements between calculated and measured solubility may require to develop an improved thermodynamic model for calculating activity coefficients in aqueous electrolyte solutions with high concentrations of dissolved chlorides and carbonates in the framework of the revised HKF model. An alternative approach would be to use local-composition based activity coefficient models such eNRTL or EUNIQUAC (e.g. Chen and Song, 2004; Hingerl et al., 2014) in conjunction with the speciation model employed in this study.

4.10.4. Standard state properties of Ca and Mg ions

The $\Delta_f G_{298,1}^0$ of the Ca²⁺ ion in the SUPCRT92 database was calculated from the $\Delta_f H_{298,1}^0$, $S_{298,1}^0$ and the standard molar entropy of the elements from the CODATA compilation (Cox et al., 1989). The values of the $\Delta_f H_{298,1}^0$ and $S_{298,1}^0$ are -543.1 ± 0.8 kJ/mol and -56.6 J/(mol·K) in Cox et al. (1989) and -542.8 kJ/mol and -53.1 J/(mol·K) in the report of Wagman et al. (1982). The reported $\Delta_f H_{298,1}^0$ of Ca²⁺ from Cox et al. (1989) was derived from the solubility data on calcite (Jacobson and Langmuir, 1974; Langmuir, 1968) and the enthalpy of dissolution of portlandite (Hopkins and Wulff, 1965; Langmuir, 1968). The standard state properties of calcite have been accurately known since the determinations of Bäckström (1925a, b). Their measured value of -178.24 ± 0.8 kJ/mol for the heat of oxide reaction to form calcite (CaO + CO₂ = CaCO₃) is almost identical to the value of -178.3 ± 1.2 kJ/mol (Chai and Navrotsky, 1993) that was adopted by Holland and Powell (1998).

Using the Gibbs energy of reaction of the portlandite solubility product reported by Hopkins and Wulff (1965) of 29.7 kJ/mol and the thermodynamic data for portlandite from Langmuir (1968) results in a $\Delta_f G_{298,1}^0$ of the Ca²⁺ ion of -553.9 kJ/mol. Combining this value for the Ca²⁺ ion with the $\Delta_f G_{298,1}^0$ of the CO₃²⁻ ion of -527.9 kJ/mol (Langmuir, 1968) and the Gibbs free energy of reaction for the calcite solubility product at 25 °C and 1 bar, the $\Delta_f G_{298,1}^0$ of calcite is calculated as -1129.8 kJ/mol. The difference between this value and the $\Delta_f G_{298,1}^0$ value of -1128.8 kJ/mol for calcite from Holland and Powell (1998) is around 1 kJ/mol. This difference is almost identical to the difference between the $\Delta_f G_{298,1}^0$ of Ca²⁺ calculated above (-553.9 kJ/mol) and the value of -552.8 kJ/mol reported by Cox et al. (1989). The $S_{298,1}^0$ of Ca²⁺ reported by Cox et al. (1989) consistent with the accepted third-law entropy value of 83.4 J/(mol·K) of portlandite and the entropy difference of the portlandite dissolution of 159.8 J/(mol·K) as calculated by Hopkins and Wulff (1965). These connections provide support for the fact that the thermodynamic properties

of calcite and all aqueous Ca and carbonate and silicate species derived in this study are highly consistent with each other.

The $\Delta_f G_{298,1}^0$ of the Mg^{2+} ion in the SUPCRT92 database was calculated from the $S_{298,1}^0$ and the standard molar entropy of the elements from the CODATA compilation (Cox et al., 1989) and the $\Delta_f H_{298,1}^0$ from Shin and Criss (1979), who evaluated the $\Delta_f H_{298,1}^0$ of the Mg^{2+} ion from the enthalpy of formation of $\text{MgCl}_2(\text{s})$ in acid HCl solutions and from the enthalpy of dilution of $\text{MgCl}_2(\text{s})$ in pure water. They used these experimental data to calculate the standard state enthalpy of $\text{MgCl}_2(\text{aq})$ at 25 °C and 1 bar (at infinite dilution). Using the enthalpy of $\text{MgCl}_2(\text{aq})$, the $\Delta_f H_{298,1}^0$ of the Cl^- ion from CODATA and applying the additivity principle, they calculated the $\Delta_f H_{298,1}^0$ of the Mg^{2+} ion.

The standard state entropy of Mg^{2+} in SUPCRT92 comes from the compilation of Parker et al. (1971), who did not reference the exact source for their thermodynamic data. Stephenson (1946) calculated the $S_{298,1}^0$ and $\Delta_f G_{298,1}^0$ of Mg^{2+} from the measured heats of reaction and heats of formation for different magnesium compounds available at that time (using a thermochemical cycle). They arrived at an $S_{298,1}^0$ value of $-136.8 \pm 4.2 \text{ J}/(\text{mol}\cdot\text{K})$, which is very close to the value of $-138.1 \text{ J}/(\text{mol}\cdot\text{K})$ reported by Parker et al. (1971). The determination of the standard state enthalpy and entropy from a thermochemical cycle results in accumulation of rather large errors amounting from the rather imprecise heat of reaction data. In addition, the heats of formation of all the reaction participants do introduce additional errors.

The standard state partial molal heat capacity $Cp_{298,1}^0$ and the c_1 and c_2 HKF parameters for the Ca^{2+} and Mg^{2+} ions were derived by Tanger and Helgeson (1988) from isobaric heat capacity measurements of aqueous calcium and magnesium electrolyte solutions. For the Mg^{2+} ion, the standard state partial molal volume ($V_{298,1}^0$) and the HKF parameters a_1 , a_2 , a_3 and a_4 that describe the pressure dependence, were derived by Tanger and Helgeson (1988) from the experimental data on partial molal volumes and isothermal compressibilities of aqueous magnesium electrolytes at 1 bar and different temperatures below 150 °C. For the Ca^{2+} ion, the $V_{298,1}^0$ was derived by Tanger and Helgeson (1988) using the data on partial molar volumes of calcium electrolytes solutions. They employed estimation techniques for the missing data for the isothermal compressibilities of aqueous calcium electrolyte solutions. Shock and Helgeson (1988) used the standard partial molal compressibility for Ca^{2+} reported by Millero (1982) and correlations between the a_1 , a_2 , a_3 , a_4 parameters, the isothermal compressibilities, and the partial molal volumes of other ions to estimate the HKF parameters for the Ca^{2+} ion. The Born coefficients ω_0 for both the Ca^{2+} and Mg^{2+} ions originate from the work of Helgeson and Kirkham (1976) who calculated them from the effective electrostatic radii of the ions.

The correction of around 2 kJ/mol on the $\Delta_f G_{298,1}^0$ of Mg^{2+} , which resulted from the global optimization is well within the uncertainties associated with the thermochemical cycles used in

the extraction of the ion properties. In the case of Ca^{2+} ion, the thermodynamic properties are strongly connected to the properties of the minerals and their solubility products, resulting in an insignificant change after the optimization process (tens of J/mol).

4.11. Conclusions and outlook

(1) The critically evaluated experimental solubility data in the Ca-Mg-Na-K-Al-Si-O-H-C-Cl system covering a wide range of conditions were used to simultaneously refine, in an internally consistent way, the standard state Gibbs energies of aqueous ions and complexes. The aqueous species properties are consistent with the Holland-Powell internally consistent dataset for minerals dataset.

(2) The thermodynamic database presented in this study and future updates will be provided at the following web-address: <http://gems.web.psi.ch/>. The files are in the format of the GEM-Selektor geochemical modeling software (Kulik et al. 2013) and enable calculation of aqueous-mineral equilibria in the system Ca-Mg-Na-K-Al-Si-O-H-C-Cl at temperatures up to 1000 °C, pressures up to 5 kbar and salt concentrations up to 5 molal.

(3) Major discrepancies were identified for the properties of Ca and Mg hydroxide and chloride species. More experimental data are needed to resolve the disagreements between the association constant data for the Ca and Mg chlorides from different studies. For constraining the stability of CaCl_2^0 and MgCl_2^0 , new experimental data that are independent of solubility are necessary at subcritical and supercritical conditions. Additional studies should look into the possible formation of higher order chloride species which could play an important role in concentrated chloride brines. New experimental data are also needed for the stability constants of the hydroxide species CaOH^+ and MgOH^+ , because at supercritical conditions there are no association constant data available that would be independent from solubility.

(4) The properties of carbonate species derived in this study are consistent with the properties of $\text{CO}_2(\text{aq})$ calculated with the Akinfiyev-Diamond model for aqueous nonelectrolytes. This model results in very a good agreement with the experimental CO_2 solubility data in water. Only limited data are available for the association constants for alkali and alkaline-earth metals carbonate and bicarbonate complexes, and future experimental studies should address their stability at supercritical conditions.

(5) More solubility experiments are needed to resolve discrepancies between calculated and experimentally measured Ca silicate solubilities, highlighted by the substantial disagreement in the system wollastonite+quartz+ H_2O . The discrepancies could be reconciled by accounting for silicate complexes that are not included into the current speciation model such as CaSiO_3^0 and MgSiO_3^0 . This would require to constrain the stability of such complexes from additional independent experiments.

Acknowledgements

This project was supported by funding from ETH Zurich, ETHIIRA grant number ETH-19 11-2 and NANOCEM internal project (Thermodynamic dataset for modelling CASHNK aqueous-solid solution systems extension of the SNF-Sinergia project). We greatly acknowledge Barbara Lothenbach for the fruitful discussion and advice regarding the thermodynamics of calcium species.

References

- Adams, B.M., Kuehn, T.H., Bielicki, J.M., Randolph, J.B. and Saar, M.O. (2015) A comparison of electric power output of CO₂ Plume Geothermal (CPG) and brine geothermal systems for varying reservoir conditions. *Applied Energy* 140, 365-377.
- Akinfiev, N.N. and Diamond, L.W. (2003) Thermodynamic description of aqueous nonelectrolytes at infinite dilution over a wide range of state parameters. *Geochim Cosmochim Acta* 67, 613-629.
- Alfredsson, H.A., Hardarson, B.S., Franzson, H. and Gislason, S.R. (2008) CO₂ sequestration in basaltic rock at the Hellisheidi site in SW Iceland: Stratigraphy and chemical composition of the rocks at the injection site. *Mineralogical Magazine* 72, 1-5.
- Altmaier, M., Metz, V., Neck, V., Müller, R. and Fanghänel, T. (2003) Solid-liquid equilibria of Mg(OH)₂(cr) and Mg₂(OH)₃Cl·4H₂O(cr) in the system Mg-Na-H-OH-Cl-H₂O at 25°C. *Geochim Cosmochim Acta* 67, 3595-3601.
- André, L., Spycher, N., Xu, T., Vuataz F.D., Pruess, K., 2006. Modeling brine-rock interactions in an enhanced geothermal system deep fractured reservoir at Soultz-Sous-Forets (France): a joint approach using two geochemical codes: FRACHEM and TOUGHREACT. Technical report, Center of Geothermal Research, Switzerland, 71 pp.
- Anderson, G.K. (2002) Solubility of carbon dioxide in water under incipient clathrate formation conditions. *Journal of Chemical & Engineering Data* 47, 219-222.
- Arcis, H., Zimmerman, G.H. and Tremaine, P.R. (2014) Ion-pair formation in aqueous strontium chloride and strontium hydroxide solutions under hydrothermal conditions by AC conductivity measurements. *Physical Chemistry Chemical Physics* 16, 17688-17704.
- Bäckström, H.L.J. (1925a) The heat of dissociation of calcium carbonate and the entropy of carbon dioxide. *J Am Chem Soc* 47, 2443-2449.
- Bäckström, H.L.J. (1925b) The thermodynamic properties of calcite and aragonite. *J Am Chem Soc* 47, 2432-2442.
- Baes, C.F. and Mesmer, R.E. (1981) The thermodynamics of cation hydrolysis. *Am J Sci* 281, 935-962.
- Baes, C.F. and Mesmer, R.M. (1976) *The Hydrolysis of Cations*. Wiley-Interscience, New York.
- Baker, T., Van Achtenberg, E., Ryan, C.G. and Lang, J.R. (2004) Composition and evolution of ore fluids in a magmatic-hydrothermal skarn deposit. *Geology* 32, 117-120.
- Bamberger, A., Sieder, G. and Maurer, G. (2000) High-pressure (vapor+liquid) equilibrium in binary mixtures of (carbon dioxide+water or acetic acid) at temperatures from 313 to 353 K. *The Journal of Supercritical Fluids* 17, 97-110.
- Bates, R.G., Bower, V.E., Canham, R.G. and Prue, J.E. (1959) The dissociation constant of CaOH⁺ from 0° to 40°C. *T Faraday Soc* 55, 2062-2068.
- Baumgartner, L. and Ferry, J. (1991) A model for coupled fluid-flow and mixed-volatile mineral reactions with applications to regional metamorphism. *Contr Min Pet* 106, 273-285.
- Bell, R.P. and George, J.H.B. (1953) The incomplete dissociation of some thallos and calcium salts at different temperatures. *T Faraday Soc* 49, 619-627.

- Bell, R.P. and Prue, J.E. (1949) Reaction-kinetic investigations of the incomplete dissociation of salts. Part I. The decomposition of diacetone alcohol in solutions of metallic hydroxides. *Journal of the Chemical Society (Resumed)*, 362-369.
- Bénézech, P., Saldi, G.D., Dandurand, J.-L. and Schott, J. (2011) Experimental determination of the solubility product of magnesite at 50 to 200°C. *Chemical Geology* 286, 21-31.
- Berg, R.L. and Vanderzee, C.E. (1978) Thermodynamics of carbon dioxide and carbonic acid: (a) the standard enthalpies of solution of Na₂CO₃(s), NaHCO₃(s), and CO₂(g) in water at 298.15 K; (b) the standard enthalpies of formation, standard Gibbs energies of formation, and standard entropies of CO₂(aq), HCO₃⁻(aq), CO₃²⁻(aq), NaHCO₃(s), Na₂CO₃(s), Na₂CO₃·H₂O(s), and Na₂CO₃·10H₂O(s). *The J Chem Thermodyn* 10, 1113-1136.
- Berner, U.R. (1992) Evolution of pore water chemistry during degradation of cement in a radioactive waste repository environment. *Waste Management* 12, 201-219.
- Brown, P.L., Drummond Jr, S.E. and Palmer, D.A. (1996) Hydrolysis of magnesium(II) at elevated temperatures. *Journal of the Chemical Society - Dalton Transactions*, 3071-3075.
- Butler, J.N. and Huston, R. (1970) Activity coefficients and ion pairs in the systems sodium chloride-sodium bicarbonate-water and sodium chloride-sodium carbonate-water. *The J of Phys Chem* 74, 2976-2983.
- Bychkov A.Y., Benezeth, P., Pokrovsky O.S., Schott J. (2007) Experimental determination of calcite solubility at 120-160°C and 2-50 bar pCO₂ using in-situ pH measurements. *Geotechnologien Science Report* 9, 47-48.
- Caciagli, N. and Manning, C. (2003) The solubility of calcite in water at 6–16 kbar and 500–800 °C. *Contr Min Pet* 146, 275-285.
- Capewell, S., Hefter, G. and May, P. (1998) Potentiometric Investigation of the Weak Association of Sodium and Carbonate Ions at 25°C. *Journal of Solution Chemistry* 27, 865-877.
- Capewell, S.G., Buchner, R., Hefter, G. and May, P.M. (1999) Dielectric relaxation of aqueous Na₂CO₃ solutions. *Physical Chemistry Chemical Physics* 1, 1933-1937.
- Chai, L. and Navrotsky, A. (1993) Thermochemistry of carbonate-pyroxene equilibria. *Contr Min Pet* 114, 139-147.
- Chen, C.-C. and Song, Y. (2004) Generalized electrolyte-NRTL model for mixed-solvent electrolyte systems. *AIChE Journal* 50, 1928-1941.
- Cox, J.D., Wagman, D.D. and Medvedev, V.A. (1989) *CODATA Key Values for Thermodynamics*. Hemisphere Publishing Company, New York.
- Crea, F., Stefano, C.D., Gianguzza, A., Piazzese, D. and Sammartano, S. (2006) Protonation of carbonate in aqueous tetraalkylammonium salts at 25 °C. *Talanta* 68, 1102-1112.
- Crovetto, R. (1991) Evaluation of Solubility Data of the System CO₂-H₂O from 273 K to the Critical Point of Water. *Journal of Physical and Chemical Reference Data* 20, 575-589.
- Dasgupta, R. and Hirschmann, M.M. (2010) The deep carbon cycle and melting in Earth's interior. *Earth and Planetary Science Letters* 298, 1-13.
- De Visscher, A., Vanderdeelen, J., Königsberger, E., Churagulov, B.R., Ichikuni, M. and Tsurumi, M. (2012) IUPAC-NIST Solubility Data Series. 95. Alkaline Earth Carbonates in Aqueous Systems. Part 1. Introduction, Be and Mg. *Journal of Physical and Chemical Reference Data* 41, 013105-013105-013167.
- Demichelis, R., Raiteri, P., Gale, J.D., Quigley, D. and Gebauer, D. (2011) Stable prenucleation mineral clusters are liquid-like ionic polymers. *Nat Commun* 2, 590.
- Diamond, L.W. and Akinfiyev, N.N. (2003) Solubility of CO₂ in water from -1.5 to 100 °C and from 0.1 to 100 MPa: evaluation of literature data and thermodynamic modelling. *Fluid Phase Equilib* 208, 265-290.
- Drummond, S.E. (1981) Boiling and mixing of hydrothermal fluids: chemical effects on mineral precipitation. PhD Thesis. Pennsylvania State University.
- Duan, Z. and Li, D. (2008) Coupled phase and aqueous species equilibrium of the H₂O-CO₂-NaCl-CaCO₃ system from 0 to 250 °C, 1 to 1000 bar with NaCl concentrations up to saturation of halite. *Geochim Cosmochim Acta* 72, 5128-5145.
- Duan, Z., Møller, N. and Weare, J.H. (1992) An equation of state for the CH₄-CO₂-H₂O system: I. Pure systems from 0 to 1000°C and 0 to 8000 bar. *Geochim Cosmochim Acta* 56, 2605-2617.

- Duan, Z. and Sun, R. (2003) An improved model calculating CO₂ solubility in pure water and aqueous NaCl solutions from 273 to 533 K and from 0 to 2000 bar. *Chemical Geology* 193, 257-271.
- Duchesne, J. and Reardon, E.J. (1995) Measurement and prediction of portlandite solubility in alkali solutions. *Cement and Concrete Research* 25, 1043-1053.
- Ellis, A.J. (1959a) The effect of pressure on the first dissociation constant of "carbonic acid". *Journal of the Chemical Society (Resumed)*, 3689-3699.
- Ellis, A.J. (1959b) The solubility of calcite in carbon dioxide solutions. *Am J Sci* 257, 354-365.
- Ellis, A.J. (1963) The solubility of calcite in sodium chloride solutions at high temperatures. *Am J Sci* 261, 259-267.
- Ellis, A.J. and Golding, R.M. (1963) The solubility of carbon dioxide above 100°C in water and in sodium chloride solutions. *Am J Sci* 261, 47-60.
- Engi, M. (1992) Thermodynamic data for minerals: a critical assessment, in: Price, G., Ross, N. (Eds.), *The Stability of Minerals*. Springer Netherlands, pp. 267-328.
- Facq, S., Daniel, I., Montagnac, G., Cardon, H. and Sverjensky, D.A. (2014) In situ Raman study and thermodynamic model of aqueous carbonate speciation in equilibrium with aragonite under subduction zone conditions. *Geochim Cosmochim Acta* 132, 375-390.
- Fein, J.B. and Walther, J.V. (1987) Calcite solubility in supercritical CO₂-H₂O fluids. *Geochim Cosmochim Acta* 51, 1665-1673.
- Fein, J.B. and Walther, J.V. (1989) Calcite solubility and speciation in supercritical NaCl-HCl aqueous fluids. *Contr Min Pet* 103, 317-324.
- Felmy, A.R., Dixon, D.A., Rustad, J.R., Mason, M.J. and Onishi, L.M. (1998) The hydrolysis and carbonate complexation of strontium and calcium in aqueous solution. Use of molecular modeling calculations in the development of aqueous thermodynamic models. *The Journal of Chemical Thermodynamics* 30, 1103-1120.
- Fockenbergh, T., Burchard, M. and Maresch, W.V. (2006) Experimental determination of the solubility of natural wollastonite in pure water up to pressures of 5GPa and at temperatures of 400–800°C. *Geochim Cosmochim Acta* 70, 1796-1806.
- Frantz, J.D. and Marshall, W.L. (1982) Electrical conductances and ionization constants of calcium chloride and magnesium chloride in aqueous solutions at temperatures to 600°C and pressures to 4000 bars. *Am J Sci* 282, 1666-1693.
- Frantz, J.D. and Marshall, W.L. (1984) Electrical conductances and ionization constants of salts, acids, and bases in supercritical aqueous fluids; I, Hydrochloric acid from 100° to 700°C and at pressures to 4000 bars. *Am J Sci* 284, 651-667.
- Frantz, J.D. and Popp, R.K. (1979) Mineral-solution equilibria—I. An experimental study of complexing and thermodynamic properties of aqueous MgCl₂ in the system MgO-SiO₂-H₂O-HCl. *Geochim Cosmochim Acta* 43, 1223-1239.
- Frantz, J.D. and Popp, R.K. (1981) The ionization constants of aqueous MgCl₂ at elevated temperatures and pressures—a revision. *Geochim Cosmochim Acta* 45, 2511-2512.
- Frezzotti, M.L., Selverstone, J., Sharp, Z.D. and Compagnoni, R. (2011) Carbonate dissolution during subduction revealed by diamond-bearing rocks from the Alps. *Nature Geosci* 4, 703-706.
- Galvez, M.E., Beyssac, O., Martinez, I., Benzerara, K., Chaduteau, C., Malvoisin, B. and Malavieille, J. (2013) Graphite formation by carbonate reduction during subduction. *Nature Geosci* 6, 473-477.
- Garrels, R.M., Thompson, M.E. and Siever, R. (1961) Control of carbonate solubility by carbonate complexes. *Am J Sci* 259, 24-45.
- Gillespie, S.E., Oscarson, J.L., Chen, X., Izatt, R.M. and Pando, C. (1992) Thermodynamic quantities for the interaction of Cl⁻ with Mg²⁺, Ca²⁺ and H⁺ in aqueous solution from 250 to 325°C. *Journal of Solution Chemistry* 21, 761-788.
- Gimblett, F.G.R. and Monk, C.B. (1954) E.m.f. studies of electrolytic dissociation. Part 7.—Some alkali and alkaline earth metal hydroxides in water. *T Faraday Soc* 50, 965-972.
- Grabman, K.B. and Popp, R.K. (1991) Experimental investigation of talc solubility in H₂O-MgCl₂-NaCl-HCl fluids in the range 500–700°C, 2 kb. *Geochim Cosmochim Acta* 55, 2819-2829.

- Greenwald, I. (1941) The dissociation of calcium and magnesium carbonates and bicarbonates. *J Biol Chem* 141, 789-796.
- Gruszkiewicz, M., Palmer, D., Springer, R., Wang, P. and Anderko, A. (2007) Phase Behavior of Aqueous Na–K–Mg–Ca–Cl–NO₃ Mixtures: Isopiestic Measurements and Thermodynamic Modeling. *Journal of Solution Chemistry* 36, 723-765.
- Gunter, W.D. and Eugster, H.P. (1978) Wollastonite solubility and free energy of supercritical aqueous CaCl₂. *Contr Min Pet* 66, 271-281.
- Harned, H.S. and Davis, R. (1943) The Ionization Constant of Carbonic Acid in Water and the Solubility of Carbon Dioxide in Water and Aqueous Salt Solutions from 0 to 50°. *J Am Chem Soc* 65, 2030-2037.
- Harned, H.S. and Scholes, S.R. (1941) The Ionization Constant of HCO₃⁻ from 0 to 50°. *J Am Chem Soc* 63, 1706-1709.
- Helgeson, H.C., Delaney, J.M., Nesbitt, H.W. and Bird, D.K. (1978) Summary and critique of the thermodynamic properties of rock-forming minerals. *Amer. J. Sci.* 278A, 230.
- Helgeson, H.C. and Kirkham, D.H. (1974) Theoretical prediction of the thermodynamic behavior of aqueous electrolytes at high pressures and temperatures; I, Summary of the thermodynamic/electrostatic properties of the solvent. *Am J Sci* 274, 1089-1198.
- Helgeson, H.C. and Kirkham, D.H. (1974) Theoretical prediction of the thermodynamic behavior of aqueous electrolytes at high pressures and temperatures; II, Debye-Huckel parameters for activity coefficients and relative partial molal properties. *Am J Sci* 274, 1199-1261.
- Helgeson, H.C. and Kirkham, D.H. (1976) Theoretical prediction of the thermodynamic properties of aqueous electrolytes at high pressures and temperatures. III. Equation of state for aqueous species at infinite dilution. *Am J Sci* 276, 97-240.
- Helgeson, H.C., Kirkham, D.H. and Flowers, G.C. (1981) Theoretical prediction of the thermodynamic behavior of aqueous electrolytes by high pressures and temperatures; IV, Calculation of activity coefficients, osmotic coefficients, and apparent molal and standard and relative partial molal properties to 600 degrees C and 5kb. *Am J Sci* 281, 1249-1516.
- Hemley, J.J. (1959) Some mineralogical equilibria in the system K₂O-Al₂O₃-SiO₂-H₂O. *Am J Sci* 257, 241-270.
- Hemley, J.J., Montoya, J.W., Christ, C.L. and Hostetler, P.B. (1977a) Mineral equilibria in the MgO-SiO₂-H₂O system; I, Talc-chrysotile-forsterite-brucite stability relations. *Am J Sci* 277, 322-351.
- Hemley, J.J., Montoya, J.W., Shaw, D.R. and Luce, R.W. (1977b) Mineral equilibria in the MgO-SiO₂-H₂O system; II, Talc-antigorite-forsterite-anthophyllite-enstatite stability relations and some geologic implications in the system. *Am J Sci* 277, 353-383.
- Hingerl, F.F., Wagner, T., Kulik, D.A., Thomsen, K. and Driesner, T. (2014) A new aqueous activity model for geothermal brines in the system Na-K-Ca-Mg-H-Cl-SO₄-H₂O from 25 to 300 °C. *Chemical Geology* 381, 78-93.
- Hnědkovský, L.r. and Wood, R.H. (1997) Apparent molar heat capacities of aqueous solutions of CH₄, CO₂, H₂S, and NH₃ at temperatures from 304 K to 704 K at a pressure of 28 MPa. *The Journal of Chemical Thermodynamics* 29, 731-747.
- Holland, T. and Powell, R. (1991) A Compensated-Redlich-Kwong (CORK) equation for volumes and fugacities of CO₂ and H₂O in the range 1 bar to 50 kbar and 100–1600°C. *Contr Min Pet* 109, 265-273.
- Holland, T.J.B. and Powell, R. (1998) An internally consistent thermodynamic data set for phases of petrological interest. *Journal of Metamorphic Geology* 16, 309-343.
- Holland, T. and Powell, R. (2003) Activity–composition relations for phases in petrological calculations: an asymmetric multicomponent formulation. *Contr Min Pet* 145, 492-501.
- Hopkins, H.P. and Wulff, C.A. (1965) The Solution Thermochemistry of Polyvalent Electrolytes. I. Calcium Hydroxide. *The Journal of Physical Chemistry* 69, 6-8.
- Hostetler, P.B. (1963) Complexing of magnesium with bicarbonate. *The Journal of Physical Chemistry* 67, 720-721.
- Jacobson, R.L. and Langmuir, D. (1974) Dissociation constants of calcite and CaHCO₃⁺ from 0 to 50°C. *Geochim Cosmochim Acta* 38, 301-318.

- Johnson, J.W., Oelkers, E.H. and Helgeson, H.C. (1992) SUPCRT92: A software package for calculating the standard molal thermodynamic properties of minerals, gases, aqueous species, and reactions from 1 to 5000 bar and 0 to 1000°C. *Computers & Geosciences* 18, 899-947.
- Kulik, D.A. and Kersten, M. (2001) Aqueous Solubility Diagrams for Cementitious Waste Stabilization Systems: II, End-Member Stoichiometries of Ideal Calcium Silicate Hydrate Solid Solutions. *J Am Ceram Soc* 84, 3017-3026.
- Kulik, D.A., Wagner, T., Dmytrieva, S.V., Kosakowski, G., Hingerl, F., Chudnenko, K.V. and Berner, U. (2013) GEM-Selektor geochemical modeling package: revised algorithm and GEMS3K numerical kernel for coupled simulation codes. *Comput Geosci* 17, 1-24.
- Kyser, K. and Hiatt, E.E. (2003) Fluids in sedimentary basins: an introduction. *J Geochemi Explor* 80, 139-149.
- Lambert, I. and Clever, H.L. (1992a) 2 - The solubility of magnesium hydroxide in aqueous systems, in: Lambert, I., Clever, H.L. (Eds.), *Alkaline Earth Hydroxides in Water and Aqueous Solutions*. Pergamon, Amsterdam, pp. 49-111.
- Lambert, I. and Clever, H.L. (1992b) 3 - The solubility of calcium hydroxide in aqueous systems, in: Lambert, I., Clever, H.L. (Eds.), *Alkaline Earth Hydroxides in Water and Aqueous Solutions*. Pergamon, Amsterdam, pp. 112-247.
- Langmuir, D. (1968) Stability of calcite based on aqueous solubility measurements. *Geochim Cosmochim Acta* 32, 835-851.
- Larson, T.E., Sollo, F.W. and McGruk, F.F. (1973) Complexes affecting the solubility of calcium carbonate in water. Illinois State Water Survey
- Lee, S.H. (2004) Molecular dynamics simulation studies of the limiting conductances of CaCl₂ using extended simple point charge and revised polarizable models. *Molecular Simulation* 30, 669-678.
- Li, D. and Duan, Z. (2007) The speciation equilibrium coupling with phase equilibrium in the H₂O–CO₂–NaCl system from 0 to 250 °C, from 0 to 1000 bar, and from 0 to 5 molality of NaCl. *Chemical Geology* 244, 730-751.
- Lothenbach, B. and Winnefeld, F. (2006) Thermodynamic modelling of the hydration of Portland cement. *Cement and Concrete Research* 36, 209-226.
- Lothenbach, B., Pelletier-Chaignat, L. and Winnefeld, F. (2012) Stability in the system CaO–Al₂O₃–H₂O. *Cement and Concrete Research* 42, 1621-1634.
- Luce, R.W., Cygan, G.L., Hemley, J.J. and D'Angelo, W.M. (1985) Some mineral stability relations in the system CaO–MgO–SiO₂–H₂O–HCl. *Geochim Cosmochim Acta* 49, 525-538.
- Majer, V. and Štulík, K. (1982) A study of the stability of alkaline-earth metal complexes with fluoride and chloride ions at various temperatures by potentiometry with ion-selective electrodes. *Talanta* 29, 145-148.
- Malinin, S.D. and Kanukov, A.B. (1972) The solubility of calcite in homogeneous H₂O–NaCl–CO₂ systems in the 200–600 degrees C temperature interval. *Geochemistry International* 8, 668-679.
- Manning, C.E., Shock, E.L. and Sverjensky, D.A. (2013) The Chemistry of Carbon in Aqueous Fluids at Crustal and Upper-Mantle Conditions: Experimental and Theoretical Constraints. *Reviews in Mineralogy and Geochemistry* 75, 109-148.
- Marshall, W.L. and Franck, E.U. (1981) Ion product of water substance, 0–1000 °C, 1–10,000 bars New International Formulation and its background. *Journal of Physical and Chemical Reference Data* 10, 295-304.
- Martynova, O.I., Vasina, L.G. and Pozdniakova, S.A. (1974) Dissociation constants of certain scale forming salts. *Desalination* 15, 259-265.
- McGee, K.A. and Hostetler, P.B. (1975) Studies in the system MgO–SiO₂–CO₂–H₂O (IV); The stability of MgOH⁺ from 10° to 90°C. *Am J Sci* 275, 304-317.
- McGee, K.A. and Hostetler, P.B. (1977) Activity product constants of brucite from 10° to 90°C. *J. Res. U. S. Geol. Surv.* 5, 227-233.
- Meinert, L.D., Hedenquist, J.W., Satoh, H. and Matsuhisa, Y. (2003) Formation of Anhydrous and Hydrous Skarn in Cu–Au Ore Deposits by Magmatic Fluids. *Economic Geology* 98, 147-156.
- Méndez De Leo, L.P. and Wood, R.H. (2005) Conductance study of association in aqueous CaCl₂, Ca(CH₃COO)₂, and Ca(CH₃COO)₂·nCH₃COOH from 348 to 523 K at 10 MPa. *J Phys Chem B* 109, 14243-24250.

- Millero, F.J. (1982) The effect of pressure on the solubility of minerals in water and seawater. *Geochim Cosmochim Acta* 46, 11-22.
- Miron, G.D., Neuhoff, P.S. and Amthauer, G. (2012) Low-Temperature Hydrothermal Metamorphic Mineralization of Island-Arc Volcanics, South Apuseni Mountains, Romania. *Clays and Clay Minerals* 60, 1-17.
- Miron, G., Wagner, T., Wälle, M. and Heinrich, C. (2013) Major and trace-element composition and pressure-temperature evolution of rock-buffered fluids in low-grade accretionary-wedge metasediments, Central Alps. *Contr Min Pet* 165, 981-1008.
- Miron, G.D., Kulik, D.A., Dmytrieva, S.V. and Wagner, T. (2015) GEMSFITS: Code package for optimization of geochemical model parameters and inverse modeling. *Appl Geochem* 55, 28-45.
- Miron, G.D., Wagner, T., Kulik, D.A. and Heinrich, C.A. (2016) Internally consistent thermodynamic data for aqueous species in the system Na-K-Al-Si-O-H-Cl. Accepted. <http://dx.doi.org/10.1016/j.gca.2016.04.026>
- Morrison, T.J. and Billett, F. (1952) The salting-out of non-electrolytes. Part II. The effect of variation in non-electrolyte. *Journal of the Chemical Society (Resumed)*, 3819-3822.
- Nakayama, F.S. (1970) Sodium bicarbonate and carbonate ion pairs and their relation to the estimation of the first and second dissociation constants of carbonic acid. *The Journal of Physical Chemistry* 74, 2726-2728.
- Nakayama, F.S. (1971) Thermodynamic functions for the dissociation of NaHCO_3^0 , NaCO_3^- , H_2CO_3 and HCO_3^- . *Journal of Inorganic and Nuclear Chemistry* 33, 1287-1291.
- Newton, R.C. and Manning, C.E. (2002) Experimental determination of calcite solubility in H_2O -NaCl solutions at deep crust/upper mantle pressures and temperatures: Implications for metasomatic processes in shear zones. *American Mineralogist* 87, 1401-1409.
- Nighswander, J.A., Kalogerakis, N. and Mehrotra, A.K. (1989) Solubilities of carbon dioxide in water and 1 wt. % sodium chloride solution at pressures up to 10 MPa and temperatures from 80 to 200°C. *Journal of Chemical & Engineering Data* 34, 355-360.
- Nordstrom, D.K. (2013) Improving Internal Consistency of Standard State Thermodynamic Data for Sulfate Ion, Portlandite, Gypsum, Barite, Celestine, and Associated Ions. *Procedia Earth and Planetary Science* 7, 624-627.
- Oelkers, E.H., Helgeson, H.C., Shock, E.L., Sverjensky, D.A., Johnson, J.W. and Pokrovskii, V.A. (1995) Summary of the Apparent Standard Partial Molal Gibbs Free Energies of Formation of Aqueous Species, Minerals, and Gases at Pressures 1 to 5000 Bars and Temperatures 25 to 1000 °C. *Journal of Physical and Chemical Reference Data* 24, 1401-1560.
- Oscarson, J.L., Gillespie, S.E., Chen, X., Schuck, P.C. and Izatt, R.M. (2001) Enthalpies of dilution of aqueous solutions of HCl, MgCl_2 , CaCl_2 , and BaCl_2 at 300, 325, and 350°C. *Journal of Solution Chemistry* 30, 31-53.
- Palmer, D.A. and Wesolowski, D.J. (1993) Aluminum speciation and equilibria in aqueous solution: III. Potentiometric determination of the first hydrolysis constant of aluminum(III) in sodium chloride solutions to 125°C. *Geochim Cosmochim Acta* 57, 2929-2938.
- Palmer, D.A. and Wesolowski, D.J. (1997) Potentiometric measurements of the first hydrolysis quotient of magnesium(II) to 250°C and 5 molal ionic strength (NaCl). *Journal of Solution Chemistry* 26, 217-232.
- Park, S., Kim, H., Kim, K., Lee, J. and Lho, D.-s. (1999) Spectroscopic measurement of the acid dissociation constant of 2-naphthol and the second dissociation constant of carbonic acid at elevated temperatures. *Physical Chemistry Chemical Physics* 1, 1893-1898.
- Parker, V.B., Wagman, D.D. and Evans, W.H. (1971) Selected Values of Chemical Thermodynamic Properties. Tables for the alkaline earth elements., NBS Technical Note. National Bureau of Standards U.S., Washington, p. 119.
- Patterson, C.S., Busey, R.H. and Mesmer, R.E. (1984) Second ionization of carbonic acid in NaCl media to 250°C. *Journal of Solution Chemistry* 13, 647-661.
- Patterson, C.S., Slocum, G.H., Busey, R.H. and Mesmer, R.E. (1982) Carbonate equilibria in hydrothermal systems: First ionization of carbonic acid in NaCl media to 300°C. *Geochim Cosmochim Acta* 46, 1653-1663.
- Pitzer, K.S. (1973) Thermodynamics of electrolytes. I. Theoretical basis and general equations. *The Journal of Physical Chemistry* 77, 268-277.

- Pizzarello, S. and Shock, E. (2010) The Organic Composition of Carbonaceous Meteorites: The Evolutionary Story Ahead of Biochemistry. *Cold Spring Harbor Perspectives in Biology* 2.
- Plank, T. and Langmuir, C.H. (1998) The chemical composition of subducting sediment and its consequences for the crust and mantle. *Chemical Geology* 145, 325-394.
- Plummer, L.N. and Busenberg, E. (1982) The solubilities of calcite, aragonite and vaterite in CO₂-H₂O solutions between 0 and 90°C, and an evaluation of the aqueous model for the system CaCO₃-CO₂-H₂O. *Geochim Cosmochim Acta* 46, 1011-1040.
- Plyasunov, A.V. (2015) Correlation and prediction of thermodynamic properties of nonelectrolytes at infinite dilution in water over very wide temperature and pressure ranges (2000 K and 10 GPa). *Geochim Cosmochim Acta*. 168, 236-260.
- Plyasunov, A.V. and Shock, E.L. (2001) Correlation strategy for determining the parameters of the revised Helgeson-Kirkham-Flowers model for aqueous nonelectrolytes. *Geochim Cosmochim Acta* 65, 3879-3900.
- Pokrovski, G.S., Schott, J., Harrichoury, J.C. and Sergeev, A.S. (1996) The stability of aluminum silicate complexes in acidic solutions from 25 to 150°C. *Geochim Cosmochim Acta* 60, 2495-2501.
- Popp, R.K. and Frantz, J.D. (1979) Mineral solution equilibria—II. An experimental study of mineral solubilities and the thermodynamic properties of aqueous CaCl₂ in the system CaO-SiO₂-H₂O-HCl. *Geochim Cosmochim Acta* 43, 1777-1790.
- Rafflaub, J. (1960) Untersuchungen über die magnesium komplex verbindungen von oxalat und carbonat. *Helv Chim Acta* 43, 629-634.
- Ramette, R.W. (1986) Copper(II) complexes with chloride ion. *Inorganic Chemistry* 25, 2481-2482.
- Rard, J.A. and Clegg, S.L. (1997) Critical Evaluation of the Thermodynamic Properties of Aqueous Calcium Chloride. 1. Osmotic and Activity Coefficients of 0–10.77 mol·kg⁻¹ Aqueous Calcium Chloride Solutions at 298.15 K and Correlation with Extended Pitzer Ion-Interaction Models. *Journal of Chemical & Engineering Data* 42, 819-849.
- Read, A.J. (1975) The first ionization constant of carbonic acid from 25 to 250°C and to 2000 bar. *Journal of Solution Chemistry* 4, 53-70.
- Reardon, E.J. and Langmuir, D. (1974) Thermodynamic properties of the ion pairs MgCO₃⁰ and CaCO₃⁰ from 10 to 50°C. *Am J Sci* 274, 599-612.
- Ridgwell, A. and Zeebe, R.E. (2005) The role of the global carbonate cycle in the regulation and evolution of the Earth system. *Earth and Planetary Science Letters* 234, 299-315.
- Robie, R.A. and Hemingway, B.S. (1995) Thermodynamic Properties of Minerals and Related Substances at 298.15 K and 1 Bar (105 Pascals) Pressure and at Higher Temperatures. U.S. Government Printing Office.
- Roselle, G.T. and Baumgartner, L.P. (1995) Experimental determination of anorthite solubility and calcium speciation in supercritical chloride solutions at 2 kb from 400 to 600°C. *Geochim Cosmochim Acta* 59, 1539-1549.
- Ruaya, J.R. (1988) Estimation of instability constants of metal chloride complexes in hydrothermal solutions up to 300°C. *Geochim Cosmochim Acta* 52, 1983-1996.
- Ryzhenko, B.N. (1963) Determination of dissociation constants of carbonic acid and the degree of hydrolysis of the CO₃⁻² and HCO₃⁻ ions in solutions of alkali carbonates and bicarbonates at elevated temperatures. *Geochem. Int.* 2, 151–163.
- Saccoccia, P.J. and Seyfried Jr, W.E. (1990) Talc-quartz equilibria and the stability of magnesium chloride complexes in NaCl-MgCl₂ solutions at 300, 350, and 400°C, 500 bars. *Geochim Cosmochim Acta* 54, 3283-3294.
- Salvi, S., Pokrovski, G.S. and Schott, J. (1998) Experimental investigation of aluminum-silica aqueous complexing at 300°C. *Chemical Geology* 151, 51-67.
- Santschi, P.H. and Schindler, P.W. (1974) Complex formation in the ternary systems Ca-H₄SiO₄-H₂O and Mg-H₄SiO₄-H₂O. *Journal of the Chemical Society, Dalton Transactions*, 181-184.
- Schulte, M.D., Shock, E.L. and Wood, R.H. (2001) The temperature dependence of the standard-state thermodynamic properties of aqueous nonelectrolytes. *Geochim Cosmochim Acta* 65, 3919-3930.
- Seewald, J.S. and Seyfried Jr, W.E. (1991) Experimental determination of portlandite solubility in H₂O and acetate solutions at 100–350 °C and 500 bars: Constraints on calcium hydroxide and calcium acetate complex stability. *Geochim Cosmochim Acta* 55, 659-669.

- Segnit, E.R., Holland, H.D. and Biscardi, C.J. (1962) The solubility of calcite in aqueous solutions—I The solubility of calcite in water between 75° and 200° at CO₂ pressures up to 60 atm. *Geochim Cosmochim Acta* 26, 1301-1331.
- Sephton, M.A. and Hazen, R.M. (2013) On the Origins of Deep Hydrocarbons. *Reviews in Mineralogy and Geochemistry* 75, 449-465.
- Seward, T.M. (1974) Determination of the first ionization constant of silicic acid from quartz solubility in borate buffer solutions to 350°C. *Geochim Cosmochim Acta* 38, 1651-1664.
- Shin, C. and Criss, C.M. (1979) Standard enthalpies of formation of anhydrous and aqueous magnesium chloride at 298.15 K. *The Journal of Chemical Thermodynamics* 11, 663-666.
- Shock, E.L. and Helgeson, H.C. (1988) Calculation of the thermodynamic and transport properties of aqueous species at high pressures and temperatures: Correlation algorithms for ionic species and equation of state predictions to 5 kb and 1000°C. *Geochim Cosmochim Acta* 52, 2009-2036.
- Shock, E.L. and Helgeson, H.C. (1990) Calculation of the thermodynamic and transport properties of aqueous species at high pressures and temperatures: Standard partial molal properties of organic species. *Geochim Cosmochim Acta* 54, 915-945.
- Shock, E.L., Helgeson, H.C. and Sverjensky, D.A. (1989) Calculation of the thermodynamic and transport properties of aqueous species at high pressures and temperatures: Standard partial molal properties of inorganic neutral species. *Geochim Cosmochim Acta* 53, 2157-2183.
- Shock, E.L., Oelkers, E.H., Johnson, J.W., Sverjensky, D.A. and Helgeson, H.C. (1992) Calculation of the thermodynamic properties of aqueous species at high pressures and temperatures. Effective electrostatic radii, dissociation constants and standard partial molal properties to 1000°C and 5 kbar. *Journal of the Chemical Society, Faraday Transactions* 88.
- Shock, E.L., Sassani, D.C., Willis, M. and Sverjensky, D.A. (1997) Inorganic species in geologic fluids: Correlations among standard molal thermodynamic properties of aqueous ions and hydroxide complexes. *Geochim Cosmochim Acta* 61, 907-950.
- Shvarov, Y. (2015) A suite of programs, OptimA, OptimB, OptimC, and OptimS compatible with the Unitherm database, for deriving the thermodynamic properties of aqueous species from solubility, potentiometry and spectroscopy measurements. *Appl Geochem* 55, 17-27.
- Siebert, R.M. and Hostetler, P.B. (1977) The stability of the magnesium bicarbonate ion pair from 10° to 90°C. *Am J Sci* 277, 697-715.
- Sipos, P., Bolden, L., Hefter, G. and May, P.M. (2000) Raman Spectroscopic Study of Ion Pairing of Alkali Metal Ions with Carbonate and Sulfate in Aqueous Solutions. *Australian Journal of Chemistry* 53, 887-890.
- Staudigel, H. (2003) Hydrothermal alteration processes in the oceanic crust, in: Rudnick, R.L., Holland, H.D., Turekian, K.K. (Eds.), *Treatise on Geochemistry*. Elsevier-Pergamon, Oxford, pp. 511-535.
- Stefánsson, A., Bénézech, P. and Schott, J. (2013) Carbonic acid ionization and the stability of sodium bicarbonate and carbonate ion pairs to 200°C – A potentiometric and spectrophotometric study. *Geochim Cosmochim Acta* 120, 600-611.
- Stefánsson, A., Bénézech, P. and Schott, J. (2014) Potentiometric and spectrophotometric study of the stability of magnesium carbonate and bicarbonate ion pairs to 150°C and aqueous inorganic carbon speciation and magnesite solubility. *Geochim Cosmochim Acta* 138, 21-31.
- Stephenson, C.C. (1946) The Standard Free Energy of Formation and Entropy of the Aqueous Magnesium Ion. *J Am Chem Soc* 68, 721-722.
- Stock, D.I. and Davies, C.W. (1948) The second dissociation constant of magnesium hydroxide. *T Faraday Soc* 44, 856-859.
- Sverjensky, D., Shock, E. and Helgeson, H. (1997) Prediction of the thermodynamic properties of aqueous metal complexes to 1000 C and 5 kb. *Geochim Cosmochim Acta* 61, 1359-1412.
- Tagirov, B.R., Zotov, A.V. and Akinfiyev, N.N. (1997) Experimental study of dissociation of HCl from 350 to 500°C and from 500 to 2500 bars: Thermodynamic properties of HCl°(aq). *Geochim Cosmochim Acta* 61, 4267-4280.

- Tagirov, B. and Schott, J. (2001) Aluminum speciation in crustal fluids revisited. *Geochim Cosmochim Acta* 65, 3965-3992.
- Takenouchi, S. and Kennedy, G.C. (1964) The binary system H₂O-CO₂ at high temperatures and pressures. *Am J Sci* 262, 1055-1074.
- Tanger, J.C. and Helgeson, H.C. (1988) Calculation of the thermodynamic and transport properties of aqueous species at high pressures and temperatures; revised equations of state for the standard partial molal properties of ions and electrolytes. *Am J Sci* 288, 19-98.
- Thien, B.M.J., Kosakowski, G. and Kulik, D.A. (2015) Differential alteration of basaltic lava flows and hyaloclastites in Icelandic hydrothermal systems. *Geothermal Energy* 3, 1-32.
- Thoenen, T., Hummel, W., Berner, U. and Curti, E. (2014) The PSI/Nagra Chemical Thermodynamic Database 12/07. Paul Scherrer Institut, Villigen PSI, Switzerland.
- Tödheide, K. and Franck, E.U. (1963) Das Zweiphasengebiet und die kritische Kurve im System Kohlendioxid-Wasser bis zu Drucken von 3500 bar, *Zeitschrift für Physikalische Chemie*, p. 387.
- Turner, D.R., Whitfield, M. and Dickson, A.G. (1981) The equilibrium speciation of dissolved components in freshwater and sea water at 25°C and 1 atm pressure. *Geochim Cosmochim Acta* 45, 855-881.
- Visscher, A.D. and Vanderdeelen, J. (2012) IUPAC-NIST Solubility Data Series. 95. Alkaline Earth Carbonates in Aqueous Systems. Part 2. Ca. *Journal of Physical and Chemical Reference Data* 41, 023105-023105-023137.
- Wagman, D.D., Evans, W.H., Parker, V.B., Schumm, R.H., Halow, I., Bailey, S.M., Churney, K.L. and Nuttal, R.L. (1982) 1982, The NBS tables of chemical thermodynamic properties. Selected values for inorganic and C₁, and C₂ organic substances in SI units. *Jour. Phys. Chem. Ref. Data* 11, 392.
- Wagner, T., Kulik, D.A., Hingerl, F.F. and Dmytrieva, S.V. (2012) GEM-Selektor geochemical modeling package: TSolMod library and data interface for multicomponent phase models. *The Canadian Mineralogist* 50, 1173-1195.
- Walker, C.S., Sutou, S., Oda, C., Mihara, M. and Honda, A. (2016) Calcium silicate hydrate (C-S-H) gel solubility data and a discrete solid phase model at 25 °C based on two binary non-ideal solid solutions. *Cement and Concrete Research* 79, 1-30.
- Walther, J.V. (1986) Experimental determination of portlandite and brucite solubilities in supercritical H₂O. *Geochim Cosmochim Acta* 50, 733-739.
- Walther, J.V. and Long, M.I. (1986) Experimental determination of calcite solubilities in supercritical H₂O. *Int. Symp. Water-Rock Interaction* 5, 609-611.
- Wiebe, R. and Gaddy, V.L. (1939) The Solubility in Water of Carbon Dioxide at 50, 75 and 100°, at Pressures to 700 Atmospheres. *J Am Chem Soc* 61, 315-318.
- Williams-Jones, A.E. and Seward, T.M. (1989) The stability of calcium chloride ion pairs in aqueous solutions at temperatures between 100 and 360°C. *Geochim Cosmochim Acta* 53, 313-318.
- Wilson, A.M., Sanford, W., Whitaker, F. and Smart, P. (2001) Spatial Patterns Of Diagenesis during Geothermal Circulation in Carbonate Platforms. *Am J Sci* 301, 727-752.
- Wimberley, P.D., Siggaard-Andersen, O., Fogh-Andersen, N. and Boink, A.B. (1985) Are sodium bicarbonate and potassium bicarbonate fully dissociated under physiological conditions? *Scandinavian journal of clinical and laboratory investigation* 45, 7-10.
- Xie, Z. and Walther, J.V. (1993a) Quartz solubilities in NaCl solutions with and without wollastonite at elevated temperatures and pressures. *Geochim Cosmochim Acta* 57, 1947-1955.
- Xie, Z. and Walther, J.V. (1993b) Wollastonite + quartz solubility in supercritical NaCl aqueous solutions. *Am J Sci* 293, 235-255.
- Xiong, Y. (2008) Thermodynamic Properties of Brucite Determined by Solubility Studies and Their Significance to Nuclear Waste Isolation. *Aquatic Geochemistry* 14, 223-238.
- Zawisza, A. and Malesinska, B. (1981) Solubility of carbon dioxide in liquid water and of water in gaseous carbon dioxide in the range 0.2-5 MPa and at temperatures up to 473 K. *Journal of Chemical & Engineering Data* 26, 388-391.

5. Outlook

This study presents a set of tools and methods as a proof of concept for deriving an internally consistent thermodynamic database for hydrothermal fluid rock interaction. In the process the mineral thermodynamic properties were taken as fixed from the database of Holland and Powell (1998), which was assumed to be fully consistent. A large dataset of solubility experiments and also experiments on speciation equilibria was critically assessed and used to optimize the properties of ions and aqueous complexes in the core system Na-K-Al-Si-O-H-Cl. Then the system was extended to include Ca, Mg, and C. The standard state Gibbs energies of formation of aqueous ions and complexes were optimized against the fixed properties of the mineral phases. The internally-consistent Holland-Powell mineral thermodynamic dataset was accepted as such, as a basis for our study, because it is comprehensive, current, well maintained and equipped with high-quality activity models for a wide range of rock-forming mineral solid-solutions. From a conceptual point of view, it is desirable that the mineral phase equilibria stability data and element partitioning data would be added to the experimental database and the optimization process. **The standard-state properties of minerals, aqueous species and complexes can then be simultaneously optimized to create a next-generation internally consistent dataset for fluid-mineral equilibria.** This could further help resolve the disagreement between the electrode potential measurements for the properties of some ions (e.g. potassium and sodium) and properties of the minerals. **To achieve such a goal, it is important to first reach a more complete understanding of the complexity of aqueous solutions.** No petrologist would want their database for minerals be perturbed and have errors introduced due to missing and unknown complexes from the aqueous phase. At ambient conditions, properties of dilute and concentrated solutions can be readily explained considering full ion dissociation and using ion-interaction models such as the one proposed by Pitzer (Pitzer et al., 1999). However, Rard and Clegg (1997) concluded from the large volume of literature data they reviewed on the CaCl₂ electrolyte system, that this system can only be represented if they explicitly included the formation of a CaCl⁺ ion pair. In concentrated and mixed electrolyte solutions, it is often difficult to distinguish between the nonideal interactions among ions and the ion pair formation (Ramette, 1986).

It is known that with increasing temperature, there is an increase in ion pairing and complex formation. This is due to a decrease in the dielectric constant of water which leads to an increase in the electrostatic attraction between oppositely charged ions (Anderson, 2005; Davies, 1962; Dolejš and Manning, 2010; Helgeson et al., 1981). Ion pairing and complex formation is embedded in the HKF model. Formation of different aqueous complexes was inferred from solubility studies (e.g. Bénézech et al., 2013; Manning et al., 2008; Newton and Manning, 2003; Stefánsson et al., 2014; Tagirov et al., 2002; Wohlers et al., 2011). However, more convincing information comes from spectroscopic studies (e.g. Brugger et al., 2010; Facq et al., 2014; Frantz et al., 1994; Fulton et al., 2006; Jones et al., 2011; Manning et al., 2008; Mookherjee et al., 2014; Newton and Manning, 2003; Pokrovski and Dubessy, 2015; Pokrovski and Dubrovinsky, 2011; Stefánsson et al., 2013; Tooth et al., 2013; Zotov and Keppler, 2002).

New spectroscopic studies involving in situ X-ray absorption spectroscopy (XANES and EXAFS), UV-Vis, and Raman are used for identifying metal complexation at different temperature

and pressure conditions. These combined with solubility studies are used to obtain the thermodynamic properties of the identified species (e.g. Brugger et al., 2010; Tooth et al., 2013). The presence of species like S_3^- at hydrothermal conditions was recently identified using in situ Raman spectroscopy (Pokrovski and Dubrovinsky, 2011). This changed the idea at that time that sulfate, sulfide, and sulfur dioxide are the major sulfur compounds at these conditions. New studies report that this species accounts for up to 50% of the total sulfur at 600-700 °C, thus having a large impact on metal mobility and ore deposit formation (Pokrovski and Dubessy, 2015). Tooth et al. (2013) used spectroscopic (XANES and EXAFS) and solubility experiments related to bismuth oxide. They used the data to extract new standard state properties and HKF parameters for the $Bi(OH)_3^0$ species. In their calculations, they used these new properties, and obtained solubilities 3 orders of magnitude larger than those predicted with the estimated parameters of Shock et al. (1997).

When Shock et al. (1997) performed their HKF parameter estimation and correlation, limited data was available for many of the considered complexes. **For many elements this situation did not improve and more experimental data is needed to further test the predictions of the HKF parameters and improve them as necessary.** Brugger et al. (2010) gives an example where the identification of $FeCl_4^{2-}$ species made it possible to explain the sharp drop in Fe solubility between 350 and 250 °C. This could not be simulated before without considering the tetrahedral iron species. In the case of Cu transport in chloride solutions, X-ray absorption spectroscopic data and ab-initio XANES calculations of Brugger et al. (2007) pointed out that $CuCl_2^-$ and $CuCl_3^{2-}$ are important at hydrothermal conditions, and that with increasing temperature, $CuCl_3^{2-}$ decreases in stability but it is not replaced by $CuCl_4^{2-}$ as was previously believed (Liu et al., 2002). Previous observations were now explained not by a change in speciation, but by a change in the solvent properties and coordination of water around the existing species (Brugger et al., 2007). It was also noted that the solubility trend measured close to the critical conditions shows an opposite trend, as compared with calculations using predicted HKF parameters (Brugger et al., 2010). All these examples point out to the usefulness of spectroscopic methods in improving our understanding of the aqueous speciation and also of the solvent properties. **Similar in situ solubility and spectroscopic studies are needed to identify possible complexes in hydrothermal fluids and extract thermodynamic data related to the identified species for major elements such as sodium, potassium, calcium, magnesium, silica, aluminium, chlorine and carbon.**

The demand is high to have a thermodynamic model together with accurate thermodynamic data that works from ambient to moderate conditions (hydrothermal ore deposition), but also at extreme pressure and temperature conditions (mantle conditions). New experimental data, theoretical relations, and information from molecular dynamics and ab-initio calculations can be further used to develop new equations of state and correlations between standard state properties of aqueous electrolytes (Akinfiev and Diamond, 2003; Akinfiev and Diamond, 2009; Dolejš and Manning, 2010; Plyasunov, 2015) or can be used to revise existing models such as the HKF model (Sue et al., 2002; Sverjensky et al., 2014). All the models have their advantages and limitations, but until now the HKF framework proved to be the most useful because of the broad predictive

capabilities over a wide range of conditions (Dolejš and Manning, 2010; Sverjensky et al., 2014). Under extreme conditions, the aqueous speciation is still poorly understood, and advances in spectroscopic techniques and new experiments will be important in identifying or denying the presence of, for example, complex polynuclear species. **For generating an internally consistent thermodynamic database that extends to extreme pressure and temperature conditions, it is essential to know and understand the aqueous solution speciation, most important to have an idea on the probable complexes that form at this conditions.** For example, Wohlers et al. (2011) find it necessary to use polymeric Na-Al-Si-bearing complexes to explain the excess in solubility predicted from the currently known ion, ion pairs, and monomer species for conditions to 600 °C and 22.5 kbar. In other cases, such as corundum solubility in alkaline solutions up to 1000 °C and 20 kbar, it was found that the known aluminum species $\text{Al}(\text{OH})_4^-$ and $\text{Al}(\text{OH})_3^0$ satisfactorily explain the measurements, and there was no indication (in the Raman measurements) for any aluminium species polymerization (Wohlers and Manning, 2009). This does not preclude the possibility that these polymers do form at even more extreme conditions.

An important tool to improve our understanding of the aqueous speciation and properties at elevated temperature and pressure conditions are molecular dynamics simulations and ab-initio calculations (see: Chialvo and Vlcek, 2015; Driesner et al., 1998; Vlcek and Chialvo, 2015). Wohlers et al. (2011) used ab-initio calculations to gain insight into the geometry and energetics of possible aluminate species, which helped them interpret their acquired in situ Raman spectroscopic data. Yui et al. (2010) performed molecular dynamics simulations for aqueous NaCl solutions at several temperatures and densities from ambient to supercritical conditions. The authors analyzed the hydration structure of the ion-pair and the interactions between ions and water in different hydration shells. They used their data to calculate logKs of association for possible “contact ion pairs” and “solvent separated ion pairs”. Their results roughly agree with ion pair association constants derived from conductance measurements (Gruszkiewicz and Wood, 1997; Ho et al., 2000; Ho et al., 1994; Zimmerman et al., 1995; Zimmerman et al., 2007). **With the increasing accuracy of such simulations, combined with conductance experiments, these type of studies will be essential in determination of the stability of different ion pairs such as earth alkali metals chloride, hydroxide, and carbonate ion pairs.**

In the HKF formulation, the g-function is defined such that the effective electrostatic ion radius decreases with temperature by the same amount (Tanger and Helgeson, 1988). Molecular dynamic simulations (Driesner et al., 1998) and EXAFS studies (Seward et al., 1999) showed that the ion hydration shell may contract or expand depending on the type of the ion, concentration, and temperature, and it can be density independent. For applications to pressures above the previous HKF limit, the models for the dielectric properties of the water solvent had to be revised, and new correlations for the parameters governing the pressure dependence were proposed (Sverjensky et al., 2014). Sue et al. (2002) have revised the HKF model to predict equilibrium constants for metal salt dissociation and metal oxide dissolution. The authors reformulated the HKF equations as a function of water density, removed the standard state volume and the pressure related parameters, and re-evaluated the g-function to expand the applicability to the near critical region (e.g.

Masoodiyeh et al., 2014). The dielectric property of water is still an essential part of their modified HKF model. The necessary parameters are Gibbs energy, enthalpy, heat capacity and conventional Born coefficient at reference state.

While the HKF model was developed using the Born solvation theory for charged species, it was empirically extended to nonelectrolytes/neutral species as well (Shock et al., 1989). However, it has been showed from theoretical and experimental consideration that the Bron-type model is not suitable for calculating and predicting the thermodynamic properties of neutral species, especially close to the critical conditions but also at supercritical conditions, (Akinfiev and Diamond, 2003; Plyasunov, 2015; Plyasunov and Shock, 2001). Plyasunov (2015) compared different sets of HKF parameters from the literature with experimental and molecular dynamics data and reached the conclusion that “*no single set of the HKF parameters for aqueous CO₂ is able to satisfactorily predict its thermodynamic properties over the whole T–P range of interest for hydrothermal geochemistry*”. **Complementary models for aqueous nonelectrolytes are needed.** A different model for nonelectrolytes was developed by Akinfiev and Diamond (2003) and can be used together with the HKF which handles the charged species.

Future studies should pursue a fruitful interplay between fundamental thermodynamics, molecular simulation, and experiment. This will help the development of comprehensive equations of state that could link molecular scale to macroscale thermodynamics thus making it possible for a smooth transition between aqueous, gas, and possibly melt phase. Understanding the chemical mechanisms at a molecular level has applications for determining mineral kinetics, dissolution/precipitation rate laws (Driesner et al., 1998; Seward and Driesner, 2004). With the development of molecular level studies, larger importance is given to intricate processes related to the solvation phenomena, such as changes in the coordination and hydration shell geometries of the ions and complexes. These processes should have a large impact on the formulation of next-generation equations of state (Chialvo and Vlcek, 2015; Seward and Driesner, 2004). **While the computational methods of molecular dynamics cannot reproduce all the aqueous solution properties with the desired level of accuracy, future developments on the theoretical side but also the increase in computational power, will help to improve the results.**

Although the present study could not conclusively solve many of the existing inconsistencies in the aqueous species thermodynamic data, it highlights some of the issues that have to be resolved in order to develop an improved thermodynamic database for hydrothermal water-rock interaction.

Chlorine is an important component in all crustal fluids, present in magmatic, metamorphic and sedimentary fluids. It strongly partitions into the aqueous phase relative to the minerals during fluid-rock interaction. Chlorine-bearing fluids can also lead to formation of Cl-enriched minerals (Kullerud et al., 2001). Chlorine is an important ligand for element transport (particularly transition metals), it forms aqueous complexes especially with alkalis and alkali-earth elements, and influences the pH and ionic strength of the aqueous solution. Thus, chlorine has a great impact on the properties of the fluid. At supercritical conditions, chlorine forms an ion pair with the hydrogen ion, HCl⁰. The properties of HCl⁰ are essential in modeling natural fluid speciation and composition at supercritical conditions (Frantz and Marshall, 1984; Hauzenberger et al., 2001;

Luce et al., 1985; Pak et al., 2003; Roselle and Baumgartner, 1995; Sverjensky et al., 1991). Even a small error in the G^0 value of this ion pair can lead to large uncertainties in the properties of other aqueous species (see Introduction section 1.5. Uncertainties). Although the study of Tagirov et al. (1997) on the HCl^0 ion pair did a good job of resolving some of the discrepancies between solubility data (Sverjensky et al., 1991) and conductance measurements (Frantz and Marshall, 1984) they did not discuss the uncertainty in their derived parameters. The uncertainties on the ion pair can be still around 0.5 log units or more. This can come from the uncertainties in the HKF model parameters or from the inability of the HKF model to accurately represent nonelectrolyte properties at elevated conditions. **New studies on the HCl^0 ion pair using improved conductance methods and newly developed electrochemical cells are necessary to get the precision and accuracy on the properties of HCl^0 to a minimum (~ 0.1 log units or lower). These studies should be complemented by spectroscopic experiments and molecular simulations.** The same is valid for other chlorine complexes. While the data for sodium and potassium complexes with chlorine is available from conductance and even molecular dynamics, this is not the case for chlorine complexes with calcium and magnesium. **Experimental data is needed for the association constants of species like CaCl_2^0 , MgCl^+ , and MgCl_2^0 to help resolve disagreements between existing conflicting data and improve the predictions of the HKF parameters of these species where there is little or no data available.** Rard and Clegg (1997) reviewed the data related to CaCl_2 solutions and remarked that the association constants for calcium chloride species are very poorly known at elevated temperatures and that the reported values below 100 °C are largely uncertain. Not much has changed since then, for both calcium and magnesium. **Spectroscopic measurements should be used to help identify the presence or absence of higher order associated chlorine species (e.g. CaCl_3^-) which have been proposed based on electrostatic considerations (Oelkers and Helgeson, 1990) but also identified in some systems (e.g. Brugger et al., 2007).** The available data at elevated temperatures for calcium and magnesium hydroxide species needs to be largely improved. When the standard state properties and HKF parameters were estimated by Shock et al. (1997) for these species, not so much data was available. For example, CaOH^+ is highly important in modeling high pH systems like portlandite and calcite solubility at elevated temperatures, or in cementitious systems.

Besides the new data on the stability of various complexes, further experiments on minerals and mineral-assemblage solubilities are necessary. Experiments such as quartz solubility in KOH solutions will help extract the properties of KHSiO_3^0 species which could be responsible for the differences between modeled and measured silica values of aqueous KOH solutions in equilibrium with quartz (see Chapter 3, section 3.7.1). There is scarce experimental data on the solubility of calcium, magnesium, and silicon neutral species, which can have an important role in high pH cementitious systems at ambient conditions, but also at high temperatures as in systems buffered by calcium and magnesium silicates.

Experiments with aluminosilicate mineral assemblages at high temperatures and pressures can help identify and extract the properties of possible Si-Al polymer species. More experiments in chloride systems that cover different hydrothermal (mainly supercritical) conditions are essential

to constrain and test the properties of chlorine complexes which are ubiquitously present in natural fluids. The study of Luce et al. (1985) is a good example of the type of solubility experiments that are essential for optimizing the standard state properties of aqueous species, but which could be also used for constraining the mineral properties. The authors make a strong call for similar future experiments: “*We urge that pertinent phase equilibrium studies be undertaken in appropriate systems to provide more insight into the types of problems we have considered on electrolyte behavior. Both conductance and phase equilibrium studies are valuable complements of one another in expanding our understanding of high temperature solution chemistry*”. Their call has remained largely unanswered. This was probably due to time and analytical difficulties concerning such experiments, although much improvement has been achieved in the experimental and analytical methods since their study.

A closer look should be given to the activity models used for calculating the activity coefficients. The existing parameters for the extended Debye-Hückel activity model are only available for 1:1 electrolytes, and little data is available on 1:2 electrolytes. The model can only calculate the activity coefficients considering just one major background electrolyte. There is also no data on how to treat a system of mixed electrolytes (in comparable amounts). One possibility would be to use an algorithm that determines which electrolytes are in the fluid and then calculates the activity coefficients using a weighted formula based on the relative amount of each electrolyte. Attention should be also given to activity coefficients calculations in systems containing a gas phase, CO₂ saturated, in equilibrium with minerals and electrolyte solutions.

With new advances in our understanding of the aqueous phase at elevated T, P conditions from molecular dynamics, ab-initio calculation, spectroscopic studies, new and improved models can be developed for calculating the properties of the solvent and of the aqueous components. The development in analytical techniques will allow many more solid-fluid phase equilibria experiments to be performed, especially at the conditions necessary to fill many of the gaps in the experimental data. This new experimental data should be subsequently used for a better refinement of the thermodynamic properties and parameters of minerals and aqueous species, to generate the next generation internally consistent database for hydrothermal fluid-rock interaction.

The dynamic method developed in this study for dataset regression together with the GEMSFITS optimization tool allows repeating the optimization procedure whenever new and improved experimental constraints become available, better thermodynamic models are developed, or when more aqueous species and chemical elements are added. The fundamental purpose of geochemical-thermodynamic models is the calculation of multi-component multi-phase equilibria with the best achievable accuracy and precision. The most rigorous test for the quality of a dataset is the comparison with large number of independent experimental solubility, phase equilibria, conductance, potentiometric and spectroscopic data, not the exact numerical value of some of the standard Gibbs energies. The present dataset undoubtedly excels in this rigorous test, and this should become obvious from the many figures in our manuscript that compare calculated with experimental data. No geochemical-thermodynamic dataset that has been published so far is

able to reproduce such a large body of experimental solubility data over such a wide range in pressure, temperature and composition

References

- Akinfiev, N.N. and Diamond, L.W. (2003) Thermodynamic description of aqueous nonelectrolytes at infinite dilution over a wide range of state parameters. *Geochim Cosmochim Acta* 67, 613-629.
- Akinfiev, N.N. and Diamond, L.W. (2009) A simple predictive model of quartz solubility in water-salt-CO₂ systems at temperatures up to 1000 degrees C and pressures up to 1000 MPa. *Geochim Cosmochim Acta* 73, 1597-1608.
- Anderson, G.M. (2005) *Thermodynamics of Natural Systems*. Cambridge University Press, Cambridge.
- Bénézech, P., Stefánsson, A., Gautier, Q. and Schott, J. (2013) Mineral solubility and aqueous speciation under hydrothermal conditions to 300 °C - The carbonate system as an example, *Reviews in Mineralogy and Geochemistry*, pp. 81-133.
- Brugger, J., Etschmann, B., Liu, W., Testemale, D., Hazemann, J.L., Emerich, H., van Beek, W. and Proux, O. (2007) An XAS study of the structure and thermodynamics of Cu(I) chloride complexes in brines up to high temperature (400 °C, 600 bar). *Geochim Cosmochim Acta* 71, 4920-4941.
- Brugger, J., Pring, A., Reith, F., Ryan, C., Etschmann, B., Liu, W., O'Neill, B. and Ngothai, Y. (2010) Probing ore deposits formation: New insights and challenges from synchrotron and neutron studies. *Radiation Physics and Chemistry* 79, 151-161.
- Chialvo, A.A. and Vlcek, L. (2015) Toward the understanding of hydration phenomena in aqueous electrolytes from the interplay of theory, molecular simulation, and experiment. *Fluid Phase Equilib.*
- Davies, C.W. (1962) *Ion Association*, Butterworth, Washington, D.C.
- Dolejš, D. and Manning, C.E. (2010) Thermodynamic model for mineral solubility in aqueous fluids: theory, calibration and application to model fluid-flow systems. *Geofluids* 10, 20-40.
- Driesner, T., Seward, T.M. and Tironi, I.G. (1998) Molecular dynamics simulation study of ionic hydration and ion association in dilute and 1 molal aqueous sodium chloride solutions from ambient to supercritical conditions. *Geochim Cosmochim Acta* 62, 3095-3107.
- Facq, S., Daniel, I., Montagnac, G., Cardon, H. and Sverjensky, D.A. (2014) In situ Raman study and thermodynamic model of aqueous carbonate speciation in equilibrium with aragonite under subduction zone conditions. *Geochim Cosmochim Acta* 132, 375-390.
- Frantz, J.D., Dubessy, J. and Mysen, B.O. (1994) Ion-pairing in aqueous MgSO₄ solutions along an isochore to 500°C and 11 kbar using Raman spectroscopy in conjunction with the diamond-anvil cell. *Chemical Geology* 116, 181-188.
- Frantz, J.D. and Marshall, W.L. (1984) Electrical conductances and ionization constants of salts, acids, and bases in supercritical aqueous fluids; I, Hydrochloric acid from 100° to 700°C and at pressures to 4000 bars. *Am J Sci* 284, 651-667.
- Fulton, J.L., Chen, Y., Heald, S.M. and Balasubramanian, M. (2006) Hydration and contact ion pairing of Ca²⁺ with Cl⁻ in supercritical aqueous solution. *Journal of Chemical Physics* 125.
- Gruskiewicz, M.S. and Wood, R.H. (1997) Conductance of Dilute LiCl, NaCl, NaBr, and CsBr Solutions in Supercritical Water Using a Flow Conductance Cell. *The Journal of Physical Chemistry B* 101, 6549-6559.
- Hauzenberger, C.A., Baumgartner, L.P. and Pak, T.M. (2001) Experimental study on the solubility of the "model"-pelite mineral assemblage albite + K-feldspar + andalusite + quartz in supercritical chloride-rich aqueous solutions at 0.2 GPa and 600°C. *Geochim Cosmochim Acta* 65, 4493-4507.
- Helgeson, H.C., Kirkham, D.H. and Flowers, G.C. (1981) Theoretical prediction of the thermodynamic behavior of aqueous electrolytes by high pressures and temperatures; IV, Calculation of activity coefficients, osmotic coefficients, and apparent molal and standard and relative partial molal properties to 600 degrees C and 5kb. *Am J Sci* 281, 1249-1516.

- Ho, P., Bianchi, H., Palmer, D. and Wood, R. (2000) Conductivity of Dilute Aqueous Electrolyte Solutions at High Temperatures and Pressures Using a Flow Cell. *Journal of Solution Chemistry* 29, 217-235.
- Ho, P., Palmer, D. and Mesmer, R. (1994) Electrical conductivity measurements of aqueous sodium chloride solutions to 600°C and 300 MPa. *Journal of Solution Chemistry* 23, 997-1018.
- Holland, T.J.B. and Powell, R. (1998) An internally consistent thermodynamic data set for phases of petrological interest. *Journal of Metamorphic Geology* 16, 309-343.
- Jones, A.M., Collins, R.N. and Waite, T.D. (2011) Mineral species control of aluminum solubility in sulfate-rich acidic waters. *Geochim Cosmochim Acta* 75, 965-977.
- Kullerud, K., Flaath, K. and Davidsen, B. (2001) High-pressure Fluid–Rock Reactions involving Cl-bearing Fluids in Lower-crustal Ductile Shear Zones of the Flakstadøy Basic Complex, Lofoten, Norway. *Journal of Petrology* 42, 1349-1372.
- Liu, W., Brugger, J., McPhail, D.C. and Spiccia, L. (2002) A spectrophotometric study of aqueous copper(I)–chloride complexes in LiCl solutions between 100 °C and 250 °C. *Geochim Cosmochim Acta* 66, 3615-3633.
- Luce, R.W., Cygan, G.L., Hemley, J.J. and D'Angelo, W.M. (1985) Some mineral stability relations in the system CaO–MgO–SiO₂–H₂O–HCl. *Geochim Cosmochim Acta* 49, 525-538.
- Manning, C.E., Wilke, M., Schmidt, C. and Cauzid, J. (2008) Rutile solubility in albite–H₂O and Na₂Si₃O₇–H₂O at high temperatures and pressures by in-situ synchrotron radiation micro-XRF. *Earth and Planetary Science Letters* 272, 730-737.
- Masoodiyeh, F., Mozdianfard, M.R. and Karimi-Sabet, J. (2014) Solubility estimation of inorganic salts in supercritical water. *The Journal of Chemical Thermodynamics* 78, 260-268.
- Mookherjee, M., Keppler, H. and Manning, C.E. (2014) Aluminum speciation in aqueous fluids at deep crustal pressure and temperature. *Geochim Cosmochim Acta* 133, 128-141.
- Newton, R.C. and Manning, C.E. (2003) Activity coefficient and polymerization of aqueous silica at 800 °C, 12 kbar, from solubility measurements on SiO₂-buffering mineral assemblages. *Contr Min Pet* 146, 135-143.
- Oelkers, E.H. and Helgeson, H.C. (1990) Triple-ion anions and polynuclear complexing in supercritical electrolyte solutions. *Geochim Cosmochim Acta* 54, 727-738.
- Pak, T.M., Hauzenberger, C.A. and Baumgartner, L.P. (2003) Solubility of the assemblage albite+K-feldspar+andalusite+quartz in supercritical aqueous chloride solutions at 650 °C and 2 kbar. *Chemical Geology* 200, 377-393.
- Pitzer, K., Wang, P., Rard, J. and Clegg, S. (1999) Thermodynamics of Electrolytes. 13. Ionic Strength Dependence of Higher-Order Terms; Equations for CaCl₂ and MgCl₂. *Journal of Solution Chemistry* 28, 265-282.
- Plyasunov, A.V. (2015) Correlation and prediction of thermodynamic properties of nonelectrolytes at infinite dilution in water over very wide temperature and pressure ranges (2000 K and 10 GPa). *Geochim Cosmochim Acta*.
- Plyasunov, A.V. and Shock, E.L. (2001) Correlation strategy for determining the parameters of the revised Helgeson–Kirkham–Flowers model for aqueous nonelectrolytes. *Geochim Cosmochim Acta* 65, 3879-3900.
- Pokrovski, G.S. and Dubessy, J. (2015) Stability and abundance of the trisulfur radical ion in hydrothermal fluids. *Earth and Planetary Science Letters* 411, 298-309.
- Pokrovski, G.S. and Dubrovinsky, L.S. (2011) The S₃⁻ ion is stable in geological fluids at elevated temperatures and pressures. *Science* 331, 1052-1054.
- Ramette, R.W. (1986) Copper(II) complexes with chloride ion. *Inorganic Chemistry* 25, 2481-2482.
- Rard, J.A. and Clegg, S.L. (1997) Critical Evaluation of the Thermodynamic Properties of Aqueous Calcium Chloride. 1. Osmotic and Activity Coefficients of 0–10.77 mol·kg⁻¹ Aqueous Calcium Chloride Solutions at 298.15 K and Correlation with Extended Pitzer Ion-Interaction Models. *Journal of Chemical & Engineering Data* 42, 819-849.
- Roselle, G.T. and Baumgartner, L.P. (1995) Experimental determination of anorthite solubility and calcium speciation in supercritical chloride solutions at 2 kb from 400 to 600°C. *Geochim Cosmochim Acta* 59, 1539-1549.
- Seward, T.M. and Driesner, T. (2004) Chapter 5 - Hydrothermal solution structure: Experiments and computer simulations, in: Harvey, D.A.P.F.-P.H. (Ed.), *Aqueous Systems at Elevated Temperatures and Pressures*. Academic Press, London, pp. 149-182.

- Seward, T.M., Henderson, C.M.B., Charnock, J.M. and Driesner, T. (1999) An EXAFS study of solvation and ion pairing in aqueous strontium solutions to 300°C. *Geochim Cosmochim Acta* 63, 2409-2418.
- Shock, E.L., Helgeson, H.C. and Sverjensky, D.A. (1989) Calculation of the thermodynamic and transport properties of aqueous species at high pressures and temperatures: Standard partial molal properties of inorganic neutral species. *Geochim Cosmochim Acta* 53, 2157-2183.
- Shock, E.L., Sassani, D.C., Willis, M. and Sverjensky, D.A. (1997) Inorganic species in geologic fluids: Correlations among standard molal thermodynamic properties of aqueous ions and hydroxide complexes. *Geochim Cosmochim Acta* 61, 907-950.
- Stefánsson, A., Bénézech, P. and Schott, J. (2013) Carbonic acid ionization and the stability of sodium bicarbonate and carbonate ion pairs to 200°C – A potentiometric and spectrophotometric study. *Geochim Cosmochim Acta* 120, 600-611.
- Stefánsson, A., Bénézech, P. and Schott, J. (2014) Potentiometric and spectrophotometric study of the stability of magnesium carbonate and bicarbonate ion pairs to 150°C and aqueous inorganic carbon speciation and magnesite solubility. *Geochim Cosmochim Acta* 138, 21-31.
- Sue, K., Adschiri, T. and Arai, K. (2002) Predictive Model for Equilibrium Constants of Aqueous Inorganic Species at Subcritical and Supercritical Conditions. *Industrial & Engineering Chemistry Research* 41, 3298-3306.
- Sverjensky, D.A., Harrison, B. and Azzolini, D. (2014) Water in the deep Earth: The dielectric constant and the solubilities of quartz and corundum to 60kb and 1200°C. *Geochim Cosmochim Acta* 129, 125-145.
- Sverjensky, D.A., Hemley, J.J. and D'Angelo, W.M. (1991) Thermodynamic assessment of hydrothermal alkali feldspar-mica-aluminosilicate equilibria. *Geochim Cosmochim Acta* 55, 989-1004.
- Tagirov, B., Schott, J., Harrichourry, J.-C. and Salvi, S. (2002) Experimental study of aluminum speciation in fluoride-rich supercritical fluids. *Geochim Cosmochim Acta* 66, 2013-2024.
- Tanger, J.C. and Helgeson, H.C. (1988) Calculation of the thermodynamic and transport properties of aqueous species at high pressures and temperatures; revised equations of state for the standard partial molal properties of ions and electrolytes. *Am J Sci* 288, 19-98.
- Tooth, B., Etschmann, B., Pokrovski, G.S., Testemale, D., Hazemann, J.-L., Grundler, P.V. and Brugger, J. (2013) Bismuth speciation in hydrothermal fluids: An X-ray absorption spectroscopy and solubility study. *Geochim Cosmochim Acta* 101, 156-172.
- Vlcek, L. and Chialvo, A.A. (2015) Single-ion hydration thermodynamics from clusters to bulk solutions: Recent insights from molecular modeling. *Fluid Phase Equilib*.
- Wohlers, A. and Manning, C.E. (2009) Solubility of corundum in aqueous KOH solutions at 700 °C and 1 GPa. *Chemical Geology* 262, 310-317.
- Wohlers, A., Manning, C.E. and Thompson, A.B. (2011) Experimental investigation of the solubility of albite and jadeite in H₂O, with paragonite-quartz at 500 and 600°C, and 1–2.25GPa. *Geochim Cosmochim Acta* 75, 2924-2939.
- Yui, K., Sakuma, M. and Funazukuri, T. (2010) Molecular dynamics simulation on ion-pair association of NaCl from ambient to supercritical water. *Fluid Phase Equilib* 297, 227-235.
- Zimmerman, G.H., Gruszkiewicz, M.S. and Wood, R.H. (1995) New Apparatus for Conductance Measurements at High Temperatures: Conductance of Aqueous Solutions of LiCl, NaCl, NaBr, and CsBr at 28 MPa and Water Densities from 700 to 260 kg m⁻³. *The Journal of Physical Chemistry* 99, 11612-11625.
- Zimmerman, G.H., Scott, P. and Greynolds, W. (2007) A New Flow Instrument for Conductance Measurements at Elevated Temperatures and Pressures: Measurements on NaCl(aq) to 458 K and 1.4 MPa. *Journal of Solution Chemistry* 36, 767-786.
- Zotov, N. and Keppler, H. (2002) Silica speciation in aqueous fluids at high pressures and high temperatures. *Chemical Geology* 184, 71-82.

Curriculum Vitae

George Dan Miron

Personal data

Address	Department of Earth Sciences NW F86.2, ETH Zürich, Clausiusstrasse 25, 8092 Zürich, Switzerland
E-mail	dan.miron@erdw.ethz.ch; mirondanro@yahoo.com
Date of birth	19 July 1985
Nationality	Romanian

Education

2012 – present	Phd in geochemistry, ETH Zürich, Switzerland.
2009 – 2012	MSc in Geology and Geochemistry, ETH Zürich, Switzerland. Graduated with distinction (5.8/6 average).
2004 – 2009	Diploma in Geology, Faculty of Biology and Geology, Babes Bolyai University, Cluj-Napoca, Romania. Graduated 1st out of 35 students (9.78/10 average).
2000 – 2004	High School, “Colegiul National Mihai Viteazul”, Turda, Romania, field of mathematics and computer science.

Phd Thesis: Internally consistent thermodynamic database for fluid-rock interaction: tools, methods and optimization.

MSc Thesis: Fluid composition and mineral equilibrium in low grade metamorphic rocks, Bündnerschiefer, Switzerland. Application of fluid inclusions and petrological modeling.

Diploma Thesis: Low-Temperature Hydrothermal Metamorphic Mineralization of Island-Arc Volcanics, South Apuseni Mountains, Romania.

- LA-ICPMS – sample and instrument handling for fluid inclusions and mineral analysis.
- Microthermometry of fluid inclusions.
- Microprobe – sample preparation, instrument calibration and analysis.
- C++ – intermediate knowledge in programming (Qt Creator).

Interests

- Thermodynamic data: measurements, derivation, databases
- Fluid-rock interaction, solubility experiments, aqueous species, mineral equilibria
- Low-grade metamorphism
- Clays and clay minerals
- Fluid inclusions
- Geochemistry and petrology related subjects

Peer-reviewed articles

George D. Miron, Dmitrii A. Kulik, Svitlana V. Dmytrieva, and Thomas Wagner (2015) GEMSFITS: Code package for optimization of geochemical model parameters and inverse modeling. *Applied Geochemistry*, 55: 28-45.

George D. Miron, Thomas Wagner, Markus Walle, and Christoph A. Heinrich (2013) Major and trace-element composition and pressure-temperature evolution of rock-buffered fluids in low-grade accretionary-wedge metasediments, Central Alps. *Contributions to mineralogy and petrology*, 165 (5): 981-1008.

George D. Miron, Philip S. Neuhoff, and Georg Amthauer (2012) Low-Temperature Hydrothermal Metamorphic Mineralization of Island-Arc Volcanics, South Apuseni Mountains, Romania. *Clays and Clay Minerals*, 60 (1): 1-17.

Recent conference and workshop talks

- GEMS training on element partitioning in aqueous-solid solution or sorption systems, 20-22 April 2015, PSI Villigen, Switzerland.
- George D. Miron**, Dmitrii A. Kulik, Svitlana V. Dmytrieva, and Thomas Wagner: GEMSFITS: A coupled code for GEMS input data optimization.
- HiTAC II, 16 April 2015, Heidelberg, Germany
 - Journee Metalogénique, 13 March 2015, Zürich, Switzerland.

George D. Miron, Thomas Wagner, Dmitrii A. Kulik, Christoph A. Heinrich: Internally consistent thermodynamic data for aqueous species in the Na-K-Al-Si-O-H-Cl system.

- ISSP16, 21-25 July 2014, KIT, Karlsruhe, Germany.
- GEMS Workshop, 7-8 May 2014, EMPA Dubendorf, Switzerland.

George D. Miron, Dmitrii A. Kulik, Svitlana V. Dmytrieva, and Thomas Wagner: GEMSFITS: A coupled code for GEMS input data optimization.

- 9th Swiss Geoscience Meeting, 2011, Zürich, Switzerland.

Miron G.D., Wagner T., Wälle M., Heinrich C.A: Fluid composition and mineral equilibria in low grade metamorphic rocks, Bündnerschiefer, Switzerland. Application of fluid inclusions and petrological modeling.

Reveiwer for scientific journals:

- Antarctic Science
- Applied Geochemistry
- Applied Clay Science
- Chemical Geology